Australian Government
Geoscience Australia

NORTHERN TERRITORY COASTAL PLAIN PROJECT

Northern Territory Coastal Plain: Mapping Seawater Intrusion In Coastal Plain Aquifers Using Airborne Electromagnetic Data

Prepared for National Water Commission, May 2012

Tan, K. P., Clarke, J.D.A., Halas, L., Lawrie, K.C., Apps, H. E., Brodie, R.C., Costelloe, M., Sumner, J. Fell-Smith, S., Christensen, N.B., Schoning, G. L., Halas, V. & Lewis, S.

Record
2012/41

GeoCat # 74100

Northern Territory Coastal Plain: Mapping Seawater Intrusion in Coastal Plain Aquifers Using Airborne Electromagnetic Data

GEOSCIENCE AUSTRALIA
RECORD 2012/41

By

Tan, K.P.[1], Clarke, J.D.A.[1], Halas, L.[1], Lawrie, K.C.[1], Apps, H.E.[1], Brodie, R.C.[1], Costelloe, M.[1], Sumner, J.[2], Fell-Smith, S.[2], Christensen, N.B.[3], Schoning, G.L.[1], Halas, V.[1], and Lewis, S.J.[1].

Australian Government
Geoscience Australia

Northern Territory Government

1. Geoscience Australia, GPO Box 378, Canberra, ACT, 2601
2. Northern Territory Department of Natural Resources, Environment, the Arts and Sport, PO Box 496, Palmerston, NT, 0831
3. Aarhus University, Denmark.

Department of Resources, Energy and Tourism
Minister for Resources and Energy: The Hon. Martin Ferguson, AM MP
Secretary: Mr Drew Clarke

Geoscience Australia
Chief Executive Officer: Dr Chris Pigram

This paper is published with the permission of the CEO, Geoscience Australia

ISSN 1448-2177
ISBN 978-1-922103-36-9
ISBN 978-1-922103-28-4 (Web)

GeoCat # 74100

Bibliographic reference: Tan, K.P., Clarke, J.D.A., Halas, L., Lawrie, K.C., Apps, H.E., Brodie, R.C., Costelloe, M., Sumner, J., Fell-Smith, S., Christensen, N.B., Schoning, G.L., Halas, V. & Lewis, S.J., 2012. Northern Territory Coastal Plain: Mapping Seawater Intrusion in Coastal Plain Aquifers Using Airborne Electromagnetic Data. Geoscience Australia Record, 2012/41, Canberra. 218p.

Australian Government
National Water Commission

Geoscience Australia acknowledges funding for this project through the National Water Commission's Raising National Water Standards program.

Cover image: Sinkhole (doline) over Koolpinyah-Coomalie Dolostone (photo by H. Apps, 2010).

Executive Summary

This report documents the findings of the 'Northern Territory Coastal Plain: Mapping Seawater Intrusion (SWI) in Coastal Plain Aquifers Using Airborne Electromagnetic (AEM) Data' project. The principal objective of this project was to assess the potential for SWI to impact on aquifers within the Darwin Rural Water Control District (DRWCD). The project was funded by the National Water Commission (NWC), with significant in-kind resources and funding provided by Geoscience Australia (GA) and the Northern Territory Department of Resources, Environment, Tourism, Arts and Sports (NRETAS). The project entailed acquisition of regional AEM data over the priority areas within the DRWCD as well as small-scale sonic and rotary drilling programs, borehole geophysical logging, groundwater sampling, laboratory analysis of pore fluids and groundwater samples, and integration, analysis and interpretation of these data.

SWI is an incipient hazard in many areas of the Northern Territory. SWI has previously been reported from an area within the project study site although the threat posed by SWI is considered to be much greater, hidden at depth in a hydrogeologically complex area with very limited appropriate data. There are 10 aquifers identified in the DRWCD, however the project has focussed on assessing the threat to the main producing aquifer (the Howard East Aquifer, HEA). The HEA consists of a highly complex succession of Proterozoic rock types in which dolostone (Koolpinyah-Coomalie Dolomite, KCD) is the dominant aquifer.

The implications of a potential threat from seawater intrusion (SWI) to the HEA are serious. This system represents a significant water source to an estimated 30,000 residents (predicted to double by 2021), a strong horticultural industry, market gardens, and a public utility providing 20% of Darwin's municipal supply. The increase in population within the region is likely to increase pressure on the water resource. The HEA also discharges to several groundwater-dependent ecosystems (GDEs) throughout much of the dry season, sustaining several important environmental and cultural sites. The project is viewed by the Northern Territory Government and the Power and Water Corporation as providing key information to assist in the assessment and management of groundwater resources, and the development of the Howard East Aquifer Water Allocation Plan.

A total of 3,875 line km of AEM data were acquired in 2008-2009 within the 3,775 km^2 of the project area, using the TEMPEST™ time domain AEM system. The survey was acquired at a range of flight line spacings, with infill acquisition acquired at 555 metre spacing over the existing and proposed borefield sites, and more broadly (1,666 and 5,000 metre spacings) outside of these areas. The AEM survey was configured to map regional-scale variations in ground conductivity that might be associated with the character of the SWI wedge, regional aquifer characteristics, groundwater conductivity and salinity. The survey was not designed for more detailed 'within-borefield' investigations. Elevation control for the interpretation of AEM data was provided by Shuttle Radar Topography Mission (SRTM), hydrologically-enforced Digital Elevation Model (H-DEM).

Data obtained from an advanced drilling technology in conjunction with existing hydrogeological information provided the basis for the validation and interpretation of the AEM dataset, and the production of a suite of derived products including maps of key elements of the aquifer system, groundwater quality (salinity) and SWI hazard.

PRINCIPLE FINDINGS OF THE REPORT

1. Limited drilling and hydrochemical analysis confirms the AEM survey has successfully mapped the SWI interface throughout the project area. This interface extends a considerable distance (up to 50km) inland associated with the upper reaches of the Adelaide and Mary Rivers, and 10km inland at Howard Springs (Figure A). The presence of highly conductive pyritic Proterozoic bedrock units necessitated mapping and masking the latter in order to produce 3D maps of SWI from the AEM conductivity data.
2. The AEM data has been used to identify potential SWI hazards to the Howard East Aquifer in four areas: Lambells Lagoon, Howard Springs, Gunn Point and Middle Point (Figure A). In each case, highly saline groundwater, interpreted as SWI ingress, appears to be facilitated by the presence of higher transmissivity structural corridors (e.g. faults at Howard Springs and faults and fractured quartz ridges at Lambells Lagoon), and/or where there are potential preferential recharge pathways in the overlying

aquifer system (e.g. through overlying palaeovalleys at Gunn Point). The greatest concern is at Lambells Lagoon, where highly saline groundwater is present at depth within 2 km of producing bores. At Howard Springs, an increase in salinity, albeit still relatively low (<250 mg/L) in a bore (RN 020730) in advance of the mapped SWI wedge, has been observed (Fell-Smith & Sumner, 2011).

3. In parallel investigations (Fell-Smith & Sumner, 2011), limited age dating and chemical characterisation of saline groundwater in the study area suggests that a there is an important distinction between 'older' deeper saline water bodies and more recent saline ingress from the coastal areas and floodplains. However, the apparent continuity of the mapped SWI wedge requires further work to establish if there are separate groundwater systems. In the confined aquifer system, the connectedness of the groundwater system and pressure responses in that system, both in terms of natural recharge and extraction from the HEA may be more important than the age of the groundwater itself in determining the dynamics of the saline ingress, and the salinity hazard to the HEA. Further data and groundwater modelling is required to understand the groundwater and salinity processes and dynamics in each of these hazard areas.
4. The AEM data in tandem with the airborne magnetics data, validated by drilling and chemical analysis, has also been used to subdivide the HEA into a number of groundwater zones based on water quality and other aquifer characteristics (Figure B; Fell-Smith & Sumner, 2011). The hydrogeological zones are: confined aquifer, low salinity aquifer, the main aquifer and saline groundwater and/or floodplain.

More detailed scientific findings:

1. A number of different inversions were carried out on the AEM data, with a Layered Earth Inversion (LEI) (Lane, 2002) providing the best fit with available borehole data. All the available borehole conductivity data were used as constraints within the final AEM inversion; therefore there is very high confidence in the inversion models within 300-500m of the borehole locations, with decreasing confidence levels in domains with little borehole control. Overall, comparison of AEM and borehole data suggest it is reasonable to assume that the modelled ground response from the inverted TEMPEST data provides a good approximation of 'true' ground conductivity as defined by the borehole conductivity tool. The final inversions of the AEM data are considered a reliable base from which to derive a suite of interpretation products including mapping the SWI interface, groundwater salinity and lithology maps.
2. There is relatively poor elevation control on the AEM data due to the wide and variable line-spacing of the AEM survey and a lack of other spatial or spot height data to constrain survey elevations. Final AEM inversions utilised an SRTM dataset corrected for hydrological features. Gridded data are estimated to have accuracies of ± 2m in the lower elevation floodplain environment, and 5-10m in the higher elevation parts of the landscape.
3. This inversion effectively mapped variations in ground conductivity at scales relevant to the regional characterisation of the SWI interface, and key elements of the hydrostratigraphy. However, the scale of the regional mapping, and lack of suitable borehole data in appropriate locations, has generally precluded the mapping of karstic porosity in the aquifer system.
4. Key elements of the hydrogeological system were mapped in three dimensions over most of the project area with the aid of AEM data. Overall, the AEM mapping has provided greater spatial detail on critical elements of the hydrostratigraphy. Importantly, most of the formations do not have unique AEM conductivity signatures due to lithological variability and highly variable groundwater salinities. Mapping of the hydrostratigraphy has been achieved through the integration of the AEM survey data with existing borehole data and five new sonic cores (drilled to ~70 metres depth). Recognition of spatial patterns in the conductivity, validated by drilling data, is a critical part of the interpretation. The study has made the following findings in regards to the geology and hydrogeology:
    a. The AEM data has mapped Tertiary weathering fronts in the area where these are electrically resistive. However, in places, it is not possible to discriminate these, particularly where more saline water overprints the weathering front. The base of weathering interface is geometrically irregular.
    b. The floodplain sediments were successfully mapped using a combination of borehole information and AEM data. It was possible to map both the thickness and extent of these sediments, including the base of the floodplain sediment sequence. Most floodplain sediments are highly conductive and water quality variations within them need to be displayed based on

fine threshold intervals. Correlation between laboratory results and conductivity data allows groundwater quality within the sediments to be derived from the AEM data.

c. Cretaceous sedimentary rocks have only been able to be mapped as undifferentiated Bathurst Island Group in the study area. Key points are:
    i. Significant palaeotopography with a relief of at least 20 m occurs along the basal unconformity, including palaeovalleys associated with the Mary and Adelaide Rivers, and very large scale karst depressions 5-10 km across. These would have formed the known as poljes when they were at the surface. The palaeovalley geometry is at least partly controlled by basement architecture. Their fill is unknown but is likely to control groundwater flow, both spillage of fresh groundwater during and following the wet season and as potential pathways fro seawater incursion should aquifers be over-pumped. The poljes have the potential to focus vertical recharge through the Cretaceous over large areas (tens to hundreds of square km) into the most permeable parts of the Koolpinyah-Coomalie Dolomite (KCD) aquifer. Both palaeovalleys and poljes may be very significant for the distribution of terrestrial and aquatic groundwater dependent ecosystems
    ii. From sonic core data it appears that the sand bodies in the Cretaceous units are relatively thin, i.e., 3 metres or less in the drilled areas. At this scale, and without marked contrast in electrical conductivities for units above or below, it is not possible to map individual sand bodies with the regional AEM data. Furthermore, groundwater storage in these sand units is likely to be low.
    iii. Drilling data and existing water bore data suggest there may be perched water tables above impermeable stratigraphic or secondary weathering-related horizons.
    iv. Borehole and coastal outcrop information show that the basal surface of the Cretaceous sedimentary rocks is highly irregular. Most Cretaceous sedimentary rocks are electrically resistive and have no significant contrast with underlying dolostone sequences; this makes it difficult to map the interface between Cretaceous sedimentary rocks and dolostone using AEM data alone. Consequently, validation using borehole and laboratory data is essential for this task. Integration of AEM and borehole data has enabled the thickness and extent of the Cretaceous sequence, and water quality variations within the sediments, to be mapped.
    v. A basal Cretaceous lag of variable thickness and very coarse grainsize composed of quartz and dolostone boulders has been described in pre-existing water bores. These lag deposits do not appear to have significant lateral extent and their distribution is probably controlled by karstic palaeo-topography beneath Cretaceous sedimentary rock cover. They cannot be mapped with AEM data.

d. Proterozoic and Archaean ‘Basement’.
    i. The depth to the top of the Proterozoic and Archaean successions was mapped successfully, including significant and previously unidentified palaeo-topography. The extent of these rocks was mapped through a layer by layer interpretation of the AEM depth slices and validated by boreholes. In general, these rocks are structurally complex, with large-scale fold patterns and faults evident in the AEM data. Interpretation of faults and dykes was assisted by integration of AEM and drilling data with airborne magnetic data.
    ii. There is less reliability in mapping the Proterozoic and Archaean basement in the eastern part of the project area due to a paucity of drillholes of sufficient depth to reach the basement.
    iii. Most of the basement rocks are of the Mount Partridge and South Alligator Group. The Finniss River Group occurs only in the south and south-west of the mapped area and the only unit known in this region is the Burrell Creek Formation. The Finniss River Group has been mapped using a combination of AEM, outcrop and borehole data.
    iv. Most dolostones in the KCD are crystalline and impermeable. Where cavernous because of dissolution or fracturing they have relatively high groundwater yields. These zones could be mapped only by using drillcore data collected at high density, together with airborne magnetics data. AEM is not able to map connectivity between sinkholes owing

to the highly resistive nature of the dolostones and the presence of fresh water in the aquifers. This AEM survey is not able to map connectivity between sinkholes owing to the highly resistive nature of the dolostones and the presence of fresh water in the aquifers. Large scale solution features, the palaeo-poljes, could be mapped through the thickening of the overlying Cretaceous sedimentary rocks. Different AEM technologies and closer line spacing may be more successful.

e. A number of dolerite dykes have been mapped in the project area using airborne magnetics and AEM data. An example is the north-west trending dolerite intrusive associated with the north-eastern Pine Creek Shear Zone (PCSZ). Dolerite dykes that cross-cut the Proterozoic successions are potential barriers to groundwater flow.

f. Quartz or quartzite ridges. Quartz-rich zones coincident with magnetic lineaments have also been mapped. These may be quartz veins, or the quartzite member (Acacia Gap Member) of the Mount Partridge Group. The quartz or quartzite is highly fractured and borehole information suggests high groundwater yields occur from this unit when it outcrops. Production bore and pump test data indicate that these may be zones of preferential recharge and groundwater flow (Fell-Smith & Sumner, 2011).

g. Fault zones. Conductivity patterns are coincident with a number of structural features interpreted from the airborne magnetics and geology maps. A major NW-SE-trending structural corridor at Howard Springs that appears to control SWI ingress, has also controlled the orientation of palaeo-drainage features in the pre-Cretaceous land surface tributary to the trunk palaeovalley of the ancestral Adelaide River.

5. The drilling of five sonic bores (to depths of ~70 metres) was critical for interpretation of the hydrostratigraphy and validation of the AEM survey data. Pore fluids have been successfully recovered from the drillcore materials. Textural and pore fluid analysis of drillcore materials have enabled the production of a suite of interpretation products including groundwater salinity maps.

More General Observations

1. In this project, survey line-spacing was based largely on matching the project area with available funds, rather than modelling of optimal survey design. Fortuitously, the infill line-spacing (550 metres) was adequate to show regional 3D patterns in electrical conductivity, and has successfully mapped the SWI interface at a broad-scale in the project area. A broader line-spacing of 1,666 metre and 5,000 metre has also been useful in defining the SWI wedge, which in this instance appears to have a relatively simple structure. In both instances, the approach has been successful due to the broad-scale variations in electrical conductivity patterns observed with SWI. Analysis of the broader 5,000 m line-spacing data shows that encroachment of the SWI interface towards the fresher groundwater resources tapped by borefields would only have been evident along individual flight lines that traversed the interface.
2. The AEM survey was not designed to map 'within-borefield' variations in texture and groundwater quality. Hints of significant variations in lithology and karstic porosity are evident in the data within individual flight lines, but the line-spacing (550 m or greater) restricts finer-scale interpretation.
3. The project was delayed due to problems encountered with data acquisition and delays in providing final survey data. Furthermore, contractor-supplied Fast Approximate Inversions using the EM Flow software were found to have poor correlation with borehole data ($r^2 = 0.338$). Inherent bias in this inversion method created an overestimate of the conductivity near the surface, since the model must compensate for the lack of conductance at depth due to assumptions about system geometry (Lane *et al*., 2004a; Brodie & Fisher, 2008). The conductivity depth sections produced using this inversion produced unreliable depth estimates of conductivity, and were found to be unsuitable for interpretation purposes. Elevation control on the AEM data was hampered by the wide flight line-spacing and a lack of complementary spatial data (e.g. LiDAR) or spot heights, limiting the utility of the AEM dataset for high resolution near-surface studies in particular. LEIs of the AEM data, incorporating borehole conductivity data as constraints, significantly improved the correlation of the AEM data with ground data.

In summary, the products and accompanying analysis and interpretation detailed in this report are being used as a key component of the hydrogeological framework in the Howard East Aquifer water allocation plan, and will provide a solid basis for future groundwater management decisions. The AEM dataset and interpretation

products are also being used to target further hydrogeological investigations and SWI monitoring programs. The new knowledge generated by the project and the specific water quality and hydrostratigraphic interpretation products will greatly assist in the parameterisation of new groundwater models.

The project has also demonstrated the potential for large survey areas in relatively inaccessible terrain to be assessed rapidly for SWI using an integrated approach based on AEM. However drilling data (especially borehole conductivity data) in a range of electrical conductivity domains are required to calibrate and validate AEM survey results and ensure a high degree of confidence in the survey results. We recommend that future studies of this nature follow a phased or staged approach to assess the available methods and technologies as part of a hydrogeological systems approach, according to previous guidelines (e.g., Spies & Woodgate, 2005; Lawrie *et al.,* 2008, 2010, 2011). This approach is critical when developing a framework for mapping groundwater systems.

PRINCIPLE RECOMMENDATIONS OF THE REPORT

NTCP Project Area-Specific Recommendations

1. There remain specific knowledge and data gaps in our understanding of the distribution of SWI, the hydrogeochemistry and hydrodynamics, and recharge and discharge processes. To assist with refining conceptual models and to improve groundwater model parameterisation and outcomes, we recommend that:
    a. A phase of additional drilling should be undertaken, targeted using the AEM-based interpretation products, to provide validation of areas of high electrical conductivity considered to result from SWI. Specifically, this will improve the validation of potential SWI encroachment at the margins of the borefield. It is recognised that this provides significant logistic difficulties, however additional data is required in key areas if the groundwater model is to be adequately parameterised. Specific sites that should be prioritised due to the higher salinity hazard include: Lambells Lagoon, Howard Springs, Gunn Point, and Middle Point.
    b. Additional drilling data and hydrogeological investigations are required to validate the revised conceptual model for recharge to the groundwater system, and to confirm potential discharge pathways, in particular the large scale karstic features (poljes) and palaeovalley tributaries identified in the AEM. Additional drilling data in specific areas may also enable further refinement of existing AEM inversions.
    c. Compilation and analysis of existing hydrogeochemical data should be undertaken to understand more fully the potential risks to water quality in the borefield, and to help with developing a conceptual groundwater model.
    d. New maps of surface recharge are required. Following the approach taken in previous investigations (e.g., Lawrie *et al*., 2010), these should incorporate existing soil and regolith maps, the new high resolution Digital Elevation Model (1-arc second SRTM), satellite remote sensing data (including vegetation change detection), radiometric data, the 0-4 m AEM depth slice, and should take into account the new conceptual model for recharge developed in this project. If possible, a high resolution LiDAR dataset should also be acquired over the project area to improve the spatial resolution of topographic features.
    e. There is sufficient confidence in the inverted electrical conductivity data and AEM-derived interpretation products to recommend that groundwater modelling, utilising these products, be undertaken to assess the SWI risk to the DRWCD and the Howard East Aquifer in particular. However, model predictions would be improved with further refinements in model conceptualisation and parameterisation. Modelling should incorporate the latest sea-level rise modelling scenarios, as well as projected population growth, expected changes to land use and variations in other environmental or socio-economic factors that may be impacted by SWI (BMT WBM, 2010).

Broader recommendations

Future AEM surveys should consider the scale of the key elements of the hydrogeological system to be mapped, with the survey designed to match this requirement. This will optimise available resources and maximise the potential for a successful project outcome. This project has highlighted that more traditional, close line spacing (100-200 m) is not always necessary (Lawrie *et al.,* 2004), depending on project objectives.

1. As with several earlier AEM-based studies (Lawrie, 2008, Lawrie *et al*., 2010, 2011), a phased or staged approach should be employed for future AEM-based SWI or karstic mapping projects and include:
    a. Collation and review of existing information for the purpose of identifying critical knowledge gaps;
    b. Scoping and technical risk evaluation to assess the methods and technologies best suited to address identified knowledge gaps, and to assist with survey design;
    c. Integrated geoscientific studies to enable key elements of the hydrogeological system to be mapped, and groundwater flow and hydrogeochemical processes to be understood;
    d. Data synthesis and interpretation using contemporary 'systems' approaches (Lawrie *et al*., 2000; Lane *et al*., 2004a, b; Spies &Woodgate, 2005; Lawrie *et al*., 2008, 2010, 2011), with an emphasis on delivering products that address specific issues and assist with the improved parameterisation of hydrogeological models; and
    e. Groundwater, surface-groundwater modelling and land use modelling to ascertain the sustainability of proposed developments. Modelling should use the best available climate data and modelling scenarios.
2. The acquisition of ground and airborne geophysical data for SWI or karstic mapping should only be considered within the broader context of integrated hydrogeological assessment of an area (Lawrie *et al*., 2010). Technical risk evaluation is required to gauge the merits of employing different geophysical approaches and technologies.
    a. Acquisition of AEM data should only proceed after completion of scoping studies to assess the likelihood of success arising from their acquisition.
    b. Scoping studies are required to identify target aquifers and groundwater systems, and the scale, depth and orientation of target objectives (where possible). This should be followed by review and assessment of suitable technologies in each area. Technology selection should include forward modelling of system responses, and should follow the best practice procedures developed by the Commonwealth, taking particular note of the ability of AEM system to map key elements of relevant elements of the hydrogeological system.
    c. AEM data analysis and interpretation should follow a 'hydrogeological systems' approach based on the methodology recommended by the Joint Academies of Science Review of Salinity Mapping Methods in the Australian Landscape Context (Spies & Woodgate, 2005). Based on these recommendations, AEM-based projects need to incorporate a drilling program, complementary ground investigations and hydrogeochemical studies to ensure appropriate survey calibration, validation and interpretation.
3. Future AEM surveys for mapping SWI and karstic systems should carefully consider the merits of using calibrated AEM systems and inversion software that can significantly shorten data acquisition and delivery schedules, and the overall project time and budget.
4. The use of sonic drilling technology was a success in this project with nearly 100% core recovery in wide range of unconsolidated and consolidated geological materials, and delivery of uncontaminated core for hydrogeochemical investigation. The use of this technology in similar studies is strongly recommended.
5. This project differed from previous federally-funded groundwater and salinity mapping projects carried out over the past decade in Australia. Specifically, the project was developed opportunistically, piggy-backing on the acquisition of a survey designed to map bedrock features as part of GA's Onshore Energy Security Program. In future, we recommend that:
    a. Where possible, forward modelling should be carried out using available ground and borehole geophysical data and relevant hydrogeological models to ascertain whether the selected

technology can map the key elements of the hydrogeological system, and to aid survey design. This is also essential to assist in project planning and resourcing.

b. Stakeholder consultation should be undertaken at an early stage to ascertain the areas and scales of interest, and the types of products required.

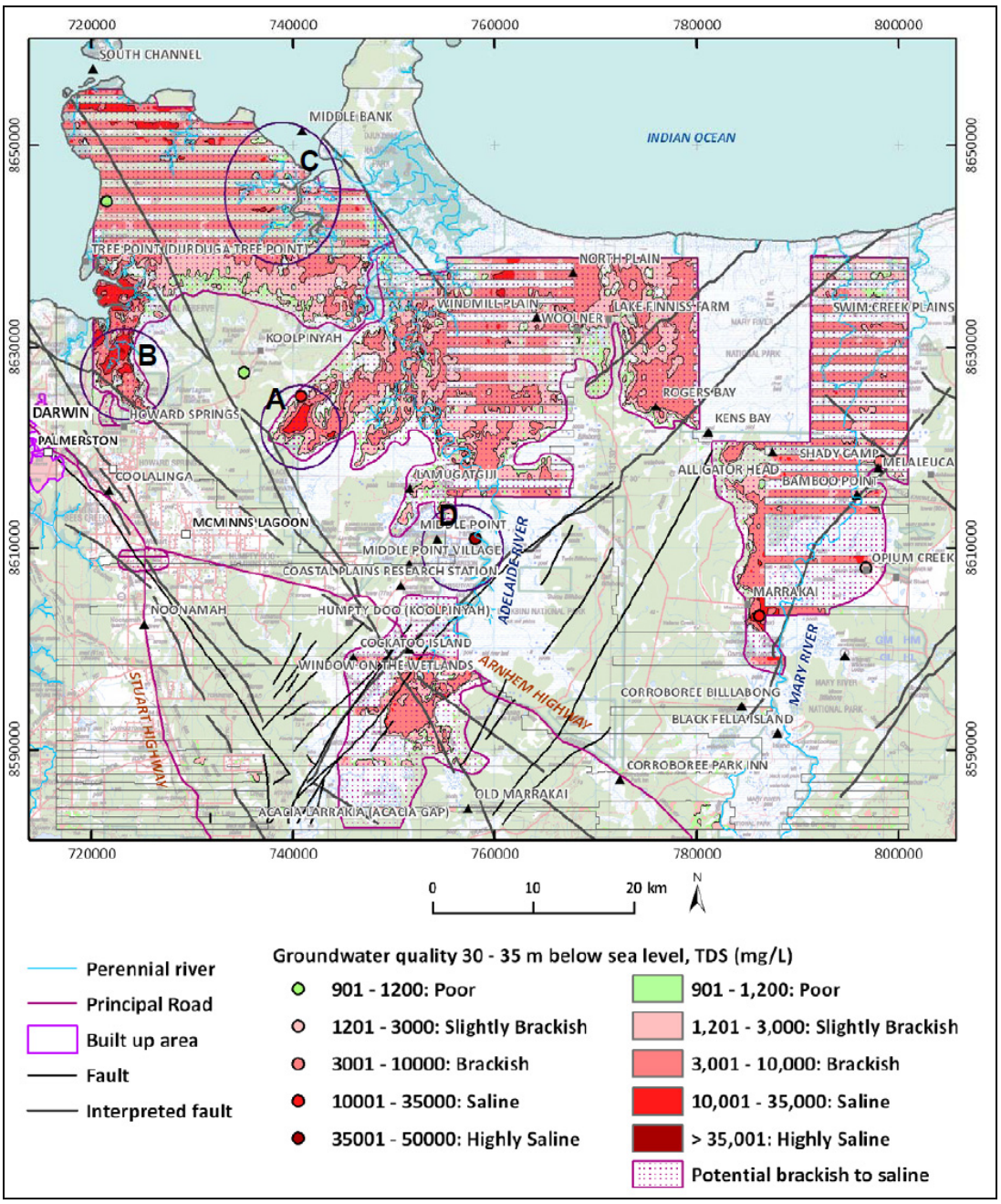

Figure A. *Map of SWI in the project area based on the AEM depth slice 30-35m below sea level. Salinity hazard areas at (A) Lambells Lagoon, (B) Howard Springs, (C) Gunn Point and (D) Middle Point, are shown.*

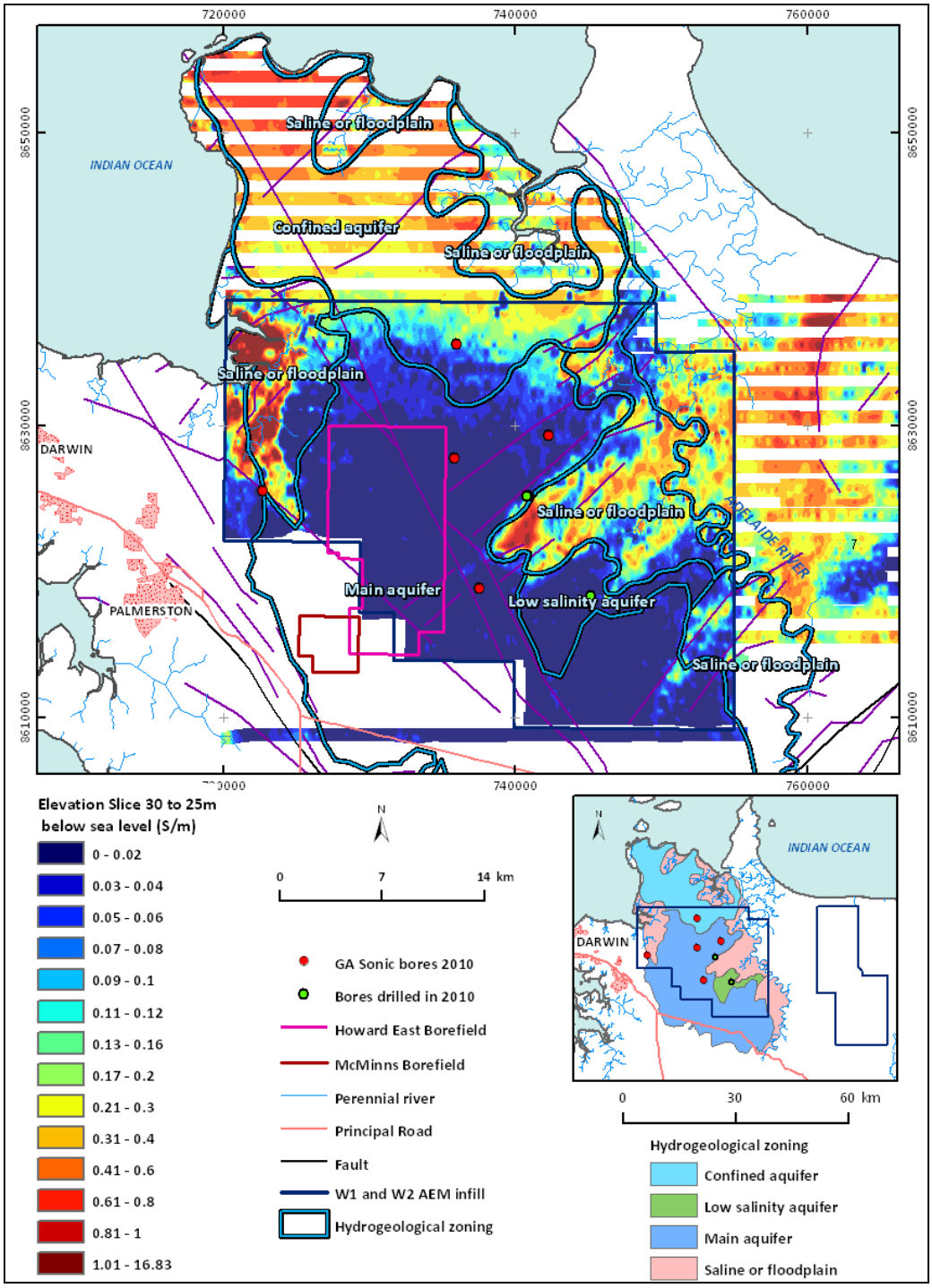

Figure B. *Hydrogeological zoning in the HEA, based on the AEM, airborne magnetics data validated by drilling. The boundaries use AEM data from several different conductivity depth slices. Comparison of the boundaries with the AEM conductivity depth slice 30-35m b.s.l. shows the correspondence with the more saline aquifer at these depths.*

Contents

List of Figures

List of Tables

1 Introduction

This report documents the findings of the National Water Commission-funded project: *'Northern Territory Coastal Plain: Mapping Seawater Intrusion (SWI) in Coastal Plain Aquifers Using Airborne Electromagnetic (AEM) Data.*' The objectives of the 'Northern Territory Coastal Plain' project were to:

1. Provide relevant baseline AEM data to support decision-making relating to water and natural resource management;
2. Combine the AEM with other key datasets to interpret aquifer characteristics and the distribution of seawater intrusion, and/or the landward extent of the seawater wedge (whether anthropogenically disturbed or not), as inputs into sustainable groundwater development in priority areas and to guide groundwater management and monitoring for the future; and
3. Act as a test-bed for guiding the planning of future AEM surveys of coastal groundwater systems in Australia, particularly where urban or community drinking water supplies are drawn from freshwater coastal aquifers and/or where irrigation is drawing on such resources.

The project was funded by the National Water Commission (NWC), with significant in-kind resources and funding provided by Geoscience Australia (GA) and the Northern Territory Department of Natural Resources, Environment, The Arts and Sport (NRETAS). The project entailed acquisition of regional AEM data over priority areas within the Darwin Rural Water Control District (DRWCD; Figure 1), small-scale sonic and rotary mud drilling programs, borehole geophysical logging, groundwater sampling, laboratory analysis of pore fluids and groundwater samples, and integration, analysis and interpretation of results.

SWI is an incipient hazard in many areas of the Northern Territory and a localised seawater intrusion hazard has previously been reported within the current project area (CSIRO, 2009a, b). However, the threat posed by SWI is considered to be much greater than presently known, hidden at depth in a hydrogeologically complex area with very limited appropriate data to fully assess the potential effects. There are ten aquifers in the DRWCD; however, this project focussed on assessing the threat to the main producing aquifer, the Howard East Aquifer (HEA). The HEA consists of a complex sequence of Proterozoic rocks in which dolostone (the Koolpinyah-Coomalie Dolostone, or KCD) provides the main source of extracted groundwater.

The implications of a potential threat from seawater intrusion (SWI) to the HEA are serious. This system represents a significant water source to an estimated 30,000 residents (predicted to double by 2021), a horticultural industry, market gardens, and a public utility providing 10% of Darwin's municipal water supply. The projected increase in population within the region is likely to increase pressure on the water resource. The HEA also discharges to several groundwater-dependent ecosystems (GDEs) in the dry season, sustaining important environmental and cultural sites. The project is viewed by the Northern Territory Government and the Power and Water Corporation as providing key information that is expected to assist greatly in the assessment and management of groundwater resources and the formulation of the Howard East Aquifer Water Allocation Plan.

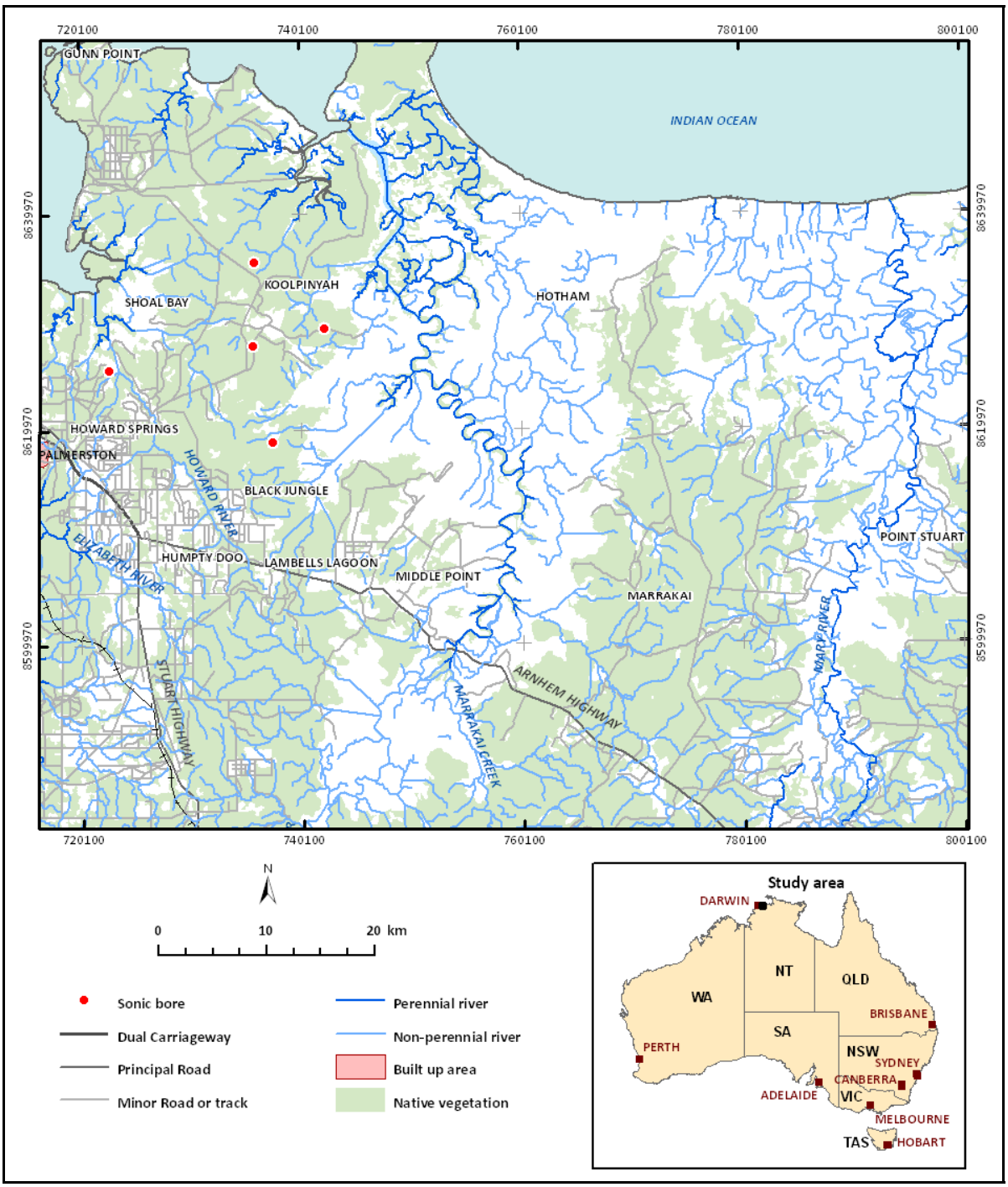

Figure 1. *Extent of the Northern Territory Coastal Plain project and adjacent areas.*

Seawater intrusion is most likely driven by over-production from the aquifer. Through the NWC-funded *Koolpinyah Dolomite Aquifer Characteristics Project*, appraisal of groundwater monitoring data indicates that the system is already under significant stress (Fell-Smith and Sumner, 2011). Accelerated groundwater development in the region since the 1990's has resulted in significant impacts on regional groundwater levels, reduced seasonal flows in the Howard River and the earlier cessation of flows from the iconic Howard Springs. Continued production at current rates is likely to increase the rate of seawater intrusion, and future population increases will further exacerbate the situation. Identification of a SWI hazard will have major consequences for management of the KCD aquifer. This is recognised by the Power and Water Authority, who have shown significant interest in the project results and have joined the project Steering Committee. The results of this project provide a strong basis for groundwater model development, and to underpin groundwater management planning. The project area is shown in Figure 1.

A total of 3,875 line kilometres of AEM data were acquired in 2008-2009 within the 3,775 km^2 of the project area, using the TEMPEST™ time domain AEM system. The survey was flown at a range of flight line spacings, with infill acquisition acquired at 555 m over the existing and proposed borefield sites, and more broadly (1.66 and 5 km spacings) outside these areas. The AEM survey was designed to map regional-scale variations in ground conductivity that may be associated with broad scale changes in the character of the SWI wedge, regional aquifer characteristics, groundwater conductivity and salinity. It was not designed for more detailed "within-borefield" investigations.

Data obtained from an advanced drilling technology (sonic coring) in conjunction with existing hydrogeological information provided the basis for the validation and interpretation of the TEMPEST AEM dataset, and the production of a suite of derived products including maps of key elements of the aquifer system, groundwater quality (salinity), and SWI hazard.

The remainder of this introductory chapter provides an overview of groundwater management in the project area, the significance of seawater intrusion more generally in the Northern Territory, the context of this NWC project (including the use of the Pine Creek AEM dataset and related groundwater projects in the area), and the broader environmental characteristics of the region.

1.1 GROUNDWATER MANAGEMENT IN THE PROJECT AREA

The Northern Territory *Water Act 1992* (the Water Act) is the legislation which provides for the investigation, allocation, use, control, protection, management and administration of water resources. The Water Act allows for the declaration of water allocation plans (WAP) within water control districts (WCD) and requires that such plans allocate water to beneficial uses. Water allocation plans define rules for the distribution and management of water resources to encourage water use efficiency within the plan area. Unlike other Northern Territory WCD's, an exemption from licensing applies within the DRWCD where extraction rates, for any purpose, do not exceed 15 L/s. Bore construction permits are required within a WCD for the construction of new bores and alterations on existing bores.

The Darwin Rural Water Control District was declared in 1999 and encompasses the Litchfield Shire and Cox Peninsula and includes the Darwin, Blackmore, Howard and Elizabeth rivers as well as many ephemeral and perennial creeks (Figure 2). The hydrogeologic setting of the area is complex with over 10 aquifer systems, although most are low yielding (<0.5 L/s).

The Howard East Aquifer (HEA) is the most significant in the DRWCD and typically yields groundwater at 1-5 L/s, although some bores may exceed 15 L/s. This aquifer underlies a significant proportion of the Darwin Rural Area from the mouth of the Howard River, south to the Arnhem Highway, east to the Adelaide River and extending north to the landward limit of Gunn Point. It encompasses Howard Springs, Girraween, Humpty Doo, Lambells Lagoon and Middle Point regions as well as Koolpinyah Station. The HEA occupies the north-eastern quarter of the Darwin Rural Water Control District.

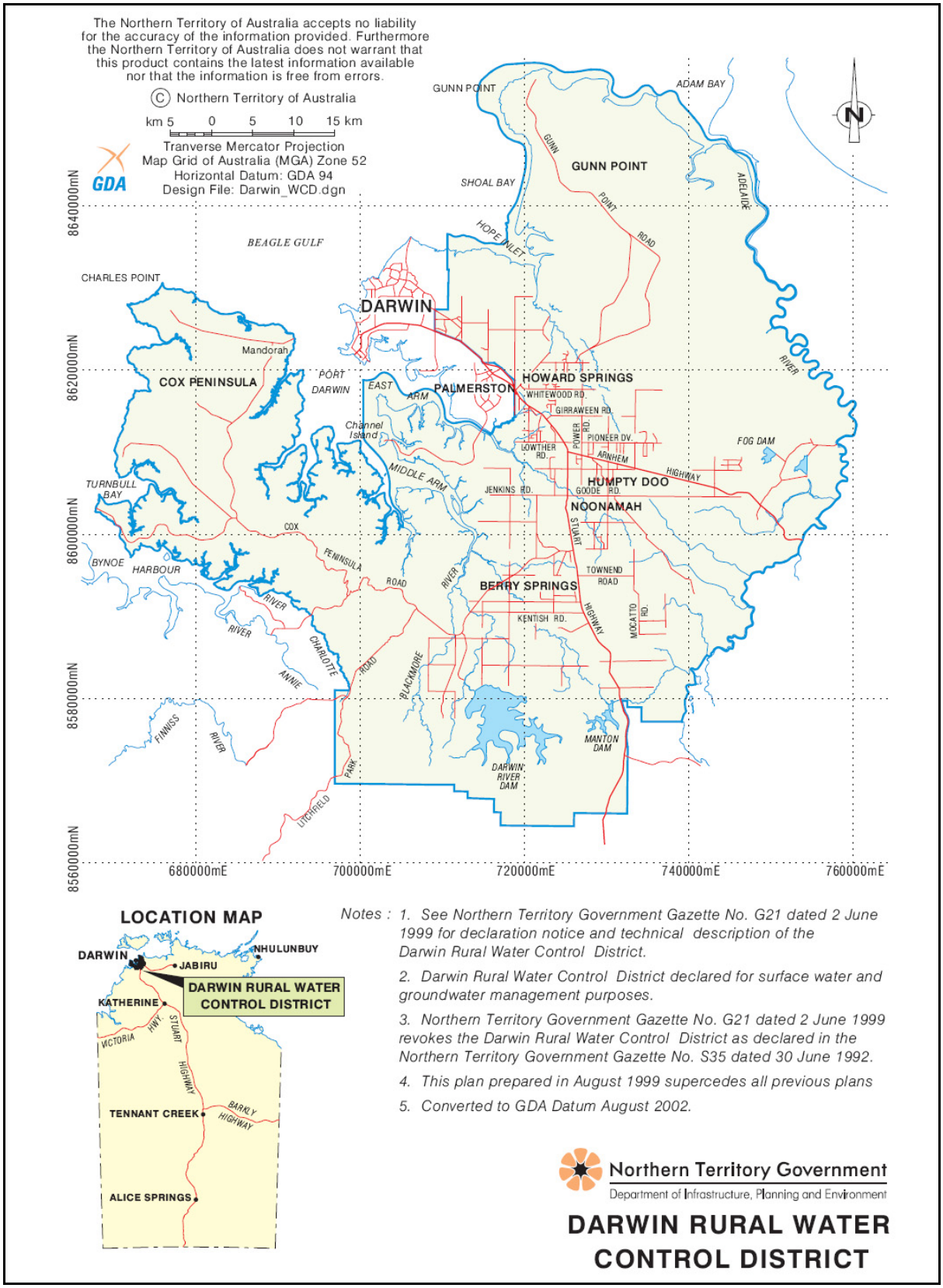

Figure 2. *Darwin Rural Water Control District.*

The HEA covers an area of 1,462 km^2 and is within the Litchfield Shire. The Litchfield Shire covers an area of 2,914 km^2. The population within the water planning area is estimated at approximately 12,000. Litchfield Shire is expected to experience rapid growth, increasing from 15,400 in 1999 to between 29,400 and 59,500

in 2021 (ABS, 2001). The increase in population is likely to increase pressure on the groundwater resources within the region.

The HEA is an important water source for agricultural and horticultural development, domestic supplies and public water use. It also discharges to several groundwater-dependent ecosystems in the dry season. Environmental and cultural sites connected to the Howard East Aquifer include Howard Springs, Howard River, Melacca Creek, Banka's Jungle, and a myriad of lagoons and several patches of spring-fed remnant jungle including Black Jungle Swamp.

The Howard East Aquifer Water Allocation Plan (Figure 3) is currently pending and will apply to all water contained in and originating from the HEA including groundwater that discharges to surface water ecosystems such as Howard Springs.

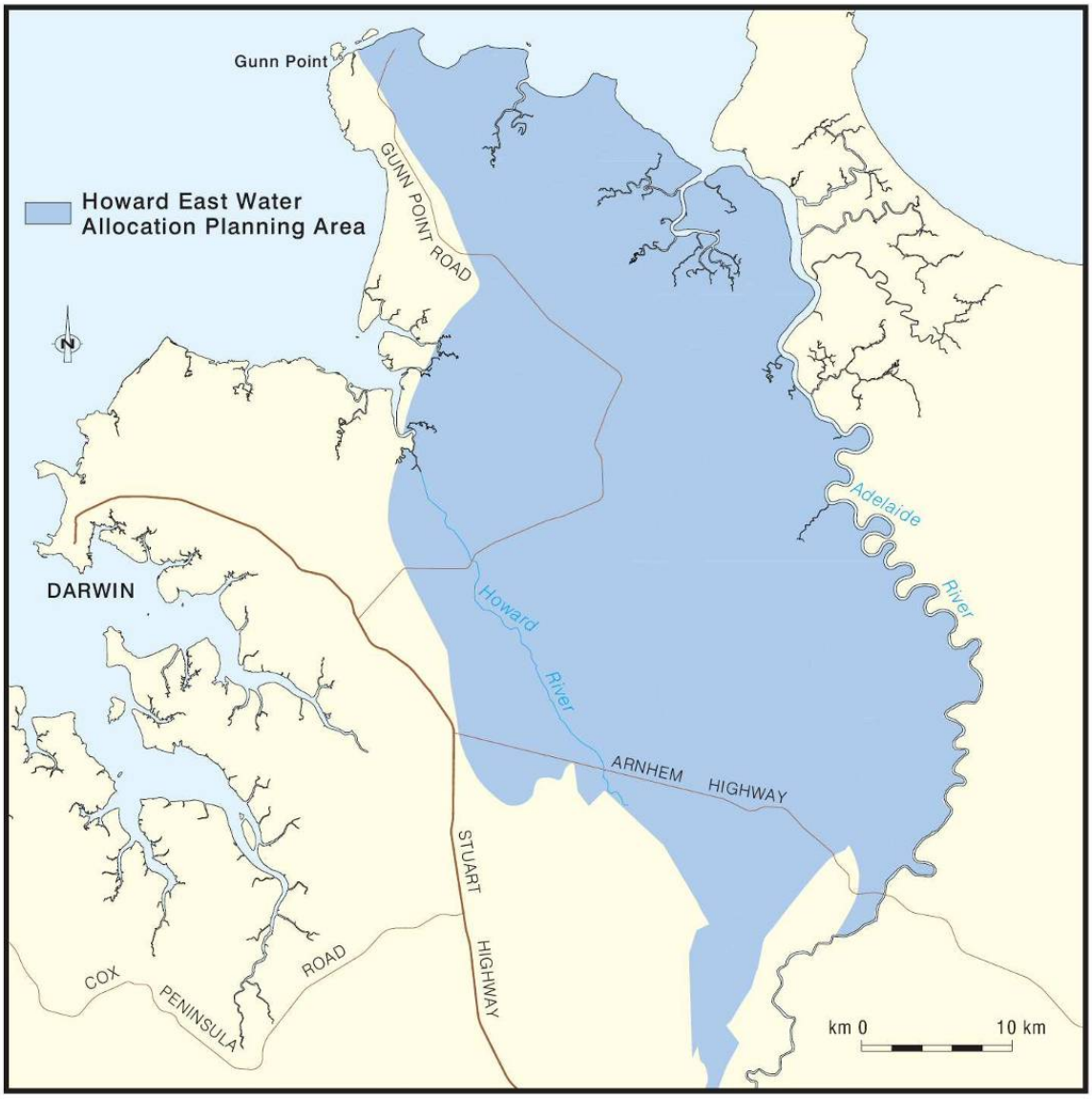

Figure 3. *Howard East Water Allocation Plan area.*

1.2 SEAWATER INTRUSION IN THE NORTHERN TERRITORY

1.2.1 Definition of seawater intrusion

Seawater intrusion (SWI) is the influx of seawater into an area (e.g., aquifer or surface water body) where freshwater normally dominates. SWI is a potentially increasing hazard in low-lying coastal areas of Australia (Dixon-Jain *et al.,* 2010; 2011) because of increased groundwater extraction for rural and urban use and because of rising sea-levels through global warming (IPCC, 2007). The following section on the general aspects of SWI is taken from Dixon-Jain *et al*. (2010), with minor additions and amendments.

SWI most commonly occurs in coastal aquifer systems as a consequence of groundwater extractions (Barlow, 2003). However, other anthropogenic influences such as urbanisation, land reclamation and drainage canals, to name a few, can also contribute. SWI may also result from natural causes including geological coastal evolution and long-term historic sea-level changes, tsunamis, climate variability and climate change. All of these processes can alter the water balance within an aquifer system. The projected sea-level rises in response to a changing global climate will also change the dynamic balance of the SWI interface, and the transition zone between fresh groundwater and seawater.

1.2.2 Development of SWI

When coastal aquifers are in hydraulic contact with seawater, an interface exists whereby less dense freshwater sits above, and adjacent to, a denser wedge of seawater (Figure 4). The leading edge of the seawater wedge is referred to as the toe, and it occurs where the seawater interface intersects with the base of the aquifer. The toe marks the maximum extent of SWI. The position of the seawater-freshwater interface can shift in response to changes in flow conditions between the aquifer and the sea. The seawater wedge decreases in thickness landward from the coast, with the toe of the wedge potentially extending several kilometres beneath freshwater reserves. Where a land mass is surrounded by seawater (e.g., islands, peninsulas and barrier dunes), opposing seawater wedges can intersect to isolate freshwater from regional groundwater systems, which may result in formation of subsurface freshwater lenses.

Mixing between freshwater and saltwater by mechanical dispersion and molecular diffusion results in a ‘transition zone’ of salinity around the interface, which can range from a few metres to kilometres in width (Figure 5). The position and width of the transition zone, and hence the extent of the saltwater wedge, is highly variable and changes with particular hydrogeologic and hydrologic circumstances (Custodio and Bruggeman, 1987). Dynamic forces such as daily tidal oscillations; seasonal and annual variations in groundwater recharge and extraction rates; and long-term changes in sea-levels will cause the transition zone to fluctuate landward and seaward over time (Barlow, 2003).

Groundwater recharge and pumping primarily control the transience and position of the interface. Aquifers with high recharge volumes may have transition zones laterally seaward of the coastline, while lower recharge areas are more likely to have transition zones that may extend many kilometres inland. Any changes in groundwater recharge or extraction volumes result in movements in the interface. The interface will gradually translate its position until it matches the new inflow-outflow regime and associated hydraulic head condition, although the time required for the interface to assume a new steady-state position after a persistent disturbance has occurred is not easily assessed or generally understood, but is thought to occur over timeframes of years to centuries.

SWI can occur through several pathways, including lateral intrusion from the ocean; upward intrusion from deeper, more saline zones of a groundwater system; and by downward intrusion from coastal waters (Barlow, 2003). SWI involving a vertical rise of saltwater from a deeper, more saline zone into an upper freshwater aquifer as a consequence of pumping is known as “up-coning”.

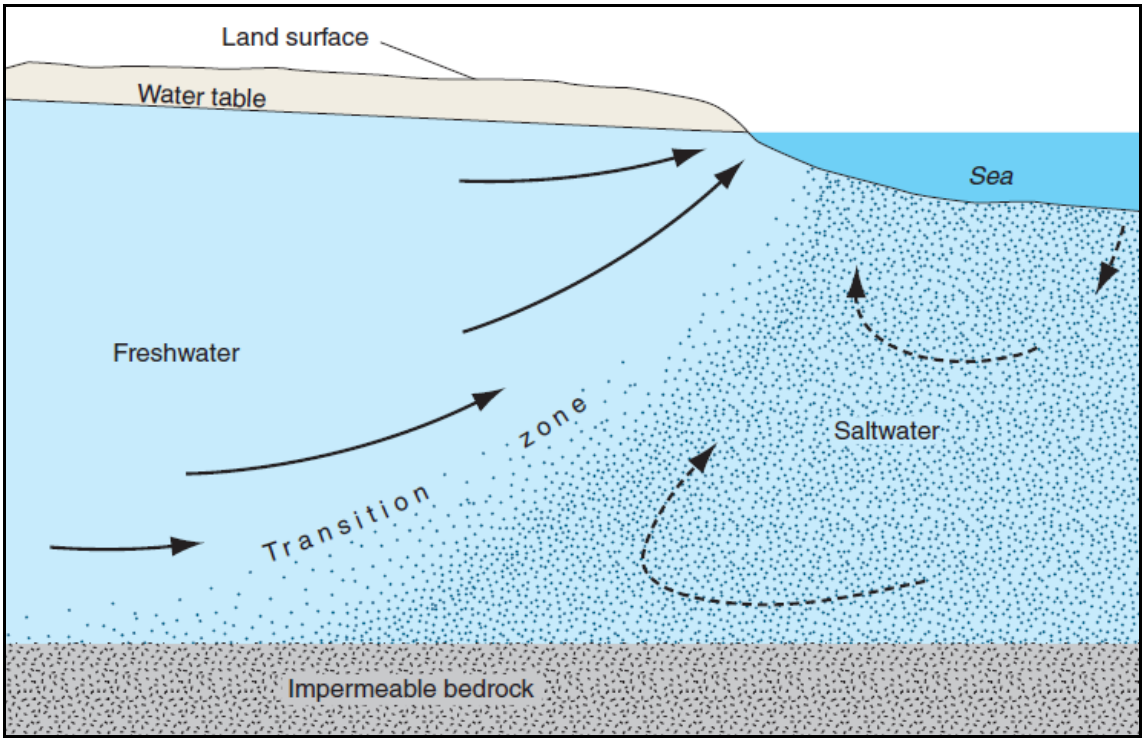

Figure 4. *Schematic of the transition zone between freshwater and saltwater in coastal aquifers (modified after Barlow, 2003). Image sourced from Dixon-Jain et al. (2010)).*

SWI is not the only mechanism by which coastal groundwater resources may become saline. Salt may be derived from other sources. For example, salinity can increase due to: dissolution of basement rock by fluids; inflow of agricultural waste products; and inflow from another aquifer containing relic seawater (Richter and Kreitler, 1993). Critical for any SWI investigation is to clearly distinguish seawater from other sources of salinity.

Seawater intrusion may produce aquifer degradation that can be difficult or impossible to reverse, so avoiding SWI is generally the objective of coastal aquifer management strategies. A foundation principle that can be used by managers of coastal aquifer systems for first-order analysis of SWI is the Ghyben-Herzberg Principle (Herzberg, 1901; Ghyben, 1888).

1.2.3 Ghyben-Herzberg lenses

The Ghyben-Herzberg principle (Figure 5) is commonly used, when and where possible, to simplify the analysis of fresh and saline water interactions and to estimate the depth to the saltwater interface.

The direction and rate of groundwater flow within a geological formation depends partly on the hydraulic gradient. The hydraulic gradient is determined by the hydraulic head difference (difference in watertable heights, or potentiometric heights in confined aquifers) within an aquifer, with flow in the direction of lowest hydraulic head. The hydraulic gradient in coastal aquifers is typically associated with the movement of groundwater from inland recharge areas to coastal discharge areas. When the freshwater-saltwater mixing zone is thin relative to the aquifer thickness it can be considered as a sharp interface; the depth to the transition zone can be estimated as a function of the depth of the watertable and the relative densities of seawater (e.g., 1,025 kg/m^{-3}) and freshwater (e.g., 1,000 kg/m^{-3}). This relationship is described for a steady-state system by the Ghyben-Herzberg equation:

$$z = 40h$$

where z is the depth to the interface below sea-level and h is the freshwater head above sea-level.

This relationship demonstrates that less dense freshwater requires a hydraulic head higher than seawater to maintain the depth to the transition zone and the persistence of fresh groundwater in the coastal zone (Figure 5). The density contrast results in 40 m of freshwater below sea-level for every 1 m of freshwater above sea-level. This relatively simple equation can be used to estimate the depth to saltwater and the thickness of freshwater in an unconfined aquifer.

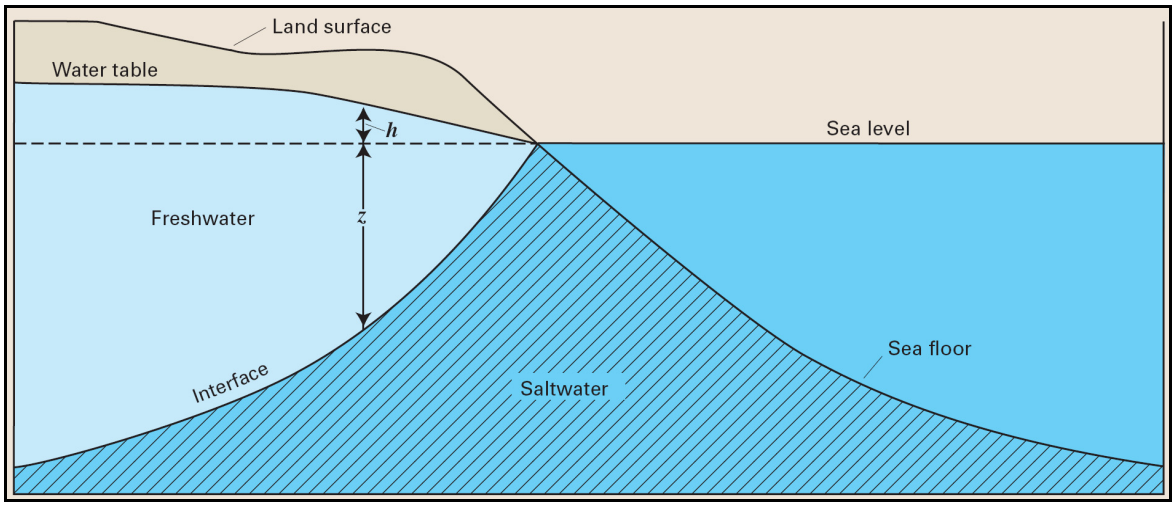

Figure 5. *Estimating the depth to the freshwater-saltwater interface using the Ghyben-Herzberg relationship (modified after Barlow, 2003). Image provided by Dixon-Jain et al., 2010.*

The Ghyben-Herzberg principle is a good approximation for situations where: the geology is relatively simple; the aquifer properties are homogeneous; and when applied away from the shoreline for an aquifer with a narrow mixing zone (Custodio and Bruggeman, 1987). However, the Ghyben-Herzberg assumption considers only horizontal flow and neglects vertical flow components and head losses in the saltwater wedge (where water is continuously circulating in clockwise rotation as shown in Figure 6). As a result, the approximation typically produces saltwater toe locations that are further inland than actually occur. In situations with more complex hydrostratigraphy, the interface is highly irregular and is characterised by complex groundwater flow paths and dynamics. Calculating the position of the interface is further complicated by aquifer recharge variations, groundwater extractions, surface-groundwater interaction processes, aquifer geometry and tidal effects. Significant hydrogeological investigation is required at local-scales to define the interface in detail and complex distributed groundwater models may be required to reliably predict groundwater interactions, flow paths and the extent of the saltwater wedge. These simple approaches are, however, useful to inform and guide future research endeavours prior to more detailed investigations and modelling.

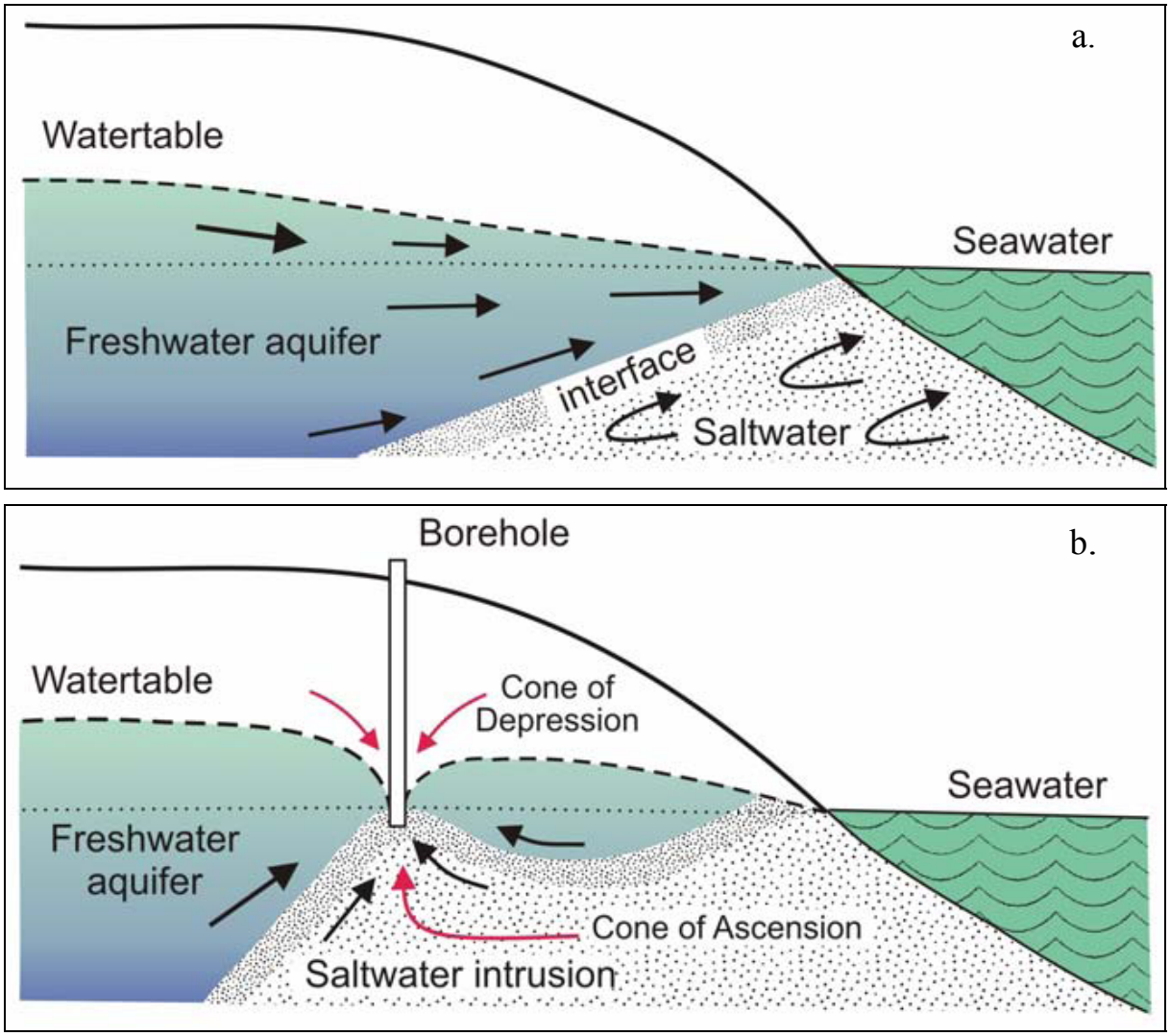

Figure 6. *The freshwater-saltwater interface: (a) in dynamic equilibrium, and (b) disturbed due to groundwater extraction. Image from Dixon-Jain et al, (2010).*

1.2.4 Factors affecting SWI

There are many factors that can disturb the dynamic equilibrium state between freshwater and seawater and contribute to the occurrence of SWI in a coastal aquifer. These influences include both natural variations, ranging from prehistoric coastal evolutionary processes influencing the position of shore-lines and sea-levels, through to present-day coastal variations which may include extreme events such as tsunamis, and anthropogenic activities. A change in hydraulic head difference between freshwater and seawater is the principal driver for movement of the transition zone. Key influences are listed below.

1.2.4.1 Groundwater extraction

Agricultural, industrial and urban uses that require extraction and/or drainage of groundwater can lower the hydraulic head of freshwater and alter the dynamic balance of the transition zone. Removal of fresh groundwater results in a hydraulic pressure drop around the extraction or drainage point. The decrease in groundwater head can produce an equivalent localised rising (up-coning) of the underlying seawater wedge and/or a shift in the seawater wedge landward. Extended periods of over-extraction can cause regional lowering of the fresh groundwater head and may result in regional SWI, or alternatively SWI can be a localised phenomenon. The intrusion of seawater may lead to the abandonment of freshwater resources in areas where the elevated salinity of the groundwater renders it unsuitable for use.

1.2.4.2 Tides

Tides are mainly caused by lunar and solar gravitational forces, although movements in the earth's crust may also generate tidal surges, e.g., tsunamis. The tidal rise and fall of sea-levels can "push and pull" the freshwater-saltwater interface in a landward direction at high tides and in a seaward direction at low tides (Barlow, 2003), thus contributing to mixing of fresh and saline water within the transition zone. Circulation of saltwater is established as a consequence of tidal influences, and saltwater may become entrained within the overlying freshwater resulting in the additional movement of saltwater in a landward direction towards the transition zone (Barlow, 2003). The tidal zone of influence decreases exponentially with distance from the coastline (FAO, 1997).

Tidal amplitudes vary with the lunar cycle and with seasonal variations. Groundwater heads in coastal aquifers will respond to tidal influences, and an oscillation in groundwater elevation will be observed within unconfined aquifer systems as tidal fluctuations occur. The influence of tides leads to elevated time-averaged watertable heights above the mean sea-level in the near-shore area (Carey *et al.,* 2009). The tidal watertable over-height (TWOH) is defined by Carey *et al.,* (2009) as "the tide-induced increase in the time-averaged watertable height above mean sea-level at the spatial location of highest astronomical tide". The TWOH is predominantly influenced by the sloping beach surface, nonlinearity of tidal groundwater waves and formation of seepage faces (Carey *et al.,* 2009).

In addition to tides, waves and storms will also influence near-shore groundwater levels and the TWOH. When defining coastal boundary conditions, e.g., in the development of conceptual and mathematical models, the analysis of TWOH is an important consideration to achieve a robust estimation of groundwater heads and hydraulic gradients in the coastal zone.

Tidal height is a significant factor for SWI scenarios in the Northern Territory because of the very large tidal range of almost 8 m along the coastline (Water Monitoring Branch 2005).

1.2.4.3 Recharge

The recharge-discharge rate of an aquifer can also contribute to SWI. Recharge can occur in several ways: infiltration of rainfall, river recharge, flooding, return irrigation flows, and artificial recharge (Narayan *et al.,* 2003). The rate at which recharge occurs is important as high recharge rates can flush out accumulated salts, dilute saline water, and also increase the hydraulic gradient and force the saltwater wedge seaward. Conversely, low recharge rates allow salt to accumulate, water to become more saline, and the transition zone to penetrate further inland (Werner and Lockington, 2006). Low recharge rates have become an issue in Australia due to ongoing drought conditions and are expected to be intensified in southern Australia by a reduction in rainfall due to climate change (Pittock, 2003). The adverse effects of low recharge rates on aquifer water quality are exacerbated by groundwater extraction.

1.2.4.4 Sea-level rise

Sea-level rise, in response to a changing global climate, can also change the dynamic balance of the transition zone. Climate change predictions by the Intergovernmental Panel on Climate Change indicate a possible rising sea-level of 59 cm (plus 10-20 cm for ice sheet melt) by 2100 (IPCC 2007) which would lead to the inland migration of the freshwater-saltwater interface (Werner and Simmons, 2009). To re-establish equilibrium with fresh groundwater in response to rising sea-levels, the transition zone is predicted to move landward and intrude coastal aquifers. Based on previous cases, SWI may cause a landward shift in the transition zone that does not return to its original position, i.e., SWI may be an irreversible phenomenon (Barlow, 2003). For example, sea-level fluctuations over the last 900,000 years in the North Atlantic Coastal Plain in the USA have produced transition zones that extend up to 60 km inland from the present-day shoreline (Meisler *et al.,* 1985). This means that some of the effects of SWI, for example a decrease in freshwater storage capacity, may be non-reversible. However, scant research has been conducted to assess why SWI in some systems appears to be permanent.

In addition to the subsurface impacts, sea-level rise may also result in the permanent surface inundation of low-lying coastal regions and increase the frequency and intensity of temporary inundation through the occurrence of storm surges. This could result in the intrusion of saltwater into freshwater reserves through downward seepage.

According to the FAO (1997), an accurate assessment of the effects of sea-level rise on coastal aquifer systems is difficult to achieve because of the time lag between cause and effect. The process of moving through one state of dynamic, hydrogeological equilibrium after another is relatively slow and it may take decades before the inflow of saline water is noted. Moreover, a relatively long time series of salinity data obtained from appropriately constructed and located monitoring bores would be required to note the changes, and these are commonly unavailable.

The impacts of sea-level rise are site-specific, and the response of the transition zone during sea-level rise will depend on the hydrogeology of the system, including the aquifer type and its geometry, aquifer parameter values (e.g., hydraulic conductivity), and system boundary conditions such as whether the aquifer is head-controlled or flow-controlled beyond the coastal fringe (Werner and Simmons 2009). Human influences such as groundwater extraction, drainage, artificial recharge and land reclamation schemes, to give a few examples, will also have an influence on extent to which sea-level rise impacts occur and/or are mitigated.

1.2.4.5 Time-scales

The time-scales for the transition zone to reach equilibrium can vary significantly depending on the processes of disturbance to the state of dynamic equilibrium (e.g., extraction, sea-level rise, recharge variations, tidal influences); magnitude and location of the disturbance; the local hydrogeological setting; and boundary conditions. Transition zones within highly permeable aquifers can have a quick response time in areas where groundwater flows and solute transport occur rapidly from a hydrogeological point of view. Nonetheless, even in these rapid systems the time-scale will still be on the order of years to decades for a new dynamic state of equilibrium to be reached. Conversely, aquifers that have incurred extensive SWI from past sea-level fluctuations are thought to have not yet reached equilibrium even after periods as long as 100,000 years (Barlow, 2003). In general, it takes considerable time for new states of equilibrium to be reached within aquifer systems because very large volumes of freshwater must be displaced by saline water in order for SWI to occur (FAO 1997). The distinction needs to be made between local and regional effects of SWI, with the latter requiring a much greater volume of freshwater to be displaced by sea water. The response of aquifers to the stresses of SWI and any subsequent rehabilitation will depend on the individual hydrogeological setting.

1.2.4.6 Geological architecture

Representations of seawater intrusion such as Figure 5 typically assume homogeneous aquifer structures. As such they are realistic only when representing simple and small-scale examples, such as seawater intrusion on a sand island or sand barrier. Most SWI scenarios are more complex, and become increasingly so as scale increases. An example of this is shown in Figure 7, which is of the Uley South area on Eyre Peninsula, South Australia. In this region there are multiple stacked aquifers, each with different hydraulic and lithologic properties (see Dixon-Jain *et al.,* 2011).

The aquifer parameters in such stacked complexes can vary significantly, such as porosity, permeability, water quality, permittivity, yield, isotropy, and response time to enforced change, to name just a few. Each aquifer will therefore respond differently to seawater intrusions. Furthermore, because different aquifers will most likely be pumped at different rates, there can be significant changes to the distribution of hydraulic heads, with the possibility of new and unforeseen aquifer connectivity developing over-time.

Modelling the manner in which such complex aquifer systems will respond to seawater intrusion requires accurate parameterisation of the aquifer and its architecture. In the NT coastal plain project area hydrogeologic complexity occurs due to the stacked aquifer systems, in the form of near-surface Quaternary

sediments, weathered Cretaceous rocks, and the underlying Proterozoic sequences. The Quaternary sediments include cheniers, tidal mud and sand flays, estuarine sediments (both coarse and fine grained), and fluvial sediments (sandy channel facies and muddy floodplain facies). The Cretaceous units consist of impermeable claystone and highly permeable gravely sandstone, with well developed secondary porosity through the deep weathering overprint. Lastly, the Proterozoic units include impermeable rocks such as massive quartzite and dolostone, slightly permeable siltstone and phyllite, and highly permeable fractured quartzite and karstic dolostone.

Furthermore, each of these successions is interconnected hydrogeologically. Proterozoic sediments are overlain by both Quaternary and Cretaceous sediments and, through sub-adjacent karstic collapse, can change the hydraulic properties of the overlying units. Cretaceous rocks incised by the Quaternary sequences can discharge laterally into the younger sediment layers.

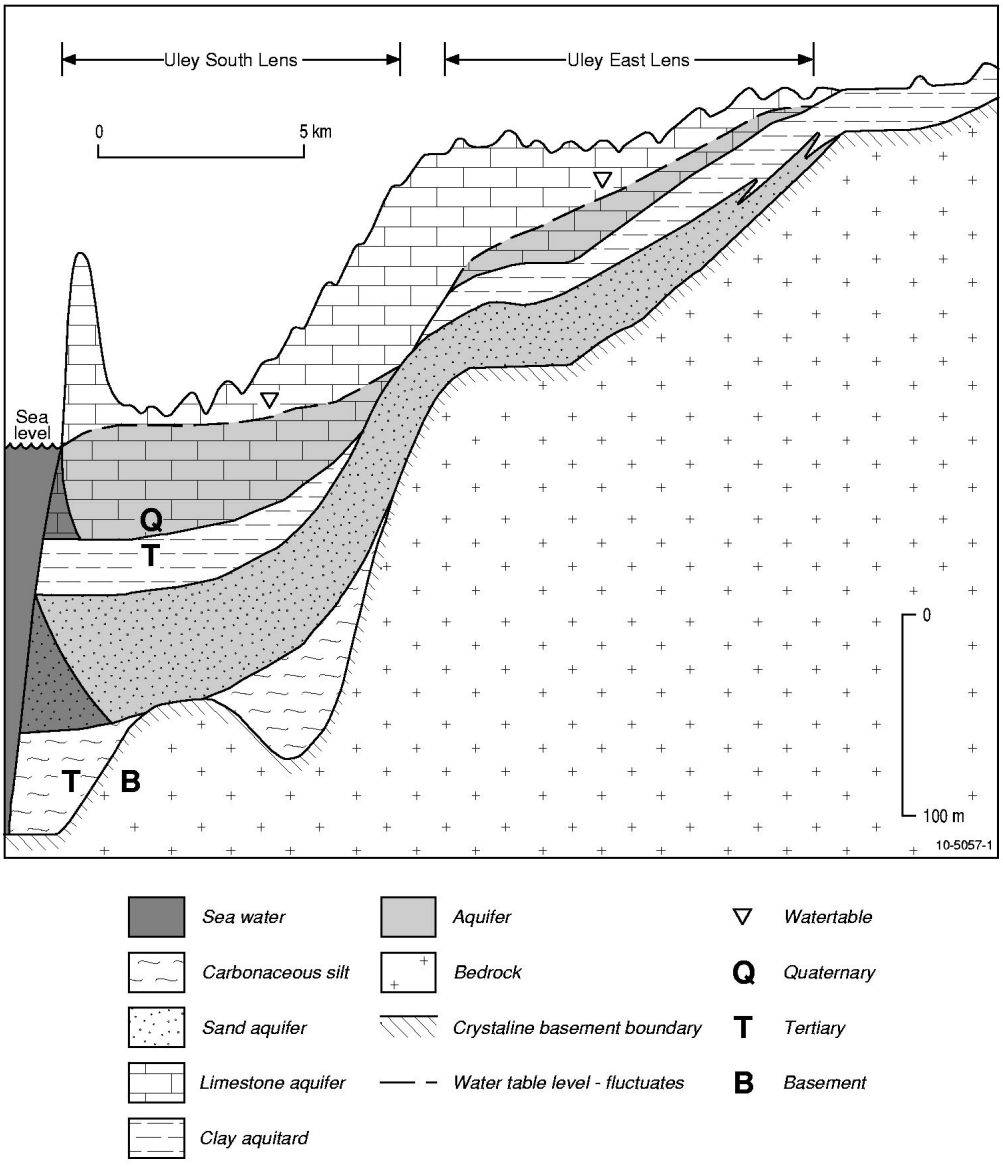

Figure 7. *Hydrogeologic cross-section from the Uley south area on Eyre Peninsula, SA, showing complexity of seawater intrusion in stacked aquifers. Image sourced from Dixon-Jain et al., (2011).*

1.2.5 Northern Territory context

SWI is an incipient hazard in many areas of the Northern Territory, potentially affecting irrigation projects, urban water supplies, and small communities (Table 1). An overview of these issues in the NT is provided by Dixon-Jain *et al.,* (2010) and the following section is taken from that study, with minor amendments and additions.

Table 1. Summary of literature on SWI studies in the NT**.** Data sourced from Dixon-Jain *et al.* (2010).

LOCATION	HYDROGEOLOGIC SETTING	AQUIFER LITHOLOGY	AQUIFER TYPE	DRIVING FACTORS	STUDIES	SALINITY TRENDS	GW LEVEL TRENDS	SWI MONITORED	SWI MNGT	LAND/WATER USE
Lambells Lagoon (Darwin Rural Area)	Consolidated	Proterozoic dolomite; carbonate massif	Unconfined	Dry season g/w extraction exceeds wet season recharge. Lambells Lagoon g/w elevations reach sea-level or below	Water levels; salinity; FEFLOW	Unknown	Decreasing	No	No	Domestic; horticulture
Warruwi (Goulburn island)	Unconsolidated/ consolidated	Weathered Cretaceous sediments	Unconfined to semi-confined	Extraction	Unknown	Unknown	Variable, depending on aquifer management	Yes	Active	Small urban
Milingimbi	Unconsolidated/ consolidated	Weathered bedrock	Unconfined to semi-confined	Extraction	Unknown	Unknown	Unknown	Unknown	Unknown	Small urban
Ngukurr	Consolidated	Fractured Proterozoic bedrock	Unconfined to semi-confined	Extraction	Unknown	Unknown	Unknown	Unknown	Unknown	Small urban
McMinns / Howard East	Unconsolidated/ consolidated	Weathered Cretaceous and Proterozoic bedrock, fractured Proterozoic	Unconfined to semi-confined	Extraction	Unknown	Unknown	Unknown	Unknown	Unknown	Urban
Milikapiti	Consolidated	Cenozoic and Cretaceous sandstones	Unconfined and confined	Extraction	No modelling known	Stable	Stable	Unknown	None	Small urban

1.2.5.1 Darwin area

Lambells Lagoon in the Darwin Rural Area is the only region in the Northern Territory where the risk of saltwater intrusion has been previously reported (CSIRO, 2009a, b). The main driving factors are groundwater extractions for horticultural and domestic use during the dry season. The groundwater resources are obtained from Proterozoic dolostone aquifers, primarily from the main KCD aquifer. Analysis by EHA (2007) indicated the amount of dry season extraction probably exceeded recharge at a number of locations in the Lambells Lagoon area at the present time. The aquifer exhibits strong seasonal variability, and natural groundwater levels were observed to rise and fall by up to 8 m in the 1970's. Under current groundwater usage, they are now observed to fluctuate 17 m/year. Although the aquifers are recharged during the wet season, they become depleted during the dry season (CSIRO, 2009a, b).

Current groundwater extraction in the Darwin Rural Area (McMinns-Howard East Section) is estimated to be 25 GL/year, and the dry season minimum groundwater levels for the main dolomite aquifer (KCD) have been declining for many years. CSIRO (2009a, b) used the FEFLOW groundwater models that were previously developed for the Darwin Rural Area (EHA 2007, 2009), as part of their sustainable yields report for Northern Australia. Their assessment indicated that groundwater levels will continue to decline under current and future climate regimes with the current level of development. In particular, the groundwater levels in the eastern section of Lambells Lagoon regularly approached or dropped below mean sea-level throughout the simulation period (2007 to 2030), posing a risk of SWI.

Reports from the CSIRO (2009a, b) also mentioned a theoretical risk of SWI into the coastal dolomite aquifer near the Adelaide River if aquifer levels were being drawn down below sea-level and if there were hydraulic connection between the aquifer and river system. However, there was insufficient data to establish this risk.

Radke *et al.,* (1998) observed minimal seawater mixing (<0.2% of the groundwater at the time of sampling) in the tidal reach areas of the lower Howard and Adelaide rivers. A distinctive hydrochemical overprint showed concentration gradients diminishing away from intrusion fronts. Greatly increased seawater mixing would be required to exceed NHMRC hydrochemical guidelines, although this may constitute a significant limit to future groundwater abstraction (Radke *et al.,* 1998).

1.2.5.2 Remote communities

Many NT coastal communities are in low-lying areas and rely on poorly defined or monitored aquifers for their water supplies. The threat of SWI is unknown but potentially high, and of considerable significance to the local communities. Examples of such communities include Warruwi on Goulburn Island (Pavelic *et al.,* 2002), Milingimbi (Yin Foo, 1980), Milikapiti on Bathurst Island (Chin, 1991), and Ngukurr in eastern Arnhem Land (Sumner, 2008). Although not yet documented to be threatened, other island communities like Umbakumba (Groote Eylandt, Tyson and Yin Foo, 1991), Wurankuwu (Bathurst Island, Moser and Chin, 1994) and Galiwinku (Elcho Island, Yin Foo, 1984) are potentially at risk. Many of these aquifers show strong seasonal variation in groundwater levels, indicating rapid responses to changes in the hydrological balance and high sensitivity to perturbation.

At Warruwi on Goulburn Island, the main aquifers are weathered Cretaceous sedimentary rocks. The aquifers are the main water supply for the community and have been investigated for managed aquifer recharge to increase storage in the dry season (Pavelic *et al.,* 2002). Brackish water at depth has been related to the marine water (Yin Foo, 1991); displacement of brackish water during injection trials has led to clogging via a clay dispersal mechanism. Sustainability of the water supply depends on the long-term management of the fresh/brackish water interface.

The aquifer supplying the Milingimbi settlement (Yin Foo, 1980; 1982) poses a number of management challenges including SWI. Capping of water extraction is required to reduce the risk of incursion of saline water.

The aquifers supplying the Milikapiti settlement on Melville Island currently discharge to the sea (Chin 1991). Extraction at the time of the report was well below that of predicted recharge and freshwater discharge occurs offshore. However, population pressures with development will require ongoing monitoring to prevent lateral SWI.

At Ngukurr in eastern Arnhem Land the main aquifer is fractured Proterozoic bedrock (Sumner, 2008). Lateral and vertical SWI is considered a major threat, requiring immediate reduction in groundwater extraction. Although the aquifer consists of fractured bedrock, incursion is controlled by palaeochannel systems.

1.2.5.3 Kakadu and other coastal ecosystems

The low-lying areas of Quaternary sediments deposited by the many river systems in the project area are, like others in the Northern Territory, close to sea-level and therefore vulnerable to sea-level rise. Cobb *et al.,* (2007) demonstrated from compilation of aerial photographs for the Wildman, West Alligator, South Alligator and East Alligator Rivers taken at intervals from 1950 through to 1991, that there had been an expansion of the mangrove ecosystem at the expense of freshwater wetlands. This was attributed to seawater intrusion caused by changes in cyclical monsoonal wind patterns rather than to sea-level rise or climate change. However, these authors also emphasised the incompleteness of the dataset and the need to acquire imagery post-1991 to further confirm the trends and test the explanations.

BMT WBN (2010) examined the threat to the South Alligator River system from various climate change scenarios. The study indicated considerable uncertainty in the different climate models for rainfall and flood events. For example, the current102 'dry' days per year could increase or decrease by up to 5 days in 2030 and increase by 18 or decrease by 13 days in 2070. "Wet days" currently total 98 annually, by 2030 these could increase by seven or decrease by nine. By 2070 "wet" days could increase by 18 or decrease by up to 34 days per year. Large flood events, currently having an average duration of 20 days each, could, in the 2030 scenario decrease by 12 days or increase by 10 days per event. For the 2070 scenario, large flood events could remain unchanged or increase by nine days per event.

BMT WBN (2010) also indicated that sea-level by 2030 will rise by 143 mm (IPCC emission scenario A1B, 95th percentile); and by 2070 possibly have risen by 700 mm (a high emissions scenario). The study modelled the impact of this on tidal ranges and storm surges. They showed that predicted sea-level rises may have significant impacts because they are efficiently propagated up the river to the limits of tidal influence. In general, tide heights would be increased by the sea-level rise for much of the tidal channel, there would be extensive overtopping of current tidal geomorphic features and encroachment of tidal influence on currently freshwater environments and the tidal limits would extend upstream. A similar propagation inland of the salt water wedge as a result of rising sea-level can be expected.

Storm surge levels, by contrast, are expected to be less altered by sea-level rise with their height increasing not being proportional to sea-level rise. Nonetheless, the limits of storm surge encroachment are expected further inland than at present because of the rise of base level, and will result in further sea water influx into areas of otherwise fresh surface water.

Although both studies occur east of the project area, the overall similarity between the floodplains and estuaries of the Alligator Rivers and of the Mary and Adelaide rivers in the project area (see Woodroffe *et al.,* 1993) suggests that similar impacts can be expected. This could affect conservation areas such as Shoal Bay Coastal Reserve, Melacca Conservation Area and Djukbinj National Park. The threat to the Mary River specifically was outlined in the Climate Change Risks to Australian Coasts report (DCC, 2009). Lateral, cross-stratal encroachment of saline water may also occur into the Cretaceous and perhaps the Proterozoic aquifers if hydraulic heads were excessively reduced through over extraction. However, the risk of sea water intrusion in these areas through sea-level rise needs to be modelled.

1.3 PROJECT BACKGROUND AND OBJECTIVES

1.3.1 The GA AEM dataset

The AEM data used in this project was acquired by Geoscience Australia as part of the Onshore Energy Security Program (OESP). Details of the data, acquisition, processing, and release are described by Costelloe and Hutchinson (2010). The survey in the Pine Creek Orogen of the Northern Territory included sections of the Pine Creek, Cape Scott, Port Keats, Fergusson River, Mount Evelyn, Katherine, Alligator River, Darwin, Fog Bay, Cobourg Peninsula, Junction Bay and Milingimbi 1:250,000 scale map sheets (see Costelloe *et al.,* 2009). As the program was aimed at providing pre-competitive mineral exploration data the survey did not include National Parks or other nature reserves. Additional areas for survey were flown in the Darwin, Adelaide River, Mary River and Rum Jungle areas with funding from the National Water Commission. The full survey areas are shown in Figure 8.

1.3.2 Northern Territory coastal plain project

The 'Northern Territory Coastal Plain: Seawater Intrusion' project used geophysical data acquired and processed by Geoscience Australia during 2008-2010 for the Pine Creek AEM survey as part of the OESP (Figure 8). This project was based on the Woolner AEM survey that extended east from Darwin across the Koolpinyah and Marrakai uplands, the floodplain of the lower Adelaide River and the western margin of the Mary River floodplain (Figure 9). The project used the AEM survey data in combination with additional geophysical, geologic and hydrogeologic datasets to assess the occurrence and potential risk of seawater intrusion into coastal aquifers in the Darwin peri-urban area. This assessment is based on the following facts and drivers:

- There is increased pressure for groundwater resources in the Darwin area due to urban growth and land-use changes such as horticultural expansion, particularly in the Koolpinyah-Marrakai coastal plain east of Darwin.
- The effects of seawater incursion into the surface environment have been registered in wetlands and floodplains of the lower Adelaide and Mary Rivers (Jonauskas and Sterling, 1992; Chin *et al.,* 1993). Saltwater intrusion into floodplain wetlands is impacting on terrestrial and aquatic GDEs, as well as on indigenous lifestyles and cultural values.
- Darwin has the highest daily water consumption per capita of all Australian capital cities at 1,000 litres-per-person, compared to average daily Australian civic use of 490 litres-per-person. Existing water supply infrastructure for Darwin is reaching the limits of current capacity. Groundwater is extracted mostly in the dry season, and water quality is generally potable except in areas close to the Timor Sea and lower floodplains where saline water intrusion is common.
- The geology and hydrogeology of the study area, part of the Pine Creek Province, is complex. Geologic features and groundwater prospects vary over short distances and, close to the coast, bedrock units and aquifers are obscured by Cretaceous sedimentary rocks and coastal muds, particularly in the lower floodplains. Geophysical information is thus required to elucidate the nature of the subsurface geology and hydrogeology.
- The *Northern Territory Coastal Plain* project will add substantial value to an investment that exceeds $2M committed by Geoscience Australia for AEM geophysical data acquisition over a 70,000 km^2 survey area. Outcomes of this complementary hydrogeologic project are relevant to the Northern Australia Stocktake, a priority of the National Groundwater Action Plan, and to our broader understanding of seawater intrusion in coastal aquifers elsewhere around Australia.
- Seawater intrusion involves the influx of highly saline seawater into an area where freshwater normally dominates, either inflow into a fresh water wetland or a freshwater aquifer. SWI can impact adversely on estuaries, lower reaches of rivers and associated billabongs and swamps, and on potable groundwater supplies. As sea-levels rise in response to climate change (or other factors such as vertical tectonic movement affecting coastal areas) seawater is able to overcome natural barriers such as sand ridges to move into low-lying areas presently dominated by freshwater. Oceanic water can also move landward in the sub-surface into freshwater coastal aquifers, an impact that may not be noticed on the surface but which could affect groundwater

supplies further inland. This project has focussed on detecting and mapping the subsurface disposition of the saltwater wedge in the NT coastal plain, particularly in areas where heavy groundwater pumping occurs and where there is risk of drawing salt water into valuable near-surface aquifers.

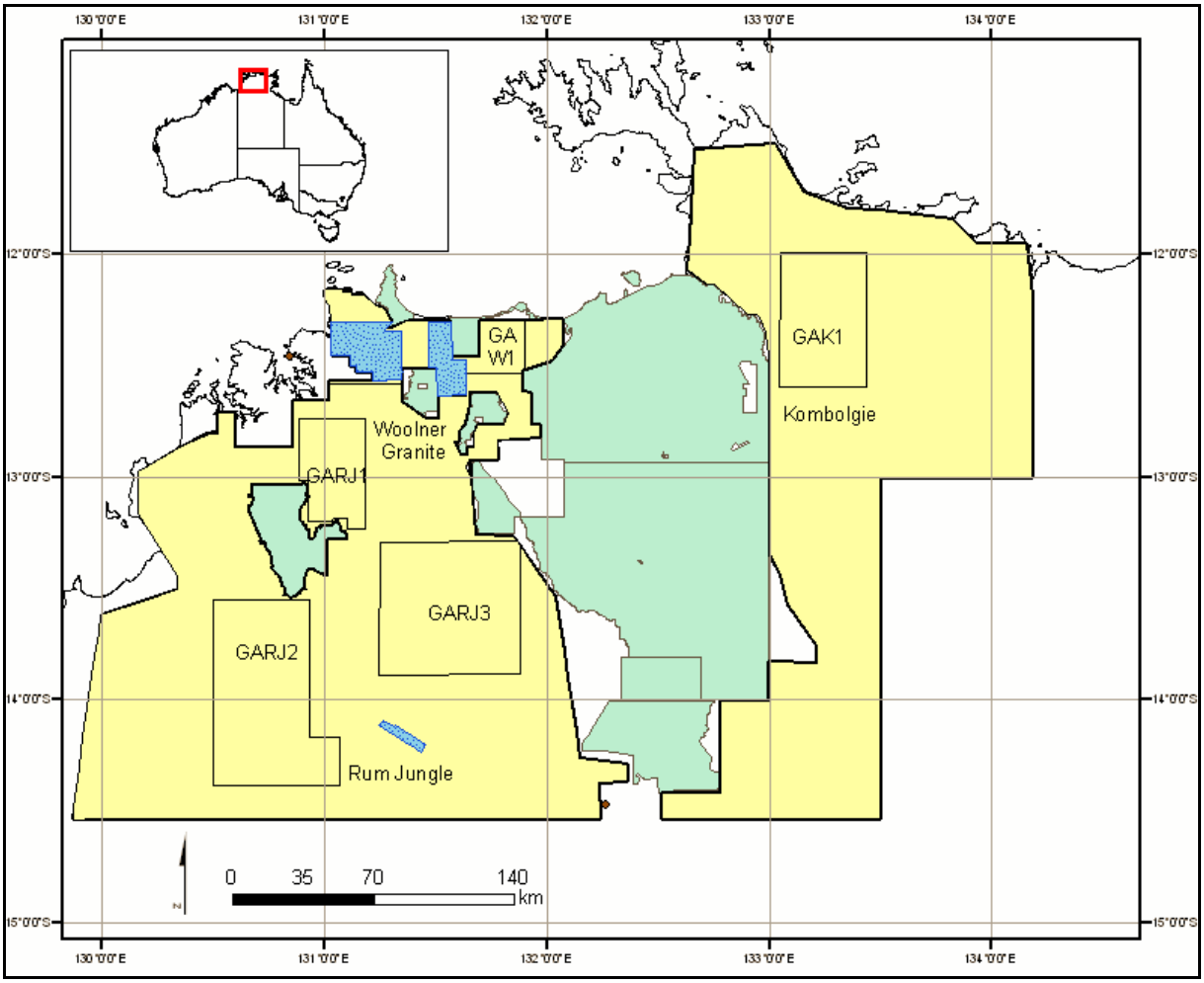

Figure 8. *Geoscience Australia funded 1,666 and 5,000 metre-spaced lines (yellow) and NWC-funded 555 m lines (blue) for the Woolner Granite, Rum Jungle and Kombolgie areas. National Parks and other reserves (green) were not flown (from Costelloe and Hutchinson, 2010).*

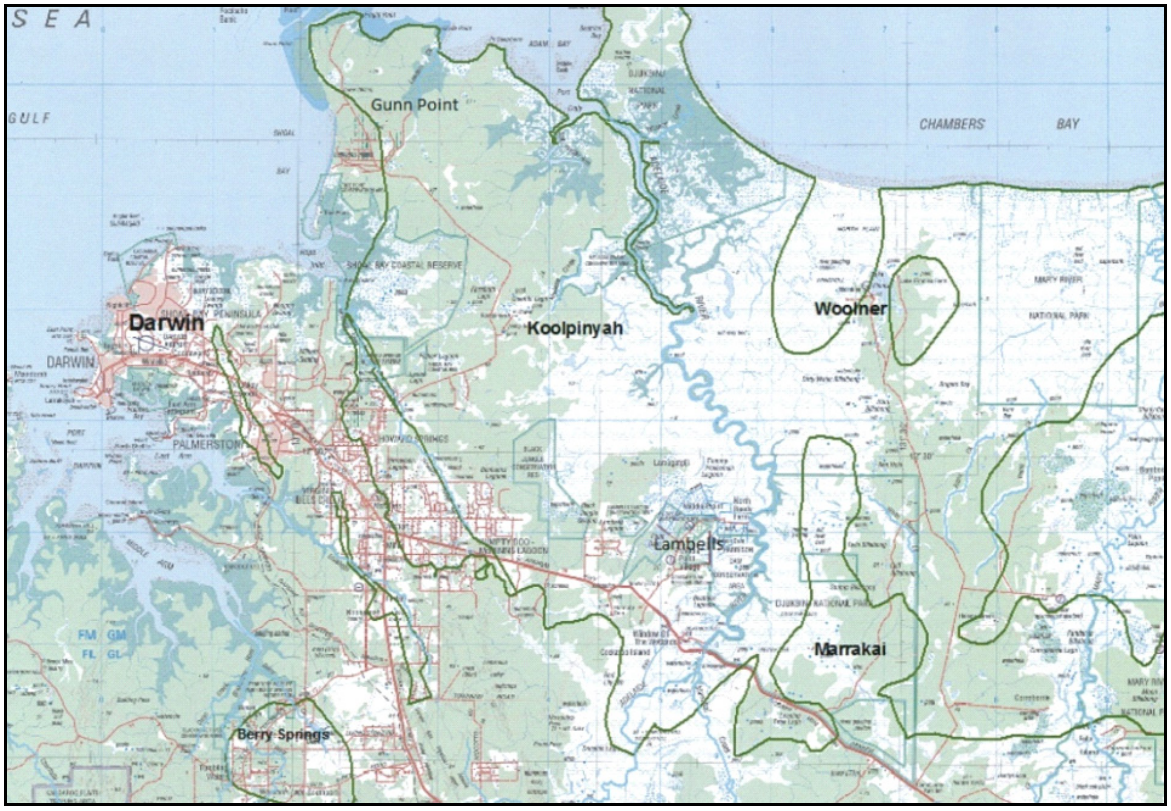

Figure 9. *Location of the Koolpinyah/Lambells area with Gunn Point in the north and the Howard River/Howard East area to the south-west of Koolpinyah. The distribution (surface and subsurface) of the KCD is enclosed by the green line, with progressively less dolostone towards the east.*

1.3.3 Related projects – Koolpinyah Dolomite Aquifer Characteristics

1.3.3.1 Project overview

The *Koolpinyah Dolomite Aquifer Characteristics* (KDAC) project was a two year project funded by the Raising National Water Standards Program (NWC). Carriage of the project, which was finalised in November 2011, was the responsibility of NRETAS. The main findings and outcomes of this project are detailed in a report by Fell-Smith and Sumner (2011).

The Koolpinyah-Coomalie Dolostone (KCD) aquifer provides up to 10% of the water supply for Darwin. It is mixed with Darwin River water. Rapid development of both public and the largely unregulated private water demands have led to increased pressure on the aquifer, leading to failure of some bores toward the end of the dry season. The climate over the last 15 years has become wetter leading to a continuing upward revision of the average rainfall. This has caused complacency with regard to water usage which may be reversed if there is a change back to a drier climate.

The 'Koolpinyah Dolomite' aquifer area refers to a complex geologic formation in which dolostone provides the dominant aquifer. It is roughly bounded in the west by the Stuart Highway, in the south by the Arnhem Highway and includes Woolner and Marrakai Stations in the eastern area. The area is largely coincident with that of the present project.

1.3.3.2 Project aims

The KDAC project concentrated on the sector to the west of the Adelaide River owing to the paucity of information further eastwards. The western area contains some 3,000 bores representing most of the groundwater use and sustainability pressures in the region. The hydrological and stratigraphic information from these bores has been used to develop the project.

The project aimed to better define the nature of the KCD aquifer, its porosity and permeability and the extent of barriers disrupting lateral groundwater flow. As the project progressed the complexity of the geological architecture both in the Cretaceous rocks and particularly the Proterozoic formations became better appreciated, which led to a strong emphasis on the geological structure and chemistry to define a new geological model.

1.3.3.3 Geology

The geological composition of the area consists of dissected Proterozoic basement rocks which are dominated by karstic dolostones and greenschist facies metasedimentary rocks (quartzite, phyllite and schist). In many places the metasedimentary rocks occur in low-lying ridges that were topographic highs on the palaeosurface. Unconformably overlying the Proterozoic basement are Mesozoic rocks, mainly Cretaceous sedimentary cover that varies from 0-100 m thick with an average thickness of about 40 m. The palaeosurface unconformity is generally deeper in the Gunn Point area in the north. Cenozoic weathering profiles with variable duricrust thickness are present over much of the area and provide a porous and ephemeral aquifer from the wet to early dry season.

Prior to this project knowledge of the Proterozoic basement geology of the area was limited because of the lack of exposure of Proterozoic rocks and a lack of mineral exploration. Because of the importance of understanding the architecture of the aquifer there was strong emphasis on defining the basement geology. This has led to an appreciation of its complexity both in terms of rock geochemistry and structure. The main historical work important in defining the basement was by uranium explorers (Urangesellschaft Australia Pty. Ltd., 1981) who cored several diamond drillholes in the central to northern part of the project area.

Drilling for the *Northern Territory Coastal Plain* (NTCP) project penetrated phyllite basement in two of the drillholes and AEM images have assisted in clarifying structural and stratigraphic details of the basement rocks. There is evidence that dolerite intrusions along Proterozoic faults probably provide barriers to horizontal groundwater flow. AEM cross-section images show the faults and conductive saprolitic dolerite contrast well against the more resistive Mesozoic sedimentary rocks.

The Mesozoic post-unconformity rocks show evidence of fluvial to estuarine transgressive facies in the Howard River, Howard East and Lambells areas, depicted in AEM data as resistive features in depth slices. Carbonaceous silts and clays in the Gunn Point area show a conductive AEM signature and represent a more benign depositional regime. The more resistive areas have minor basal high-energy indurated sandstones, with the overlying Howard Sand Member formed in places. Above the Howard Sand Member clays and silts dominate, with minor sand lenses.

1.3.3.4 The aquifers

As mentioned above the relatively porous weathering profile acts as a seasonal aquifer. Other aquifers occur in various sand lenses within the Cretaceous sequences. At the base of the Cretaceous section there is a major aquifer in lag deposits on the Proterozoic palaeo-surface that is connected to the karst aquifer in dolostone at (or near) the palaeo-surface. Karst dolostone may also occur at depth, presumably associated with fracturing. Further information on the aquifers of the study area is provided in Chapter 3.

The KDAC project addressed the porosity and connectivity of these aquifers relevant to groundwater flow and their effects on the potentiometric surface. The project also addressed groundwater outflow from streams and springs and drawdown from both town and private bores.

1.4 ENVIRONMENTAL FRAMEWORK

1.4.1 Hydrology

Key hydrological features within the NTCP study area include the Howard, Adelaide and Mary Rivers, and Melacca, Banka, Black Jungle and Howard springs. The Adelaide and Mary Rivers have extensive floodplains whereas the Howard River appears to be fault-controlled; it drains to the north-west within the Koolpinyah uplands (Figure 10, Figure 11). The Adelaide River previously drained into Chambers Bay before meandering westwards to drain into Adam Bay on the west side of Cape Hotham approximately 3,000 years ago (Woodroffe *et al.,* 1993).

Tides in the Darwin region are macrotidal with a range of 7-8 m, and have a mean spring tidal range of 5.5 metres and a mean neap tidal range of 1.9 metres. Tidal influence on the Adelaide River extends approximately 130 km inland (Woodroffe *et al.,* 1993). Fresh wet season water of approximately 200 million cubic metres is progressively replaced in the river when runoff subsides. Tidal flows in a year can be up to ten times the annual peak flow of the river (Kingston *et al.,* 1982).

Rapid tidal creek extension on the Lower Mary River Plains has occurred since the 1940's resulting in the degradation of 17,000 ha through salt water intrusion. Many barrages have been constructed on the plains to abate the SWI and these have met with mixed success (Jonauskas and Sterling, 1992).

Surface runoff in the study area is largely determined by rainfall with minimal runoff occurring in the dry season. There is an initial lag to runoff at the start of the wet season as soil and vegetation moisture deficits are satisfied. Studies in the Howard East catchment (Cook *et al.,* 1998a, b) determined runoff to the Howard River of 570 mm for the wet season and 20 mm for the dry. From February to May total catchment runoff averages 60% of rainfall. In June and July, mean runoff is greater than mean rainfall indicating that the Howard River is largely sustained by groundwater flows at this time. The upper Howard River, and occasionally Howard Springs, ceases to flow late in the dry season.

Melacca, Banka, Black Jungle and Howard springs are fed by groundwater from the KCD aquifer (discussed further in Chapter 3). Over 100 perched lagoons also exist in the study area, many of which fill in the wet season and then progressively dry out from May to October. A strong correlation exists between faults and photo lineaments and the location of shallow lagoons, suggesting a structural influence in their formation. The lagoons are likely to be karstic depressions.

1.4.2 Climate

The study area to the south-east of Darwin has a tropical monsoonal climate with a wet season lasting from October to April. Most annual rainfall occurs between December and March. Mean monthly rainfall ranges from 410 mm at the height of the wet season to 5 mm in the middle of the dry. The mean annual rainfall at Darwin Airport is 1,715 mm, as recorded over the last 70 years by the Bureau of Meteorology (BoM). The highest recorded annual rainfall is 2,776 mm and the lowest is 1,025 mm. Temperatures are highest in November, when the mean maximum is 33.3°C and the mean minimum is 25.3°C. The coolest month is July when the mean maximum is 30.5°C and the mean minimum is 19.3°C. Evaporation usually exceeds rainfall throughout the year, except in the wet months. The monthly evaporation ranges from 170 mm in February to 270 mm in October. The mean annual evaporation is 2,650 mm, measured over 27 years (1967-1994) at the Darwin Airport DE014015 meteorological station (BoM, 2011).

1.4.3 Geomorphology

Verma (2002) divided the Darwin 1:250,000 scale map sheet into five geomorphic units. Some of these divisions are shown in Figure 10 and Figure 11. The regolith geology of the region is shown in Figure 12 and Figure 13.

The geomorphic divisions are: 1) coastal and estuarine plains, 2) alluvial plains, 3) northern plains, 4 dissected foothills and 5) dissected uplands. In detail, they consist of (after Verma 2002, with lithologic

information from Pietsch, 1985, and Pietsch and Stuart-Smith, 1987). These are described in more detail below.

1.4.3.1 Coastal and estuarine plains

This unit consists of muddy foreshores, beaches, chenier ridges, and low lying coastal floodplains. The main sediment types are estuarine, saline and calcic mud, clay and silt, with chenier ridges of shelly sand standing up to 7 m above sea-level. Creeks and rivers are influenced by tides for up to 60 km inland.

1.4.3.2 Alluvial plains

Alluvial plains occur immediately behind beaches away from the estuaries and extend inland. They are flat with gentle gradients that grade from the coastal plains. Flood plains, incised channels and levee banks occur adjacent to rivers and major creeks. Deep sandy or silty soils dominate, with seasonal inundation.

1.4.3.3 Northern plains

The northern plains are areas of moderate to low relief with flat to undulating loam-, sand- or gravel-bearing soils (commonly with ferruginous pisolites). These plains are underlain by ferruginous duricrusted Cretaceous sedimentary rocks and very low rises of Proterozoic rocks (for examples see Tickell, 2009). The northern plains are marked by subtle dissolution features leading to a pseudo-karstic landscape (McFarlane *et al.,* 1995).

1.4.3.4 Dissected foothills

These occur in the south-western part of the project area and consist of rises up to 50 m above sea-level with skeletal, gravely, dissected detrital ferruginous soils and Lower Proterozoic rocks. Ferruginised benches result from erosion of Cretaceous rocks.

1.4.3.5 Dissected uplands

These occur in the southern part of the project area rising up to 200 m above sea-level with shallow, gravely, rocky skeletal soils and Lower Proterozoic rocks. They form prominent strike ridges and boulder-strewn hills.

1.4.4 Soils and vegetation

Shallow sandy soils (yellow and massive) dominate the upland regions and grey cracking clays dominate the floodplains. Upland soils are typically loamy topsoils grading into light sandy clay loam subsoils. Dense ferruginised gravels are widespread. The surface is characterised by a lamination of coarse, loose sand and ferruginised gravels, ranging from dark brown to yellow brown.

Moderately deep sandy red massive earths occur with the above soil types, although they are not as extensive on the gently undulating surface. They grade from a sandy loam surface to sandy clay loam subsoil with gravel abundance increasing with depth. This profile is usually 70 to 100 cm deep and overlies weathered ferruginous parent material. The surface is dark brown and the subsoil red to reddish brown.

Vegetation across the Koolpinyah and Marrakai uplands is open forest standing up to 15 m tall. The understorey is common Sorghum sp. (speargrass) and the canopy consists of Eucalyptus tetradonta and Eucalyptus miniata (Beringer *et al.,* 2003). Surrounding the floodplains and other poorly drained areas Pandanus sp., Melaleuca sp. and Acacia auriculiformus dominate, with sedge grasses on the floodplains (Fogarty, 1980). Patches of monsoon vine forest occur in seepage areas around creeks and lowlands and are likely groundwater dependent.

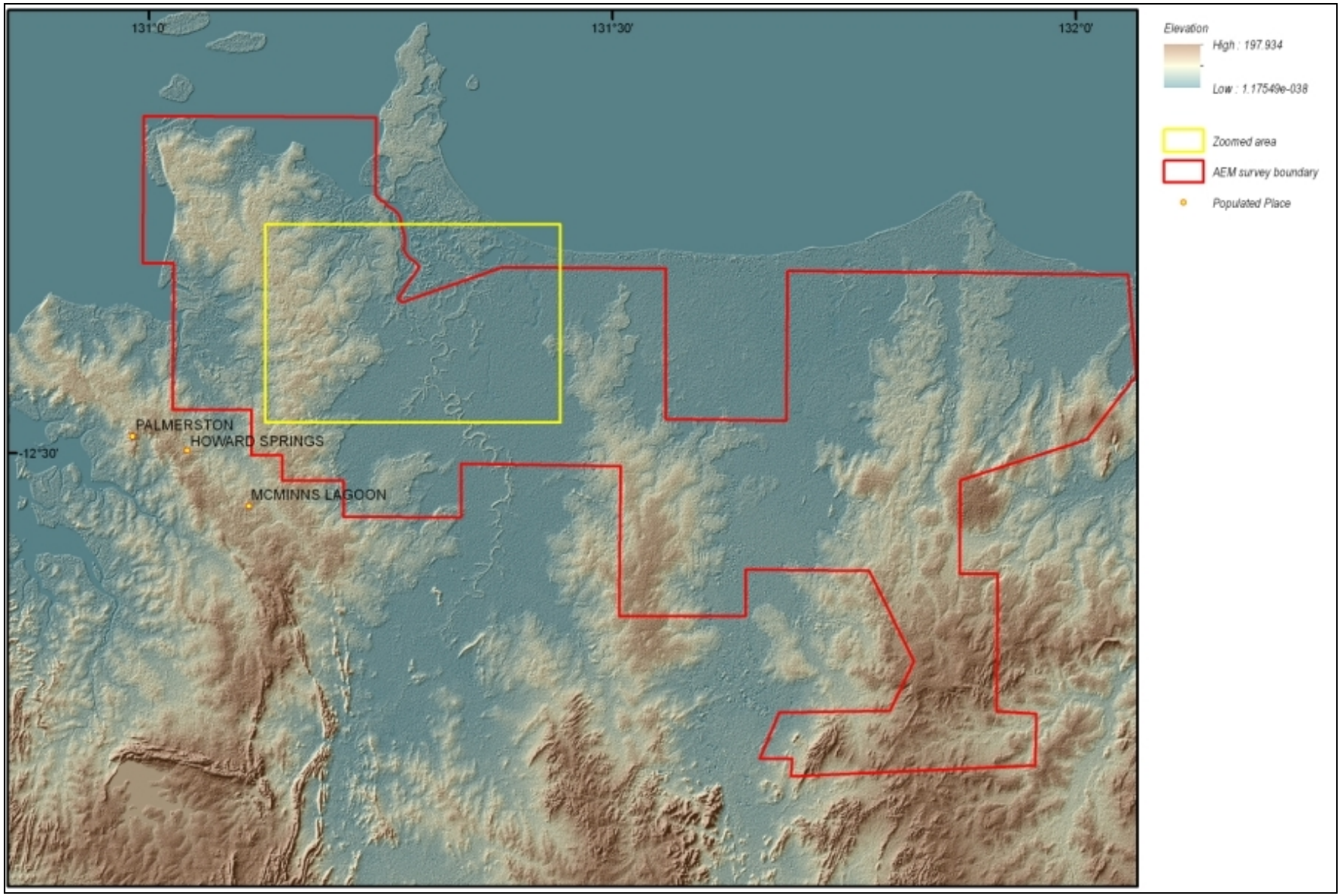

Figure 10. *Shaded digital elevation model (DEM) of the NT coastal plains region produced from 1-arc second Shuttle Radar Topographic Mission (SRTM) data. The AEM survey area is outlined in red, with the yellow box showing detailed area presented in Figure 11.*

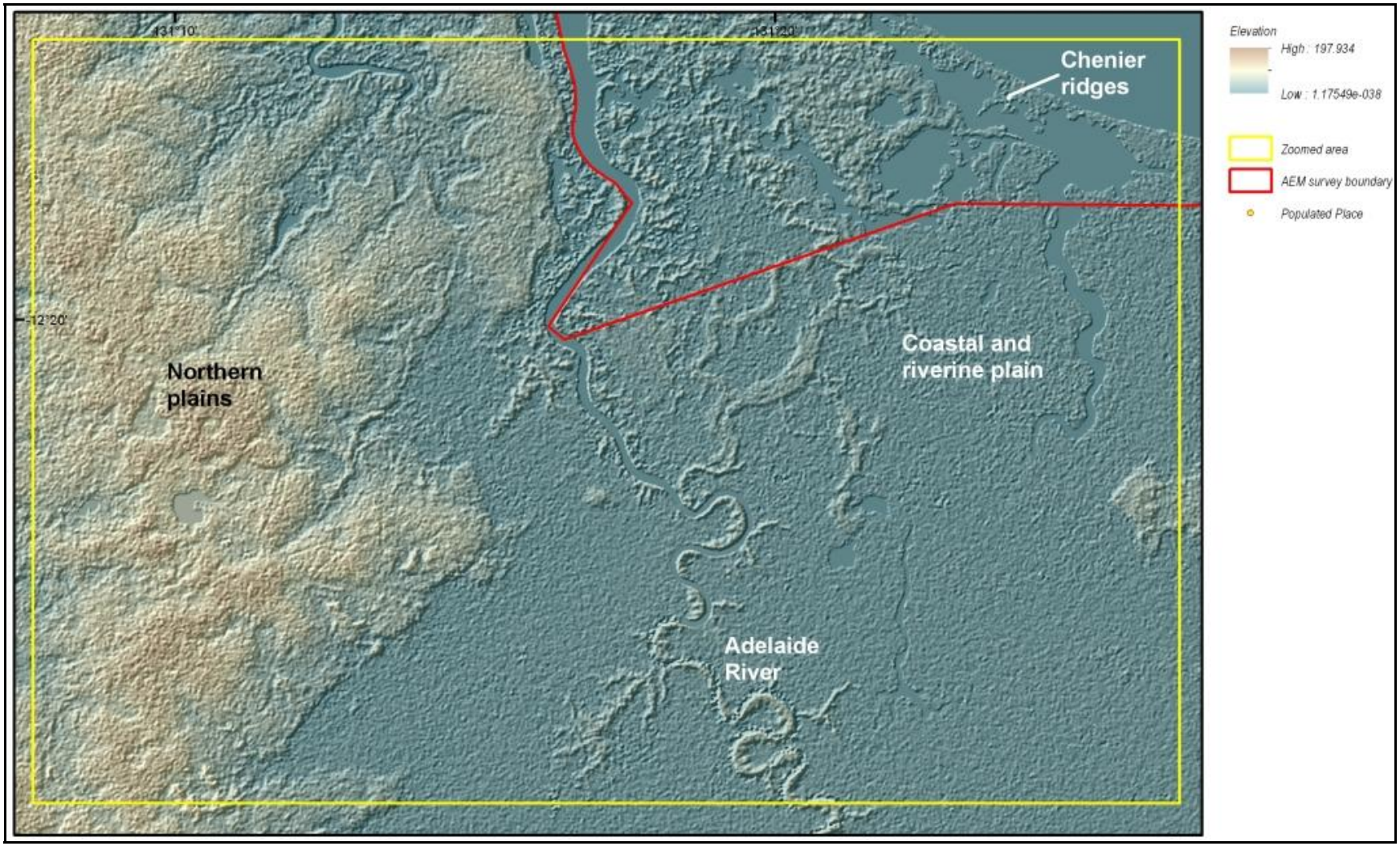

Figure 11. *Zoomed region of the 1-arc second DEM from Figure 10 highlighting specific landscape features. The coastal, estuarine, and riverine plains cannot be readily differentiated using the SRTM data, although surface water bodies such as the Adelaide River are evident.*

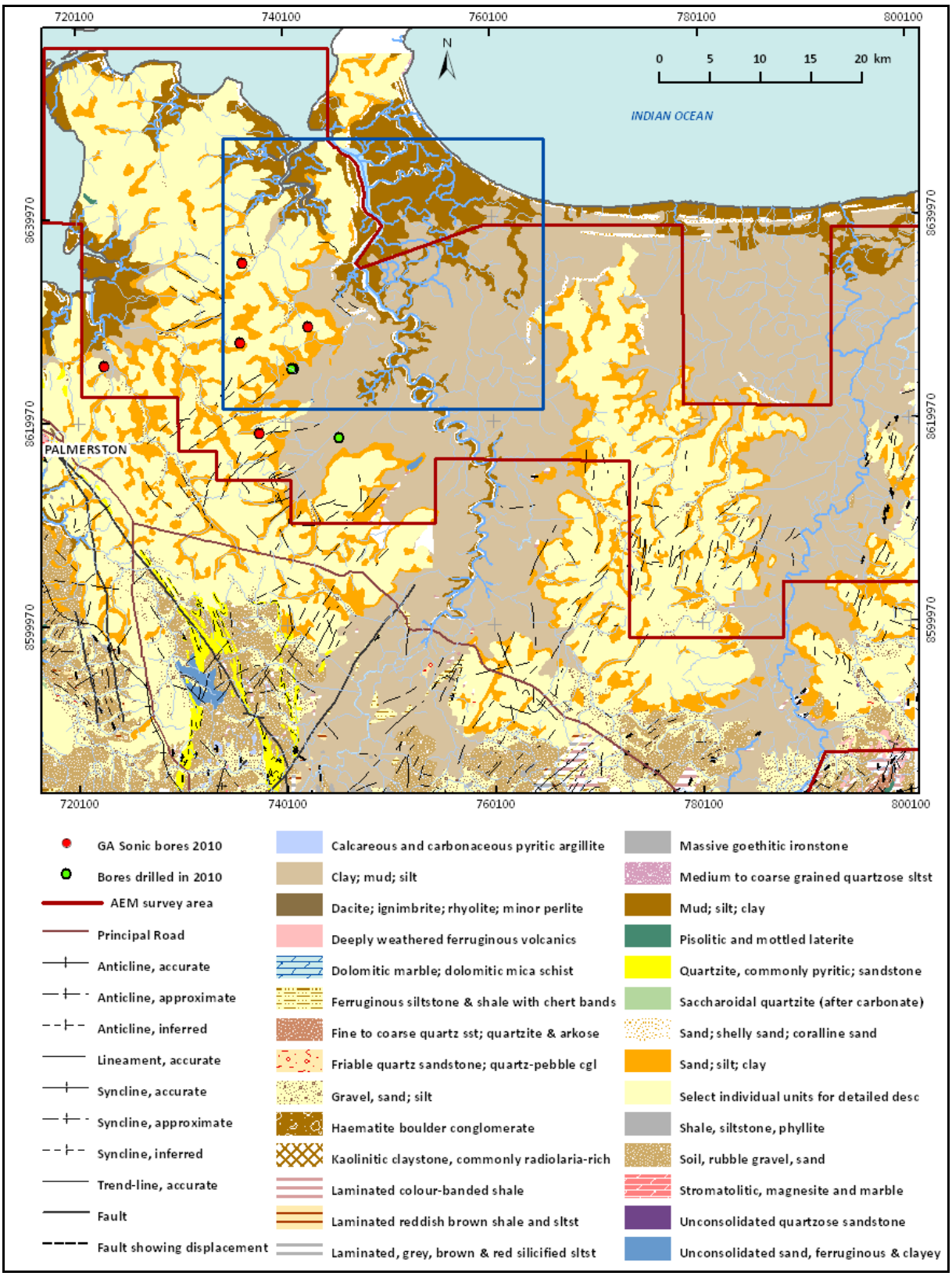

Figure 12. *Cenozoic geology and regolith of the NT Coastal Plains study region (blue box is area shown in Figure 13).*

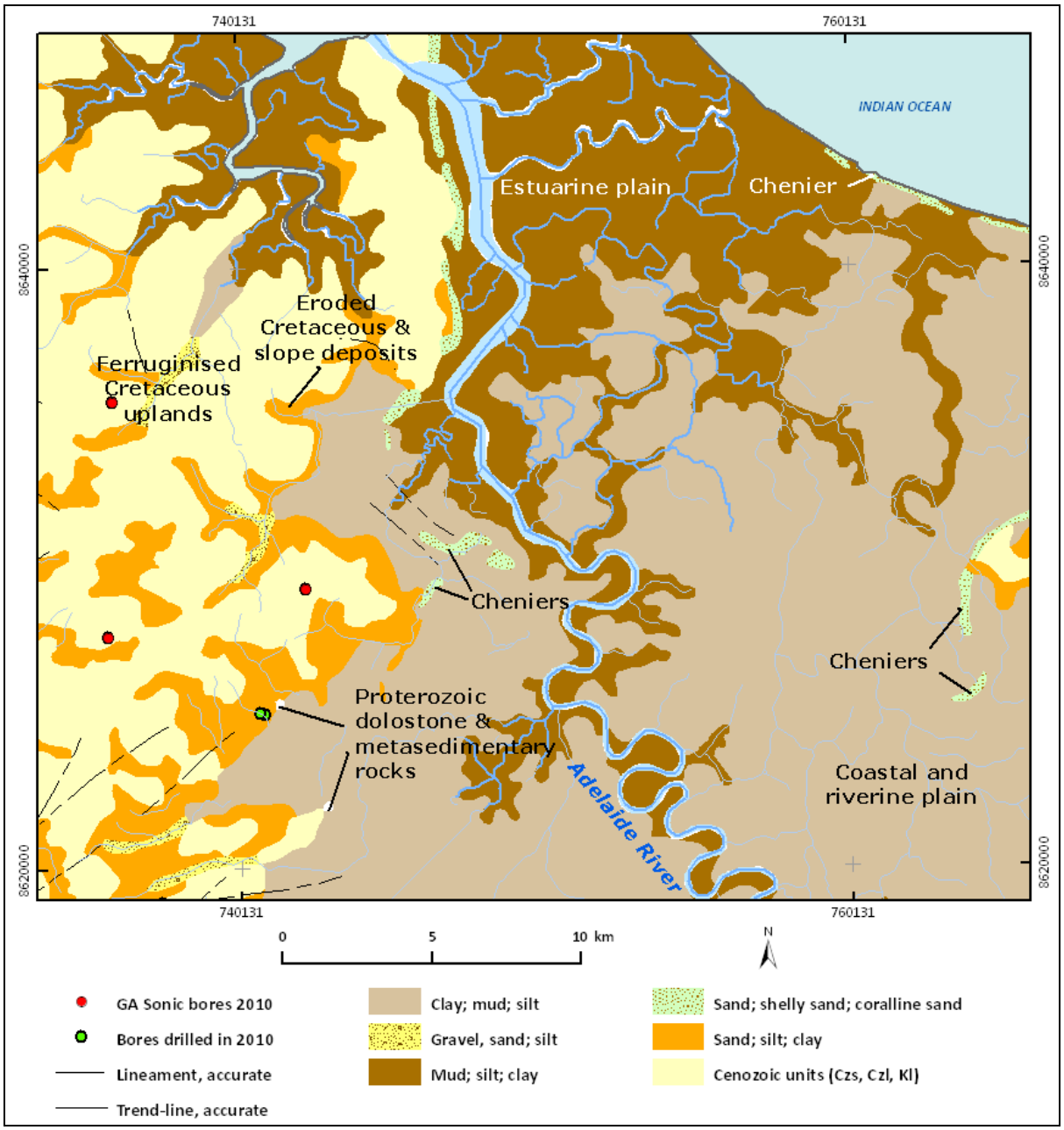

Figure 13. *Zoomed part of the NT Coastal Plains study region (from previous figure) showing some of the main features of the Cenozoic geology and regolith, with specific features labelled. Basement trend lines are shown through cover.*

2 Geological Framework

2.1 BASIN ARCHITECTURE AND STRUCTURE

2.1.1 Regional architecture

At the regional scale bedrock structure is dominated by the fabric of the Pine Creek Orogen (PCO) formed in the Paleoproterozoic (Ahmad *et al.,* 2006). The PCO consists of a north-west to south-east trending Central Trough of highly deformed sedimentary rocks up to 4 km thick, with Archaean bedrock inliers to the south-west (the Rum Jungle Complex) and the north-east (Woolner Granite). The architecture of the PCO is shown in Figure 14. The following geological descriptions are largely based on Worden *et al*. (2008) unless otherwise cited.

2.1.2 Major structures

Tight folding of the Proterozoic sediments is evident in the processed aeromagnetic data from the survey area, with fold axes trending north-easterly (Figure 15). The bedrock stratigraphy is cut by two major fracture systems, the north to north-west trending Pine Creek Shear Zone (PCSZ) and the north-east trending Giants Reef Fault (GRF). These are shown in Figure 16. The PCSZ, part of the larger Noonamah-Katherine lineament, was interpreted by Simpson *et al.,* (1980) as a major crustal fracture system with sinistral movement. The PCSZ was active during the 1,780-1,760 Ma Shoobridge Event. The GRF is a dextral strike-slip fault extending for more than 200 km from the Halls Creek Mobile Zone in Western Australia, 5-8 km of lateral offset is recorded (Ahmad *et al.,* 2006).

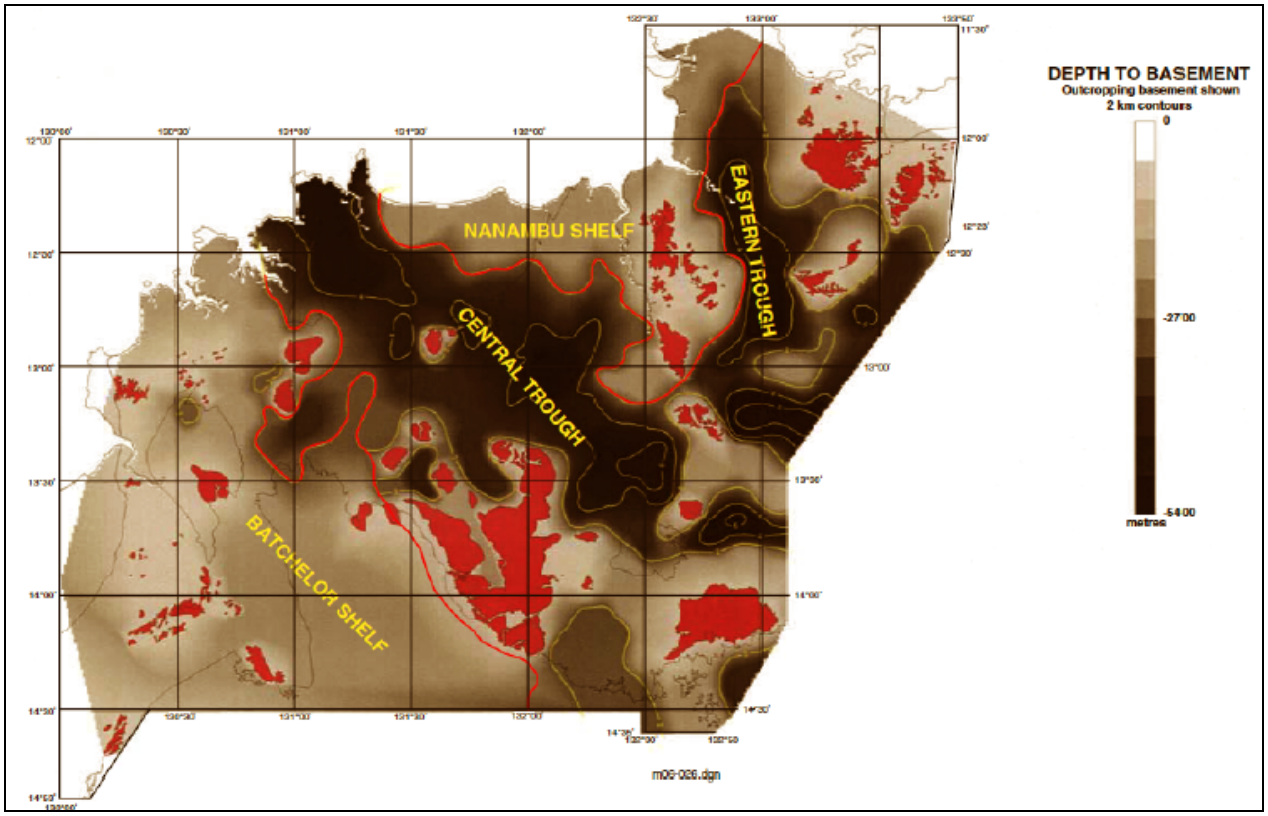

Figure 14. *Architecture of the Pine Creek Orogen derived from regional gravity data (after Ahmad et al., 2006)*

.

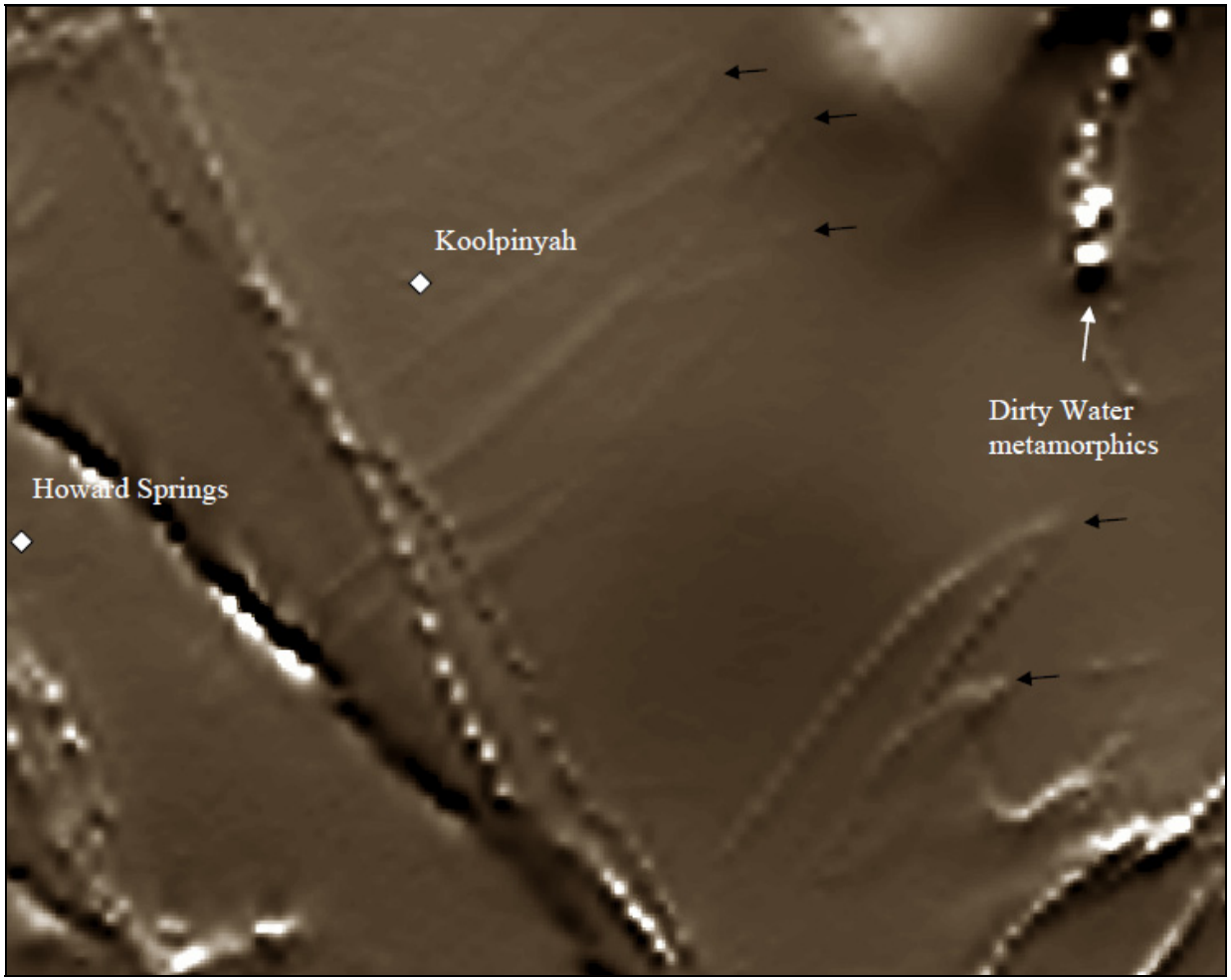

Figure 15. *1st vertical derivative of regional airborne magnetic data showing (with arrows) NE-SW trending fold structures in Proterozoic meta-sedimentary rocks (north to top). Image width is 43 km across. North-west trending linear structures are dykes associated with Pine Creek Shear Zone. The positions of Koolpinyah Homestead and the Howard Springs ranger station are also shown.*

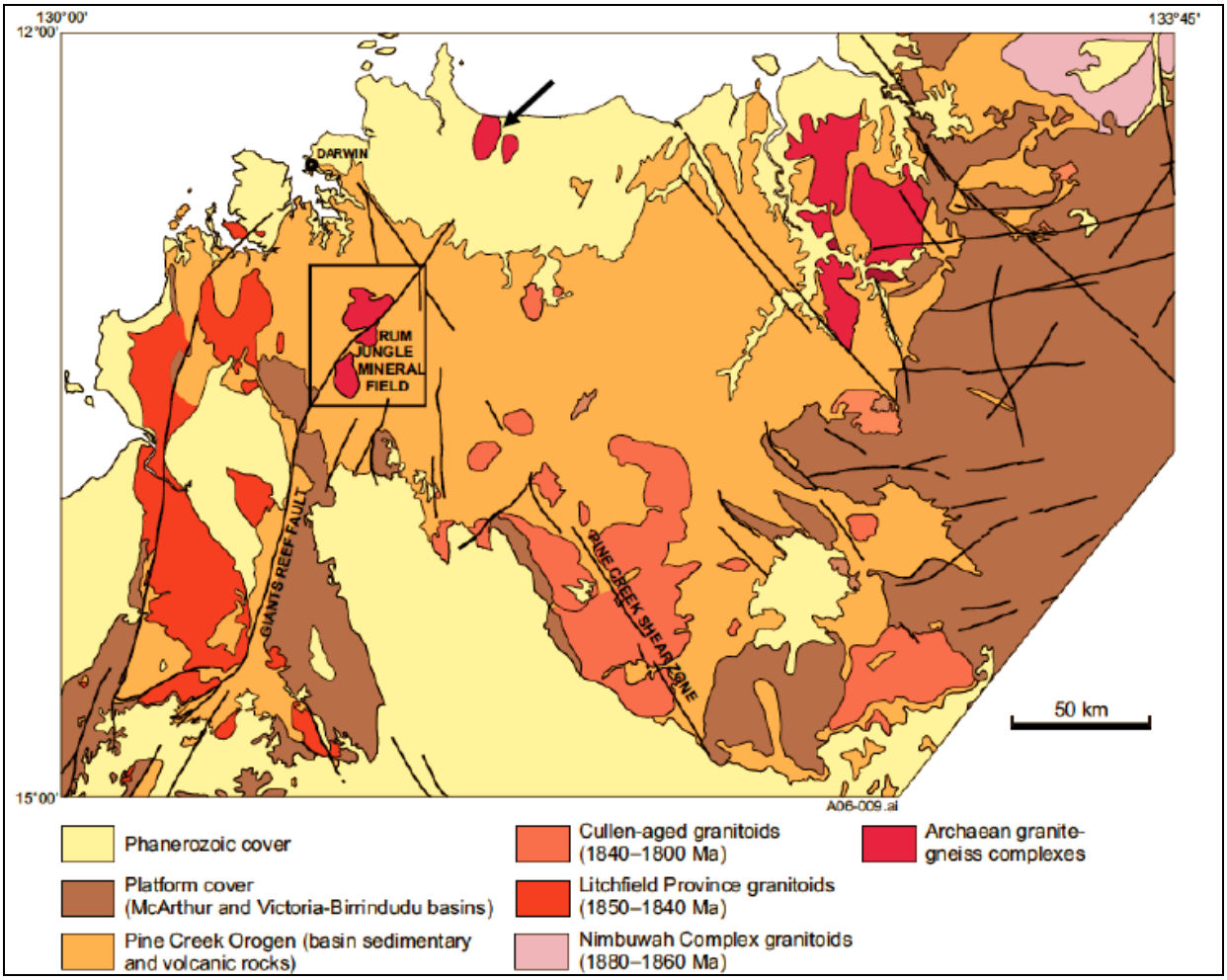

Figure 16. *Regional geological setting of the study area showing major structural-stratigraphic elements. Archaean Woolner Granite is arrowed. Image modified after Ahmad et al. (2006).*

2.2 STRATIGRAPHY AND LITHOLOGY

The regional stratigraphic units are summarised in Table 2, focusing on those that occur in the project area. The stratigraphic architecture (from Worden *et al.,* 2008) is shown in Figure 17.

2.2.1 Archaean

Archaean granites (the Woolner Granite) subcrop in the northern part of the study area. They are the oldest rocks in the region, dated at 2.675 Ga (Worden *et al.,* 2008). These granites are correlates of the Rum Jungle Complex further to the south-west, outside the study area (Figure 17). The Archaean rocks are considered the source of much detrital material in the overlying Proterozoic succession. Surrounding the granites and intruded by them are the Dirty Water Metamorphics. These consist of biotite schist, amphibolite, gneiss, and migmatite, suggesting highly metamorphosed supracrustal rocks. The top of the Archaean succession is unconformably truncated by the Proterozoic succession.

Table 2: Project area stratigraphy.

ERA/AGE	GROUP	FORMATION	MEMBER	LITHOLOGY
Quaternary				Sands, silts, clays, locally carbonaceous. Shelly sands
Cretaceous	Bathurst Island	Darwin		Siltstones, claystones, some radiolarian rich, fine to medium sandstone, pyritic, carbonaceous, phosphatic, and glauconitic when fresh
			Howard Sand	Pebbly coarse sand
Mesoproterozoic	Finniss River	Burrell Creek		Siltstone, shale and greywacke with interbedded volcanics at base
	South Alligator	Mount Bonnie		Shale and siltstone with minor sandstone and chert
		Gerowie Tuff		Cherty tuff and greywacke, minor argillite, ironstone, siltstone and chert
		Koolpin		Ferruginous siltstone with chert bands and nodules, carbonaceous pyritic shale, silicified dolomite, minor jasper, ironstone, and phyllite
Palaeoproterozoic	Mount Partridge	Wildman Siltstone		Laminated pyritic and carbonaceous shale, silty shale and siltstone. Minor silicified dolostone, sandstone and quartzite
			Acacia Gap Quartzite	Pyritic quartzite. Interbedded shale, sandstone, and phyllite
		Whites		Calcareous and carbonaceous pyritic mudstone, dolostone, sandstone
		Koolpinyah/ Coomalie Dolomite		Silicified dolostone, magnesite, marble and phyllite
		Crater Formation / Mundogie Sandstone		Sandstone, quartzite and arkose
Archaean	Woolner Granite			Granite
	Dirty Water Metamorphics			Biotite schist, amphibolite and migmatite

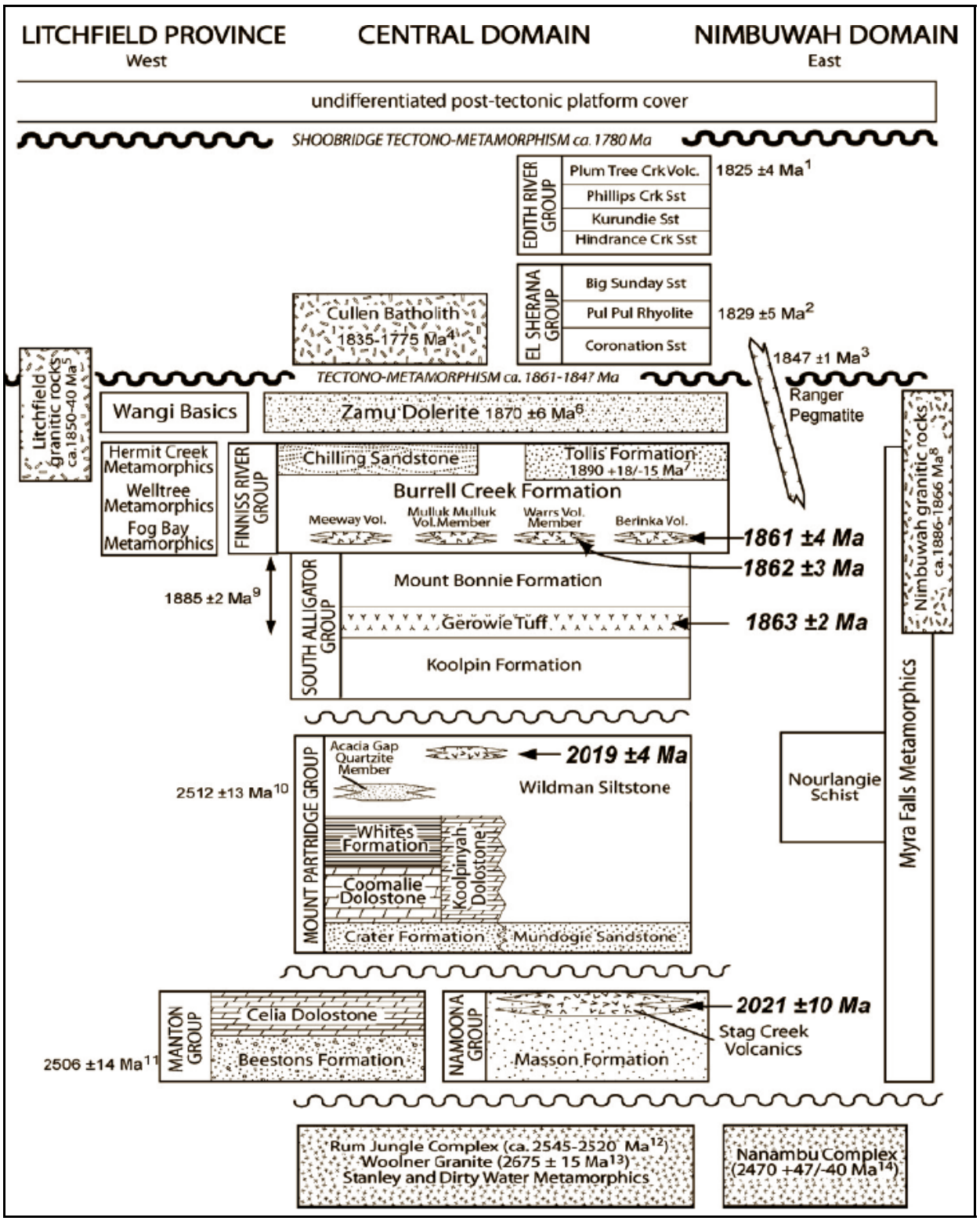

Figure 17: *Archaean and Proterozoic stratigraphy of the Pine Creek Orogen, taken from Worden et al., (2008).*

2.2.2 Paleoproterozoic

2.2.2.1 Stratigraphic units

The main rock units in the project area belong to the Mount Partridge Group and rest unconformably on Archaean basement (Figure 18). The Mount Partridge Group has been highly deformed and regionally metamorphosed to lower greenschist facies by the Nimbuwah Event that occurred at 1861-1847 Ma. The rocks are poorly exposed in the project area and this, combined with their structural complexity, has led to confused stratigraphic nomenclature.

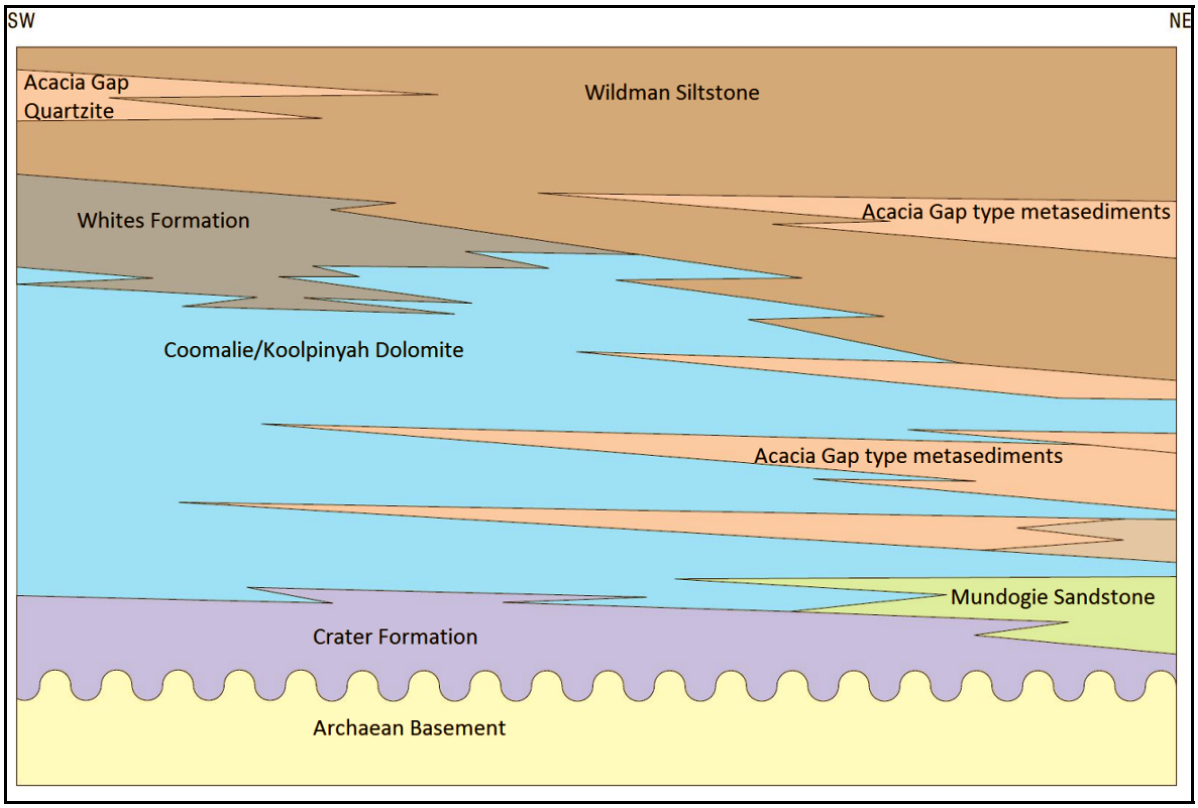

Figure 18: *Conceptual stratigraphic relationships for the Paleoproterozoic rock units within the study region (after Fell-Smith and Sumner, 2011).*

2.2.2.1.1 Crater Formation

This formation is the basal, clastic-dominated part of the Mount Partridge Group and unconformably overlies the Archaean basement. Rocks of this formation have low permeability due to strong induration, except where fractured. This formation is one possible host for the weak magnetic units whose folding is visible in the aeromagnetic data. The presence of the Crater Formation, and its lateral equivalent, the Mundogie Sandstone, in the project area is unconfirmed (Fell-Smith & Sumner, 2011).

2.2.2.1.2 Wildman Siltstone Formation

This formation consists mainly of fine-grained carbonaceous and pyrite-bearing shales and silty shales, locally metamorphosed to phyllite. The sulfides and organic carbon fraction are visible only at depth. Tuffaceous units near the top give an age of 2.019 Ga. Worden *et al*., (2008) suggested that the Wildman Siltstone is laterally equivalent to three other units (from top to bottom): the Acacia Quartzite Member, the Whites Formation, and the Coomalie Dolomite. The Coomalie Dolomite is partly to wholly equivalent to the Koolpinyah Dolomite.

2.2.2.1.3 Koolpinyah-Coomalie Dolomite

The published nomenclature of this unit is very confused. The early literature refers to the dolostone in the area as the Coomalie Formation (e.g., Needham and Stuart-Smith, 1984) and correlated with other occurrences in the Rum Jungle area. Pietsch (1985) appears to have been the earliest to use the term "Koolpinyah Dolomite" for the dolostone on the Koolpinyah 1:100,000 map sheet, although the justification for this is unclear.

We consider that Coomalie Formation is probably the better term for this unit, having priority and better representing the heterogeneous lithology (see below). However, Koolpinyah Dolomite is well entrenched. Thus, this report will use the term Koolpinyah-Coomalie Dolomite (KCD) to reflect this.

The KCD is lithologically variable. Tickell (2009) reported that although KCD is widespread over the northern Darwin 1:250,000 hydrogeological map sheet, a detailed investigation of the supposed dolostone where intersected by drilling shows it typically consists of coarse-grained (sandstone, quartzite) or fine-grained (shale, phyllite) clastic rock types (Figure 19). There is also calcite veining, silicification and development of secondary porosity after sucrosic dolomite. Locally significant karst breccias occur. Drilling in the course of this project has shown that the phyllites are mostly sericite-chlorite with silty sized quartz grains.

We concur with Worden *et al.,* (2008) regarding the lateral equivalence between the Wildman Siltstone and the KCD and consider them to be interfinger within the project area. Diamond drillhole Y22 (602 m) (744335 8628785), which has been analysed with the Hylogger, to the east of Koolpinyah homestead on the edge of the floodplain provides evidence for this relationship. In the upper part of the hole there are two significant KCD dolostone beds separated by metasedimentary rocks, whereas the lower part of the drillhole contains more abundant metasedimentary rocks (mostly phyllite, schist and quartzite) with beds of dolostone.

Borehole RN37330 (156 m total depth) (721460mE, 8622700mN), which is 1.5 km west of Howard Springs, was drilled in the KDP drilling program and penetrated rocks identified as the Whites Formation, with a basal pyritic zone appearing conductive in the AEM, then a zone transitional to dolostone and finally massive KCD dolostone, giving insight as to the nature of the top of the KCD.

The Proterozoic rocks encountered in diamond drillhole Y19 (291 m total depth) (727565mE, 8623750mN) 5 km east of Howard Springs consist of massive dolostone. Fifteen chemical analyses of carbonates sampled from the KCD indicate that the dolostone is chemically uniform, except for two samples where near complete (presumably Veitch-style) magnesite development has occurred. In both of these samples karstic features are not well developed.

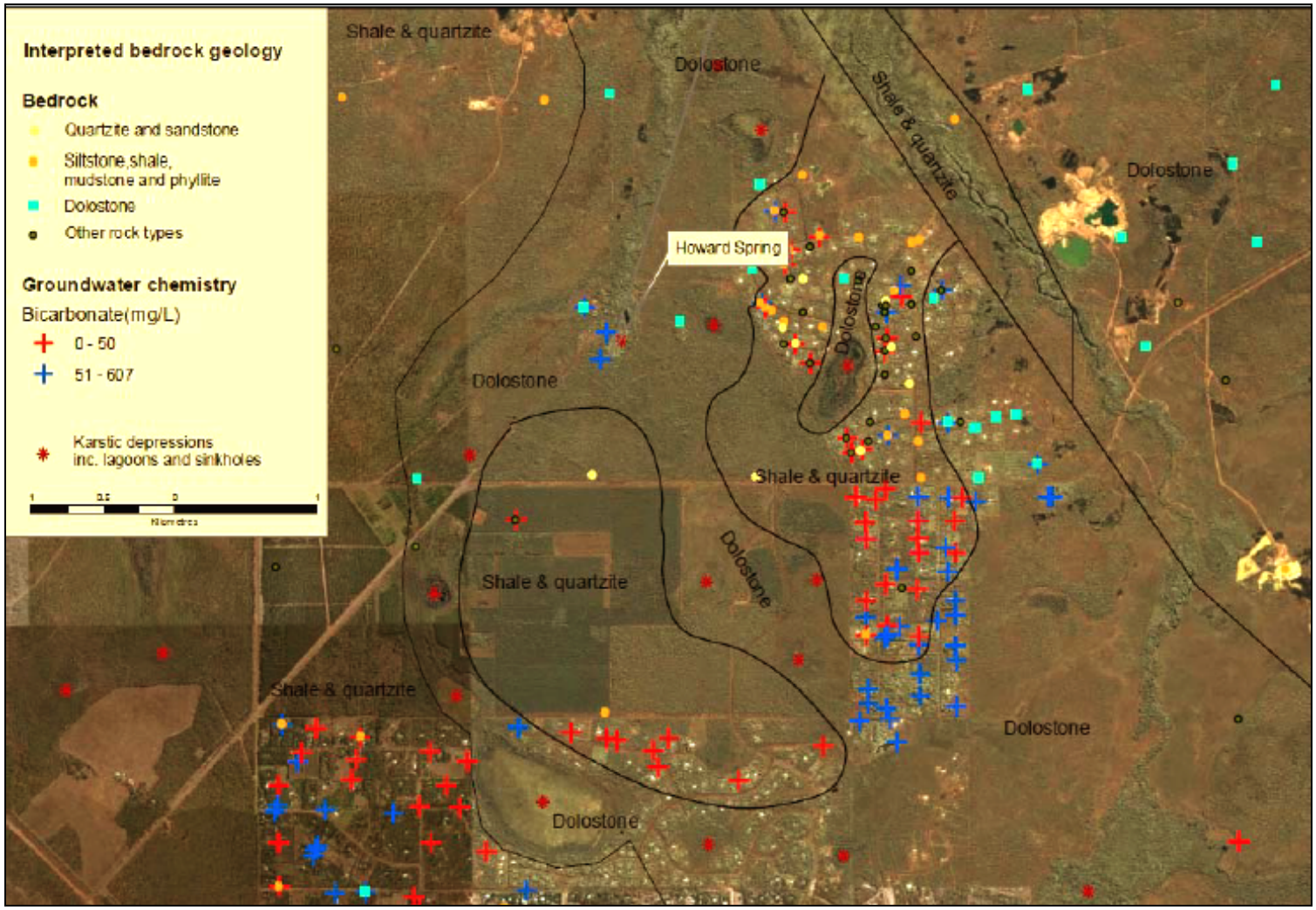

Figure 19: *Rock types and groundwater compositions encountered by drilling in the Howard Springs area. Image modified slightly from Tickell (2009).*

Although different rock types occur in consistent domains, it is not possible to determine coherent structural or stratigraphic patterns. However, the distribution of collapse features and associated springs in the area interpreted to be forming sub-adjacent karst (e.g. Howard Springs, Tien 2006, Haig and Townsend, 2003, McFarlane *et al.,* 1995) remains consistently associated with pure dolostone in drilling, despite its more restricted occurrence.

The hydrogeologic implications of the widespread heterogeneity are significant. The sequences dominated by karstic dolostones and associated overlying lag deposits are highly permeable. Brecciated zones, sometimes at depth, have high permeability not only in the dolostones, but also in the Whites Formation and in quartzites, whereas permeability in phyllites is low. Zones of silicification in the dolostone and the quartzite beds will have very low permeabilities, except where cut by fractures. Chemical analyses within the KCD indicate that silicification and other alteration in the weathered zone and 'silicified dolomite' is very weak and that any real silicification is probably only at the dolostone/groundwater boundary, and is thus due to weathering.

2.2.2.1.4 Whites Formation

This fine-grained shale, siltstone and locally phyllite-bearing formation is distinctively carbonaceous and pyritic and also contains thin dolostone interbeds. Permeability is generally low, except in places enhanced by fracturing.

2.2.2.1.5 Acacia Gap Quartzite Member

This is a distinctive coarse-grained quartzite unit containing interbedded fine-grained pyritic shale and phyllite. The formation is one possible host sequence for the folded and weakly magnetic bodies visible in the regional aeromagnetic data (Figure 15). With respect to hydrogeological properties, permeability is expected to be moderate to low in the siltstones and phyllites and low in the quartzite, except where fractured. These quartzite units will act as groundwater flow barriers if impermeable or, conversely, may be flow pathways if pervasively fractured.

2.2.2.2 Deformation

The Mount Partridge Group was deformed at 2.512 Ga ± 13 Ma (Worden *et al.,* 2008). The folded sedimentary rocks were subsequently eroded prior to the deposition of the overlying Mesoproterozoic succession.

Dolerite dykes dated at ~1,870 million years old intruded the Mt Partridge Formation and older rocks in the area subsequent to deformation. Many of these have intruded along major structural zones such as the Pine Creek Shear Zone and the Giants Reef Fault. The dykes belong to the Zamu Dolerite.

2.2.2.3 Typical lithologies

Typical Paleoproterozoic rock types from the project area are illustrated in Figure 20. These images show the permeability variations that occur in the project area, ranging from the very high permeability in the karstic breccias to the moderate to low permeability in phyllitic rocks, to the very low permeability (except where fractured) in massive dolostones.

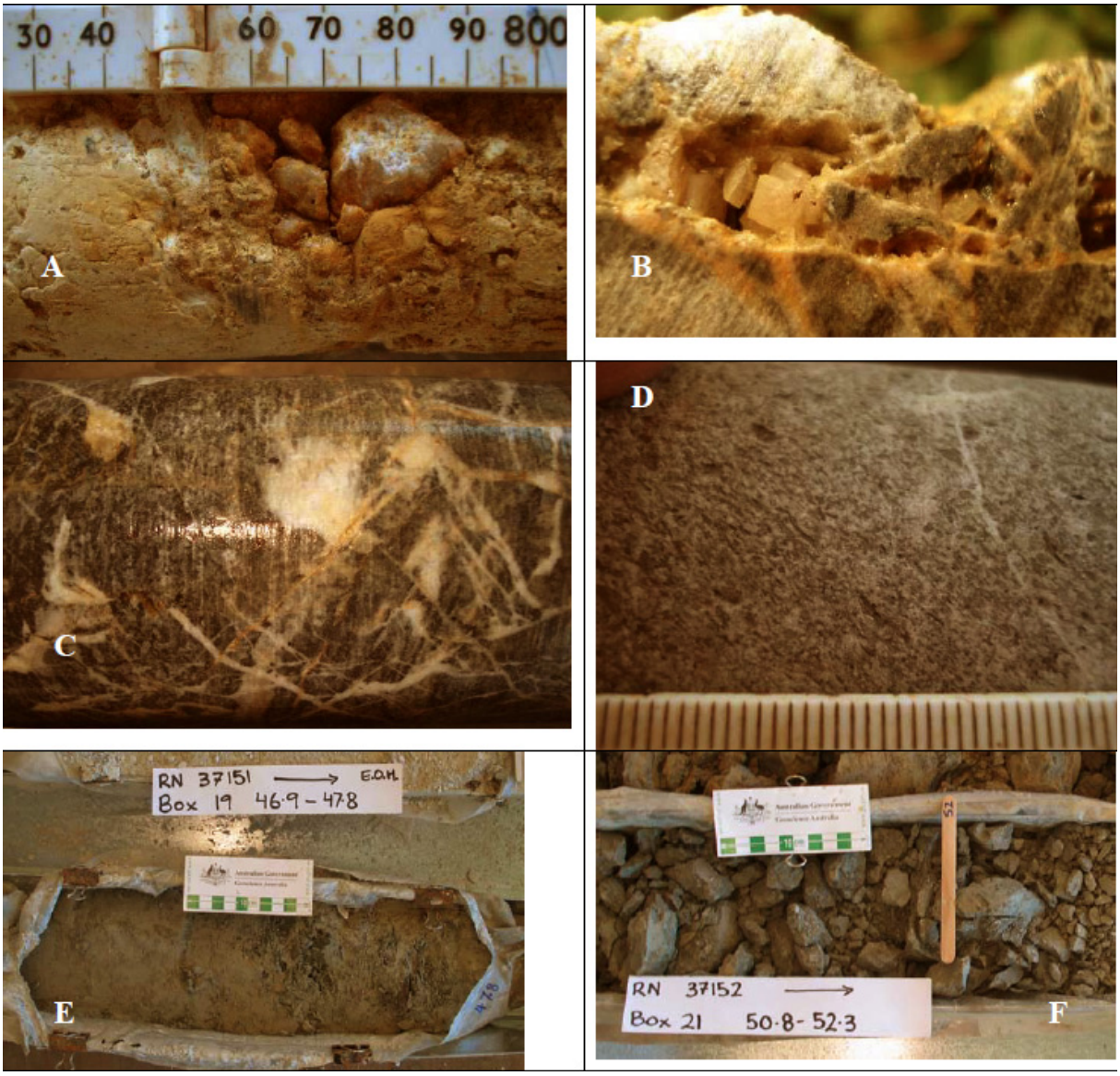

Figure 20: *Typical Proterozoic rocks from the project area. A: RN36530, close up of Core 4, 41.4 m, karstic breccia with large fragment of quartz (from Tickell 2009). B: RN36530, close up of Core 6, 51.0 m, dolomite rhombs in a cavity etched out along a calcite vein (from Tickell 2009). C: RN36530, close up of Core 6, 51.1 m, dolostone, strongly veined with calcite (from Tickell 2009). D: RN36531, close up of Core 1 showing detrital dolostone and quartz and 70° dip (from Tickell 2009). E: RN37151 (KD003) fresh fragmented phyllite. F: RN37152 (KD002) fresh, slightly carbonaceous phyllite and siltstone.*

2.2.3 Mesoproterozoic

2.2.3.1 Stratigraphic units

Mesoproterozoic units lie outside the project area but are included here because they occur in the south and south-western parts of the mapped area. They consist of the Finniss River and South Alligator Groups (Worden *et al.,* 2008, Ahmad *et al.,* 2006).

The South Alligator Group in the mapped area consists of the following formations:

Koolpin Formation

The Koolpin Formation rests unconformably on the Paleoproterozoic sediments of the Mount Partridge Group and consists of ferruginous and carbonaceous shale and siltstone, with minor cherty to jasperoidal

horizons. Chert nodules, banded ironstone and tourmalinite beds are locally present. Finer-grained lithologies become phyllite where subjected to higher metamorphism.

Gerowie Tuff

The Gerowie Tuff conformably overlies the Koolpin Formation. In the project area it is composed of cherty green-black tuff, laminated light grey silicified siltstone, red and black argillite, thin banded ironstone and greywacke (Ahmad *et al.,* 2006, Pietsch 1985). Worden *et al.,* (2008) assigned an age of 1.863 Ga to the formation.

Mount Bonnie Formation

The Mount Bonnie Formation conformably overlies the Gerowie Tuff and consists predominantly of red to brown shale and siltstone with minor fine to medium sandstone, ironstone and chert beds.

Burrell Creek Formation

The Burrell Creek Formation is the only geologic unit of the Finniss River Group in the study area. It consists of fine-grained clastic lithologies, principally siltstone, shale, and greywacke. Some interbedded volcanics occur at the base. The contact with the underlying Mount Bonnie Formation is transitional (Ahmad *et al.,* 2006), and is marked by the disappearance of ironstone and chert units characteristic of the older Formation and Group. Dating of the interbedded volcanics at the base has yielded ages of 1.861-1.862 Ga (Worden *et al.,* 2008).

2.2.3.2 Deformation

The Mesoproterozoic rocks were deformed at ~1.885 Ga (Worden *et al.,* 2008).

2.2.3.3 Typical lithologies

Mesoproterozoic rocks were not encountered by drilling in the project area so example rock types and their hydrologic properties are not discussed in this report.

2.2.4 Mesozoic

2.2.4.1 Stratigraphic units

The Mesozoic rocks of the project area are assigned to the Bathurst Island Group (Mory, 1988). This consists of numerous formations, most of which occur only offshore. However, the Darwin Formation and the Wangarlu Formation both occur in the project study area (Doyle, 2001). Their relationships are shown in Figure 21.

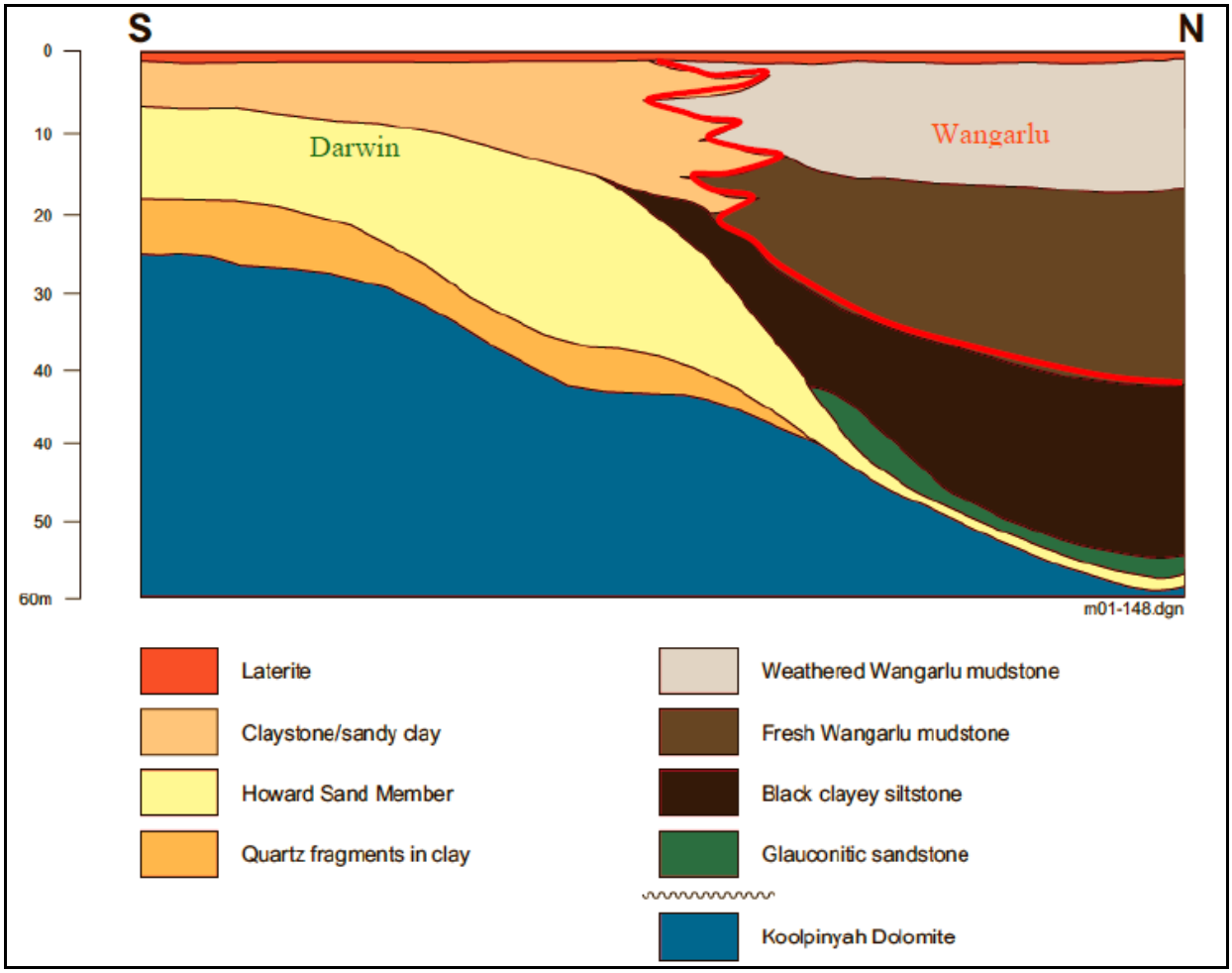

Figure 21: *Stratigraphy of the Bathurst Island Group in the broader region encompassing the project area. The upper 'laterite' layer is probably a deep saprolite weathering profile. Image modified slightly from Doyle (2001).*

2.2.4.1.1 Basal lag deposits

These consist of coarse-grained detritus that built up on the eroded and weathered Proterozoic basement surface prior to deposition of Cretaceous sediments. These deposits are variably thick and typically range from <1 m to 3 m. The clasts are heterogeneous, and include silicified dolostone, quartzite, quartz, ironstone, ferruginised sandstone and pegmatite (Fell-Smith & Sumner, 2011).

2.2.4.1.2 Darwin Formation

The Darwin Formation forms the basal unit of the Bathurst Island Group. Doyle (2001) described it as claystone and sandy claystone, with sand- (some glauconitic) and conglomerate-layers near the base. The formation thins to the north and becomes strongly carbonaceous and pyritic. Phosphatic horizons are present and fossilised molluscs, including bivalves, ammonites, and belemnites are common. Bioturbated horizons also occur. The Darwin Formation was deposited in the Early Cretaceous, spanning the Aptian (104 Ma) to Valanginian (135 Ma). The dominantly fine-grained clay-rich composition of the Darwin Formation means that it acts as an aquitard, confining groundwater in the underlying Howard Sand and Proterozoic aquifers and restricting downward leaching of weathering products.

2.2.4.1.3 Howard Sand Member

This unit is composed of coarse-grained, pebbly sand and pebbly gravel. It unconformably overlies Proterozoic rocks and fills collapse features formed in dolostone. The Howard Sand Member lacks fossils, but is inferred to be Early Cretaceous (Valanginian, 135 Ma). It forms a major aquifer in the project area.

2.2.4.1.4 Wangarlu Formation

The Wangarlu Formation overlies and replaces the Darwin Formation to the north of the project area. It mainly consists of grey clay-rich mudstone. The clays are rich in montmorillonite and glauconite units, phosphate nodules, pyrite nodules, and radiolarian-rich beds occur. The age of the Formation is Cretaceous, Maastrichtian (65 Ma) to Albian (104 Ma). Like the Darwin Formation it is an aquitard, confining groundwater in the underlying Howard Sands and Proterozoic aquifers and restricting downward leaching of weathering products.

In practice, it is difficult to differentiate between the Darwin and Wangarlu Formations in the project area because of the effects of strong physical and chemical weathering during the Cenozoic. Post depositional weathering has resulted in formation of thick regolith where Cretaceous stratigraphic units are indistinct. Remobilisation of iron and silica has developed indurated beds of massive, pisolitic, and nodular ferricrete and porcelainite alternating with strongly leached zones that extend through much or all of the Cretaceous successions. Therefore, for the purpose of this report, the Cretaceous successions are simply amalgamated and referred to as the Bathurst Island Group, without attempting to differentiate individual formations. The exception to this is the Howard Sand Member, which is a distinct lithologic and stratigraphic unit forming a significant aquifer.

2.2.4.2 Typical lithologies

Typical Cretaceous rocks are shown in Figure 22. Noteworthy are the fine-grained soft claystone and siltstones of the unweathered Cretaceous which provide an aquitard (A and B) and the highly permeable (and oxidised) Howard Sand Member (C and D). Also noteworthy is the contrast between the unweathered (A and B) and weathered (E and F) Bathurst Island Group sedimentary rocks, where weathering has resulted in extensive iron mobilisation, precipitation and leaching, and reprecipitation of silica.

2.2.5 Weathering

The entire lithologic succession in the study region has been extensively weathered, including both the Proterozoic and the overlying Mesozoic rocks. Weathering of the Proterozoic generally extends from a few metres in depth to several 10’s of metres. It is not clear whether this is a buried weathering horizon, weathering post-burial through passage of highly oxidised fluids through the basal Howard Sand Member of the Bathurst Island Group, or the result of both. However, the presence of residual quartz pebble lag in some holes (e.g., sonic drillcore in RN37151/KD003) suggests that there is at least locally preserved evidence of pre-Cretaceous weathering.

Chemical analyses within the KCD indicate that silicification and other alteration in the weathered zone and 'silicified dolomite' is very weak. Any real silicification probably occurs only at the dolostone-groundwater boundary; this is also interpreted as a weathering-related feature although its timing is uncertain.

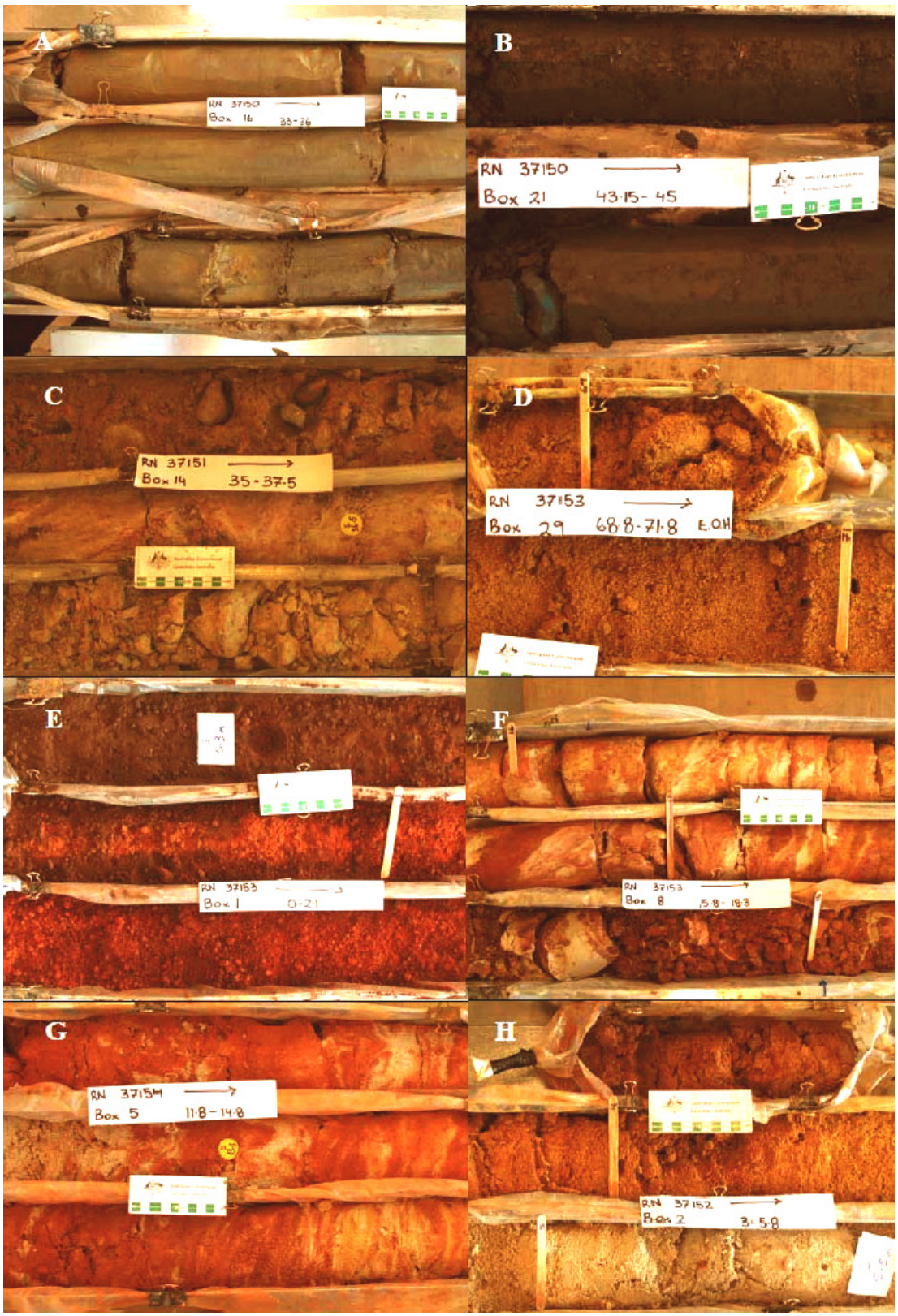

Figure 22: *(Photographs shown on previous page): Typical lithologies in Cretaceous and Quaternary sediments and the regolith. A: RN37150 (KD001) green, bioturbated Cretaceous claystone. B: RN37150 (KD001) black carbonaceous Cretaceous silty claystone. C: RN37151 (KD003) contact between base of Cretaceous and weathered Proterozoic. Top row coarse pebbly sand (Howard Sand Member), middle and bottom rows weathered Proterozoic phyllite. D: RN37153 (KD004) Howard Sand Member (coarse clean sand) in bottom of hole. Note that "pebbles" are actually cemented sand. E: RN37153 (KD004) Pisolitic ironstone duricrust at top of hole. F: RN37153 (KD004). G: RN37154 (KD005) banded and mottled fine clay-cemented Cretaceous sandstone. H: RN37152 (KD002) weathered coarse sand of probable Quaternary age, showing gradation from haematite staining at the top, to goethitic staining in the middle, to beached or iron-free clay-cemented sand at bottom.*

Weathering of the Cretaceous succession is probably continuous through to the present, as indicated by ongoing iron precipitation in contemporary sediments (Doyle, 2001; Fell-Smith and Sumner, 2011).

Most of the previous work on the weathering and landscape evolution has focused on the Darwin area further to the north and west of the study site (e.g., Nott, 1994; McNally *et al.,* 2000). However, the main observations from Darwin appear equally applicable in this project area. The similarity in the depth to base of Cretaceous and the depth to base of weathering in the Darwin area suggests that there at least pre-Cretaceous weathering is preserved (Figure 23).

Deep weathering has permeated most of the Mesozoic succession. The regolith is heterogeneous, with maghemite-bearing ferruginous pisolites at the top and variable leaching and induration below. Considerable chemical weathering has affected the originally carbonaceous and glauconitic claystones, siltstones, radiolarites, and fine sandstones of the Bathurst Island Group. For example, organic carbon has been mostly destroyed, and iron and silica have been extensively leached and reprecipitated as haematite- and goethite-rich layers, bands, and nodules, as well as bands of porcelainite (McNally, 2000).

The deeply weathered Cretaceous rocks have been eroded in some locations due to incision by the major rivers such as the Adelaide and the Mary. The toes of the slopes at the foot of the incisions are characterised by ongoing induration of resedimented material from the weathered plateau (Doyle, 2001). Likewise the slope deposits formed along the margins of sub-adjacent karst features are also undergoing active iron cementation through spring discharge (Tickell, 2009).

Weathering effects on the Howard Sand Member appear to differ from other Cretaceous units. Even where overlain by relatively unweathered sedimentary material (e.g., evidence from drillhole RN37151/KD003) it is relatively oxidised. Although this may be in part due to deposition in an originally oxidising atmosphere, the presence of an oxidation halo affecting carbonaceous sediments immediately above the Howard Sand Member (in RN37151) suggests that this aquifer has been a major conduit for through-flowing oxidised groundwater for considerable time.

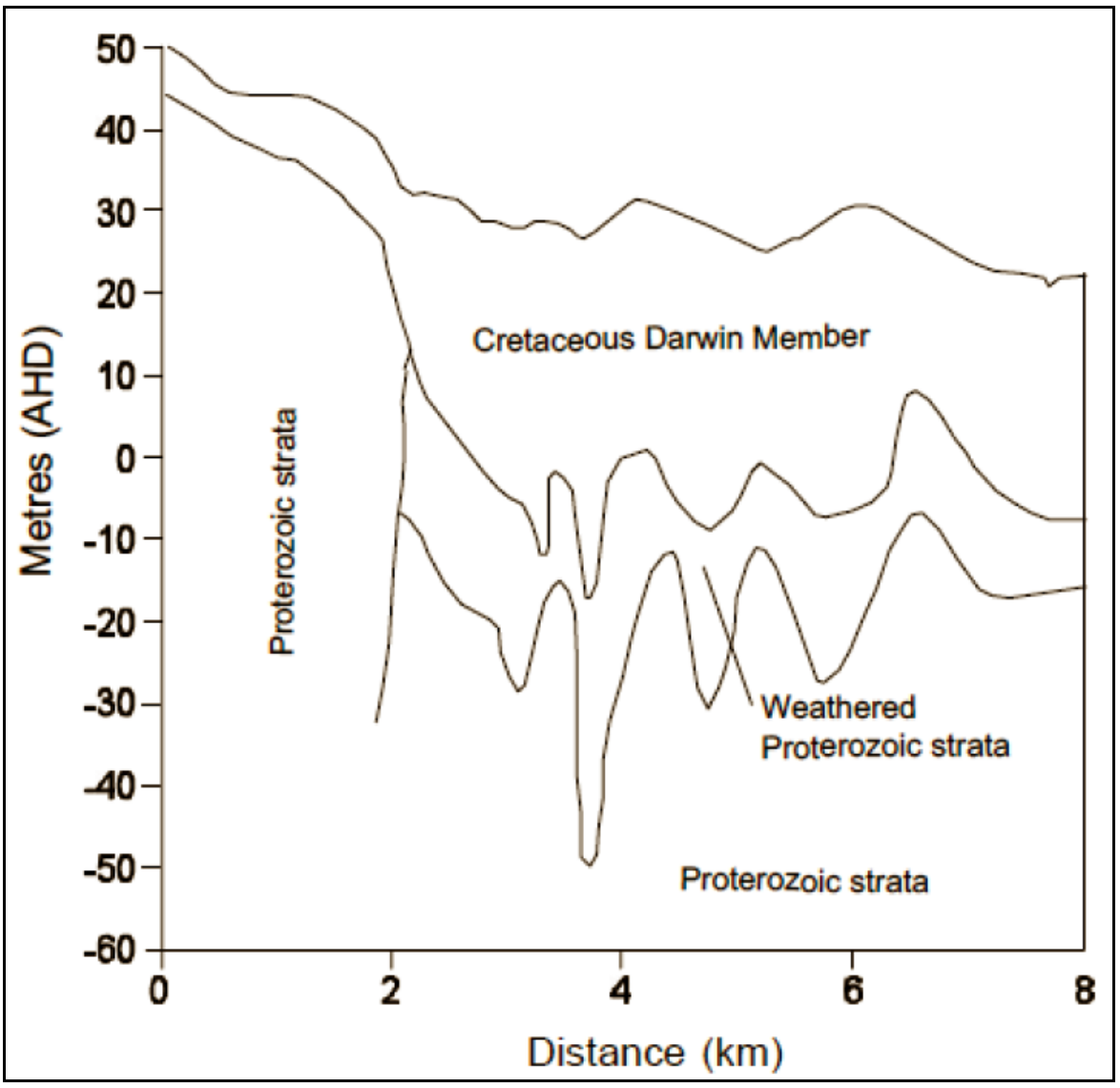

Figure 23: *Similarity between the morphology of the base of Cretaceous and the base of weathering in the underlying Proterozoic successions. Image sourced from Nott (2003).*

The aggressive weathering nature of groundwater has resulted in extensive dissolution and thus karst-like phenomena in what would normally be considered relatively insoluble rocks of the Cretaceous sequence (McFarlane *et al.,* 1995). The development of such a karstic landscape in normally non-soluble rocks is termed pseudo-karst. Dissolution has opened up numerous cavities and channels. The original nature of the dissolved lithologies is obscure; they may have been radiolarians, root channels, phosphate nodules, fossils or various combinations of all of these precursors (Doyle, 2001; Fell-Smith and Sumner, 2011). Whatever their origin, they have created significant porosity and water storage potential in the affected rocks. Furthermore, they allow water to bypass the otherwise impermeable claystone and porcelainite units and recharge the basal Howard Sand Member aquifer, which is a major groundwater target in the region (Radke *et al.,* 1998).

The ferruginous duricrust ("laterite" in older reports) sheds water laterally to low points in streams and floodplain boundaries and provides a reservoir for vertically induced recharge during the wet season.

2.2.6 Quaternary

The coastal, estuarine, and riverine plains occupy valleys incised into and in some cases through the Cretaceous cover, exposing Proterozoic bedrock. These incised valleys have been filled by Quaternary sediments, the most extensive of which appear to be of Holocene age.

Holocene sediments were not intersected by the drilling program for this project. The following description is therefore from published sources.

Woodroffe *et al.,* (1993) summarised extensive studies of the coastal and estuarine plains in the NT between the Adelaide River in the west and the South Alligator River in the east. The Mary River (Mulrennan and Woodroffe, 1998) can be taken as typical (Figure 24) of these environments.

In the estuaries these authors found that a Holocene transgressive-regressive estuarine succession up to 12 m thick was deposited on older Quaternary alluvial sediments with a well developed palaeosol along the contact. Radiocarbon dating indicated that the transgression phase occurred between 8,000 and 6,800 years ago. This was followed by the "Big Swamp" phase 6,800 to 5,300 years ago which, as the name suggests, was characterised by extensive mangrove swamps over much of the estuarine area. This was followed from 5,300 to the present with more restricted mangrove development along channels and seaward parts of the floodplain. Deposition in this phase has been slow, with only a few centimetres of sediments being deposited by the fresh water environments.

In contrast, the coastal plain sediments consist of saline sandy mudflats with sparse chenier ridges of shelly sand. As with the estuarine sediments evidence of an initial transgressive event followed by a forced coastal regression through sediment accretion is recorded in these sediment layers. The earliest sediments are mangrove muds deposited during transgression from 6,700 to 6,300 years accompanying a sea-level rise of about 8 m. This was followed by the progradation of the sandy mudflats and chenier ridges of the modern sedimentary environment. In excess of 5 km of progradation is known to have occurred. These sediments built up to approximately 2 m above AHD. The surface of the coastal plain is locally veneered by freshwater sediments from seasonal inundation.

Very little information exists on the earlier Quaternary sediments in the project area. These are likely to be older Pleistocene estuarine, fluvial, and coastal plain sediments. These sediments were probably intersected in sonic drill core from RN37152 (KD002) where 13.1 m of inferred Quaternary sediments overlie weathered Proterozoic phyllites. The basal 10 cm consists of graded sand to clay beds overlain by quartz cobbles in a clayey matrix. The sediments consist mostly of coarse clayey sand. The top 4.4 m has been iron-stained, with haematite grading downwards to goethite stains, and then abruptly into unstained white clayey sand. The top 1 m consists of haematic gravel with whitish clay clasts and overlies a dark brown sandy palaeosol.

The Quaternary sands range from low to high permeability, depending on clay content. They are important hydrologically as they are the conduit through which marine waters come in contact with the main aquifers in the Cretaceous and Proterozoic rocks.

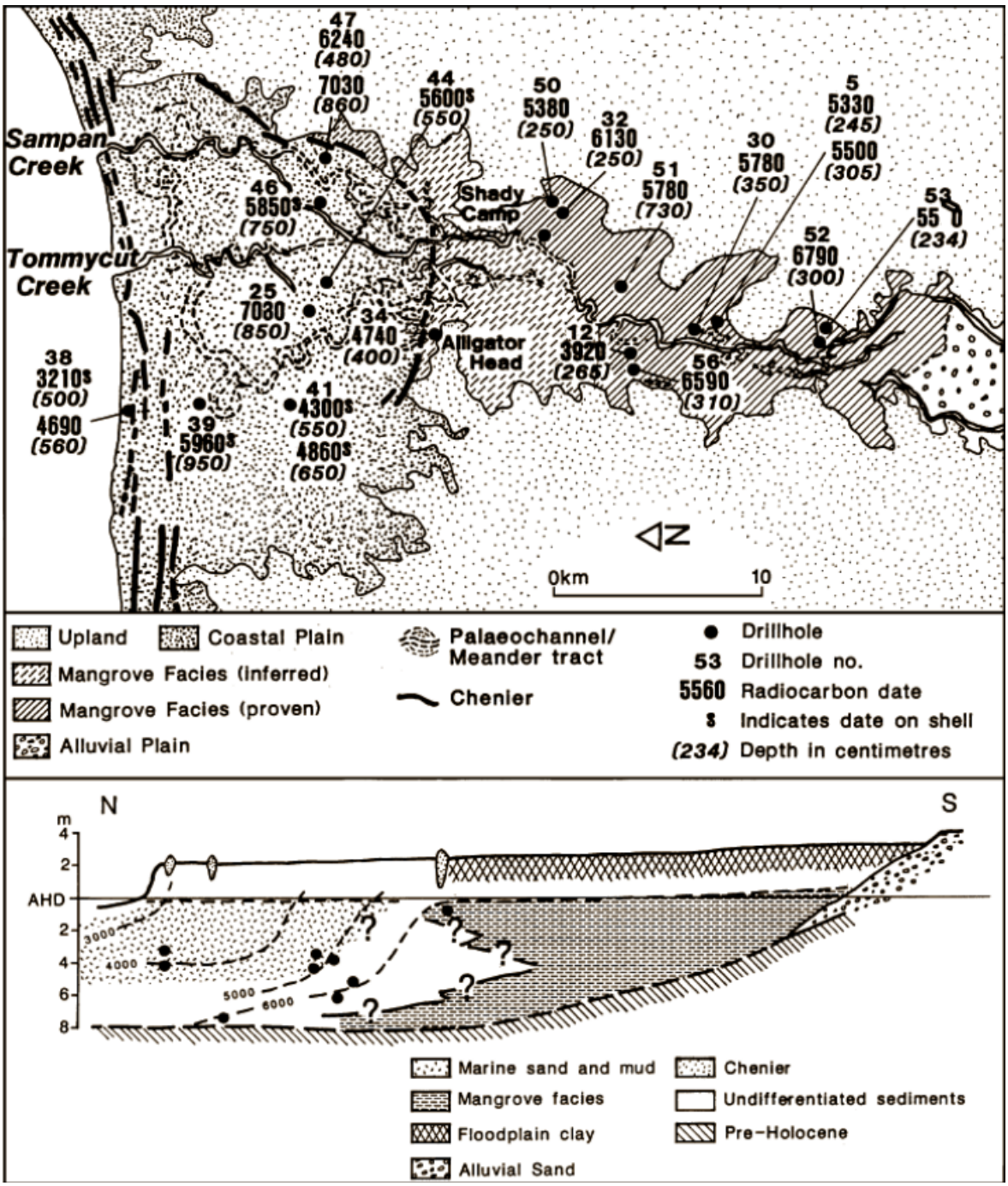

Figure 24: *Coastal progradation in the Mary River estuary (after Woodroffe et al., 1993).*

3 Hydrogeological Framework

The account of the regional hydrogeology presented in this chapter is taken (with some amendment and modification) from Haig & Townsend (2003) and Fell-Smith &Sumner (2011).

3.1 PRINCIPLE AQUIFERS

Jolly (1983) showed that there are three main aquifer systems underlying the coastal plains of the project study area (Figure 25). These include aquifers developed in:

- Cretaceous sedimentary rocks and their weathered near-surface equivalents;
- Palaeoproterozoic Koolpinyah-Coomalie Dolomite (KCD); and
- Fractured rocks in the Proterozoic basement sequences, such as the Whites Formation.

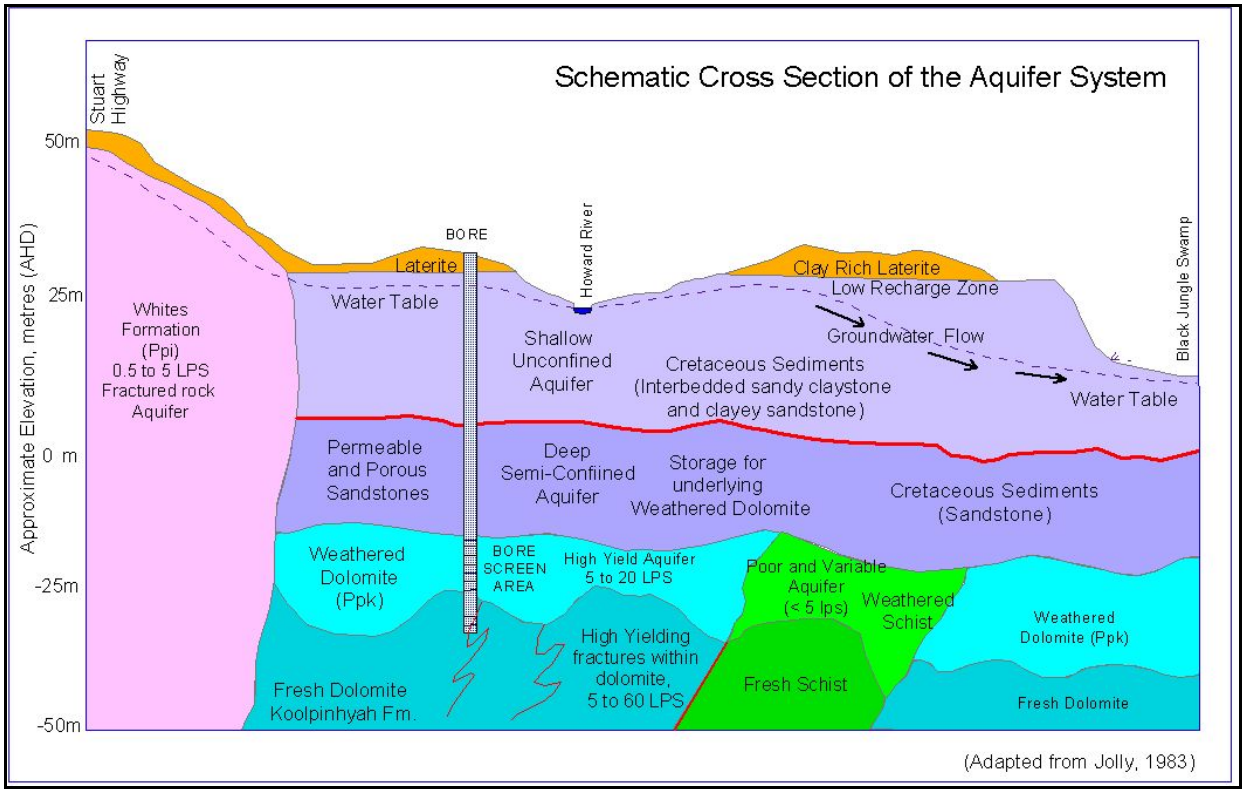

Figure 25: *Schematic diagram showing groundwater movement in the Howard East area. The 'laterite' layer at surface is probably a deep saprolite weathering profile (adapted from Jolly, 1983).*

3.1.1 Saprolite and Cretaceous aquifers

The distribution and continuity of Cretaceous sedimentary rocks (Bathurst Island Group) varies over the study area due to facies changes and local variations in depositional processes (Fell-Smith and Sumner, 2011). A widespread weathering profile is well developed within the upper ~30 m of the Cretaceous sedimentary profile, although the depth and degree of weathering depends on the original sediment composition and susceptibility to weathering. The saprolite aquifer is highly permeable, especially in the mottled zone (upper 12 metres below surface), although storage potential is generally low as groundwater readily drains from this zone to low-lying areas during the dry season. Below the weathering profile the composition of the Cretaceous rocks varies from claystone through to sandstone, with the highest yielding aquifers typically in medium- to coarse-grained friable sandstone lenses; these may have yields of 2-5 L/s (Jolly, 1983).

Basal Cretaceous gravel and sand deposits occur at the contact with the underlying Proterozoic rocks. These are variably interspersed with relict surficial lag deposits which mark the erosional remnants of the palaeo-

surface that existed on the Proterozoic rocks prior to the onset of deposition in the Mesozoic deposition. This transitional zone, also known as the McMinns Hydrostratigraphic Unit, provides some high-yielding intervals for groundwater extraction. However, the permeability of the transitional unit is highly variable due to the common presence of fine-grained sediments (e.g., clay) in the matrix. Such zones have poor aquifer potential.

3.1.2 Koolpinyah-Coomalie Dolomite (KCD) aquifer

The KCD aquifer is widespread in the NT coastal plain region, and one of the primary sources of groundwater extracted throughout the Darwin Rural Water Control District. Aquifer permeability varies significantly due to deformation (folding and fracturing) and differential weathering of the various rock types that occur within the formation, e.g., dolostone, schist and quartzite (Jolly, 1983). In places, localised faulting has focused groundwater flow and led to extensive dissolution features which may have distinct surface expression, e.g., sinkholes. The highest groundwater bore yields in the region occur in areas of karstic weathered dolomite or where extensive fracturing has disrupted the basement rocks. The unfractured metasedimentary layers of the KCD (e.g., phyllite and schist) generally have very low permeability and poor bore yields.

Widespread structural deformation and disruption, coupled with multiple steeply dipping dolerite dykes (Figure 26), have created many distinct hydrogeologic zones in the KCD aquifer (Fell-Smith and Sumner, 2011). Groundwater characteristics such as salinity, major and minor ion compositions, and recharge/discharge processes vary between these different zones. Based on the results of their detailed investigation Fell-Smith and Sumner (2011) defined four major hydrogeological zones within the KCD of the study area, with five significant sub-zones recognised in the main aquifer system (Figure 27). According to Fell-Smith and Sumner (2011) the key features of the four main zones are listed below.

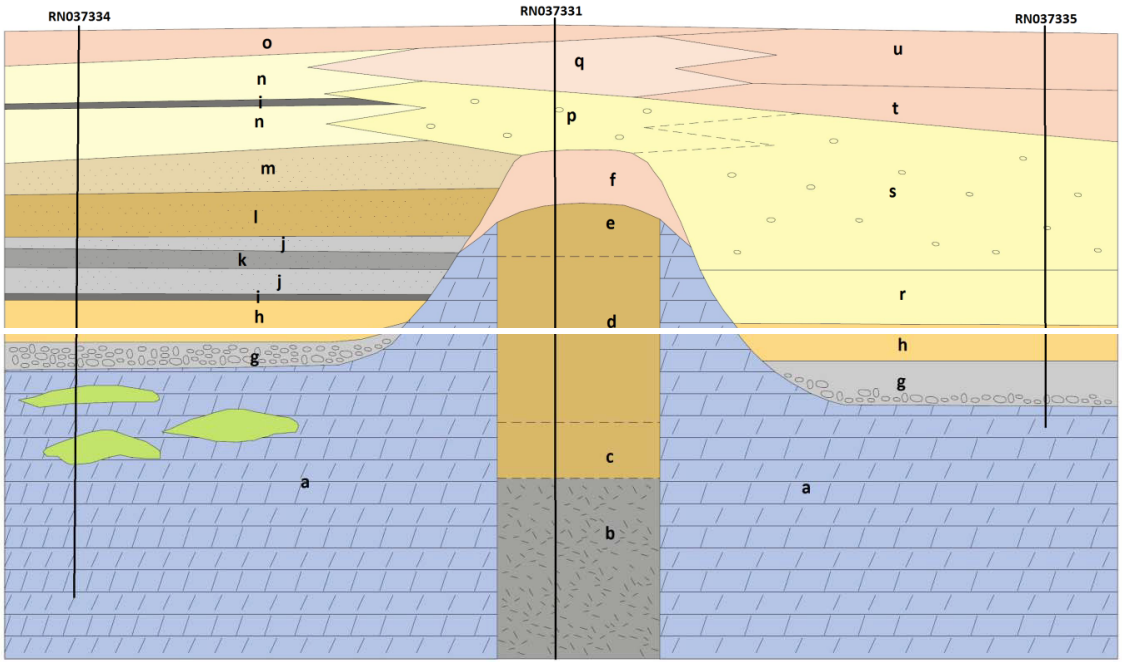

Figure 26: *Schematic view of dolerite dyke which has intruded the Proterozoic KCD and formed a resistant basement ridge overlain by younger Cretaceous rocks and Quaternary sediments. Resistant dolerite ridges are known to occur in several places in the project area and likely have an effect on groundwater flow (modified from Fell-Smith and Sumner, 2011). The labels for rock types are: a – dolostone; b – fresh dolerite; c – chloritic dolerite; d – fragmented dolerite saprolite with relict zeolite vughs; e – brown clay with relict zeolite vughs; f – light red clay of probable dolerite origin; g – grey sand with fragments of dolostone and silicified dolostone; h – yellow sandy clay; I – ironstone; j – grey weak sandstone; k – hard ferruginised sand; l – brown clay; m – mottled clay and some sand; n – beige sandy clay; o – ferruginous sandy clay; p – poorly sorted sand, clay, gravel with ironstone clasts; q – as for p, but no ironstone; r – clayey sand; s – clayey sand with ironstone clasts; t – sandy clay; u – clayey sand.*

3.1.2.1 KCD Zone 1

This aquifer zone occurs in the north of the study area (Gunn Point) and is bounded by distinct structural features. Groundwater contained in the central and northern parts of this zone is confined by the widespread distribution of organic-rich clays with low permeability that occurs in the mid to lower part of the Cretaceous sequence. Basal sand lenses provide the main aquifer sequence but have low storage capacity. Direct recharge may occur in the southern region. Groundwater discharge occurs mainly towards Melacca Creek, and through palaeovalleys incised into the overlying Cretaceous rocks.

3.1.2.2 KCD Zone 2

Groundwater movement within KCD Zone 2 is highly compartmentalised, at least in part by Proterozoic dolerite dykes that have intruded along pre-existing structures. A well defined and highly saline groundwater body occurs within folded strata in a major anticline, and there is only limited connection of this groundwater body to the other parts of the zone. A relatively thin fresh water lens may overlie the saline groundwater in some places. Other parts of KCD Zone 2 lie under the river floodplains and have low capacity to accept direct recharge.

3.1.2.3 KCD Zone 3

This is an area of relatively low salinity around the Lambells Lagoon floodplain. Major NW-directed faults and dolerite dykes, cross-cut by other deformed basement structures, also play an important role in the development of groundwater flow patterns within this zone. Part of KCD Zone 3 also occurs below the Adelaide River floodplain and receives only limited direct recharge. However, the work of Fell-Smith and Sumner (2011) showed that fresh groundwater does occur below the floodplain and encounters the saline water interface approximately 5 km away from the river. Fresh groundwater throughflow moves into this region from the south-west, i.e., the main recharge zone within the area. Direct infiltration to the groundwater system occurs only around Lambells Lagoon.

3.1.2.4 KCD Zone 4

This is the main hydrogeologic zone in the KCD aquifer and occurs between the western and southern extremities of the formation and a major NW-trending dyke. Groundwater bore yields and rock types vary substantially between the five different sub-zones. A topographic high situated west of the Howard River Fault focuses groundwater flow. Recharge mounds develop during the wet season adjacent to the western margin and in the central part of this zone. There is significant rural development that uses the groundwater resources of KCD Zone 4, and major draw-downs occur in the dry season. Natural discharge to springs (e.g., Howard Springs) and baseflow to rivers (e.g., Howard River) also occurs widely across the zone, and supports extensive GDEs in the local area.

3.1.3 Fractured rock aquifers

Fractured rock aquifers may occur in other basement rock formations (Mesoproterozoic and older) that underlie the NT coastal plains region to the east and south-east of Darwin. Complex multi-stage fault systems dissect much of the Proterozoic bedrock and, in places, have created extensive bedrock fracturing and brecciated zones, creating localised enhanced hydraulic conductivity. Groundwater yields range from 2-15 L/s in some highly fractured zones, although the spatial distribution of productive aquifer zones is highly variable. The hydrochemical composition of groundwater in fractured rock aquifers may be locally influenced by the lithologic composition of the host rocks, e.g., groundwater extracted from fractured rock systems in the Whites Formation commonly has elevated iron contents due to the extensive pyrite veining that occurs in this formation.

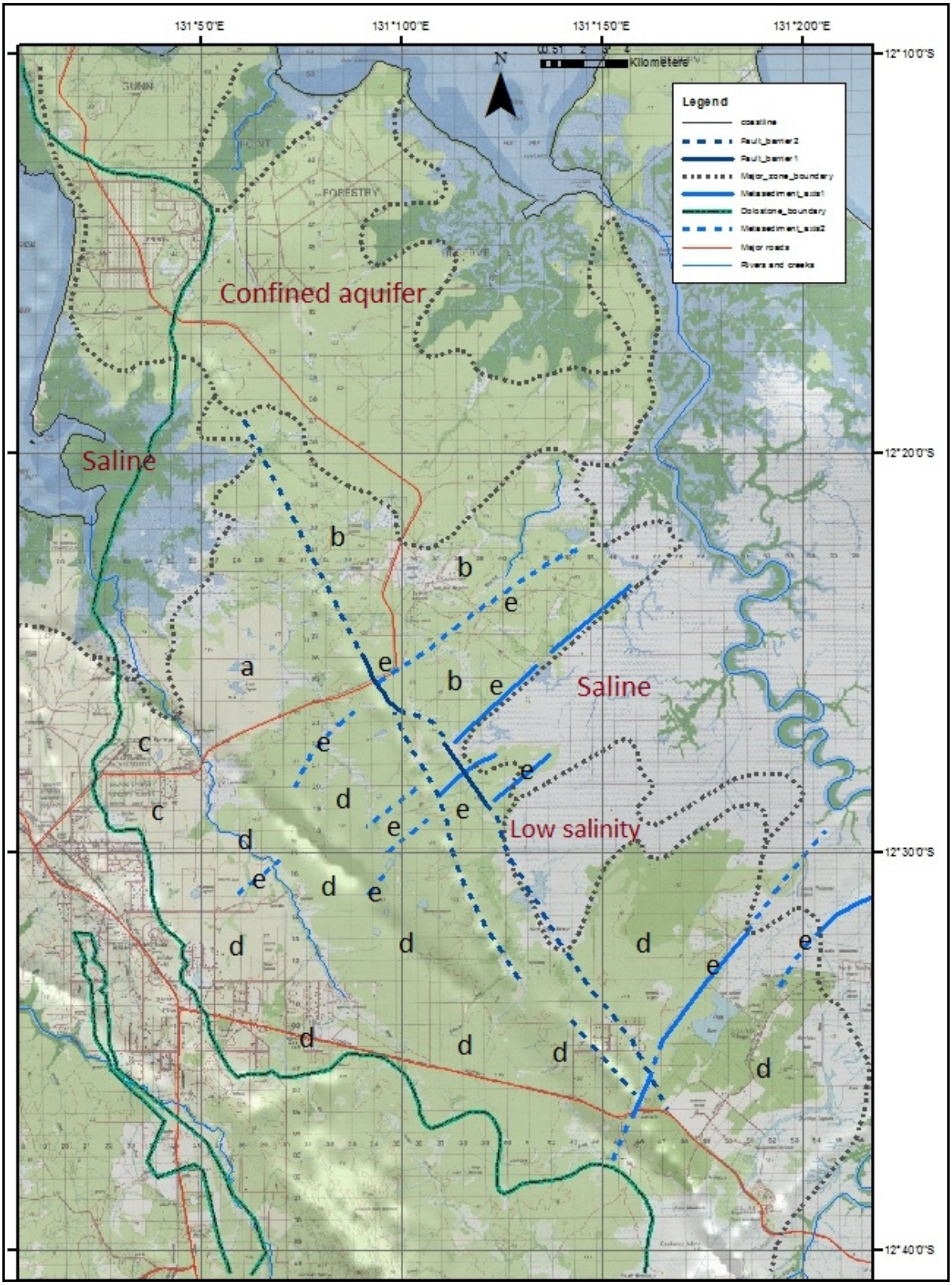

Figure 27: *Hydrogeological zonation of the KCD aquifer as defined by Fell-Smith and Sumner (2011). The major hydrogeologic zones and barriers are depicted on the 1:100,000 topographic map sheet. Sub-zones within Zone 4 of the KCD aquifer are shown as a–e.*

3.2 RECHARGE AND DISCHARGE TO THE KCD AQUIFER

Recharge in the study area occurs during the wet season (Figure 28) as a result of direct infiltration of water into the regional aquifers. The water table is significantly higher at the end of the wet season, especially in the high recharge zones around Howard Springs. In contract, Figure 29 shows a much reduced groundwater mound over the high recharge zone near Howard Springs. Rainfall data show that recharge typically occurs from January to May. In some years, recharge can begin as early as October and end as late as June. Monthly total rainfalls above the threshold level of 165 mm (Cook *et al.,* 1998a, b) are necessary to satisfy the soil moisture deficit. In most cases, this threshold must be reached before rivers will begin to flow and for rainfall seepage to recharge regional aquifers.

Previous hydrologic studies have indicated that the long-term average pre-development recharge over much of the regional Cretaceous cover sequence is approximately 200 mm per hectare per year, e.g., Cook *et al.,* (1998a, b). In areas covered by clay-rich ferruginous duricrust, recharge estimates can be as low as 20 mm per hectare per year due to the low permeability of this material. Recharge to the deeper bedrock aquifer occurs as a result of vertical infiltration through macropores in the overlying ferricrete, saprolite, and Cretaceous sedimentary units (Figure 25). The oldest Cretaceous rocks, named the Howard Sand Member by Doyle (2001), form the most reliable aquifer in the upland regions.

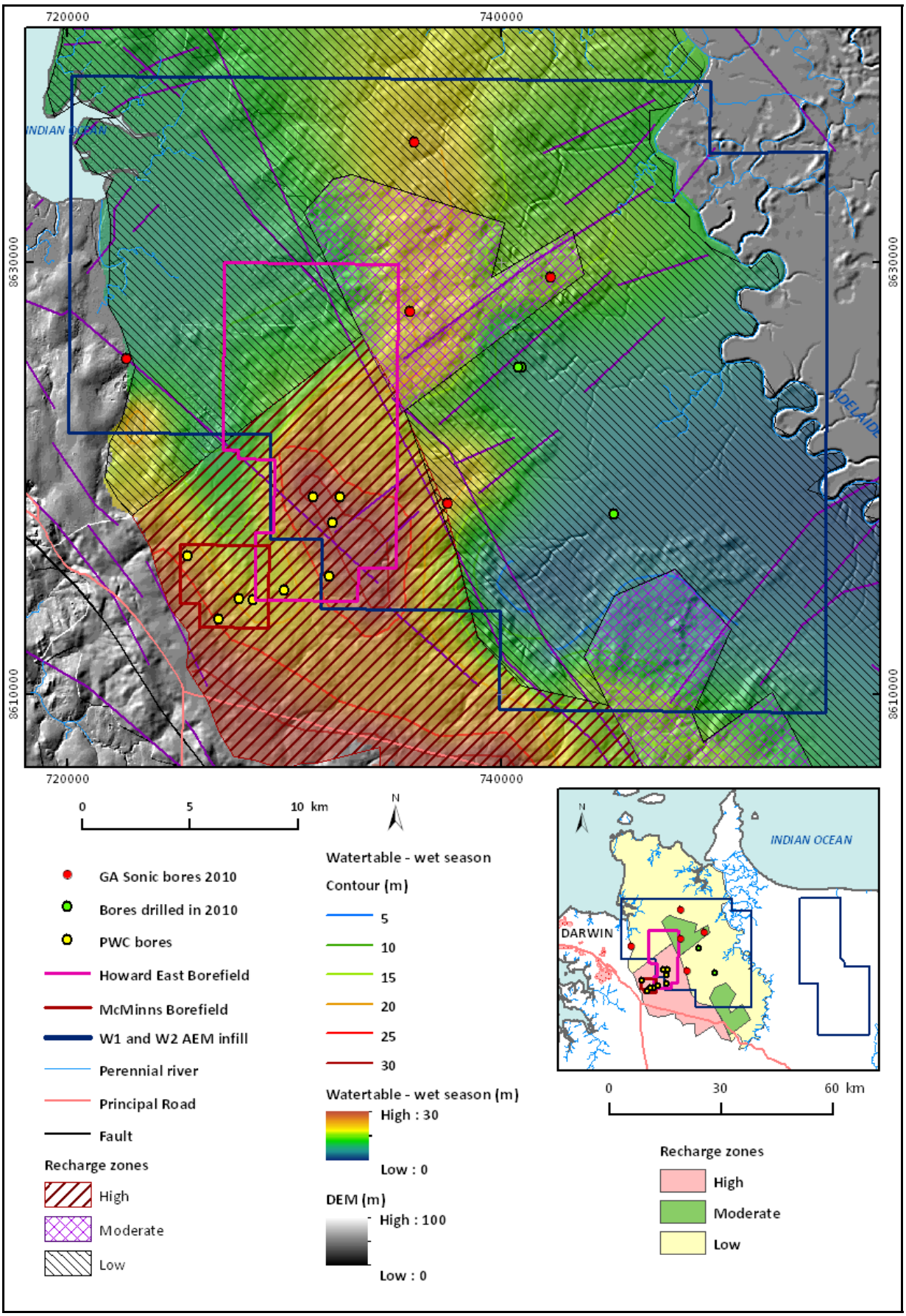

Figure 28. *Water table at the end of the wet season as generated from bore data.*

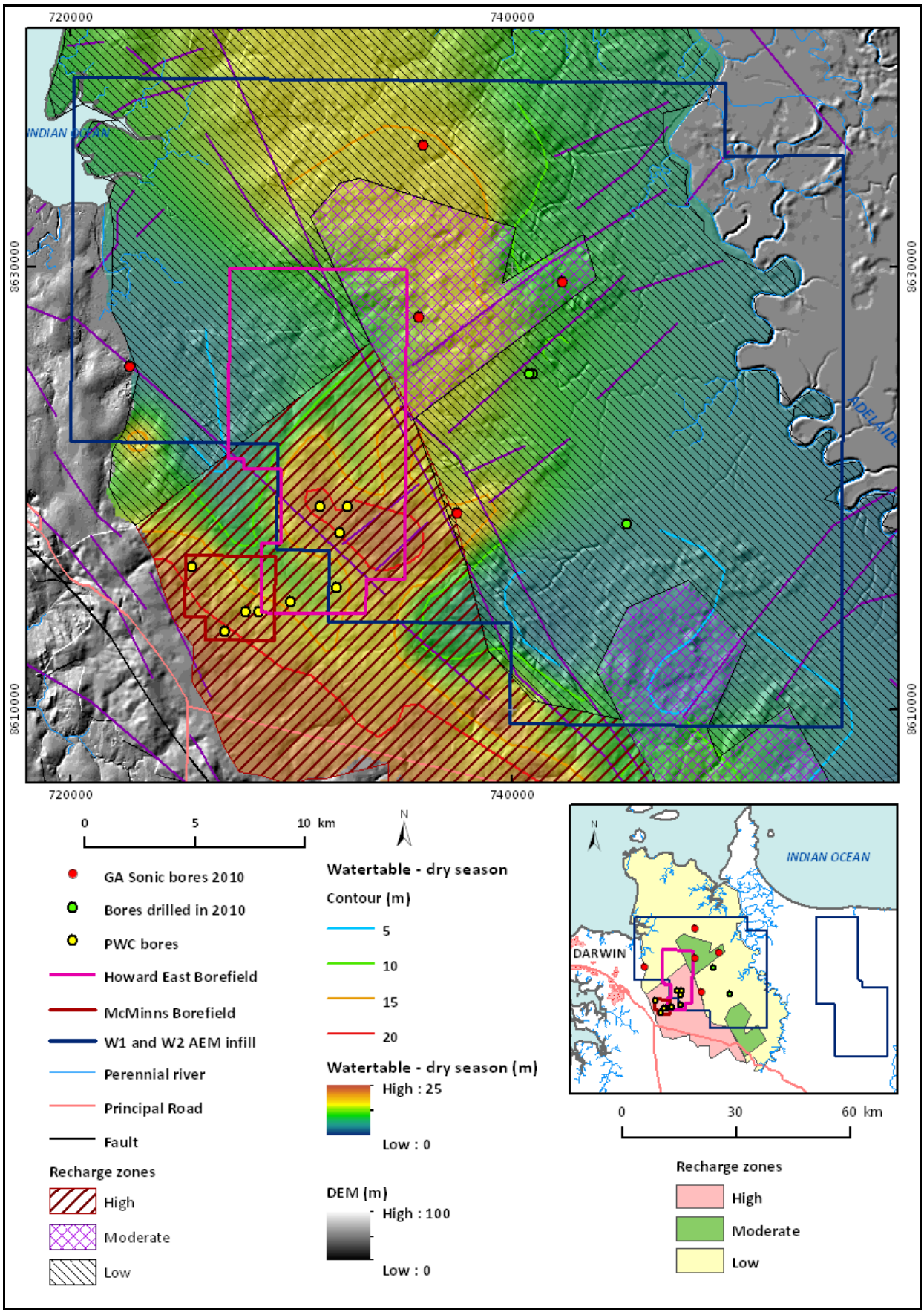

Figure 29. *Water table at the end of the dry season as generated from bore data.*

The silicified upper surface of the Proterozoic unconformity is commonly overlain by a metre or more of the relatively transmissive Howard Sand Member. Sands and gravels have accumulated on the unconformity

filling irregularities in the weathering surface and providing yields of up to 5 L/s. In some of the deeper paleosurface depressions and expansive karstic voids (McFarlane *et al.,* 1995), where significant thicknesses of Howard Sand Member have accumulated, yields may exceed 15 L/s. Extensive fracturing in quartzite and solution cavities in massive cherty dolostone can double this yield.

Fell-Smith and Sumner (2011) used the bicarbonate to chloride ratio of groundwater sampled for the NRETAS *Koolpinyah Dolomite Aquifer Characteristics* project to determine variations in groundwater recharge to the KCD aquifer. The main recharge zone (defined by the highest HCO3:Cl ratios) occurs in the uplands of the south-west compartment of the aquifer, around the Howard River. In this area there are two prominent recharge mounds developed over sand-rich Cretaceous rocks and the underlying Proterozoic basement. Moderate recharge also occurs in two separate areas away from this region, including upland areas of Koolpinyah Station and near Lambells Lagoon and Middle Point. Stable isotope data further indicate that large rainfall events in the wet season provide the main source of recharge to the KCD aquifer (Fell-Smith and Sumner, 2011).

Groundwater flows are controlled by topography and by the ability of the aquifer to transmit water. The direction of groundwater flow is generally based on topographic variations, from relatively high to low elevation. The areas of discharge in the Howard River catchment are the Howard River, the small tributaries that drain into the black soil plains to the east, and subsurface throughflow below Gunn Point (Jolly, 1983). In Figure 31, the direction of groundwater flow is from the topographically higher Howard River area to the Black Jungle Swamp.

The age of groundwater in the Howard River catchment was determined, by measuring tritium activity, to be <25 to 60 years, and 25 to 40 years in the Adelaide River catchment (Radke *et al.,* 1998). These results were consistent with those of Cook *et al.,* (1998a, b) using CFC-12. Fell-Smith and Sumner (2011) undertook a broader program of measuring groundwater residence times in the KCD aquifer away from the Howard East area, using 14C dating. Uncorrected 14C ages ranged from 1,300 to 17,315 years, with three samples having ages of around 15,500 to 17,500 years. Evidence from this hydrogeochemical and groundwater dating study, combined with the AEM data, was used to interpret the existence of highly saline 'fossil' groundwater bodies, which are believed to have developed below the Adelaide River floodplain during the widespread Holocene marine transgression (~6,500 years ago). This 'Big Swamp' phase of landscape evolution was characterised by extensive mangrove development over much of the floodplain (Fell-Smith and Sumner, 2011).

Groundwater discharge predominantly from the KCD aquifer has been observed at only a few sites (Figure 30). These areas are defined on the basis of groundwater dependent ecosystems, such as vine forests. Examples of this type of flow are Melacca Creek and Howard Springs. Flow at Howard Springs varies from 300 L/s in early March, at the peak of the wet season, to 20 L/s or less at the end of the dry. The schematic model for groundwater flow at Howard Springs is shown in Figure 32.

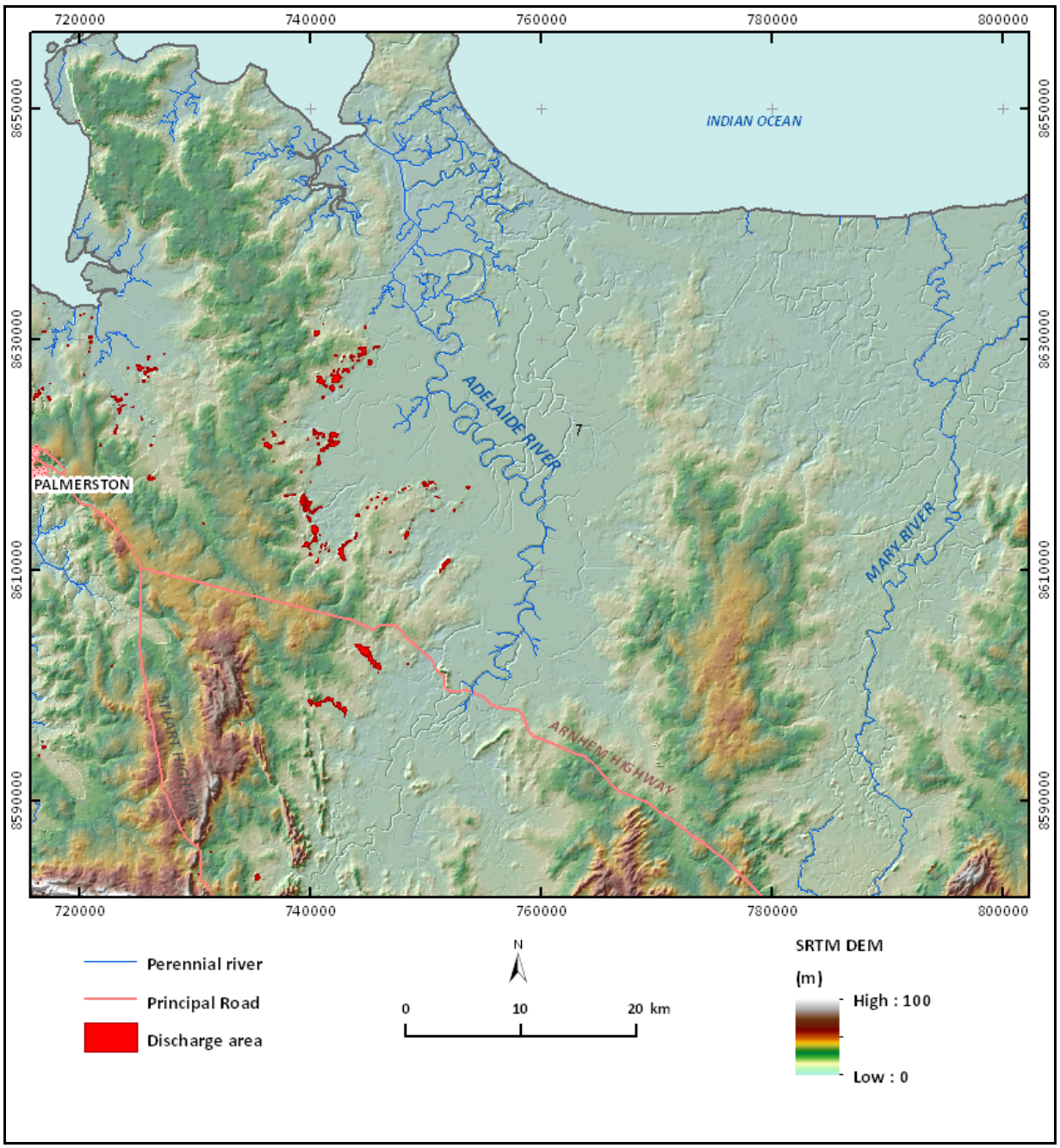

Figure 30: *Discharge areas as indicated from distribution of groundwater dependent ecosystems.*

3.3 SEASONAL VARIABILITY

The process of shallow groundwater drainage begins at the end of the wet season. Areas of higher elevation dry-out earlier than areas of low elevation. In general, end of dry season surface discharges from groundwater are associated with areas of lower elevation. Figure 31 shows schematic cross-sections of the annual flow regimes in the Howard River from the wet season to the end of the dry season. At the end of the dry season, there are areas of wetland that persist after the surrounding region has been drained of shallow groundwater. This process forms "perched lagoons" in areas where ground depressions have caused ponding of wet season rainfall. The base of the wetland has a layer of organic mud that acts as a semi-impermeable boundary. The rate of evaporation of the lagoons is approximately 2 metres per year. In comparison, the regional water table drops an average of 8-10 m from the peak of the wet season to the end of the dry season (in some places up to ~15 m variation). As a result, the shallow depressions, which form the "perched lagoons", are left above the water table. There are numerous examples of this phenomenon throughout the upland regions.

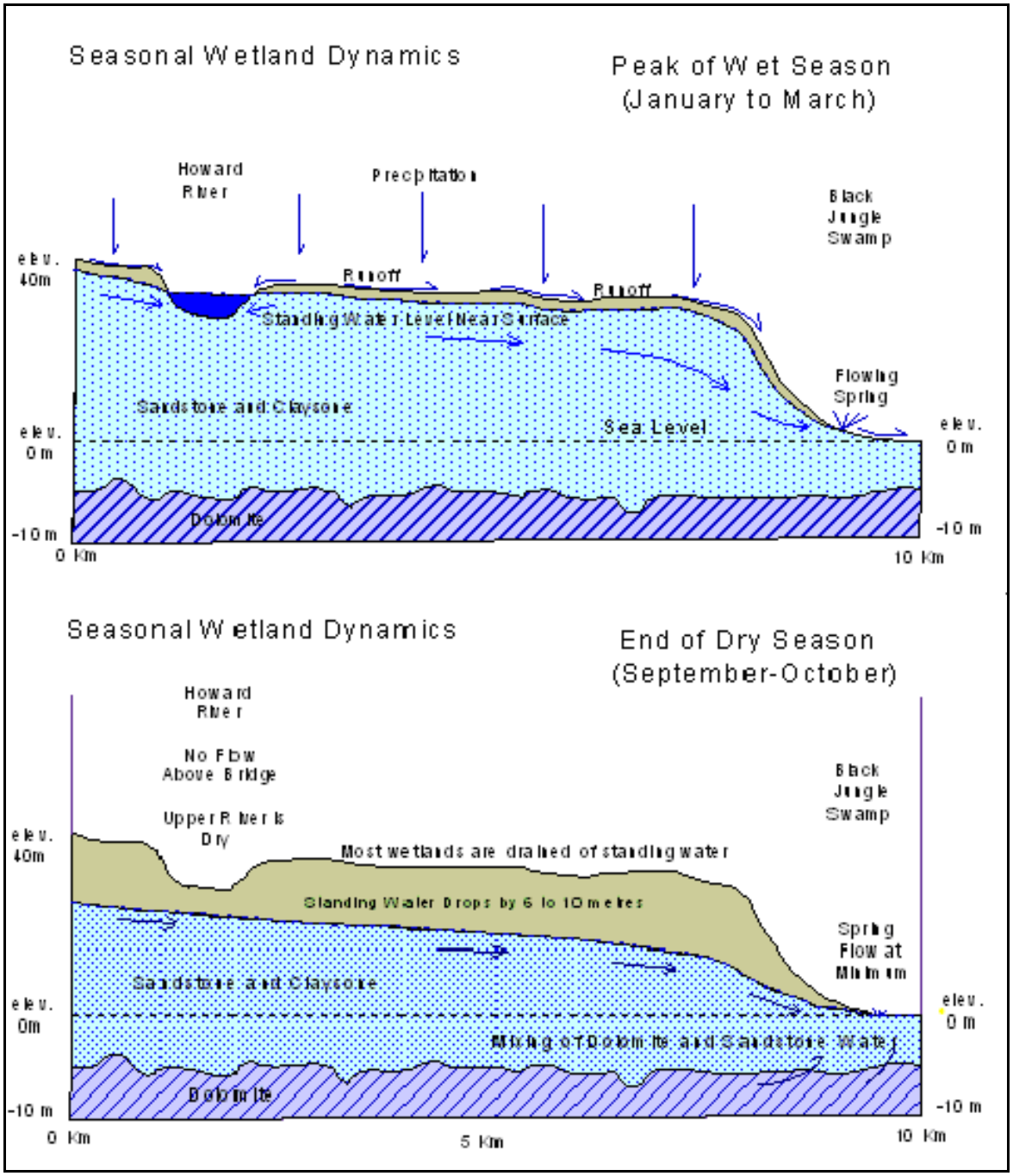

Figure 31: *Seasonal wetland dynamics of the Howard River and Black Jungle region (adapted from Haig &Townsend, 2003).*

Howard Springs, Howard River, Black Jungle and Holland's Creek, show seasonal change in water quality (Table 3). Early dry season chemical analyses of spring discharge indicate that the water source is the shallow Cretaceous aquifer. By the end of the dry season there is a change in water chemistry that indicates the discharge water is derived from both the shallow aquifer and from the deeper dolomite aquifer.

Seasonal groundwater levels tend to vary by 8 m in the undeveloped parts of the upland study area. Extraction in developed areas has increased this to 12 m. Groundwater usually comes to within 2 m of the surface at the peak of its oscillation. The groundwater level trend is increasing slightly in undeveloped areas and falling moderately in the developed areas.

Table 3: *Reported springs flowing from dolostone aquifers in the study region with historical range of electrical conductivity (EC) and pH data (after Tien, 2006).*

NAME	EASTING	NORTHING	EC (µS/cm)	pH
Howard Springs Reserve At Spring	723030	8621960	340-360	7.1-7.9
Howard River At Koolpinyah Stn	726430	8621410	280-380	7.0-7.8
Black Jungle Creek At Spring	740530	8612860	360	7.5
Black Jungle Spring Near G8170083	741030	8612360	42	7.5
Holland's Creek At Black Jungle	740130	8611560	337-370	7.2-7.5

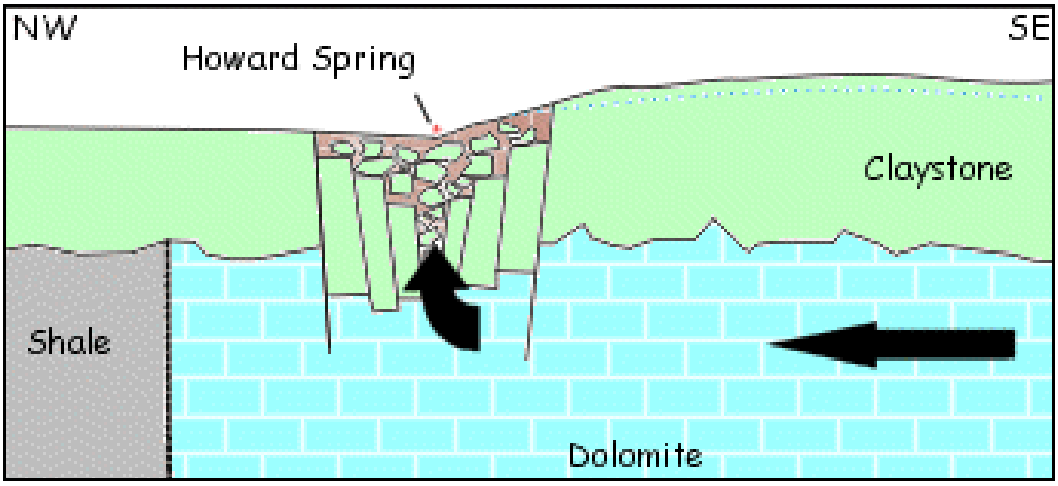

Figure 32: *Schematic cross-section of Howard Springs (source: NRETAS website).*

3.4 HYDROCHEMISTRY

Groundwater in the Darwin region can be broadly grouped into three main categories (Verma, 2002): i) fresh carbonate water, ii) fresh non-carbonate water and iii) saline water. Water quality is a function of various parameters, such as the aquifer type, distance from the sea, time the water has spent in contact with the aquifer material and distance from the recharge source.

Fresh carbonate water comes from the deeper, dolomite aquifer and carbonate rocks. This water tends to be alkaline and hard; pH ranges from 7 to 9 with hardness values averaging about 150 mg/l. The water is potable, with total dissolved solids ranging from 200 to 500 mg/l (Verma, 2002). The water chemistry of typical fresh carbonate water from Howard Springs is shown in Table 4.

Fresh non-carbonate water is found in the Cretaceous sandstones of the shallow aquifer, or other non-carbonate rocks. The water is similar to rain water in that it is acidic, with a pH that ranges from 5 to 7. The water tends to be soft and has low total dissolved solids that tend to be lower than those of the carbonate rocks.

In coastal areas subject to tidal influence, groundwater tends to be brackish with salinity levels greater than 1,000 mg/l. Salinity levels above 1,000 mg/l are considered undesirable for human consumption and give water a salty taste. Acceptable salinity levels for irrigating crops depend on many factors, such as soil type, drainage and vegetation type. Salt tolerant crops are highly variable and may span a range from 500 to 3,500 mg/l. Salinity levels of 4,000-5,000 mg/l are the maximum limits to which stock can adapt without loss of production (ANZECC, 2000). Depending on the proximity of the marine environment, salinity levels can be as high as 60,000 mg/l (Verma, 2002).

Groundwater within the aquifers constitutes a mixing system with recharged rainfall and intruded seawater as end members. Ionic ratios comparable to seawater (e.g., Cl/Br), and mixing curves interpreted from 36C1/C1 ratios, indicate a seawater component of up to 0.2% within the aquifers in the lower Howard and Adelaide River (Harrison Dam area) catchments. The variable fracturing and inferred preferential flow paths of high transmissivity in the KCD, as well as its presence down to 20 m below sea-level confers vulnerability to increased salinisation by seawater intrusion when groundwater abstraction exceeds annual recharge (Radke *et al.,* 1998).

Table 4: *Typical composition of fresh carbonated groundwater from Howard Springs (data from NRETAS website).*

GROUNDWATER COMPOSITION		
TDS	(mg/l)	170
Conductivity	(µS/cm)	320
pH		7.4
Temperature	(°C)	30
Sodium	(mg/l)	3
Potassium	(mg/l)	1
Calcium	(mg/l)	37
Magnesium	(mg/l)	17
Hardness	(mg/l)	163
Chloride	(mg/l)	6
Sulfate	(mg/l)	2
Bicarbonate)	(mg/l	198
Fluoride	(mg/l)	0.1
Silica	(mg/l)	14

Radke *et al.,* (1998) reported that groundwaters from weathered dolostone contain relatively low concentrations of inorganic trace elements, although some areas exceed the aesthetic value for iron (0.3 mg/l). Fell-Smith and Sumner indicated that higher iron contents mostly occur in the KCD aquifer adjacent to the Whites Formation. This is mainly because pyrite veining is extensive in the Whites Formation and leaching of pyrite leads to increased levels of iron in groundwater. Further analytical work by Fell-Smith and Sumner (2011) largely confirmed the earlier work of Radke *et al.,* (1998) in that trace element concentrations are low (i.e., below recommended drinking water limits) for most inorganic constituents. However, faecal indicator bacteria are widespread in groundwater within the developed rural areas. The bacteria are suspected to originate from either the poor standard of head works for private bores or septic tanks occurring near bores on domestic blocks. *Burkholderia Pseudomallei* was detected in 14% of samples. Later work by the Menzies School of Health (Mayo *et al.,* 2011) detected *B. Pseudomallei* in 30% of domestic bores.

3.5 WATER MANAGEMENT

The management and protection of regional water resources is controlled under the Water Act 1992 and the National Water Quality Management Strategy (NWQMS). The Water Act declares the extent to which both surface water and groundwater can be used and for what purposes. Through the declaration of "beneficial users", management goals are set to determine how and why the community and government want to protect, manage and use the water resource (Wood, 2002). Seven beneficial uses have been identified and are listed in Table 5. The categories of beneficial use have been modified from, but are consistent with, those of the Australian and New Zealand Environment and Conservation Council (ANZECC, 1992).

Table 5: *Beneficial water use categories.*

BENEFICIAL USE	DESCRIPTION
Environment	Maintain the health of aquatic ecosystems
Cultural	Aesthetic, recreational and cultural needs
Agricultural	Irrigation water for primary production
Public Water Supply	Drinking purposes delivered through community water supply systems
Manufacturing and Industry	Secondary industry
Riparian	Public rights and ownership to take water for domestic and stock purposes
Aquaculture	Commercial production of aquatic animals

The McMinns Borefield has been in production as a public water supply since 1971. The groundwater extracted represents approximately 10% of the total municipal water supply with the remainder coming from Darwin River Dam. The borefield has a total of six production bores, but only three bores are used at any given time. The NT Power and Water Corporation are licensed to extract up to 8.4 GL/year but currently draw 5 GL/year.

Table 6: *Estimation of groundwater consumption in the Darwin Rural Area (*metered value).*

MAJOR USE	CONSUMPTION (ML/YEAR)
Domestic bores in the rural area	12,000
Agricultural bores in the rural area	13,500
Power and Water bores at McMinns borefield	4,992*

The total number of producing bores in the Darwin Rural Area is approximately 3,000 (Figure 33), with around 75 new bores drilled each year. Approximately 400 irrigation bores are in use. Bores pumping greater than 15 l/s require an extraction licence and are required to report volume usage. The groundwater consumption levels for domestic and agricultural bores presented in Table 6 were estimated by M. Miles (2011, pers. comm.).

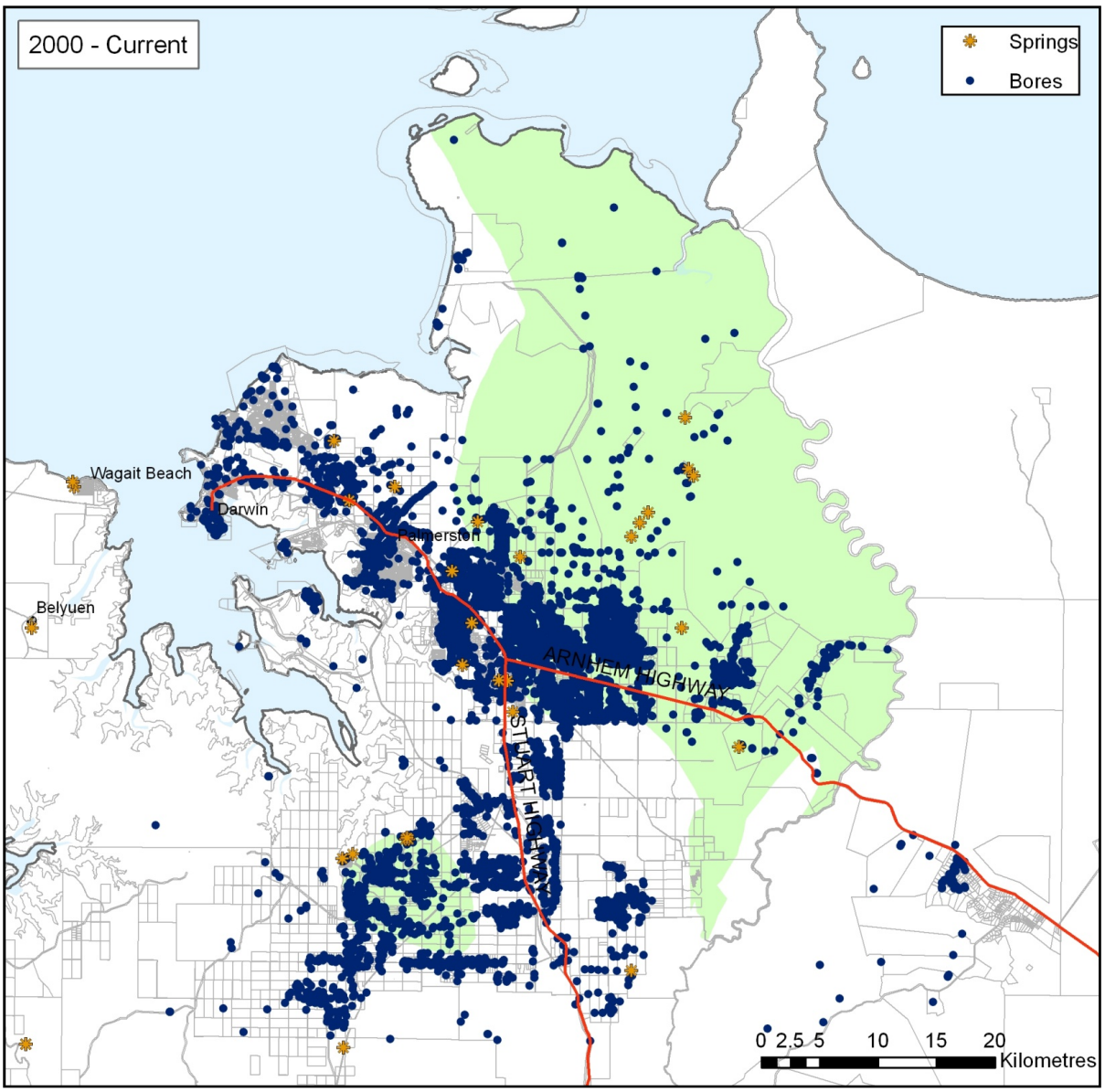

Figure 33: *Distribution of bores and groundwater use for agriculture in the Darwin Rural Area. The region in green is the Howard East Water Allocation Plan area.*

4 Project Data Acquisition and Analytical Methodology

4.1 PREVIOUS STUDIES AND APPLICATIONS OF AEM FOR SEAWATER INTRUSION MAPPING AND MANAGEMENT

A review facilitated by the Australian Academy of Sciences and the Australian Academy of Technological Sciences and Engineering for the Australian Federal Government's Natural Resource Management Ministerial Council in 2005 found that airborne geophysical techniques, combined with ground and borehole control, are important tools in understanding salinity and hydrology at depth at a variety of scales. The review also concluded that the only broadacre, remote sensing technique that can detect and resolve groundwater salinity in the sub-surface deeper than the root zone is airborne electromagnetics (Spies and Woodgate, 2005).

A wide range of AEM systems and acquisition platforms are available (Allen, 2005; Spies *and* Woodgate, 2005), and the technology is now recognised as mature, capable of mapping complex salinity relationships in a variety of landscape settings. AEM systems cover large areas rapidly and generally penetrate to significant depths, often providing important broader contextual information on hydrogeological systems. AEM systems also provide a logistical advantage in being able to acquire data systematically over difficult or inaccessible terrane. Borehole EM technologies provide important constraints on sub-surface salinity distribution and are an essential component in calibration and validation of AEM inversions; ground-EM and in-river EM systems are particularly effective at mapping near-surface salinity with high resolution (Allen, 2005; Spies and Woodgate, 2005).

George *et al*. (2003) emphasised the need to match the appropriate technology to the groundwater salinity management issues to be addressed, and articulated a phased methodology to achieve a successful management outcome using airborne geophysics. Based largely on the lessons articulated by George *et al*. (2003), AEM surveys have increasingly been designed over the past 6 years to address specific land and groundwater management questions within the context of broader natural resource management strategies (Walker *et al*., 2004). Using this approach, a number of AEM surveys have been shown to be cost-effective in addressing salinity and land management issues (Lawrie *et al*., 2003a, b, 2008, 2009a, b; Walker *et al*., 2004; Munday *et al*., 2007, 2008). Overall, this approach has played a crucial role in demonstrating the relevance of AEM-based information products for salinity, groundwater and broader land and environmental management (Munday *et al*., 2003 a, b; Paine, 2003; Walker *et al*., 2004; Chamberlain *and* Wilkinson, 2004; Lawrie, 2006b; Cresswell *et al*., 2007; Lawrie *et al*., 2009a, b). Successful outcomes from these projects have been attributed not just to advances in science, technology, project design, the calibration and validation of AEM data, and development of customised information products (George *et al*., 2003; Spies *and* Woodgate, 2005), but also to a high level of consultation between scientists, decision makers and local community groups at all stages in project design, implementation, delivery, knowledge transfer and follow-through (Walker *et al*., 2004).

AEM data is particularly useful in helping to map the distribution and extent of seawater intrusion (SWI) in near-coastal aquifers due to the elevated sub-surface conductivity contrasts that exists between saline and fresh groundwater. Previous SWI investigations using AEM data have occurred in the USA (Fitterman *and* Deszcz-Pan, 1998), Indonesia (Siemon and Steuer, 2011), Mexico (Supper *et al*., 2009) and the Galapagos Islands (D'Ozouville *et al*., 2008). Prior to this study AEM has been used to map SWI in Coffin Bay (Munday *et al*., 2007; Auken *et al*., 2009a; Ward *et al*., 2009), and more recently in the Gascoyne coastal region (Munday, pers. comm. 2011).

The benefits from AEM surveys are maximised when these technologies are employed within multi-disciplinary, systems-based approaches to the analysis of problems and the development of customised interpretation products (Lawrie *et al*., 2000; Lawrie *et al*., 2003a, b; Spies and Woodgate, 2005). Systems-based approaches incorporate an understanding of landscape evolution and scale, utilise modern investigative

approaches to the conceptualisation of aquifer systems, and incorporates data on water, salinity and vegetation dynamics to provide key constraints on aquifer systems (Lawrie *et al*., 2000, 2008, 2009a).

Over the past 5 years, a staged approach to survey design combined with forward modelling studies have ensured that appropriate AEM technologies are selected to match the target objectives (Green and Munday, 2004; Lawrie, 2006; Munday *et al*., 2007, 2008d; Lawrie *et al*., 2009a, b). In Australian landscape settings AEM-based products are particularly effective at providing high resolution baseline data on the spatial distribution of aquifers and aquitards as well as water quality and salt stores in shallow (<120m) floodplain sediments (Mullen *et al*., 2007; Tan *et al*., 2005; Munday *et al*., 2006, 2007; Lawrie *et al*., 2009a). However, while these datasets and information products address specific gaps in the biophysical knowledge framework, addressing salinity and land management questions usually requires an understanding of underlying biophysical processes and dynamics that often cannot reliably be determined from analysis of spatial patters of conductivity alone (Cresswell *et al*., 2007).

While increasing sophistication of AEM-derived products (e.g. porosity-corrected lithology products, maps of salt load, salt hazard etc; Tan *et al*., 2009) has improved their utility and up-take by land managers, much of the success of AEM surveys in the past 5 years has come from demonstration of relevance through incorporation of AEM-derived products in regional planning and decision support tools and in groundwater modelling frameworks (Chamberlain and Wilkinson, 2004; Walker *et al*., 2004). The high resolution (in 2D and 3D) afforded by AEM datasets enables key elements of the hydrogeological system to be mapped and characterised with greater certainty. This has contributed to improved parameterisation of models, and enables more reliable quantitative assessments to be made of the uncertainties and confidence levels in model predictions. It is the adoption of these multi-disciplinary, multi-scale system approaches that underpin the development of more effective salinity and groundwater management strategies, and enable more targeted salinity management actions (Lawrie, 2008; Lawrie *et al*., 2009a).

To date, a large variety of modelling approaches have incorporated AEM-derived products, reflecting the diversity of salinity management questions tackled. The approaches vary from GIS-based modelling platforms to fully distributed groundwater flow models. For example, building on the availability of a number of AEM surveys that have been conducted along the River Murray, modelling studies include: the impacts of broad-scale land use planning including land clearing along the River Murray (RCSM: Walker *et al*., 2005; Doble *et al*., 2005, 2008); salt loads in the Murray River (SIMPACT; Wang *et al*., 2005); the links between groundwater processes, evapotranspiration and vegetation health (WINDS; Munday *et al*., 2008c); leakage from salinity disposal basins (Munday *et al*., 2008), and the potential impacts of flooding and environmental watering in the River Murray Corridor using fully distributed finite difference (MODFLOW) groundwater models (Richardson *et al*., 2007; Yan *and* Howe, 2008; H. Middlemass, pers. com. 2008).

In particular, new insights into the lateral and vertical connectivity of the aquifer systems are required to assist with groundwater management. Similarly, new insights into distribution of sand and gravel aquifers in 3D are required to better understand the extent of surface-groundwater interactions, and to identify preferential recharge and infrastructure leakage in the landscape. These are essential to improve the management of surface water, groundwater, salinity, and broader environmental management. To constrain the hydrogeological models it is necessary to better map water quality (salinity), aquifer boundaries, and elements of the sedimentary system, particularly the upper and lower gravels and their connectivity, as groundwater flow is highest through these units. Gaining a better understanding of where the potential increased evaporation and or discharge zones occur would also be desirable. Ultimately, it will be necessary to construct an improved 3D map of the aquifer systems.

The power and long-term value of AEM-based datasets for salinity management lies largely in providing stakeholders with a range of customised information products that help address specific salinity and land management questions (George *et al*., 2003). This necessitates translating conductivity measurements to estimates of salinity extent, salt hazard and ‘loads’ and groundwater quality, and requires the differentiation of host lithologies and other hydraulic parameters (such as texture and porosity) acquired through drilling.

To address most questions other than those related simply to salinity extent, it is also necessary to relate these map-based products to an understanding of salinity dynamics and processes by carrying out hydrogeochemical studies and incorporating the AEM-derived products within hydrogeological and land use models (Walker *et al*., 2004; Cresswell *et al*., 2007).

The NTCP project AEM data was acquired utilising an AEM system (TEMPEST) selected for regional energy and mineral mapping purposes, rather than its ability to map key elements of the hydrogeological system related to SWI. Nevertheless, TEMPEST data has been used successfully to map groundwater salinity in a range of environments Lane *et al*., 2002; Chamberlain *and* Wilkinson, 2004). In this study, there was limited drilling data available however a multi-disciplinary approach was taken to the generation of interpretation products.

4.2 ELEVATION DATA

Accurate high resolution elevation data is critical in the generation of AEM-derived products. Without accurate surface information, interpretation of any features at depth is not possible. Initially released AEM products (Tan *et al*., 2011) were hung off a gridded 5 km Digital Elevation Model (DEM; Figure 34) that was unsuitable for near-surface mapping. Elevation data at this resolution is not fit for use in such mapping studies. Final AEM-derived products discussed in this report were hung off a Shuttle Radar Topography Mission (SRTM) 1-second, hydrologically enforced DEM (H-DEM; Figure 35). This dataset has a spatial resolution of 30 m, an absolute geolocation error of 7.2m, an absolute height error of 6 m and a relative height error of 4.7 m (Rodriguez *et al*., 2006). Figure 34, Figure 35 and Figure 36 shows scatter plots comparing the elevation data from the two DEMs with respect to the spot elevations. The SRTM H-DEM has a better fit than the initial DEM.

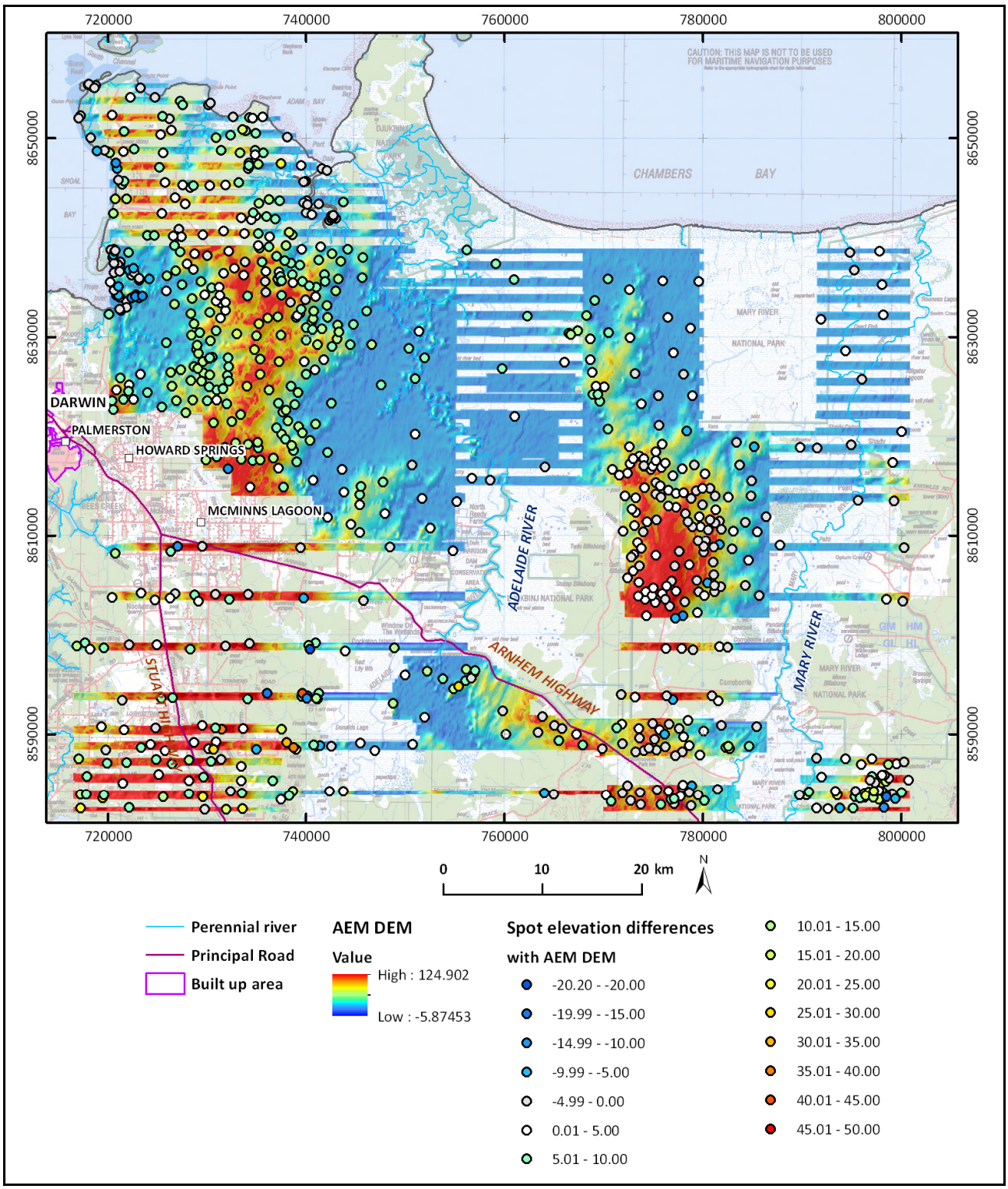

Figure 34. *Difference between initial DEM used for AEM inversion and spot elevations.*

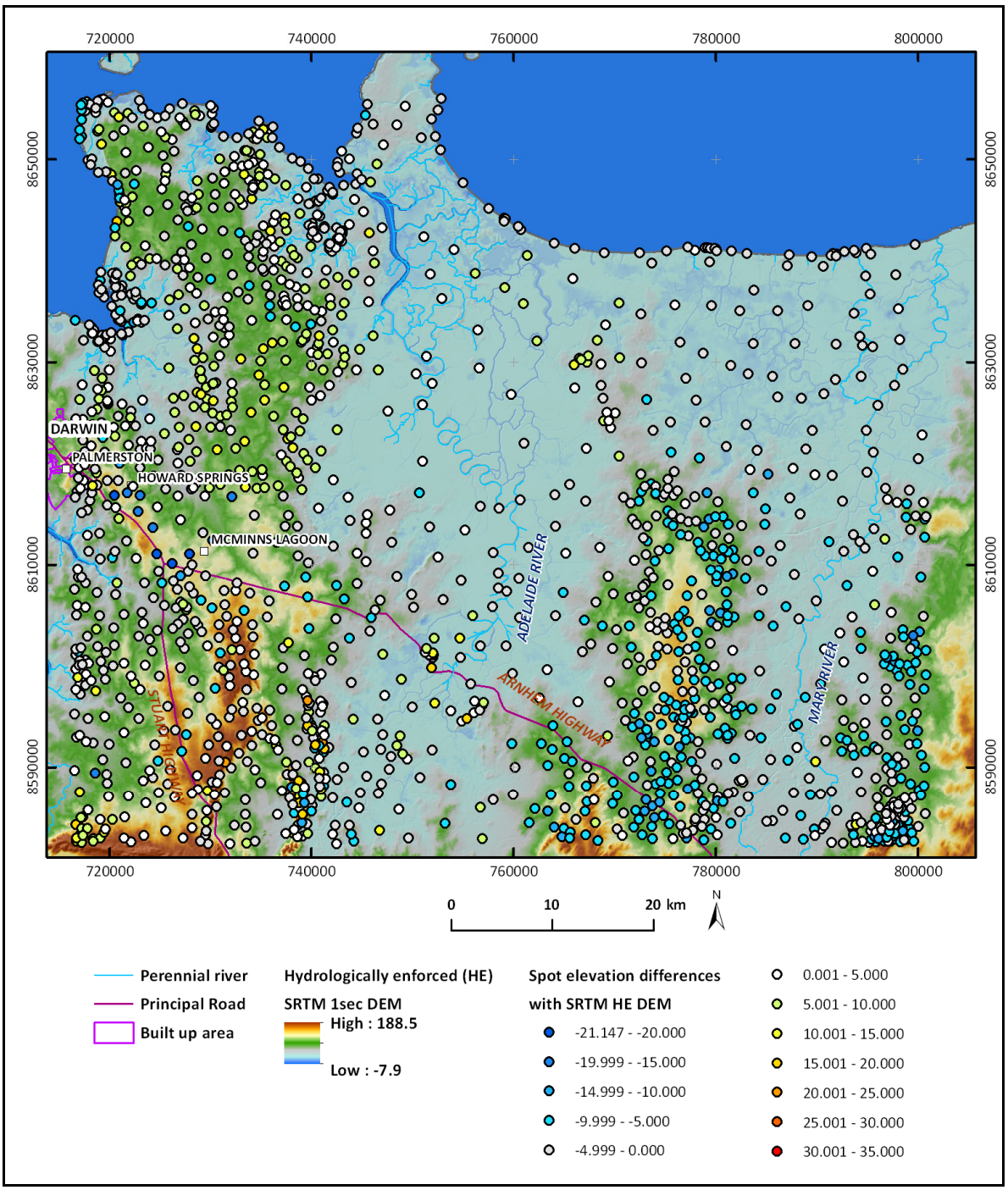

Figure 35. *Difference between hydrologically enforced SRTM 1 second DEM and spot elevations.*

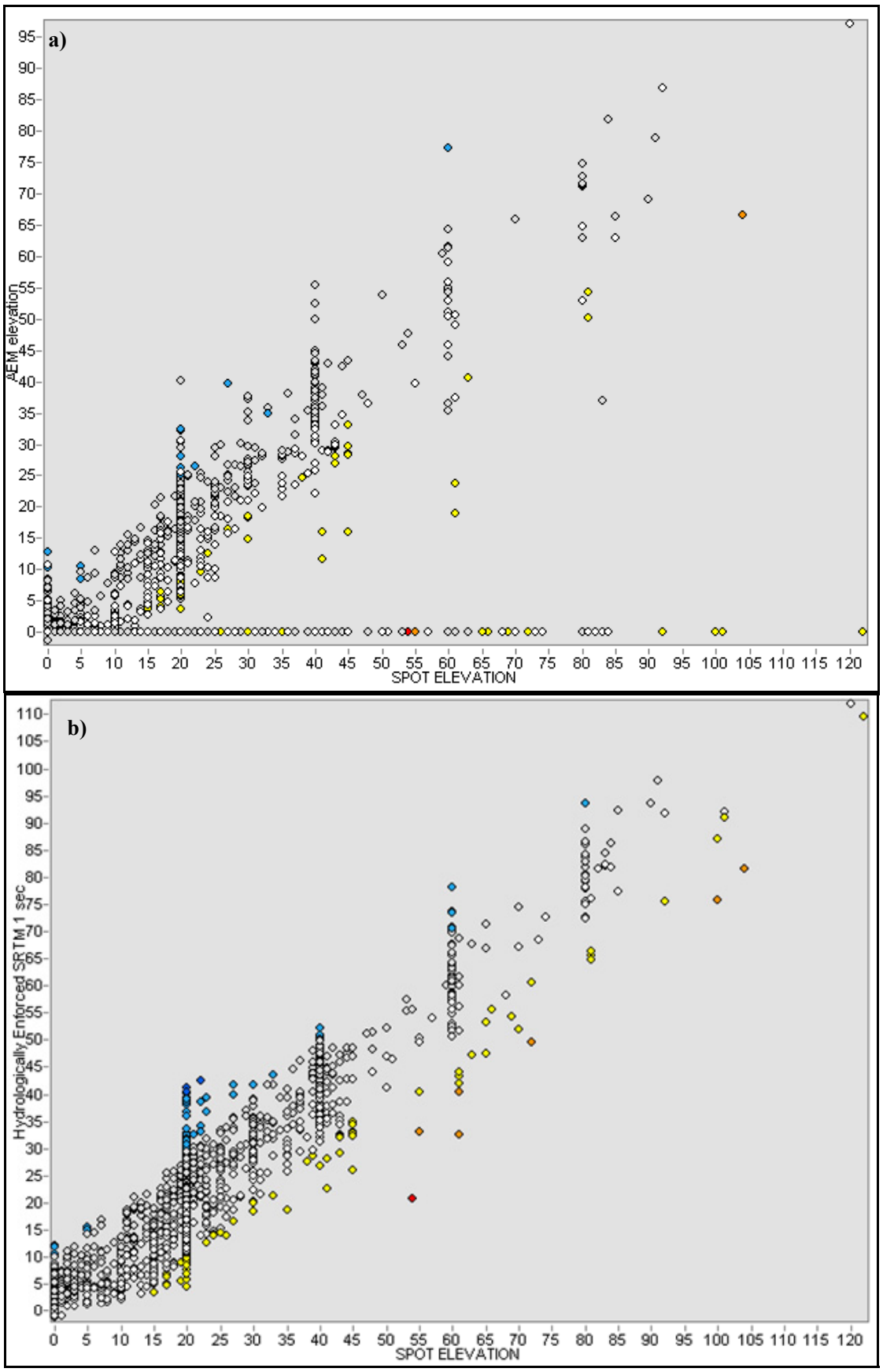

Figure 36. *Scatter plots comparing elevation between spot heights and a) initial DEM and b) hydrologically enforced DEM.*

4.3 AIRBORNE ELECTROMAGNETICS

4.3.1 Introduction

Fugro Airborne Surveys (FAS) were contracted to fly the AEM surveys using their TEMPEST™ system during 2008-2009. A total of 21,100 line km of data were acquired along variably spaced flight lines (Figure 37), a subset of which was used for the NT Coastal Plain project. Survey lines funded by Geoscience Australia were flown at 1,666 and 5,000 m spacings, and the National Water Commission lines were flown at a spacing of 555 m. The FAS contractor supplied data were publicly released by Geoscience Australia in 2009 (Costelloe and Hutchinson 2010).

4.3.2 TEMPEST™ AEM system

The following data acquisition section is taken from Costelloe and Hutchinson (2010) with modification where required. The TEMPEST AEM System (Lane *et al.,* 2000) used in the survey was installed on two aircraft (Figure 32). A summary of the system configuration is shown in Table 7. The survey areas, acquisition and processing of the survey data are detailed in Lawrence and Stenning (2009a) and Lawrence and Stenning (2009 b) respectively.

The TEMPEST system is a fixed-wing time-domain system. It employs an approximate square-wave 50% duty cycle current waveform with a base frequency of 25 Hz. The current is transmitted through a single turn transmitter (TX) loop draped around the nose, wings and tail of the aircraft. The survey was flown with the TX loop at 122 m above ground level (average height).

The receiver (RX) coils are housed in a 'bird' towed approximately 120 m behind and 35 m below the aircraft. The RX consists of three orthogonal coils that sense the rate of change of the magnetic field (dB/dt) flux threading each coil. The axes of the three coils are nominally aligned in the horizontal flight line direction (X-component), horizontal direction perpendicular to the flight line (Y-component), and vertical directions (Z-component). However, only the X- and Z-components are recorded and processed at full resolution and thus available for interpretation.

The TX height and the orientations and relative separations of the TX and RX are known as the system geometry. The system geometry continuously varies as the aircraft moves along each flight line. The TEMPEST instrumentation includes a GPS unit to measure the aircraft's horizontal position, radar and laser altimeters to measure its height above ground level, and gyroscopes to measure its roll, pitch and yaw angles (i.e. its orientation). The relative separations of the TX and RX and the orientation of the RX are not measured by the system because of the logistical difficulty in doing so.

Since the system geometry affects the measured response, it must be used as an input into quantitative forward modelling, and hence estimation of subsurface conductivity from the recorded data. Therefore, in the data processing the unmeasured elements of the system geometry need to be estimated. For the TEMPEST system this involves separation of the measured total field response into its primary field (due to direct coupling between TX and RX) and secondary field (due to eddy currents induced in the ground) components. This requires an assumption to be made about the unknown subsurface conductivity, which typically is that the subsurface is resistive at depth. Once separated into primary and secondary components, the horizontal and vertical offsets between the TX and RX can be analytically determined from the primary field if it is assumed that the receiver bird is orientated with zero roll, pitch and yaw. It is these estimated and assumed values of system geometry that are taken to be the real values in standard algorithms for estimating subsurface conductivity from the measured data.

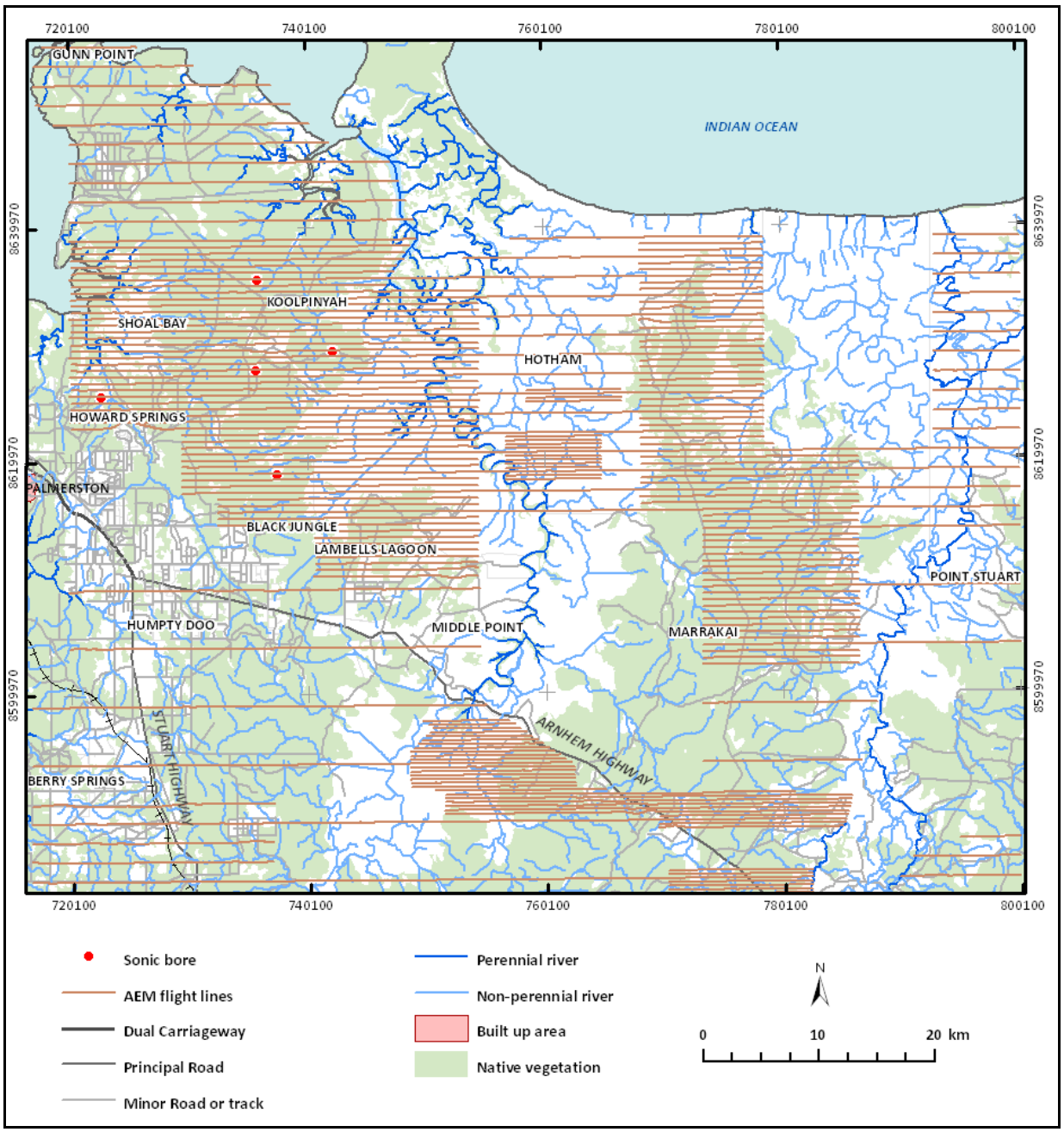

Figure 37: *AEM survey flight lines in the project area.*

Figure 38: *The two aircraft used for the TEMPEST survey. A: modified CASA 212-200 Aviocar registration VH-TEM. B: modified Shorts SC-7 Skyvan registration VH-WGT.*

Table 7: *TEMPEST AEM system specifications (from Lane et al., 2000).*

FEATURE	SPECIFICATION
Base frequency	25 Hz
Transmitter area	221 m2 (VH-TEM)
Transmitter turns	1
Waveform	Square
Duty cycle	50%
Transmitter pulse width	10 ms
Transmitter off time	10 ms
Peak current	280 A (VH-TEM)
Peak moment	61880 Am^2 (VH-TEM)
Average moment	30940 Am^2 (VH-TEM)
Sample rate	75 kHz on X and Z
Sample interval	13.333 microseconds
Samples per half cycle	1500
System bandwidth	25 Hz to 37.5 kHz
TX Loop flying height (nominal)	121.1 m (subject to safety considerations)
TX Loop flying height (average)	122.4 (VH-TEM)
EM sensor	Towed bird with 3 component dB/dt coils
TX Rx horizontal separation average	120.1 (VH-TEM)
TX Rx vertical separation average	34.5 (VH-TEM)
TX Rx horizontal separation standard	120 m (geometry corrected standard)
TX Rx vertical separation standard	35 m (geometry corrected standard)
Stacked data output interval	200 ms (~12 m)
Number of output windows	15
Window centre times	13 µsec. to 16.2 msec.
Magnetometer	Stinger mounted caesium vapour
Magnetometer compensation	Fully digital
Magnetometer output interval	200 ms (~12 m)
Magnetometer resolution	0.001 nT
Typical noise level	0.2 nT
GPS cycle rate	1 second

4.3.3 AEM inversions

4.3.3.1 Introduction

The initial data release included conductivity predictions produced by FAS from the industry standard EM Flow CDI algorithm (Macnae *et al.,* 1998; Stolz and Macnae, 1998). EM Flow is a fast approximate transformation method based on the concept that the response of a quasi-layered earth can be approximately represented by a mirror image of the transmitter dipole that recedes below the surface and expands with delay-time. By determining the vertical depth distribution of the mirror image dipoles a quasi-layered estimate of the subsurface conductivity can be estimated. Since the routine relies on the estimates of the system geometry that are made during the FAS data processing the accuracy of the resultant conductivity estimates are dependent on the accuracy of the geometry estimates. Accordingly, the estimates tend to be biased towards producing results that are consistent with the assumptions made in the FAS data processing, namely a resistive basement earth model. This bias can in turn create an overestimate of the conductivity near the surface, since the model must compensate for the lack of conductance at depth (Lane *et al.,* 2004a; Brodie & Fisher, 2008).

A further problem is caused by the assumptions made in the system geometry estimation that the receiver is orientated in its nominal position (i.e. with zero roll, pitch, and yaw). If the receiver is in fact rotated from its nominal position, which is generally the case, it may be impossible to simultaneously fit both the X- and Z-component data using the same subsurface conductivity distribution because the data are inconsistent with the system geometry information provided to the routine. For this reason it is often necessary to calculate the

EM Flow estimates using just the X- or just the Z-component data. Although this is possible, a different conductivity model will result from each component.

Consequently, the contractor-supplied inversions of the AEM data were found to have extremely poor correlations with available borehole data (r^2=0.338; Lawrie *et al.,* 2009). The spatial conductivity patterns observed in the initial products were crudely valid; however, the conductivity-depth relationships generated by the EM Flow CDI modelling were not properly assigned and were very unreliable. The initial CDI models were inappropriate for this case study, and constrained inversions of the data were required. To assist with targeting a drilling program, the AEM data were initially re-inverted by project geophysicists using the EM Flow software. This produced an improvement in the correlations with boreholes (r^2=0.592; Figure 39), although this was still considered inadequate.

4.3.3.2 GA inversions

Two inversions were performed by GA. Both used the GA-LEI inversion method to invert the TEMPEST data Costelloe and Hutchinson (2010). The following text has been taken from their report, with minor modification. That report should be consulted for additional details.

Conversion of the non-linear electromagnetic response obtained by the system into estimates of subsurface conductivity allows for much easier and more accurate integration with independent subsurface information and facilitates better interpretation. The conversion can use either approximate transformation methods or geophysical inversion, both of which produce model-dependent conductivity estimates.

These same issues have been encountered in previous AEM projects and led to the development of the Geoscience Australia layered earth inversion (GA-LEI) algorithm (Lane *et al.,* 2004a, b). In the GA-LEI inversion algorithm, the idea is to not rely on the primary field separation and hence geometry estimates made in the standard FAS data processing. Instead, the total field (primary plus secondary) field data are inverted directly. The inversion solves not only for a layered earth conductivity model, but it simultaneously solves for the horizontal and vertical separations between the TX and RX and the pitch of the receiver coils. By solving for the system geometry during the final inversion the method allows the information from both the X- and Z-components to be simultaneously fitted using a single common conductivity model. It prevents the assumptions made during the standard data processing from being automatically imposed onto the inversion results. Furthermore, if prior information exists about the electrical structure of the survey area, these can be included as specific constraints on the inversion results.

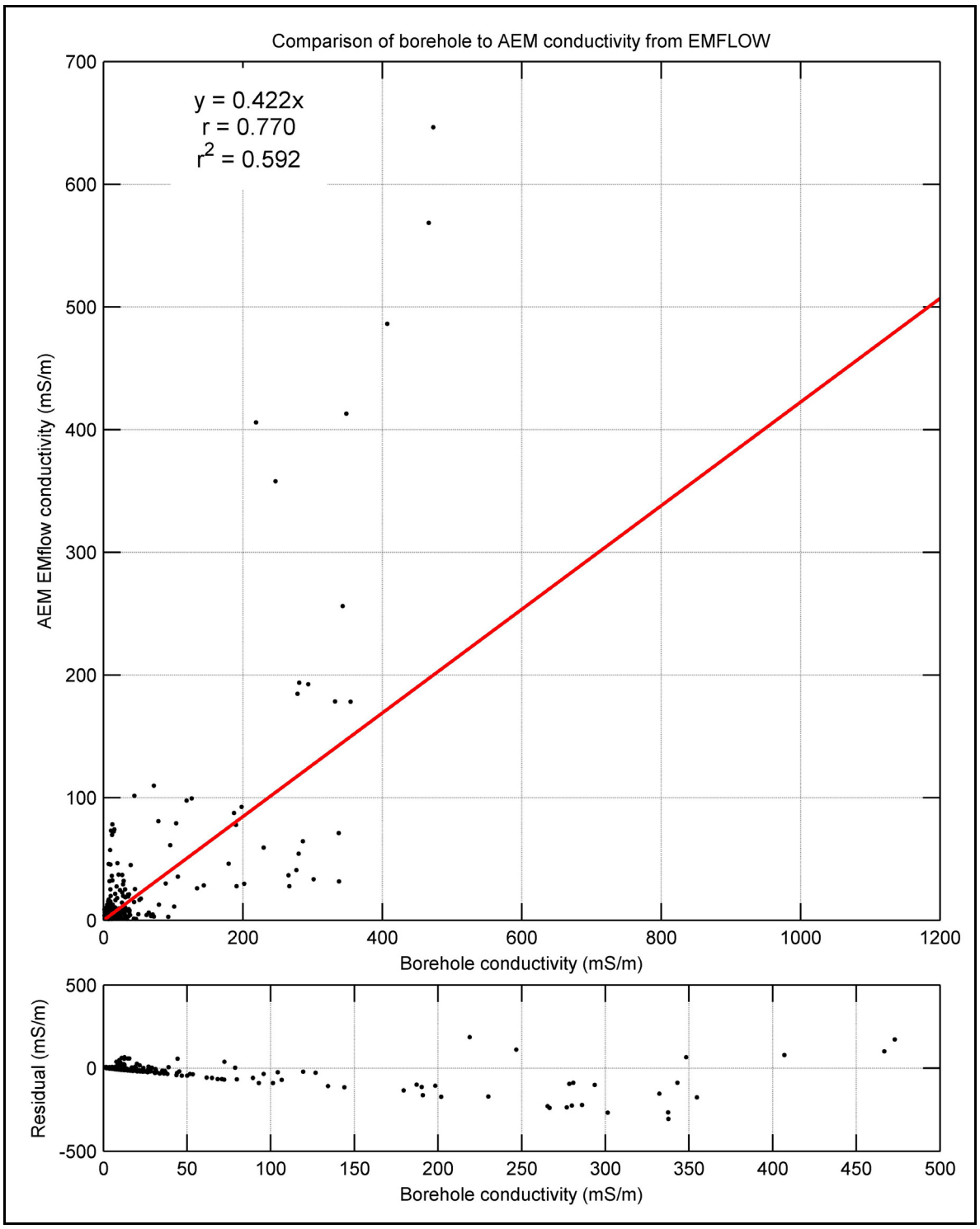

Figure 39: *Fiducial point comparison between the AEM data inverted using the EM Flow software package versus borehole induction data from 27 bores in the project area. This correlation represents only a moderately good fit of the data, although it is much better than that obtained using the earlier contractor-supplied EM Flow inversions.*

4.3.3.3 Detailed description of AEM inversions

The GA-LEI is a 1D "sample-by-sample" inversion in which each of the airborne samples, acquired at approximately 12 m intervals along a flight line, are inverted independently of their neighbours. The inversion of each individual sample involves the estimation of a 1D layered earth conductivity structure, and three elements of the system geometry, that are consistent with the data. A 1D layered earth conductivity structure means that the earth is considered to be a series of horizontal layers stacked in layer-cake fashion (Figure 40). Each layer extends to infinity in the horizontal direction and the conductivity within each layer is constant. Once all samples are inverted they are compiled into a pseudo-3D model by 'stitching' the 1D

model together. A detailed technical description of the GA-LEI is provided in Appendix 2 of Costelloe and Hutchinson (2010).

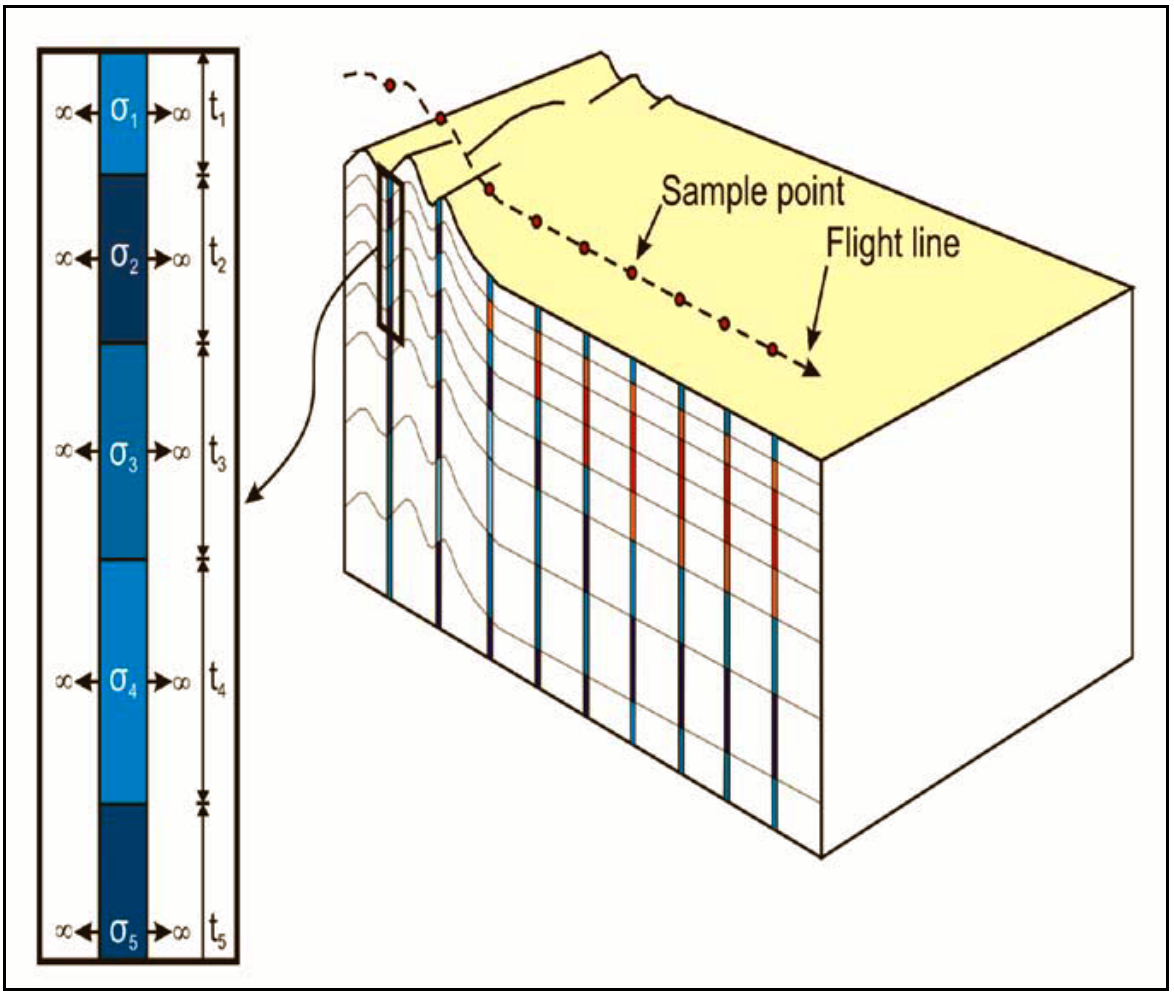

Figure 40: *Schematic diagram of 1D vertically smooth layered earth model used in the GA-LEI. The thickness of each layer (t_n) is fixed, but the conductivity (σ_n) is not fixed and can vary between layers. Image modified from Brodie and Fisher (2008) (from Costelloe and Hutchinson, 2009).*

Since the data are non-linear with respect to the model parameters, an iterative inversion technique is used. Starting from an initial estimate, the layer conductivities and system geometry parameters are iteratively updated until the forward response of the model replicates the measured data satisfactorily, i.e., to within the noise levels. The estimated conductivity model is constrained to be vertically smooth and to be as close as possible to a reference conductivity model. The aim of these smoothness and reference model constraints is to ensure that the model is as simple as possible, and complex structure is only permitted where necessary (see for example Constable *et al.,* 1987).

For the initial inversions of the Pine Creek Survey data the subsurface was parameterized with 30 layers where thicknesses were chosen and remained fixed throughout the inversion (i.e. they were not solved for, see Costelloe and Hutchinson 2010 for original layers). For this project we have used only the top 19 layers, reflecting the zone of interest for a seawater intrusion study. These layers are shown in Table 8.

Table 8: *GA-LEI model layer thicknesses and depths from surface (modified from Costelloe and Hutchinson 2010).*

LAYER NUMBER	THICKNESS (m)	DEPTH TO TOP (m)	DEPTH TO BOTTOM (m)
1	4.00	0.00	4.00
2	4.40	4.00	8.40
3	4.84	8.40	13.24
4	5.32	13.24	18.56
5	5.86	18.56	24.42
6	6.44	24.42	30.86
7	7.09	30.86	37.95
8	7.79	37.95	45.74
9	8.57	45.74	54.31
10	9.43	54.31	63.74
11	10.37	63.74	74.11
12	11.41	74.11	85.52
13	12.55	85.52	98.07
14	13.81	98.07	111.88
15	15.19	111.88	127.07
16	16.71	127.07	143.78
17	18.38	143.78	162.16
18	20.22	162.16	182.38
19	22.24	182.38	204.62

4.3.4 Comparison of airborne and ground EM responses

In an effort to assess the quality of the inverted AEM survey data, the results of the inversions were compared with borehole inductive conductivity logs. The logs from 27 bores were compared with a GA 30-layer sample by sample inversion (Figure 41) and a 40 layer EM Flow transform.

The limitations of this comparative technique need to be appreciated. Line spacing in the W1 and W2 survey areas is 555 m and the bores are not necessarily located on the flight lines. The footprint of the TEMPEST AEM system is a square 470 m x 470 m (Reid and Vrbancich, 2004) and the footprint of the conductivity tool is a circle of 2 m radius.

A detailed FID point comparison was also completed to assess the quality of the AEM data and constrain the inversion products. Inductive conductivity data for 26 boreholes was used for this comparison. Rigorous data selection and validation methods were applied to ensure that only the highest-quality data were used, e.g., bores selected only if within 200 m of AEM flight lines. Several different FID point comparison methods were applied, and the overall result provided confidence that the AEM and borehole conductivity data are consistent for this study, with >95% correlation.

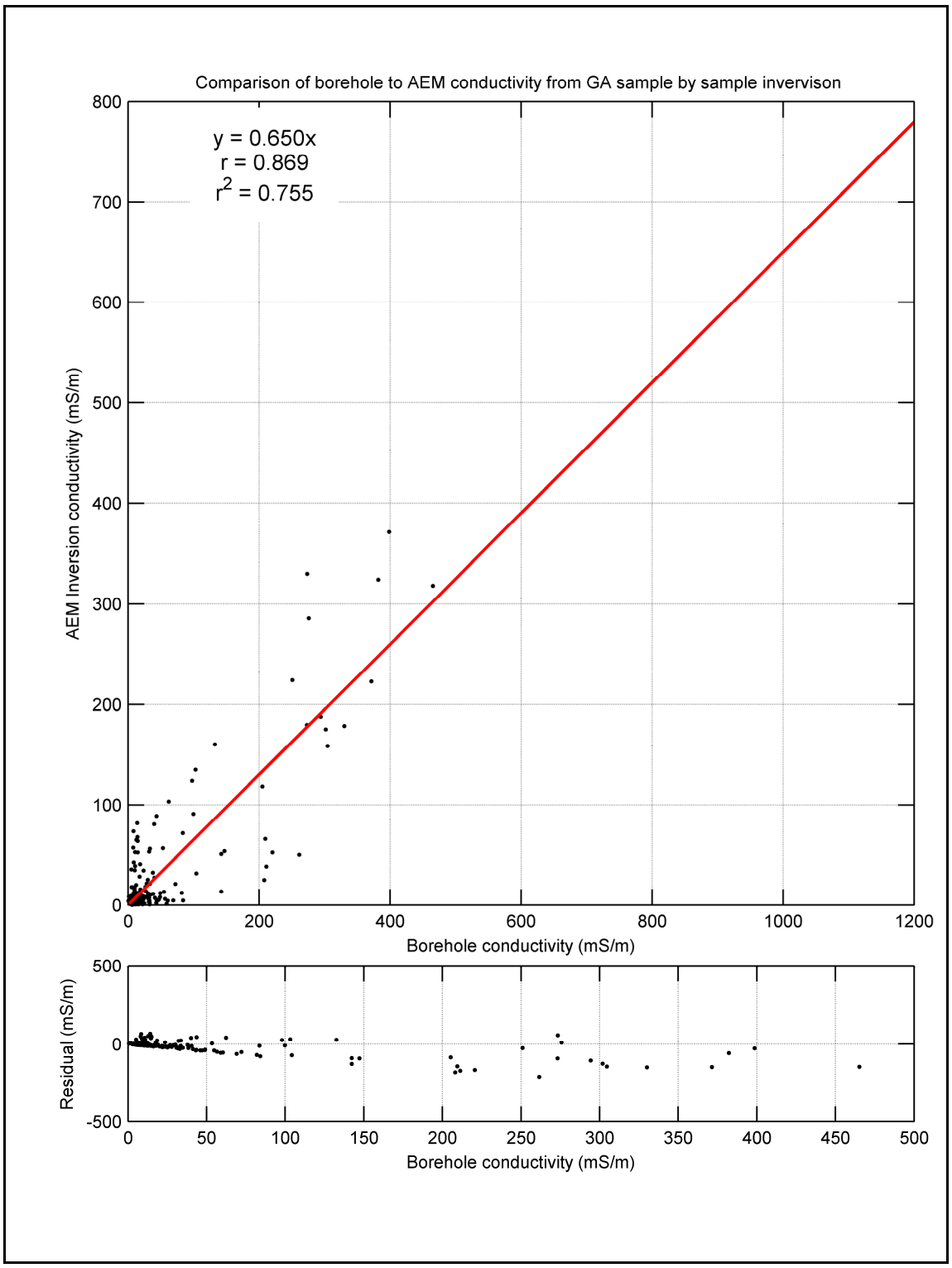

Figure 41: *Comparison of borehole to AEM conductivity from GA sample by sample inversion.*

4.3.4.1 Reference model

Conductivity logs can be used to create a detailed reference model that varies across the survey in order to constrain the inversion when the solution becomes non-unique. In the Pine Creek survey, only 16 conductivity logs were available to use in the inversion. Since there were relatively few conductivity logs available over a large survey area, it was not feasible to define a conductivity reference model that was spatially variable. Therefore, the reference model used in this inversion is simply a half-space of homogeneous conductivity across the survey area to basement. The reference model was also used as the starting model for the iterative inversion.

For the TX to RX horizontal and vertical separation inversion model parameters we used the values (i.e. different for each sample) estimated during the standard FAS data processing as the starting and reference model values. We used zero for the starting and reference model value for the receiver coils' pitch parameter.

4.3.4.2 Final LEI FiD point comparisons

The borehole induction logs selected for use in the FiD point comparsion were selected using the following process of quality control:

- A FID point comparison is meaningless for bores too far away from the nearest AEM sounding. We chose a limiting distance of 200 m. Bores further away than 200 m were discarded.
- One of the bores were a duplicate of another bore and was discarded.
- Some of the bores had conductivity logs that were predominantly negative. These were discarded.
- One bore was in the list, but there was no data file: discarded.
- Strange-looking bores that made no geological sense were discarded.

The bores that were left were edited as necessary. Several of the conductivity logs had intervals with negative data, some of these probably caused by metal at the top of the casing. The negative data were excluded plus an interval of 50 cm to each side of the negative interval to make sure that distorted data were not included in the analyses. Other intervals with negative data occur where the conductivity values are very small and they are probably due to poor calibration of the tool, in particular poor zero leveling. Rapidly oscillating sections and intervals with overly steep gradients at the top or bottom of the bores were also deleted. In Table 1, an overview of the logs and their assessment is given, and in Figure 1, three examples of the editing that took place are given. A complete set of plots of logs before and after editing are found in two accompanying pdf files listed in Appendix A.

To assess whether the models derived from inversion of AEM data are in accordance with the conductivities measured by borehole conductivity logs, the so-called ``FID point comparison'' has been carried out. In this approach, the borehole conductivity is compared with the model conductivities obtained from inversion of AEM data from the location closest to the borehole.

There are several issues that need be acknowledged in connection with any type of comparing borehole conductivity logs and the models resulting from AEM inversion, the most important of which is the huge scale difference between the volume occupied by the sensitivity of the log tool and the corresponding volume for the sensitivity function of an airborne TEM measurement. At early delay times for the TEMPEST data, the ratio between the log volume and the AEM volume is of the order of $1{:}10^5$ while for late times, the ratio is of the order of $1{:}10^7$. The scale issue is more complex than can be considered here. However, it must be kept in mind that in a comparison between conductivity values coming from geophysical methods with such disparate sensitivity distributions, there will potentially be many cases of apparent, but false, inconsistency between the borehole conductivity and the AEM conductivity, and likewise there will be many cases of apparent, but false, consistency.

Another issue worth clarifying is that both the layer conductivities found in AEM inversion and the borehole conductivity log measurements are associated with an uncertainty. In the AEM inversion, estimates of the uncertainty of the AEM data are included in the inversion process in such a way that data with a small uncertainty will influence the inversion model more than data with a high uncertainty. In the inversion process, data uncertainty propagates to the model so that the layer conductivities are associated with an uncertainty which is estimated in the inversion process. Likewise, borehole conductivity logs are associated with an uncertainty determined by how well the tool is calibrated, amplifier stability, thermal drift, etc. When deriving measures of the difference between AEM and borehole conductivities, these differences must be interpreted in the light of the uncertainties of the both terms. In the following, two measures of the difference have been used: one assuming no errors on either AEM nor borehole conductivity, and the other taking the uncertainty of the borehole conductivity into account.

Beside calculating misfit measures, functional relationships have also been derived between AEM and borehole conductivity. These will be derived under three different assumptions: one assuming no errors on either AEM nor borehole conductivity, one taking the uncertainty of both AEM and borehole conductivity into account, and one taking only the uncertainty of the borehole conductivity into account.

The log samples are assigned a basic absolute noise level and a relative noise level (Ley-Cooper and Davis, 2010), meaning that the variance of the borehole conductivity is:

$$\mathrm{var}\left(\sigma^{log}\right) = \left[\Delta\sigma_{abs} + \Delta\sigma_{rel} \cdot \sigma^{log}\right]^2 \tag{1}$$

In a previous study (Lawrie *et al*., 2012), values of $\Delta\sigma_{abs} = 10$ mS/m and $\Delta\sigma_{rel} = 0.05$ were recommended (Ley-Cooper and Davis, 2010), but inspection of the selected logs from the NTCP project area indicates that the above figures are probably too optimistic. In depth intervals where the borehole conductivity is very low, subintervals of negative values, but with small absolute values, were also found. This may indicate poor calibration of the log tool, specifically poor zero leveling, and the noise model values have therefore been set to $\Delta\sigma_{abs} = 20$ mS/m and $\Delta\sigma_{rel} = 0.07$.

The uncertainties on the AEM layer conductivities are estimated for every sounding after the inversion has been carried out. The expression used for the uncertainty on the $\log_{10}$ of the layer conductivities is (Menke, 1989):

$$\mathrm{var}_{LEI} = \mathrm{diag}\left[\frac{1}{a^2}\left(\mathbf{J}^T\mathbf{C}_e^{-1}\mathbf{J} + \frac{1}{a^2}\mathbf{I}\right)^{-1}\right] \tag{2}$$

where J is the Jacobian matrix, referring to the derivatives of the data with respect to the base 10 logarithm of the parameters and $\mathbf{C}_e$ is the data error covariance matrix containing the estimated data variances in the diagonal. In the multi-layer inversions used for the AEM data, the matrix $\mathbf{J}^T\mathbf{C}_e^{-1}\mathbf{J}$ is generally very poorly conditioned and to ensure numerical stability in the inversion of the expression in the parentheses, the term $\left(1/a^2\right)\mathbf{I}$ is included. The effect of this term is to introduce a maximum on the posterior variances of a^2. The posterior variance is subsequently renormalised through the factor $\left(1/a^2\right)$ so that the dynamic range of the posterior covariance becomes 1 with a maximum of the variance of 1 corresponding to completely undetermined parameters.

4.3.4.2.1 Quantitative measures of the difference between borehole and AEM conductivity

The misfits have been expressed through a least squares residual, i.e. the sum of the squares of the differences between the two parameters to be compared. This sum is then divided by the number of terms to give an average value, and finally the squareroot is taken to deliver a result that reflects the difference and not the square. The formula for this residual is:

$$R^{Raw} = \sqrt{\frac{1}{M}\sum_{i=1}^{M}\left(\sigma_i^{aem} - \sigma_i^{log}\right)^2} \tag{3}$$

where σ_i^{log} is the borehole conductivity values and σ_i^{aem} is the layer conductivity of the AEM model at that same depth, and M is the number of samples involved in the sum. The raw residual has the dimension of conductivity.

However, a residuals normalised with the variance of the borehole conductivity is also calculated. By dividing each term with the variance, the difference is weighted according to how much the borehole conductivity terms can be trusted. If the difference has a large uncertainty, its contribution to the residual is down-weighted, and vice versa. This ensures that the value of the residual carries a reasonable significance

in expressing the overall, mean difference between the two parameters to be compared: a certain difference is considered more serious if the uncertainties are small and less serious if the uncertainties are large. The normalised residual thus measures the difference in units of the uncertainty on the borehole conductivity and is dimensionless. If the normalised residual has a value of unity, it means that, on average, the expected difference between the parameters is of the same order of magnitude as the uncertainty on the borehole conductivity, i.e. statistically they cannot be claimed to be different.. The formula for the normalised residual is:

$$R^{YNorm} = \sqrt{\frac{1}{M}\sum_{i=1}^{M}\frac{\left(\sigma_i^{aem} - \sigma_i^{log}\right)^2}{\mathrm{var}\sigma_i^{log}}} \tag{4}$$

where var σ_i^{log} is the variance (the square of the standard deviation) of the borehole conductivity. This residual is dimensionless.

All residuals for all 26 boreholes for all types of comparisons are listed in Table 2. All 26 plots pertaining to the boreholes in the NTCP area are included in pdf files and are stored in Encapsulated PostScript format. See Appendix A for a list of the supplementary files.

Functional relationships between borehole and AEM conductivity

To find a functional relationship between the AEM conductivity and the borehole conductivity, the borehole conductivity is plotted as a function of the AEM conductivity in a loglog plot and the best-fitting linear relationship between the logarithms of the two conductivities is found, i.e. the parameters a and b are determined so that

$$y = a + b \cdot x \tag{5}$$

minimises the misfit. In this equation, y is log σ^{log} and x is log σ^{aem} and M is the number of samples involved in the regression. The linear regression is done under some or all of the assumptions: (a) that there is no noise on neither log σ^{log} nor log σ^{aem}; (b) that there is noise on both parameters, and (c) that there is noise on log σ^{log}, but not on log σ^{aem}. The misfits to be minimised under these assumptions are:

a) Error on neither x nor y: $$R_{Regress}^{NOerr} = \sqrt{\frac{1}{M}\sum_{i=1}^{M}\left[y_i - \left(a + b \cdot x_i\right)\right]^2} \tag{6}$$

b) Error on both x and y: $$R_{Regress}^{XYerr} = \sqrt{\frac{1}{M}\sum_{i=1}^{M}\frac{\left[y_i - \left(a + b \cdot x_i\right)\right]^2}{\mathrm{var}\left(y_i\right) + b^2 \cdot \mathrm{var}\left(x_i\right)}} \tag{7}$$

c) Error on only y: $$R_{Regress}^{Yerr} = \sqrt{\frac{1}{M}\sum_{i=1}^{M}\frac{\left[y_i - \left(a + b \cdot x_i\right)\right]^2}{\mathrm{var}\left(y_i\right)}} \tag{8}$$

For all of the above regressions, a correlation coefficient R^2 is calculated. In the case when uncertainty is neglected, R^2 is given by the traditional expression for linear regressions:

a) Error on neither x nor y: $$R^2 = 1 - \frac{SS_{err}}{SS_{tot}} = 1 - \frac{\sum\left[y_i - \left(a + b \cdot x_i\right)\right]^2}{\sum\left(y_i - < y >\right)^2} \tag{9}$$

where SS_{err} is the unnormalised difference between the data and the predicted response and SS_{tot} is the total variability of the data, and $< y >$ is the mean value of y. In the case where the uncertainty on both x and y is taken into account, a generalisation of the above formula must be derived. The normalisation of the residual term is already defined in equation (11) so, in the same way, the expression for the total variability normalised with the variance must be derived. It is easy to prove that the covariance between y_i and $< y >$ is zero so the variance of the difference is the sum of the variances:

$$\mathrm{var}\left(y_i - < y >\right) = \mathrm{var}\, y_i + \mathrm{var} < y > = \mathrm{var}\, y_i + 1/\sum_{i=1}^{N} \frac{1}{\mathrm{var}\, y_i} \tag{10}$$

The correlation coefficient R^2 is therefore given by:

b) Error on both x and y:
$$R^2 = 1 - \frac{\sum \frac{\left[y_i - (ax_i - b)\right]^2}{\mathrm{var} y_i + b^2 \cdot \mathrm{var} x_i}}{\sum \frac{\left(y_i - < y >\right)^2}{\mathrm{var} y_i + 1/\sum\left(1/\mathrm{var}\, y_i\right)}} \tag{11}$$

Analogously, in the case where only errors on y is taken into account is given by:

c) Error on only y:
$$R^2 = 1 - \frac{\sum \frac{\left[y_i - (ax_i - b)\right]^2}{\mathrm{var} y_i}}{\sum \frac{\left(y_i - < y >\right)^2}{\mathrm{var} y_i + 1/\sum\left(1/\mathrm{var}\, y_i\right)}} \tag{12}$$

All of the regression computations have been done using the freely available MATLAB script york_fit.m (York *et al.*, 2004).

4.3.4.3 The NTCP survey: Results and FiD point comparison

To illustrate the comparisons, plots have been made for all 26 boreholes depicting the comparisons outlined above. Representative examples are shown below.

4.3.4.3.1 Comparing borehole conductivity data with AEM layer conductivities

In this comparison, the raw residual and the Y-normalised residual are used, i.e. the one normalised with the variance of the log conductivity, see Equations (3) and (4). M is the number of borehole log measurements, σ_i^{log} is the borehole log conductivity measurements at the i'th depth, and σ_i^{aem} is the AEM layer conductivity at that same depth.

Figure **42** shows a plot of the comparisons for borehole RN025421. An explanation of the plot is given in the figure caption. The general conductivity level displayed in the borehole conductivity log is reproduced by the AEM inversion model, but the relatively thin conductive layers at 35 m and 45 m depth are of course not resolved by the AEM model. The raw residual, 19 mS/m is of the same order of magnitude as the conductivity values themselves, and the normalised residual is equal to 0.7, meaning that the difference is of the same order of magnitude as the uncertainty of the borehole conductivity data. Figure **42** also shows the comparisons for borehole RN036537. This borehole is in a relatively high-conductivity environment and it is seen that the AEM model reproduces the conductivity high between 5 m and 40 m depth. The unnormalised residual acquires a value of 80 mS/m between the maximum and the minimum values of the borehole log, and the normalised residual is equal to 2.1.

The mean value of the raw residuals is 30 with a standard deviation of 31, while the mean value of the normalised residuals is 1.0 with a standard deviation of 0.8.

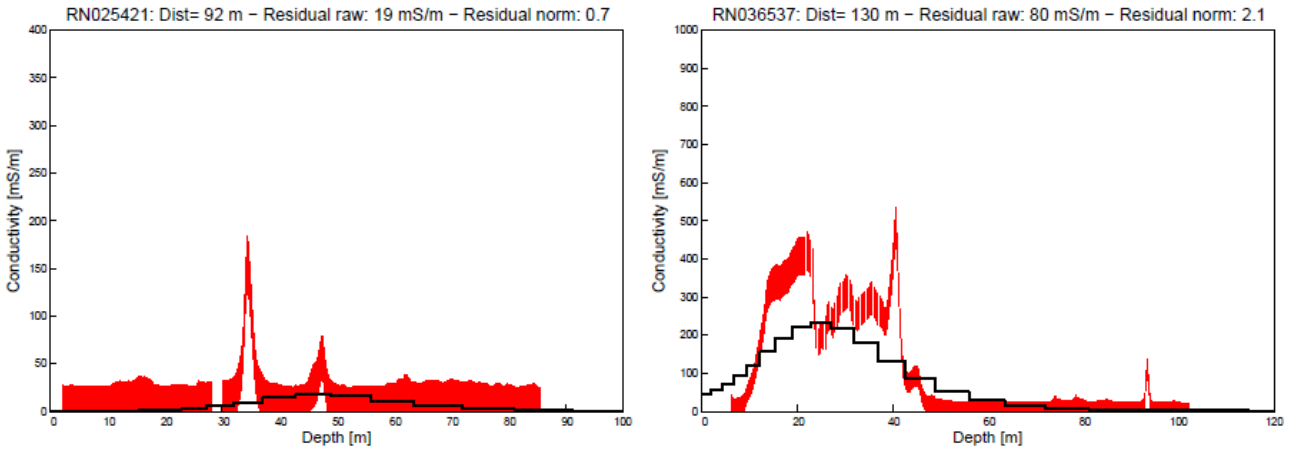

Figure 42: *FID comparison plots for the RN025421 and RN036537 boreholes. The borehole conductivity plotted in red as vertical line segments indicating the uncertainty. The 30-layer AEM model closest to the borehole is plotted in black. The distance between borehole and AEM model is given in the plot title together with the raw and the normalised residuals.*

To see if the residuals are correlated with the distance between the borehole and the AEM sounding position, Figure 43 shows the residuals plotted as a function of the borehole-AEM distance. Apparently there is no correlation.

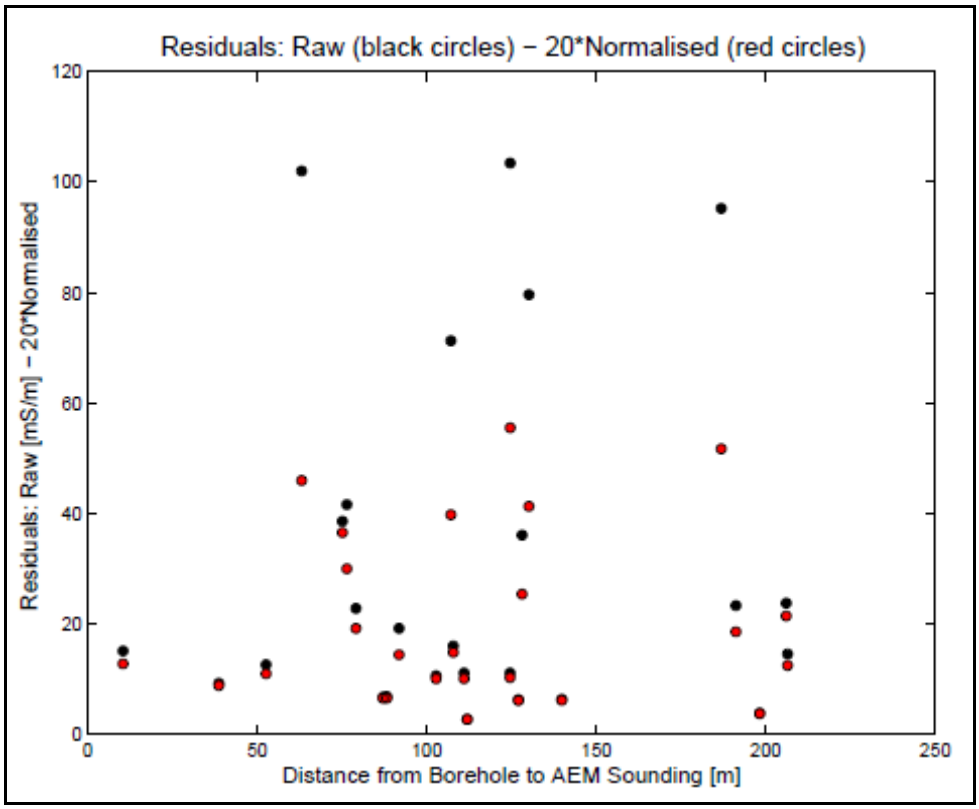

Figure 43: *Raw and normalised residuals as a function of the distance between the borehole and the closest AEM sounding. It is seen that there is no correlation between the two parameters.*

4.3.4.3.2 Comparing depth interval averages

In this section we compare the averages over depth intervals of borehole conductivity and AEM conductivity. Computations are carried out for both a 2 m and a 5 m depth discretisation. Both the raw residual and the Y-normalised residual are used.

The average of the borehole conductivity is calculated taking the estimated errors on the borehole conductivity into account, i.e. the average in the j'th depth interval is found as:

$$< \sigma_j^{log} >= \sum_{i=1}^{N} \frac{\sigma_i^{log}}{\mathrm{var}\sigma_i^{log}} / \sum_{i=1}^{N} \frac{1}{\mathrm{var}\sigma_i^{log}} \tag{13}$$

where the N samples of the average are the ones in the j'th depth intervals. The variance of the average is given as:

$$\mathrm{var} < \sigma_j^{log} >= 1 / \sum_{i=1}^{N} \frac{1}{\mathrm{var}\sigma_i^{log}} \tag{14}$$

If there are no borehole conductivity data in the interval, it is excluded from the analysis.

The averages of the AEM conductivities are found as simple mean values of the layer conductivities weighted with the relative contributions from the AEM model layers to the j'th depth interval and the variance of the average is calculated in the same way.

4.3.4.3.3 Depth intervals of 2 m

For the 2 m discretisation, Figure 44 shows a plot of the comparisons for borehole RN025421. An explanation of the plots is given above and will not be repeated here.

The raw residual pf borehole RN025421, 17 mS/m is of the same order of magnitude as the conductivity values themselves, and the normalised residual is equal to 4.3, meaning that, on average, the difference is slightly higher than the uncertainty of the borehole conductivity data. The unnormalised residual acquires a value of 75 mS/m between the maximum and the minimum values of the borehole log, and the normalised residual is equal to 12.5.

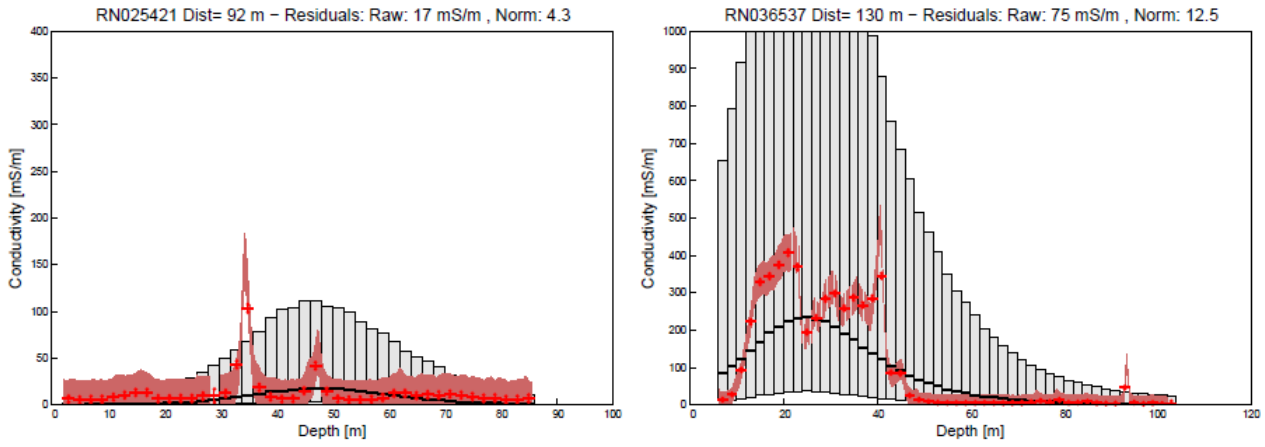

Figure 44: *Comparison plots for the RN025421 and RN036537 boreholes for the 2 m depth discretisation. The borehole conductivity data are plotted in dark red as vertical line segments indicating the uncertainty. The averages of the AEM model closest to the borehole are plotted in black with uncertainties indicated by the gray bars. The borehole conductivity averages are plotted in red with uncertainties indicated by the vertical red error bars. The distance between borehole and AEM model is given in the plot title together with the raw and the normalised residuals.*

Plotting the residuals (of the comparison between 2 m averages) as a function of the distance between the borehole and the AEM sounding position showed no apparent correlation (Figure 43).

The distributions of the raw and the normalised residuals for all boreholes are illustrated in the histograms of Figure 45. All residuals are listed in Table 9. For the raw residual, the mean and standard deviations are 29 mS/m and 29 mS/m, respectively, and for the normalised residuals, the values are 6.1 and 4.7, respectively.

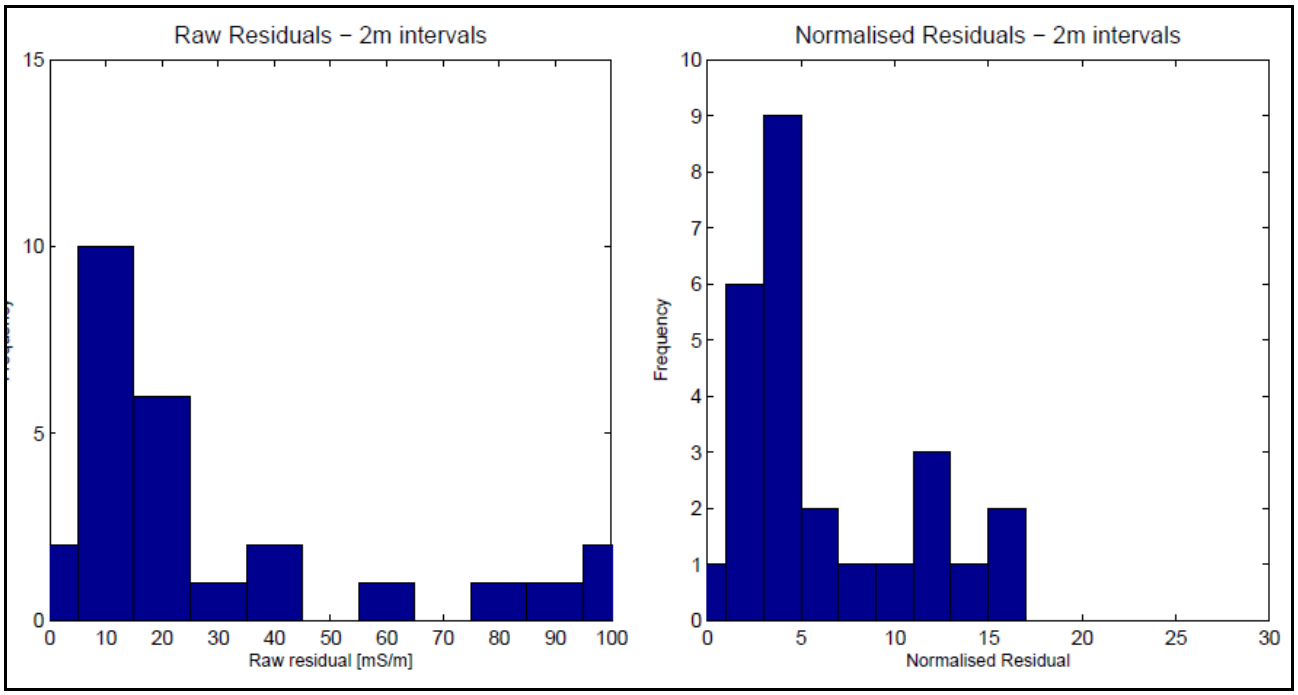

Figure 45: *Histograms showing the distribution of the raw (left) and the normalised (right) residuals for the 2 m depth discretisation listed in Table 2.*

In Figure 46, the borehole layer conductivity is plotted as a function of the AEM layer conductivity with the regression lines corresponding to the assumption of no parameter errors (equation 6), errors on both (equation 7), and errors on only the borehole layer conductivity (equation 8). See table 3 for a list of the regression parameters. The R^2 values of the regressions are 0.435, 0.998 and 0.721, respectively, for the three regression lines.

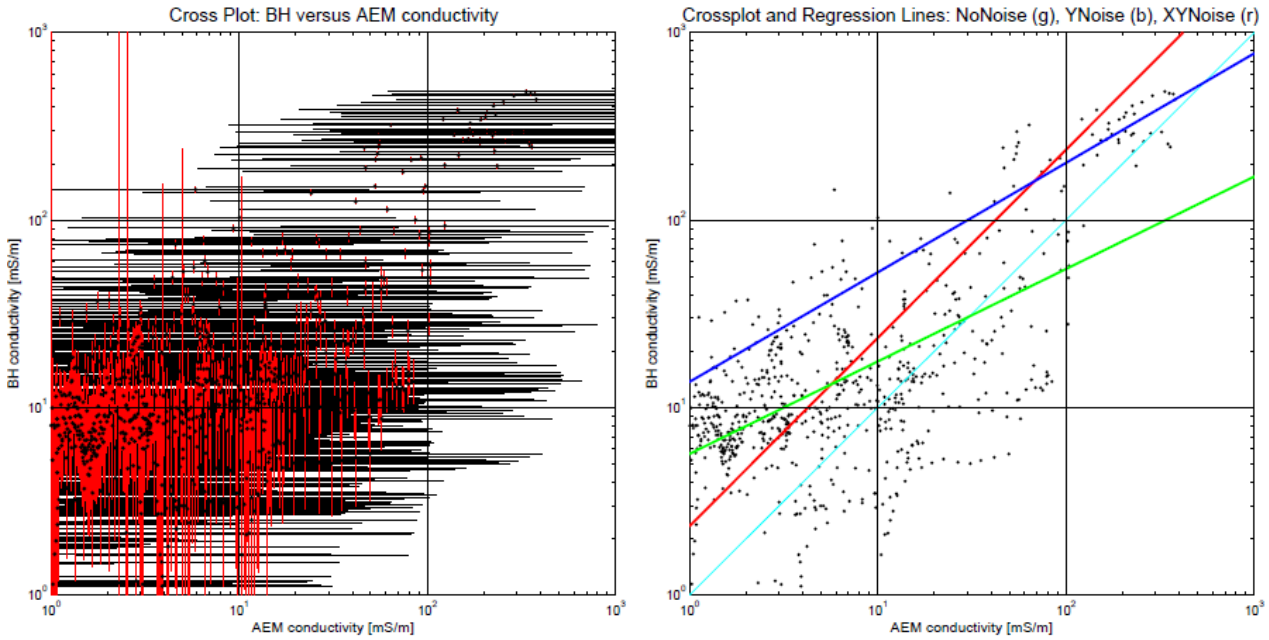

Figure 46: *Cross plots on a logarithmic scale of the borehole layer conductivity as a function of the AEM layer conductivity for the 2 m depth discretisation; left: with error bars, and right: without, for clarity. The identity mapping is shown with a thin cyan line while the least squares linear fit corresponding to an assumption of no errors, errors on borehole conductivity and errors on both parameters are plotted as thicker green, blue and red lines, respectively.*

Table 9. *Residuals of all types for all selected bores within the NTCP survey area.*

RESIDUALS FOR ALL BOREHOLES

Label	Dist	ResRaw	ResNorm	ResRaw_2m	ResNorm_2m	ResRaw_5m	ResNorm_5m
RN020967	125	103	2.8	98.4	16.9	92.8	26.1
RN021012	76	42	1.5	38.5	9.1	36.1	14.2
RN021047	111	11	0.5	10.9	3.1	10.3	4.6
RN021761	206	15	0.6	14.2	3.9	13.6	5.9
RN021768	108	16	0.7	15.8	4.6	15.7	7.3
RN021769	88	7	0.3	7.2	2.0	6.8	3.1
RN022060	87	7	0.3	6.6	2.0	6.5	3.1
RN022065	198	4	0.2	3.8	1.1	3.7	1.7
RN024402	112	3	0.1	2.7	0.8	2.6	1.2
RN024770	140	6	0.3	6.5	1.8	6.5	2.8
RN025420	128	36	1.3	32.9	7.4	29.9	11.2
RN025421	92	19	0.7	17.1	4.3	12.3	5.4
RN025422	127	6	0.3	6.2	1.9	6.2	2.9
RN025423	39	9	0.4	9.1	2.7	8.9	4.1
RN029425	191	23	0.9	19.6	4.8	16.0	6.1
RN031977	107	71	2.0	59.0	11.8	34.4	12.0
RN035864	206	24	1.1	23.5	6.7	22.0	10.0
RN036537	130	80	2.1	75.1	12.5	64.3	17.8
RN036810	125	11	0.5	10.9	3.2	10.9	4.8
RN036811	53	13	0.5	12.1	3.4	10.6	4.7
RN037150	63	102	2.3	98.9	13.8	96.5	20.2
RN037151	187	95	2.6	87.9	15.7	76.3	22.4
RN037152	75	39	1.8	39.0	11.4	40.1	17.4
RN037153	103	11	0.5	10.8	3.1	10.4	4.9
RN037154	79	23	1.0	22.1	5.9	21.3	9.1
RN037218	10	15	0.6	16.8	3.8	21.2	5.7

STATISTICAL PARAMETERS

Label	ResRaw	ResNorm	ResRaw_2m	ResNorm_2m	ResRaw_5m	ResNorm_5m
MEAN	30.3	1.0	28.7	6.1	26.0	8.8
STDDEV	31.4	0.8	29.3	4.7	26.5	6.7

LEGEND

Dist: The distance between the borehole and the nearest AEM sounding in [m].
ResRaw: Unnormalised residual, all borehole data.
ResNorm: Normalised residual , all borehole data.
ResRaw_2m: Unnormalised residual, averages over 2m intervals.
ResNorm_2m: Normalised residual , averages over 2m intervals
ResRaw_5m: Unnormalised residual, averages over 5m intervals.
ResNorm_5m: Normalised residual , averages over 5m intervals.

4.3.4.3.4 Depth intervals of 5 m

The plots pertaining to a depth discretisation of 5 m are shown in Figure 47, Figure 48 and Figure 49 and the explanation for the plots will not be repeated here.

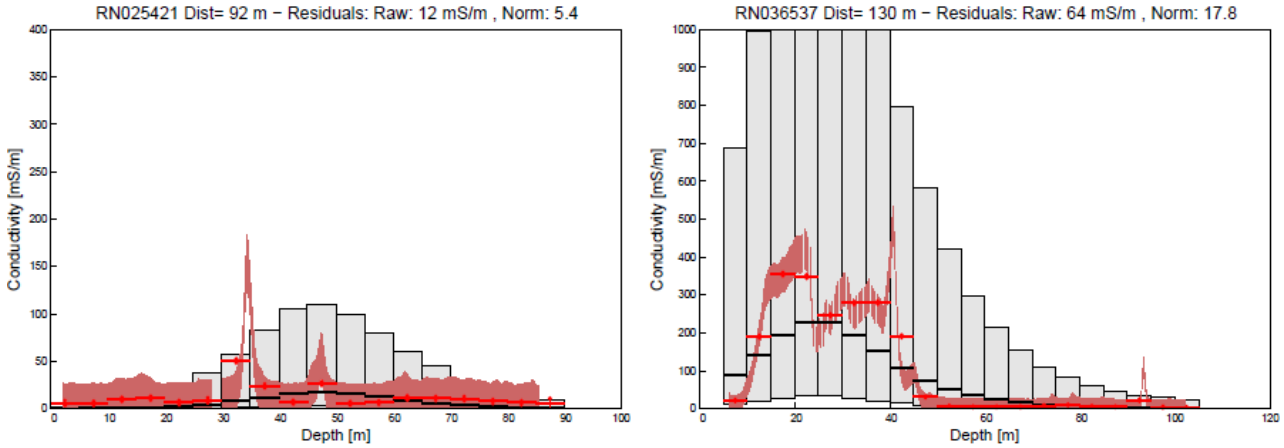

Figure 47: *Comparison plots for the RN025421 and RN036537 boreholes for the 5 m depth discretisation. The borehole conductivity data are plotted in dark red as vertical line segments indicating the uncertainty. The averages of the AEM model closest to the borehole are plotted in black with uncertainties indicated by the gray bars. The borehole conductivity averages are plotted in red with uncertainties indicated by the vertical red error bars. The distance between borehole and AEM model is given in the plot title together with the raw and the normalised residuals.*

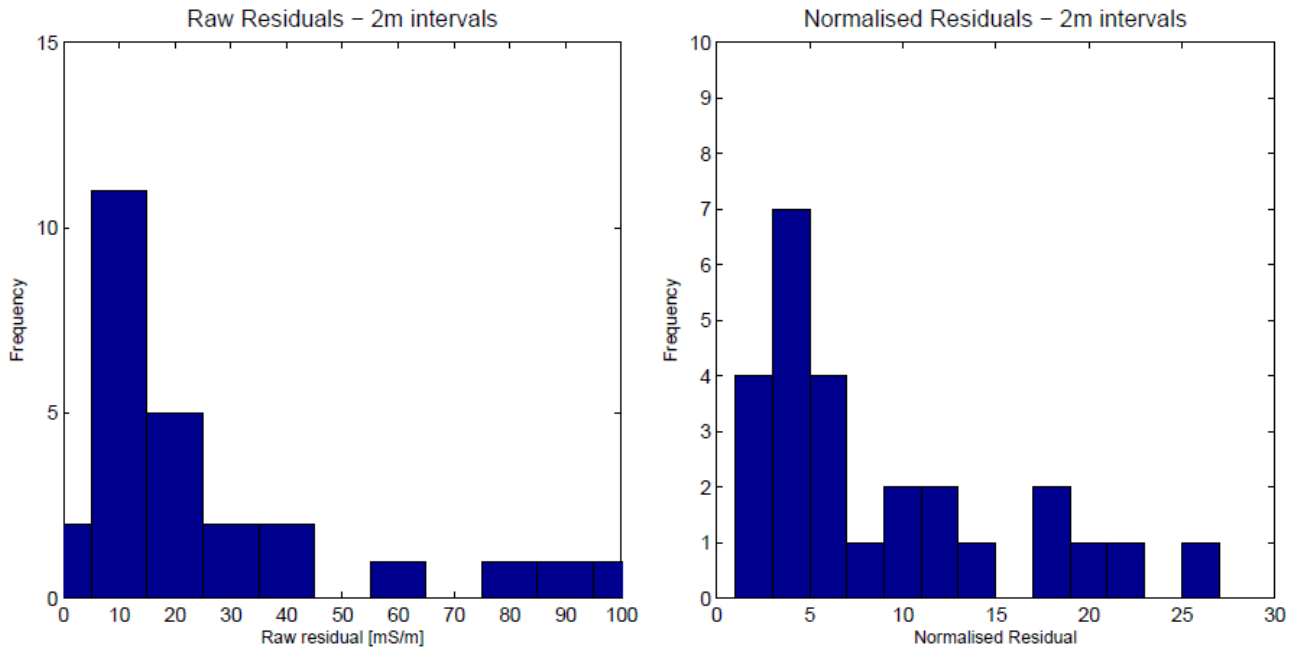

Figure 48: *Histograms showing the distribution of the raw (left) and the normalised (right) residuals for the 5 m depth discretisation listed in Table 9.*

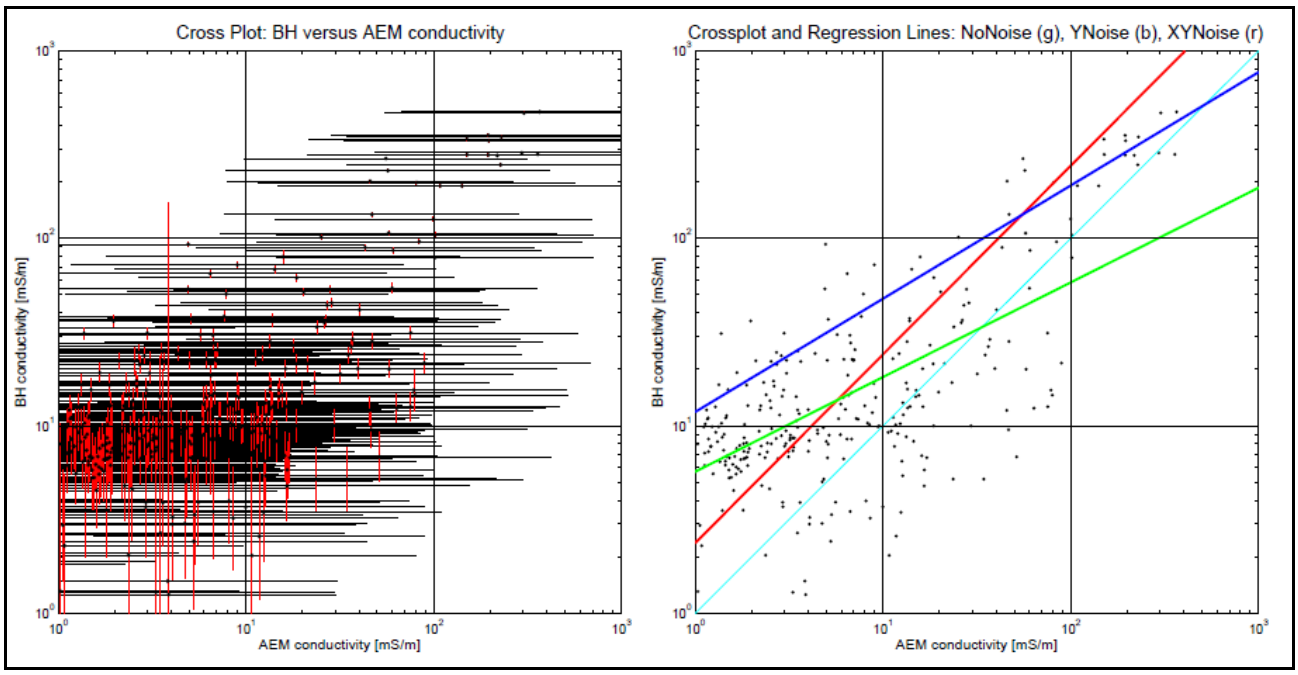

Figure 49: *Cross plots on a logarithmic scale of the borehole layer conductivity as a function of the AEM layer conductivity for the 5 m depth discretisation; left: with error bars, and right: without, for clarity. The identity mapping is shown with a thin cyan line while the least squares linear fit corresponding to an assumption of no errors, errors on borehole conductivity and errors on both parameters are plotted as thicker green, blue and red lines, respectively.*

4.3.4.3.5 FID point comparisons: Summary

The FID point comparisons have been carried out in three different ways: based on every single measured borehole conductivity value, based on averages over 2 m depth intervals, and over 5 m depth intervals. For each of these, the misfit between borehole conductivity and AEM conductivity has been expressed through least squares residuals: assuming no error on either parameter, and assuming errors on only the log conductivities.

In Figure 49 it is evident that the raw residuals are mostly the same for the three methods of comparison. However, for the normalised residuals there is a clear tendency that they increase with the width of the averaging interval. This is mainly due to the fact that if the averaging interval doubles, there will be twice the number of samples in the average and, consequently, the estimated error of the average goes down with a factor of $\sqrt{2}$ see Equation (13) and (14). When the error decreases, the normalised residual increases. In the first comparison, every log sample is used with a sampling distance of 0.05 m, in the comparison of averages over 2 m intervals, there will be 40 samples in each average and the estimated error will go down with factor of 6. Correspondingly, for the 5 m averages, there will be 100 samples in each average and the estimated error will go down with factor of 10. The normalised residuals will therefore increase approximately with those factors and that is actually what is observed.

Through the different methods of FID point comparison, the feature that stands out most clearly is that the borehole conductivities seem to be higher than the ones found in the AEM inversion; in particular, where small conductivity values are indicated in the AEM inversion, the borehole conductivity seems considerably higher. This is evident in the cross plots of Figure 46 and Figure 49. There are several possible explanations for his: poor AEM data, poor inversion (not likely, see above) or poor log calibration, in particular poor zero calibration preventing the measured log conductivity to go below 5-10 mS/m. One of the reasons for the difference is that the background model in the inversion of the TEMPEST data was set to be 1 mS/m (Ross Brodie, GA, personal communication), meaning that the AEM models will gravitate towards that value where conductivities are low and therefore not resolved by neither AEM data nor borehole logging. In this context it is also relevant to consider that the boreholes selected for the FID point comparison are generally in a more resistive terrain than what is average for the whole survey area (Ross Brodie, GA, personal

communication). It must also be remembered that the contribution to the measured borehole conductivity from the water in the borehole - which is generally more conductive than the formation itself - is relatively higher when logs are carried out in a resistive environment, and it skews the results towards higher conductivities. This author regards a combination of the above issues to be the most likely explanation for the observed conductivity distribution in the crossplots.

Concerning the linear regression and the functional relationship between AEM and borehole conductivity, the regression lines derived assuming errors on both parameters is the one with a slope closest to unity. If errors are not taken into account, the asymmetrical distribution of conductivities makes the regression lines have a slope of less than unity and the same effect is seen when only errors on the borehole conductivity are taken into account. The R^2 values are closest to unity when errors on both parameters are taken into account and the smallest when errors are neglected.

Overall, the raw residual, i.e. the average difference between AEM and borehole conductivity, is of the same order of magnitude as the uncertainty of the borehole conductivity. The conclusion that can be drawn from this is that: given the borehole and the AEM conductivities and given that the errors are properly estimated, there is little in the FID point comparison to suggest that there are inconsistencies between the borehole and the AEM conductivities.

At first, this might seem at odds with the quite evidently asymmetrical conductivity distributions in the crossplots mentioned above, but the contradiction is only superficial: the major discrepancies in the crossplots appear for the very low conductivities and that is where the errors on both the borehole conductivity and the AEM conductivity are the largest.

4.3.4.4 Impact of improved processing

NRETAS found that the spatial conductivity patterns using these inversions are quite reliable. In addition to borehole data, comparison with floodplain geomorphic data shows a good correlation between the near-surface conductivity patterns and the overlying geomorphic units. Notably, there is a good correlation between the alluvial plains and conductivity. This also gives confidence in the data, as higher conductivities are expected to be associated with seawater in the shallow coastal floodplains.

4.3.5 Inversion products

4.3.5.1 Depth of investigation

The conductivity model estimated by the inversion is determined not only by the AEM data, but it is also influenced by an *a priori* estimate of conductivity. This estimate of conductivity, known as the reference model, is used as the initial model and is iteratively updated until an acceptable solution is reached. It is important to ascertain how much the solution is determined by the reference model and how much it is determined by the AEM data itself.

The relative contributions of the data and the reference model can be estimated by defining a parameter called the percent data influence (PDI); which compares two inversions created from different reference models. In this work, the PDI is defined as:

$$PDI = 100\left(1 - \frac{\log(\sigma_{i1}) - \log(\sigma_{i2})}{\log(\sigma_{r1}) - \log(\sigma_{r2})}\right)$$

where $\sigma i1$ and $\sigma i2$ are the two inverted conductivities at a given location and $\sigma r1$ and $\sigma r2$ are the corresponding reference model conductivities (Lane *et al.,* 2004a). We define the PDI using the logarithm of the conductivity, since this is the quantity used in each inversion.

If the PDI is greater than 50% then the inversion is deemed to be more influenced by the AEM data than the reference model, whereas if it is less than 50% then the reference model is deemed to be dominant. The depth of investigation (DOI) is defined as the depth at which the PDI is 50%. Thus the DOI marks the depth to which the inverted conductivity is relatively robust. Note that the 50% PDI threshold is arbitrary and a different threshold is possible.

4.3.5.2 Grids and gridding

The 2D grids of the original survey have been created in two different categories:

1. Single inversion layers (the fundamental parameters from the 30 layer GA-LEI model); and
2. Depth slices.

A conductivity depth slice is the average estimated conductivity over a given constant depth interval below the topographic surface. The point-located conductivity estimates were gridded using the (base-10) logarithm of conductivity, since this is the solved value within the inversion.

The AEM survey data were gridded using Intrepid Software and are stored in binary files as ER Mapper single band IEEE4Byte Real data types. An ER Mapper header (.ers) file is associated with each grid file, which describes the data type and the coordinate systems used to spatially reference the grid. Gridded data are stored in a projected coordinate system only; in this case Universal Transverse Mercator (metric) coordinates of the Map Grid of Australia Zone 52 using the Geodetic Datum of Australia 1994. Technical details of the projection can be found in the appendices of Costelloe and Hutchinson (2010).

The surveys had a line spacing of 5 km. Data was not interpolated across the 5 km spaced lines to reduce artefacts that would obscure structural features. In this area the data appears as coloured stripes with null values in between.

Copies of all AEM cross-section and depth slice images acquired and used for the *NT Coastal Plains SWI* project are included in Appendix 1 (digital copies only).

4.4 DRILLING

4.4.1 Introduction

A sonic drilling program was designed to develop a ground truth model for the AEM data that was flown for the *NT Coastal Plains SWI* project. The aim of the drilling was to obtain relatively undisturbed core as basis for chemical and physical analyses of the sediments in the laboratory, to relate these findings to the observed AEM responses. A total of five sonic holes (Table 10) were drilled between December 2009 and September 2010, situated in areas with probable different rock types and variations of conductive response.

Table 10: *Details of the sonic drilling program.*

SITE	REGISTERED BORE NO.	EASTING	NORTHING	AREA	TARGETED AEM FEATURE	DEPTH	BASEMENT
KD-001	RN037150	735987	8635546	Koolpinyah North	north high conductivity	54 m	Dolomite suspected
KD-002	RN037152	722689	8625528	Howard Springs	floodplain north high conductivity	52.3 m	Siltstone
KD-003	RN037151	742280	8629311	Koolpinyah Airstrip	north medium conductivity	47.8 m	Phyllite
KD-004	RN037153	375790	8627734	Koolpinyah Gates	central low conductivity	71.8 m	Dolomite suspected
KD-005	RN037154	737530	8618858	Black Jungle	south low conductivity	59.7 m	Phyllite

Significant problems were experienced with the sonic drilling rig (Figure 50) initially provided by the contractor (Boart-Longyear). Multiple breakdowns caused a significant delay in the drilling program. The rig was deemed faulty, and a second rig mobilised to complete the drilling program. However, due to the effects of a cyclone, only five of the ten holes originally planned were completed. These were drilled to the maximum depths of the rig capability (~70m).

The slow rates of drilling meant that further drilling would not have been possible due to budget constraints. The location of the five sonic bores is shown in Figure 51. Figure 52 shows a photograph of representative sonic core recovered for textural and pore fluid analysis (section 4.5).

Figure 50: *Boart-Longyear Delta base 320 sonic drill rig on site at RN37150.*

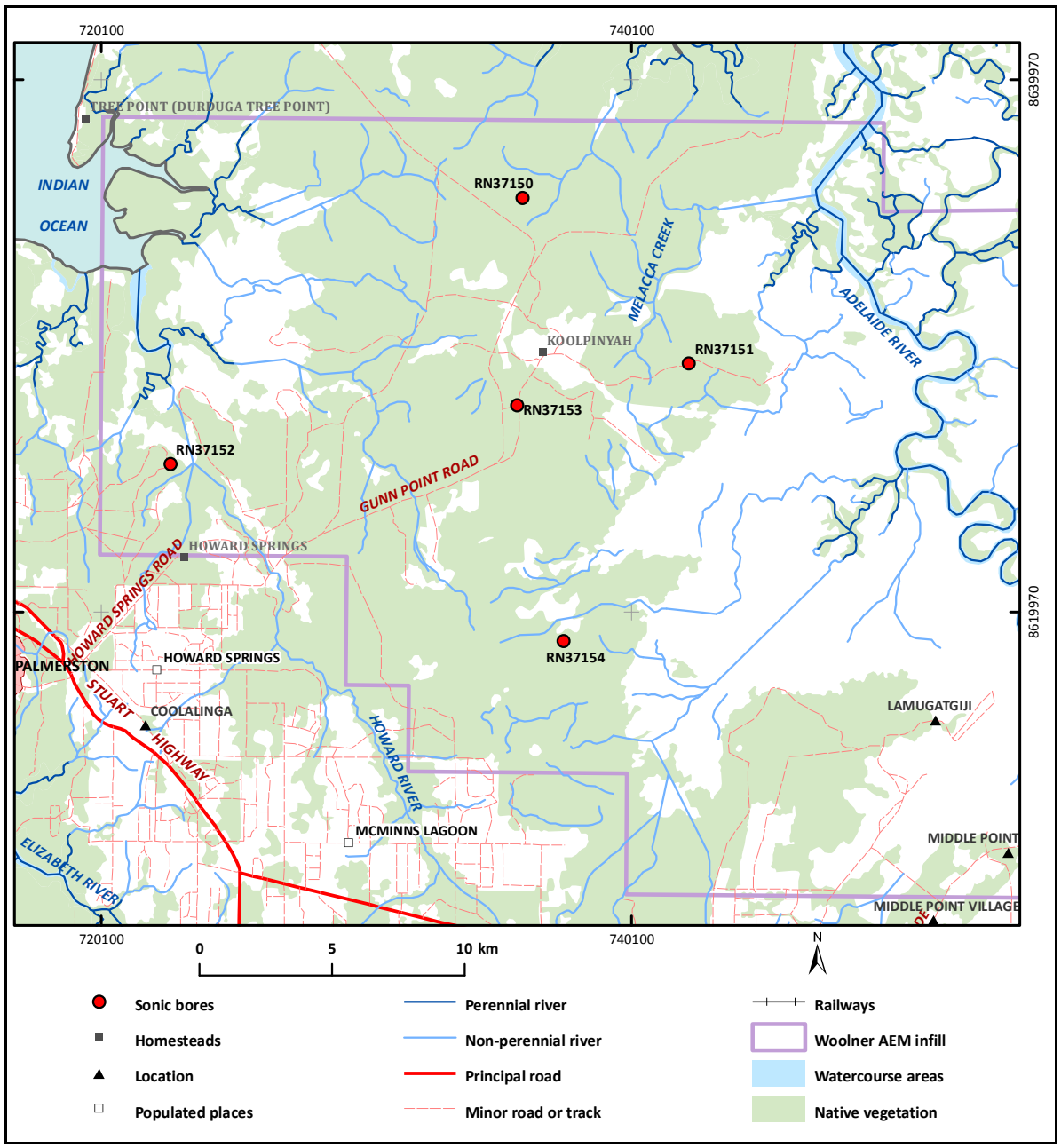

Figure 51: *Map showing the location of five sonic boreholes drilled for the project.*

4.4.2 Drilling methodology

Sonic drilling was chosen as the most reliable method for collecting samples of unconsolidated through to consolidated sediments known to be the dominant rock types in the target areas. The holes were drilled by Boart-Longyear with a Delta Base 320 sonic drilling rig, which is a relatively small, lightweight track-mounted rig suitable for drilling on floodplains. The drilling process normally requires the injection of only relatively small amounts of water that remains as a contaminant only on the outer skin of the core.

The core was encased in a plastic sleeve on extraction from the core-barrel and then taken daily to a cold room where the temperature was kept just above freezing until it was transported to the laboratory in Canberra. This slowed any possible migration of contaminating water from the outer skin of the core inwards, maintaining an uncontaminated central zone of the core for the analytical procedures.

Figure 52: *Sonic core recovered for the 8.0-9.6 m interval in the Cretaceous sandstone sequence from borehole RN37151.*

In addition to the sonic drilling program NRETAS used their Bourne Kelly rotary mud rig (Figure 53) to drill five other bores with the aim of targeting conductivity anomalies possibly associated with the seawater intrusion wedge. Although the cuttings produced by the rig have a tendency to be contaminated by cave-in of sediments from further up-hole, the airlifted water quality readings and sediment samples provide good approximation of *in situ* parameters. The original rotary drilling program was also curtailed by the early onset of wet conditions and only five holes were completed successfully.

Figure 53: *NRETAS rotary drilling rig at the RN37218 floodplain site.*

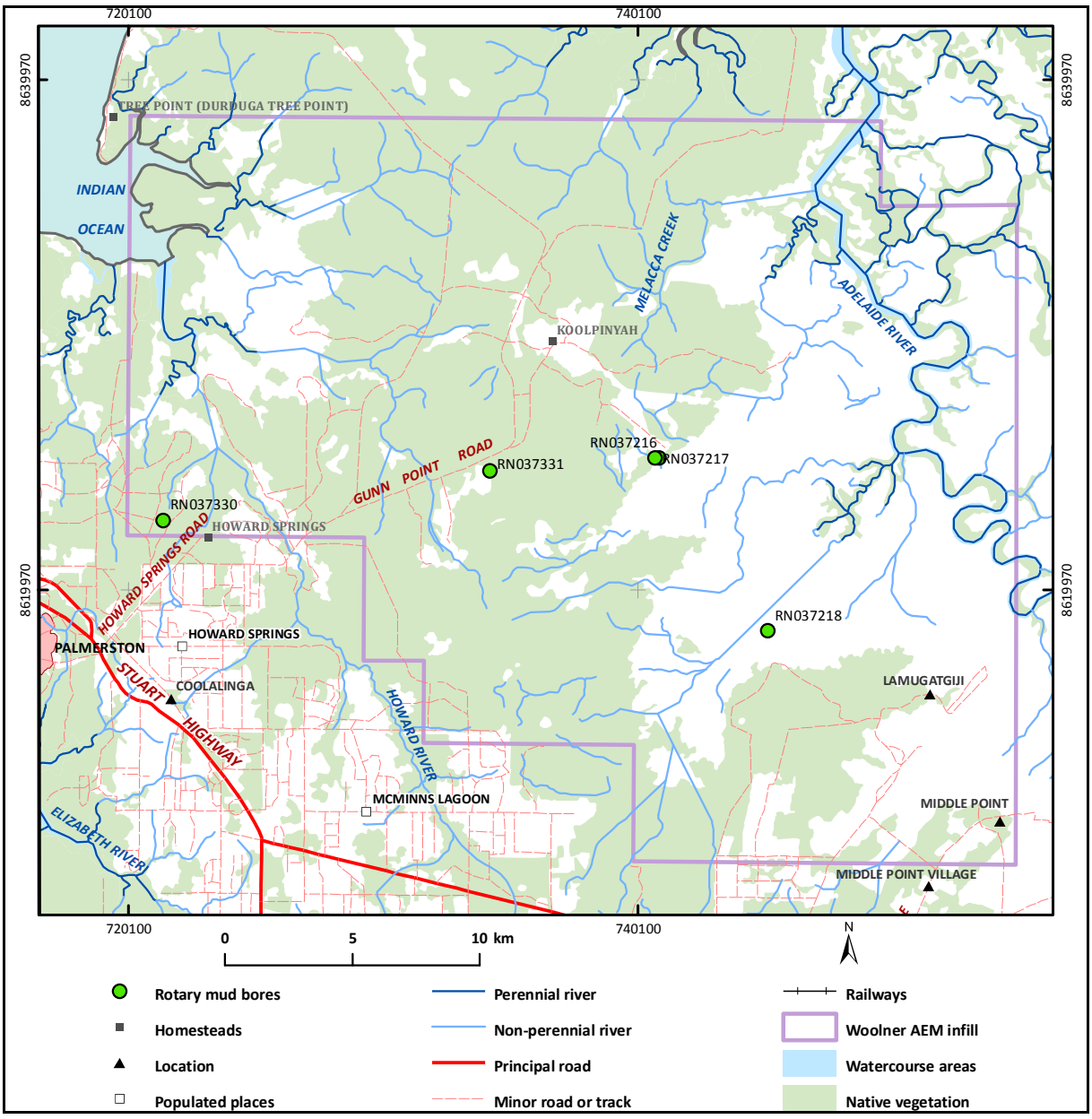

Figure 54: *Location of boreholes in the NTCP study area constructed using the NRETAS rotary drilling rig.*

4.5 DOWN HOLE GEOPHYSICS

4.5.1 Equipment

Down hole geophysical logging involves lowering or raising a tool at a steady rate within a drillhole using a winch and wireline. The tool is attached to the end of the wireline and data are sent via an inner conductor through the winch to a data logger attached to a laptop. Inductive conductivity logging utilises a tool containing two coils, a transmitter and a receiver. The transmitter emits a primary magnetic field which induces current flow in the material surrounding the bore. The more electrically conductive a material is the greater the current flow. This current flow generates its own magnetic field, known as the secondary magnetic field, and this is measured by the receiver coil (Figure 55). The measurement is converted to an apparent conductivity value in milli Siemens-per-meter (mS/m) by software on the laptop using a lookup curve generated from calibration readings using a series of known conductive sources.

The penetration of an inductive conductivity tool is proportional to the coil spacing. Typically, the radius of material investigated is 300-1,000 mm from the tool with most of the response coming from 300 mm (McNeill *et al.,* 1990). The tool operates in PVC cased or uncased boreholes. Steel casing swamps the inductive conductivity signal and provides meaningless data. Highly saline water in the bore can also swamp

the response. The tool responds to electrical conductivity contrasts due to stratigraphy, weathering, fracturing and salinity. Interplay of numerous factors affects the response. In order of decreasing importance, they are (Hallenburg, 1984; Lane, 2002):

- Porosity and water content;
- Water chemistry (i.e., salinity);
- Rock chemistry and mineralogy;
- Degree of rock alteration and mineralisation;
- Amount of evaporates;
- Amount of humic acids, and
- Temperature.

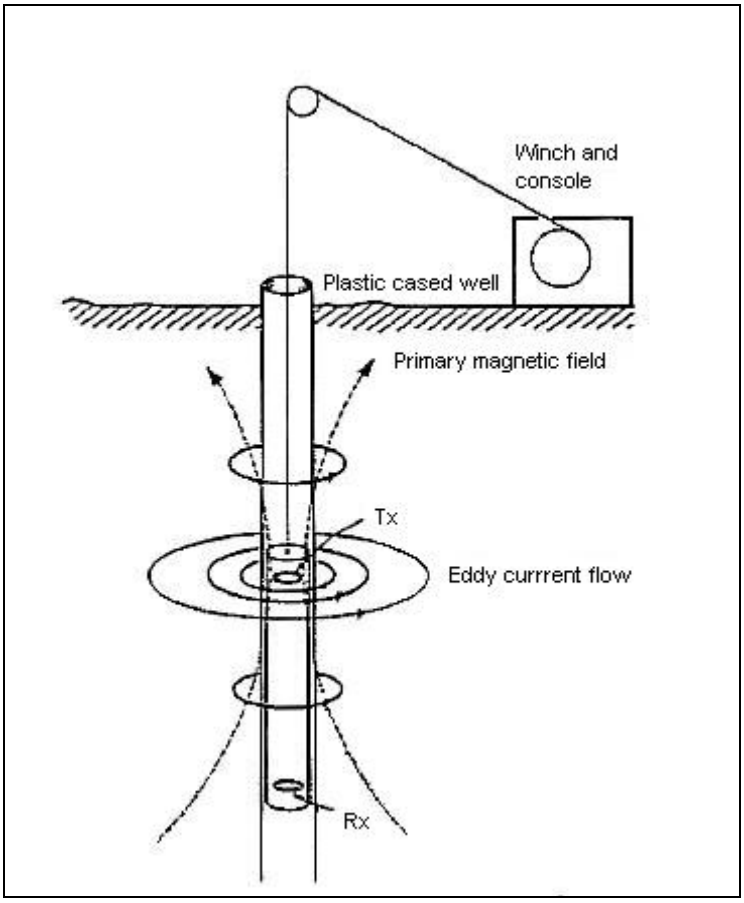

Figure 55: *The principle of operation of inductive conductivity borehole logging tools (after McNeill et al., 1990).*

The natural gamma tool records the total gamma radiation detected in a borehole within a selected energy range. In rocks not otherwise contaminated by artificial radioisotopes the most significant naturally occurring, gamma emitting radioisotopes are potassium 40 and daughter products of the uranium and thorium decay series (Keys, 1990). The gamma tool contains a sodium iodide crystal activated with thallium, NaI (Ti), which scintillates when subject to ionising radiation. These pulses are amplified and counted to provide measurements from the gamma tool in counts per second (cps). This value may be calibrated to American Petroleum Institute (API) gamma ray units.

The natural gamma tool most effectively characterises stratigraphy based on variations in potassium content. It is commonly used to map sedimentary rocks in a basin or the depth of weathering over a craton. Varying proportions of clay versus sand reveal upwardly fining or coarsening facies changes. Basement unconformities show prominently. Correlation of strata between levelled boreholes allows thickness

variations and dips to be determined. The inductive conductivity and natural gamma tools used in this project are supplied by Auslog. The specifications of each are shown in Table 11 and Table 12.

Table 11: *Specifications of the Auslog A034 inductive conductivity tool.*

MODEL	A034
Serial Number	002
Diameter	38 mm
Length	1400 mm
Weight	5 Kg
Temperature Rating	70 °C
Pressure Rating	10000 KPa
Nominal Power	24 VDC
Nominal Current Consumption	80 mA
Conductivity Range	1 – 3000 mS/m
Noise Level	< 0.5 mS/m
Accuracy	3%
Sensor	two coil system
Intercoil spacing	500 mm
Operating Frequency	~26 Hz

Table 12: *Specifications of the Auslog A031 natural gamma tool.*

MODEL	A031
Serial Number	S073
Diameter	43 mm
Length	1130 mm
Weight	4.4 Kg
Temperature Rating	60°C
Pressure Rating	21000 KPa
Nominal Power	24 VDC
Nominal Current Consumption	40 mA
Detector Type	NaI Crystal
Crystal Size	25 mm x 76 mm

4.5.2 Calibration

The borehole logging software used by NRETAS during the project is Auslog Version 6.2g which accepts only a two point calibration for the tools. The inductive conductivity tool was calibrated using a free air measurement (0 mS/m) and a 500 mS/m calibration disk. Calibration was completed at the start and finish of each logging campaign and bore RN035972, slightly outside of the Woolner survey area to the south-west, was used for repeat measurements to verify the calibrations.

The natural gamma tool was calibrated at the NRETAS depot prior to the survey. It was calibrated in counts per second using the jig and standard gamma source supplied with the tool. All logs were run at 6 to 8 m per minute.

4.6 LABORATORY ANALYSES

The methodology used for analysis of the core samples was derived from that developed for sonic drilling in the Ord Irrigation area (Lawrie *et al*., 2010) and simplified from that used in the Broken Hill study (Lawrie *et al*., 2012).

The cores were transported by road to Geoscience Australia in Canberra where the plastic sleeving was cut open and the core described in detail, photographed and sampled. Borehole logging data and core

photographs are in Appendix 3 and 4, respectively. The core samples were analysed for: i). grainsize (using sieving for the gravel fraction and laser granulometry for the sand and finer fractions), ii).bulk density, iii). moisture content, and iv). PIMA analysis and identification of clay types using Spectral Geologist™ software. Pore fluids were also extracted using either hydraulic press or saturation extract method to analyse their hydrochemical compositions. Grainsize data is shown in Appendix 5, and geochemistry data for solid phases and pore fluids recovered from sonic coring is shown in Appendix 6. The analytical techniques utilised are X-ray fluorescence (XRF) and inductively coupled plasma mass spectrometry (ICP-MS). Compiled sonic borehole logs showing downhole variations in geochemistry for solid phases (including PIMA results) and for pore fluids is shown in Appendix 7.

4.7 METHODOLOGY FOR CREATING INTERPRETIVE MAPS AND MODELS

Previous studies have developed multi-disciplinary and multi-scale 4D system approaches to the integration, analysis and interpretation of complex hydrogeological, hydrogeophysical and hydrogeochemical datasets, such as those in the Ord Valley Interpretation Project (Lawrie *et al.,* 2000; Lawrie, 2008; Lawrie *et al.,* 2009). These approaches incorporated an understanding of landscape evolution and scale, and used modern investigative approaches for conceptualising and mapping of aquifer systems and aquitards. State-of-the-art hydrogeochemical and hydrogeophysical techniques were also applied to assess the main hydrogeological processes.

In this study, the specific approach used to produce maps of key elements of the hydrostratigraphy, including geology maps at specific elevation intervals, is described in detail below. The groundwater quality and SWI models are also developed to help establish the potential SWI threat pose to the existing and proposed bore fields.

4.7.1 Mapping of Geological Units

The objective of the mapping of geological units is to establish the spatial extent of the Quaternary sediment, Cretaceous, Proterozoic and Archaean rocks.

4.7.1.1 Available Information

Available data used were:

- 1 arc-second shuttle radar topographic mission (SRTM);
- 1st vertical derivative of the total magnetic intensity (TMI);
- LANDSAT Thematic Mapper imagery;
- AEM conductivity estimates as 5m thick elevation slice grids
- Lithological information from 360 historic boreholes obtained from the NRETAS website (http://www.ntlis.nt.gov.au/hpa-services/borereport?bore=RN000190);
- 9 project boreholes with lithological and water quality information, consisting of 5 sonic bores and 4 mud-rotary holes.

Geological and hydrogeological information are also obtained from the interpreted geological map series (2010) and hydrogeological map of Darwin (2004) (Map Sheet SD52-4). The Proterozoic and Archaean stratigraphic nomenclature are summarised in Worden *et al*. (2008) and are used in the interpretation of the borehole lithology.

4.7.1.2 Borehole Interpretation

Borehole lithological information is translated from hard copy (drillers' logs as pdf document) to Excel spreadsheet and imported into ArcMap™. The lithology is interpreted in a GIS environment together with the surface geology, solid geology and hydrogeological layers, and structural patterns observed on the 1st vertical derivative TMI. Based on the lithological description, geological formations and Groups are assigned to the bore depth intervals.

The drillers' logs, which span across five decades, vary in clarity of spelling, detail in lithological description and ambiguity in lithology. These affect the confidence of the interpretation and the assigned geological units, and the accuracy of delineating the Cretaceous-Proterozoic unconformity.

4.7.1.3 AEM Interpretation

The AEM conductivity estimates are available in both depth slice and elevation slice grids. Depth slices represent the average conductivity over a given interval below the topographic surface. Elevation slices represent the average conductivity over given intervals above or below zero elevation, where elevation is defined by the project's digital elevation model described in Sections 4.2. Considering the varying topography of the study area, i.e. from low lying floodplain to hills and ridges, the elevation grids are better suited for geological interpretation and mapping. The elevation slice grids are in 5m interval, and 15 alternate grid slices are interpreted (Table 13) which starts from 45m above sea level to 95m below sea level.

Since the floodplains and undulating plains dominate the landscape as the hills and ridges are only present in the south, limited areas with apparent conductivity values are present in elevation slices 20-25 mAHD, 30-35mAHD and 40-45mAHD. In addition, these areas are dominantly resistive due to crystalline bedrock, except where conductive sulphides or carbonaceous materials are present. In the Cretaceous rock, weathered mud-rich units are weakly conductive (< 0.3 S/m).

Table 13. *The 15 AEM elevation slices used in the geological mapping.*

From (mAHD)	To (mAHD)	Thickness m
45	40	5
35	30	5
25	20	5
15	10	5
5	0	5
0	-5	5
-10	-15	5
-20	-25	5
-30	-35	5
-40	-45	5
-50	-55	5
-60	-65	5
-70	-75	5
-80	-85	5
-90	-95	5

Extensive areas of high conductivity (1-8 S/m) are present in elevation slices +5 to 0 mAHD, 0 to -5 mAHD and -10 to -15 mAHD. These conductive areas are associated with saline Quaternary alluvium and estuarine sediment. Areas of moderate to high conductivity (~0.5 S/m to 1.5 S/m) persist at lower elevation (-45 mAHD) and are associated with Cretaceous, Proterozoic and Archaean saprolite. Conductivity continues to decrease with depth as the geological domains pass from saprolite to fractured bedrock and variably weathered saprolith. In the south, more distinct conductive features are attributed to the sulphide bearing Proterozoic rocks. On contrary to the saprolite, the apparent conductivity of sulphide bearing rocks increase with depth.

There are also large resistive tracts present throughout the elevation slices. Hydrogeological information suggests that apart from the Koolpinyah / Coomalie Dolomite, the fractured Proterozoic and Archaean units have typically low yield (< 0.5 l/s). The Koolpin and Whites Formations may have low to moderate yield (0.5 - 5.0 l/s). Thus, the resistive signal is a result of the dominant crystalline matrix with low porosity. For Koolpinyah / Coomalie Dolomite, its a range of factors including crystalline, fractured and karst environment with fresh water that results in very low electrical conductivity.

AEM cross sections along flight lines show the vertical conductivity structures. In general, the high conductivity passing into low or moderate conductivity demarcates the Quaternary – Cretaceous unconformity. The low conductivity overlying resistive areas separates the Cretaceous from the Proterozoic rocks. However, there are areas where resistive Cretaceous sedimentary rocks overlie resistive Proterozoic rocks and the availability of borehole lithological information becomes imperative to distinguish between the two geological units.

The Cretaceous unit such as Wangarlu and Darwin Formations are mapped as undifferentiated Bathurst Island Group as they cannot be readily differentiated in these data. Soils, colluvium and weathering zone (e.g. ferruginous duricrust) are not mapped due to the lack of conductivity contrast with the surrounding saprolite and bedrock and the potential thinness of the unit (e.g. 1-2m thick soil).

4.7.1.4 Geological Mapping – A GIS Approach

Two sets of digitised geological polygon templates (shape files) are created. The first template emphasize on the Proterozoic and Archaean geology whereas the second focus on Tertiary and Cretaceous units, with the Proterozoic units attributed as undifferentiated. Interpreted geological formations from borehole lithology suggest that Cretaceous rocks do not persist below -60 mAHD. Thus, the Proterozoic and Archaean geology template is used to represent the geology across intervals -60 to -65mAHD, -70 to -75 mAHD, -80 to -85 mAHD and -90 to -95 mAHD. In comparison, the Tertiary and Cretaceous units have to be digitised across the 11 elevation intervals, from -55 mAHD to 45 mAHD.

The Pine Creek Solid geology map is used as the base map for the Proterozoic and Archaean geology. However, patterns from 1st vertical derivative TMI, conductivity from AEM grids and information from interpreted borehole geological formations suggest the need to amend the Pine Creek Solid Geology polygons. Overall, four areas are amended, these include:

1. The addition of a polygon in the northwest corner (east of Gunn Point).
2. The addition of a polygon in the north (Hotham).
3. The subtraction of a polygon in the middle (Middle Point)
4. The addition and amendment of polygons in the south and southeast (south of Marrakai in the vicinity of the Arnhem highway).

The AEM grid at -90 to -95 mAHD shows a conductive feature near Gunn Point. This conductivity feature is associated with basement rock rather than salinity and is confirmed from available borehole information, which indicates the presence of graphitic/carbonaceous slate. This feature is interpreted as the Whites Formation rather than the mapped Koolpinyah Dolomite (Figure 56).

The Archaean Woolner Granites and Dirty Water metamorphics rocks are mapped as two elliptical bodies. The western edge of the Archaean rocks can be observed in the AEM more than the eastern edge partially due to weathering. Borehole RN027200, located north of the smaller ellipsoid, recorded weathered granite at -14 mAHD and fresh granite at -54 mAHD. Thus, a new polygon of Woolner Granite is added and the two elliptical bodies are joined as one (Figure 57).

At Middle Point, a tightly folded elongated body is evident from the 1st vertical derivative TMI. This is mapped as Wildman Siltstone in the Pine Creek Solid Geology. This unit is resistive and there is no conductivity contrast with the surrounding Koolpinyah / Coomalie Dolomite. Available borehole at the edge of the "Wildman Siltstone" indicates the presence of dolomite. This unit is thus interpreted as Koolpinyah Dolomite (Figure 57).

South of Marrakai is the presence of a set of strongly conductive features. Available borehole lithology indicates the presence of shale, siltstone, slate, schist and phyllite with both presence and absence of sulphides. Based on the patterns observed from the 1st vertical derivative TMI, stratigraphic and structural

information gathered from the Pine Creek Solid Geology, the conductive features are mapped as Koolpin Formation rather than Wildman Siltstone (Figure 56).

To map the extent of Quaternary and Cretaceous units from 45 to -55 mAHD requires a convoluted process. To ensure consistency in the polygons, mapping starts from the base (-50 to -55 mAHD) to the top (45 to 40 mAHD), using the bottom layer as a template for the consecutive upper layer.

Definition query on interpreted borehole geological age is first set up. For example, for interval -20 to -25 mAHD, the query used is as follows:
[“Age” = ‘Proterozoic’ and “from_mAHD” > -22.5 or “Age” = ‘Archaean’ and “from_mAHD” > -22.5].

This ensures that boreholes with Cretaceous-Proterozoic/Archaean unconformity shallower than the mid-point of the interval (-22.5 mAHD) are selected. The extent of the selected bores gives an approximation of the areas where pre-Phanerozoic rocks are present within the interval. Boreholes not selected using the query indicates either the presence of Cretaceous rock or an absence of lithological information within the interval (i.e. shallow bores).

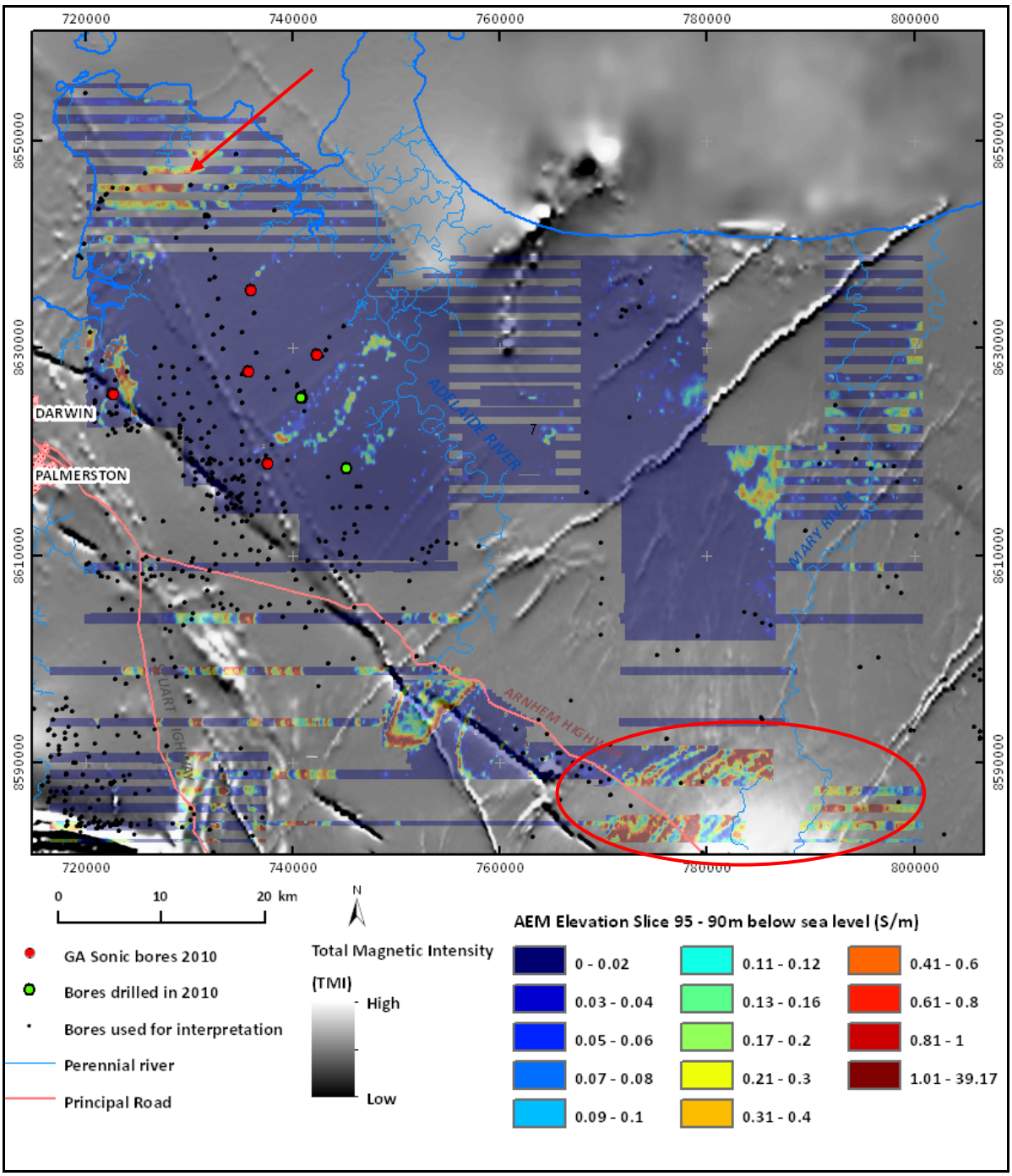

Figure 56. *Conductive features interpreted as Whites Formation in the north-west (indicated with red arrow) and Koolpin Formation in the south (indicated with red circle).*

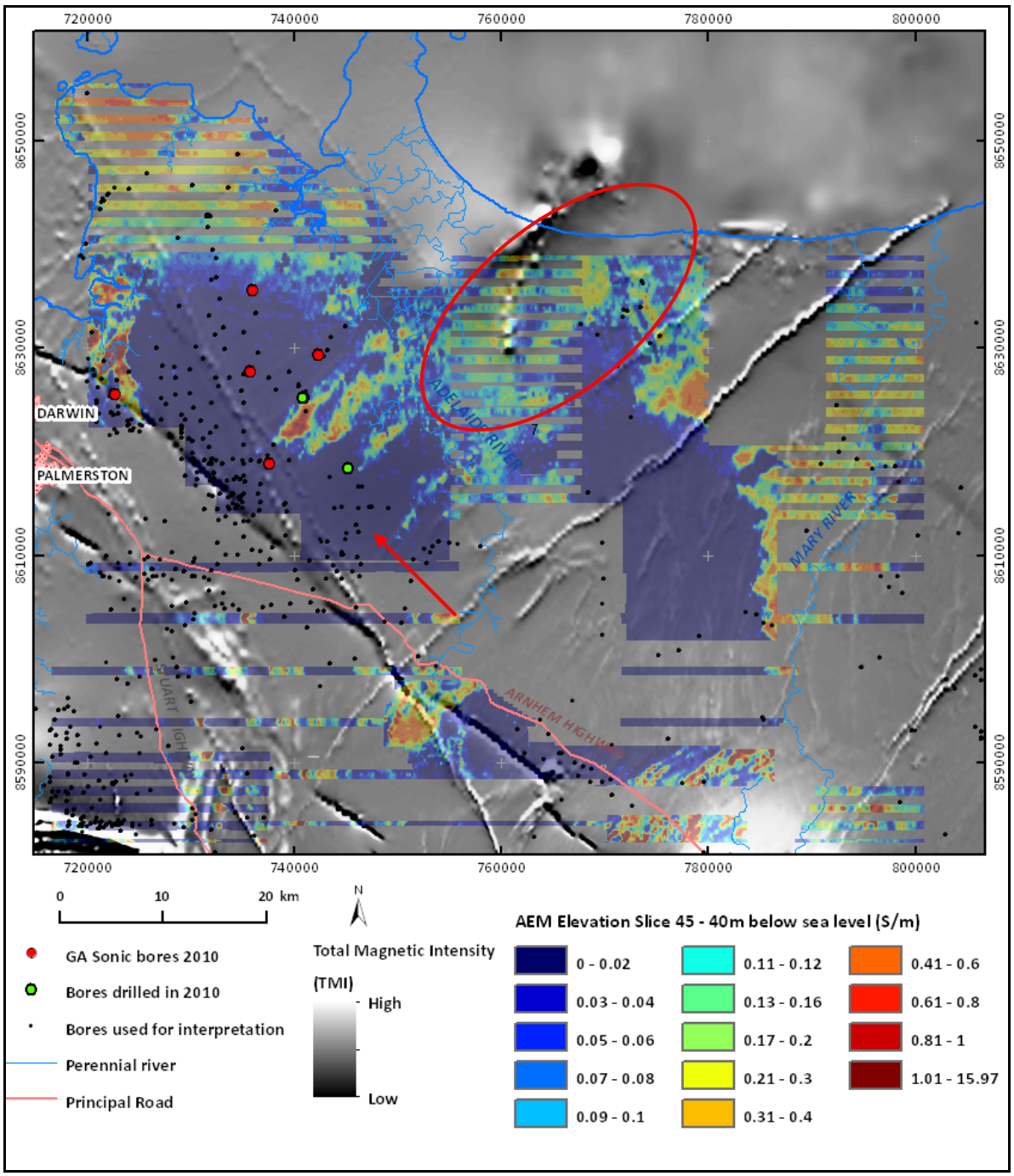

Figure 57. *TMI and AEM signatures demarcate the western boundary of the Archaean units (red circle). No conductivity contrast exists at Middle Point between the Wildman Siltstone and Koolpinyah Dolomite (red arrow).*

To ensure that subtle conductivity values are observable, the AEM grids are grouped into 14 customized threshold classes (Table 14) and these are kept consistent throughout the 15 interpreted layers. Polygons are then digitised according to observable patterns, range of conductivity values and in concur to the borehole geological information.

Table 14. *Conductivity thresholds use to display the AEM grids*

Low (S/m)	Moderate (S/m)	High (S/m)
0.02, 0.04, 0.06, 0.08, 0.1	0.12, 0.16, 0.2, 0.3, 0.4	0.6, 0.8, 1, >1

Polygons from the surface geology map are used to represent the extent of Quaternary sediment for elevation intervals 5 to 0 mAHD and 0 to -5 mAHD. Since these polygons are mapped at a scale of 1:250,000, they are refined using higher resolution AEM grids and LANDSAT image. Borehole lithology information suggests the presence of Quaternary sediment extending into interval -10 to -15 mAHD and these polygons are used to constrain the sediment's maximum extent and modified based on conductive AEM features. From the surface geology map, isolated outcrops of Proterozoic rocks occur within the floodplain. These polygons are incorporated into the interval 5 to 0 mAHD, and extend as subcrops in intervals 0 to -5 mAHD and -10 to -15 mAHD.

Quaternary estuarine and floodplain sediment does not exist above 10 mAHD and the area represented by the AEM grids is drastically reduced. To obtain a realistic rather than pixelated outline from the AEM grids, four smoothed contour polylines using 1 arc-second SRTM data are created at 10, 20, 30 and 40 mAHD. These are converted into polygons and used as template to map the geology for grids 15 to 10 mAHD, 25 to 20 mAHD, 35 to 30 mAHD and 45 to 40 mAHD. Using mainly the query function on borehole geological age and the surface geology map, the Cretaceous and undifferentiated Proterozoic rocks are digitised for these four elevation intervals.

To derive the final geology of the upper intervals (i.e. 45 mAHD to -55 mAHD), the shape files of the elevation intervals are merged with the Proterozoic and Archaean geology shape file, using the geological attributes of the latter to replace the undifferentiated Proterozoic of the earlier.

Overall, there is less reliability in mapping the Proterozoic and Archaean basement in the eastern part of the project area due to a paucity of boreholes of sufficient depth to reach the basement.

4.7.2 Salinity and Seawater Intrusion Models

Groundwater salinities from approximately 360 bores were compiled from the NRETAS web site (bores are shown in Appendix 8). In addition, data from project bores, which includes the 5 sonic project bores and 4 mud-rotary bores drilled by NRETAS were used. Amongst the data are depths and elevations of the screen intervals, water bearing zones or sample depths. Other information used includes the geological groups and formations. This information is matched with the relevant AEM model elevation grids to obtain the conductivity values at the bore locations. The geological information was used to separate the data into Quaternary sediment, Undifferentiated Cretaceous sedimentary rocks and Proterozoic meta-sedimentary rocks.

No groundwater salinity information is available in the highly conductive estuarine areas. To calculate the salinity of the estuarine sediments, a coefficient between AEM conductivity and salinity needs to be established. To achieve this, AEM grids at 0m to 5m below sea level is used. The conductivities of 20 individual points over the sea along the coast were averaged. The resulting averaged value is 7.17 S/m, which should equate to sea water salinity of 35000 mg/l TDS and dividing this TDS value with the average conductivity results in a coefficient of 4880.

However, this coefficient represents conductivity of water, rather than water-laden sediment. To derive the coefficient of the sediment, the formation factor, which is largely influenced by the total porosity of unconsolidated sediment, needs to be assumed. In this case, a total porosity of 30 vol % appears to be reasonable for estuarine mud and interbedded sandy mud and sand of the Quaternary alluvium. The coefficient of the sediment is calculated using the following formula.

TDS (mg/l) = 4880 x total porosity x AEM conductivity (S/m)

TDS (mg/l) = 4880 x 1 / 0.3 x AEM (S/m)

TDS (mg/l) = 16266 x AEM (S/m) Equation 1

Equation 1 is used to calculate the groundwater water salinity of the Holocene estuarine sediment, Quaternary alluvium, Cretaceous and Proterozoic rocks that have undergone varying degree of weathering. For GIS application, the coefficient in Equation 1 is rounded down to 16000.

Although there is a large number of salinity data, approximately 360, there are only 10 bores with high salinity. In addition, most of these bores are located in areas between strips of AEM data and thus do not allow direct correlation between salinity (TDS) and AEM conductivity. Thus, these bores are inferred validation point for the calculated salinity model.

A graph of groundwater salinity against AEM conductivity reveals the presence of three populations (Figure 58). The first group has high salinity but low conductivity (data lie along the x-axis), and mainly composed of Proterozoic Mount Partridge Group meta-sedimentary rocks. The second group has moderate conductivity and high salinity, and composed of both Cretaceous and Proterozoic rocks. The third population has low salinity but moderate conductivity (data lie along the y-axis), and composed of both Cretaceous and Proterozoic rocks. The first population represents fractured Proterozoic bedrock aquifer where the crystalline matrix dominate the low AEM signal, albeit the presence of saline water. The second population is associated with weathered materials, where the presence of clay, salinity and porosity has resulted in elevated conductivity. The third population is related to either conductive geological minerals in Proterozoic rock, or smectite-bearing clay facies of the Cretaceous rock, where conductivity is influenced principally by smectite rather than salinity. Cretaceous rock with brackish water is also present in this population.

The presence of the first population suggests that the calculated salinity model may underestimate the groundwater salinity in resistive fractured crystalline rock. Thus, haloes of approximate 500m to 1km are drawn around the conductive seawater intrusion zones to reflect the possible presence of brackish to saline water in AEM resistive crystalline aquifers, which include both Cretaceous and Proterozoic rocks, with the latter having higher potential to host saline groundwater. These haloes are not drawn for elevation slices bsl 0-5m and 10-15m as weathered Cretaceous and Proterozoic rocks containing saline water should be moderately conductive rather than resistive.

Using Equation 1, grids of modelled groundwater quality were generated for elevation slices 0-5m, 10-15m, 20-25m, 30-35m, 40-45m, 50-55m and 60-65m below sea level. The screen intervals and salinity (TDS in mg/l) of bores were compiled and 116 sample results were available for comparison with the predicted salinity. The results show a general trend along 1:1 relationship, with a spread within 1 order of magnitude (Figure 59). Thirteen samples, or 11 % of the data, lie beyond 1 order of magnitude. Considering the diverse range of geological formations from unconsolidated, partly or fully weathered sedimentary rocks to karstic and fractured meta-sedimentary rocks, the formation factors will influence the accuracy of the AEM to predict the water quality. Thus, the salinity model provides an overview of the range across the study area and at various depths.

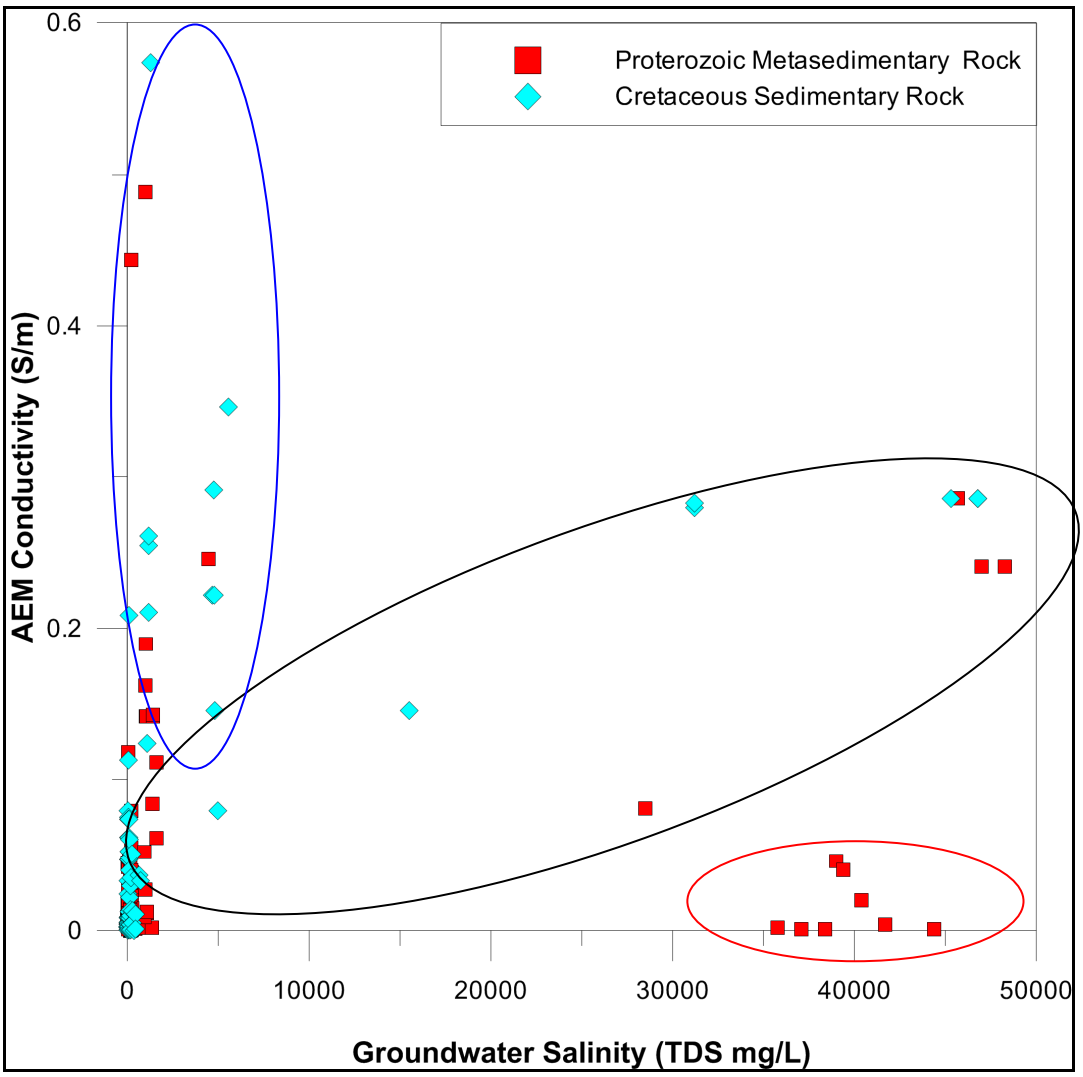

Figure 58. *Graph of borehole groundwater salinity and the AEM conductivity values showing the presence of three populations (denoted by ellipses).*

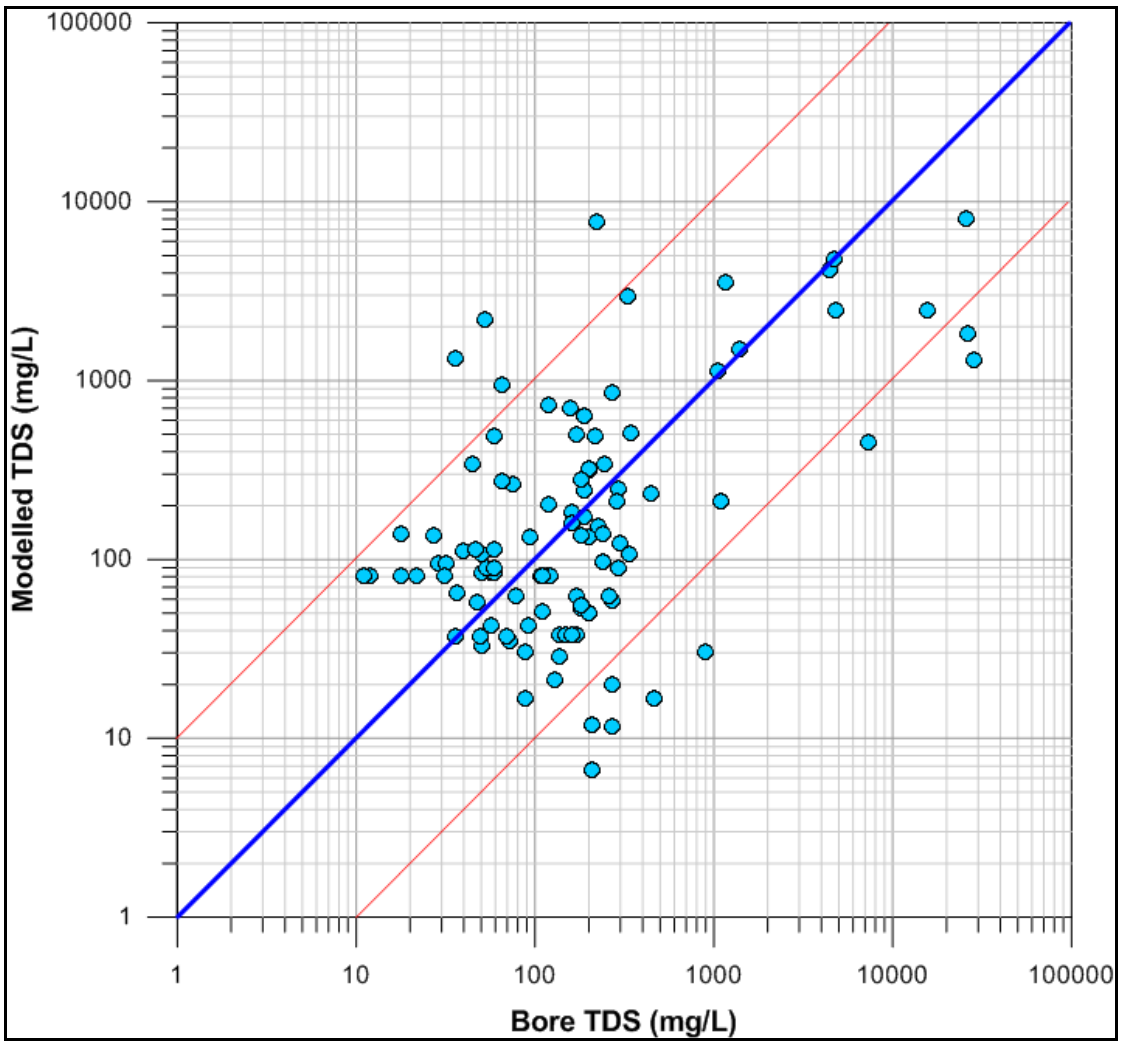

Figure 59. *Graph of modelled TDS versus measured groundwater salinity from boreholes.*

4.7.2.1 Exclusion of AEM data

Geological units such as pyritic or haematitic shale and graphitic slate are intrinsically conductive. Geological formations containing these materials have moderate to high conductivity signal. However, it is not possible to use AEM threshold values to discriminate between saline groundwater induced versus mineral induced conductivity. Nevertheless, shallow conductive outcrops and shallow sub-crop can be identified from borehole lithological information, geological maps, or from digital elevation model where the formation occurs as ridges and hills. In low lying areas where saline conductive alluvium or conductive Cretaceous rocks are present, it becomes a challenge to discriminate the conductive geological units occurring at depths. Where present, borehole lithological information is used to confirm the relative depth of the conductive geological units.

In general, the AEM conductivity associated with saline environment generally decreases with depth whereas conductive geological formations increase in values with depths. To derive a spatially robust method, new conductivity grids are generated by subtracting consecutive AEM depth interval grids, i.e. subtracting the upper grid by the lower. The resulting 'grid of difference' shows negative, near zero, and positive values. Negative values indicate increase in conductivity with depth, near zero values suggests no or minimal change in conductivity and positive values indicate a decrease in conductivity with depth. At a given location, a transition between positive to negative values suggest a potential change from saline environment to conductive geological formations (Figure 60). These depth interval grids are validated using borehole information. Moderate conductor of the Cretaceous sedimentary rock passing into saline conductive Proterozoic saprolite may also result in negative values. These outliers are identified in each depth interval and omitted from the classification. Polygons are subsequently drawn around the negative values associated with conductive mineral-bearing units and applied over the calculated groundwater salinity grid to represent

areas of data exclusion. To generate the 3D whirlwind model however, since no 'mask' can be applied to the grid, the AEM data from the conductive geological formations are removed prior to the calculation of groundwater salinity grids.

Evidence from borehole RN37150 shows the presence of conductive smectite-bearing Cretaceous clay facies. Fluids extracted from the clay are neither brackish nor saline. This facies have been identified to occur between 5m above sea level to 10m below current sea level. Polygon masks are drawn over the facies extent and are excluded in the calculated groundwater salinity grids.

4.7.2.1.1 Displaying of Groundwater Quality and Seawater Intrusion Data

The Groundwater Quality model is displayed using the seven water quality categories collated from the Australian Water Resources Assessment (2000) and the Australian Drinking Water Guidelines (2011) (Table 15). The polygons associated with conductive geological formation are applied as masks. In contrast, the SWI model uses five categories by omitting the good water categories (0-600, 600-900 mg/l TDS). The conductivity grids associated with conductive geological formations were converted to null prior to transforming the conductivity grid into the SWI model.

Table 15. *Subdivision of water quality for the groundwater quality and seawater intrusion models.*

Category	Groundwater Quality (mg/l TDS)	Seawater Intrusion (mg/l TDS)
Good	0 - 600	
Fair	601 - 900	
Poor	901 – 1,200	901 – 1,200
Slightly Brackish	1201 – 3,000	1201 – 3,000
Brackish	3000 – 10,000	3000 – 10,000
Saline	10,000 – 35,000	10,000 – 35,000
Highly Saline	>35,000	>35,000

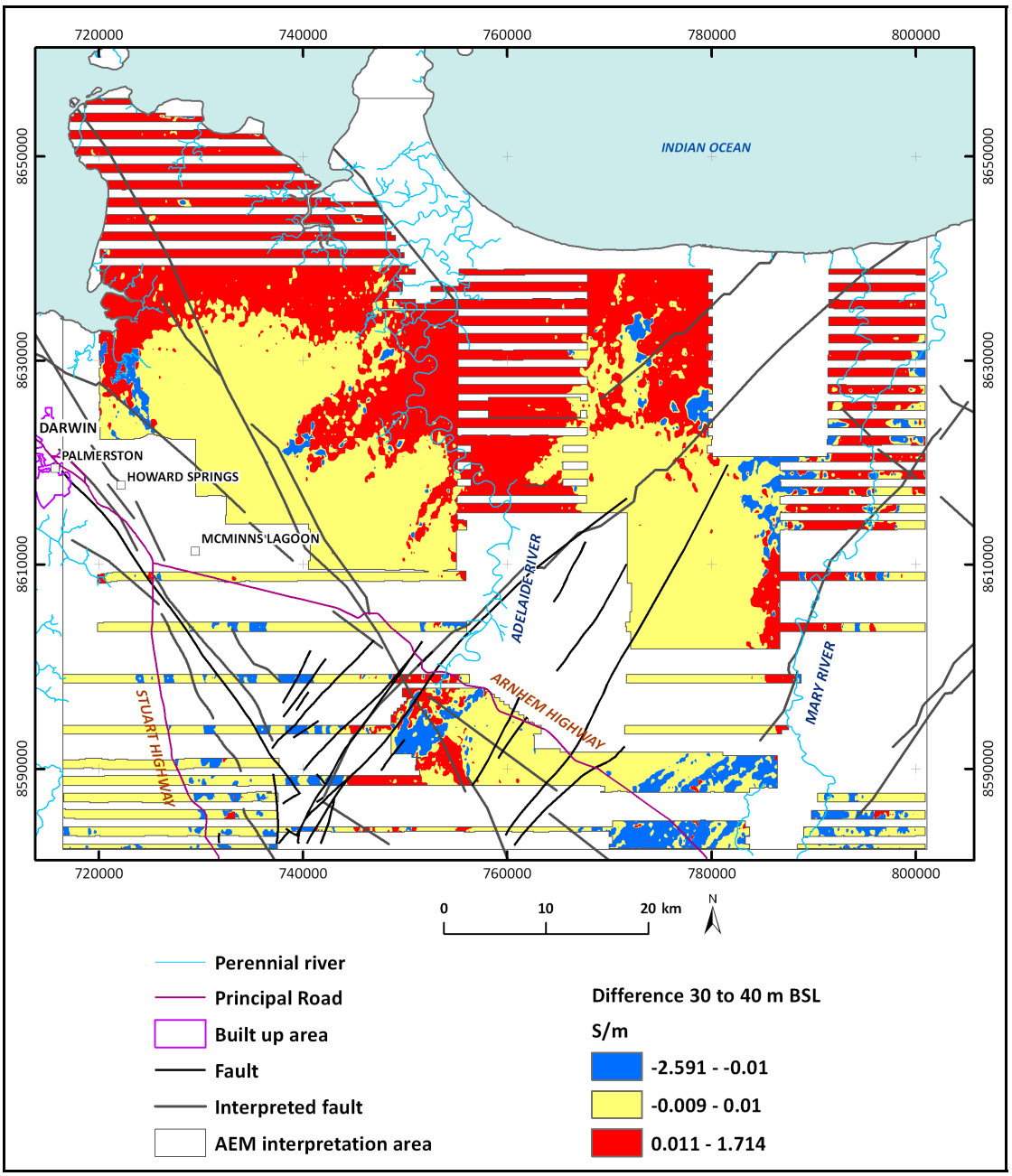

Figure 60. *New AEM grids are generated by subtracting the upper grid by the consecutive lower grid. In this case, AEM grid at interval -30 to -35 mAHD is subtracted by grid at -35 to -40 mAHD. The result shows areas of decreasing (red) or increasing (blue) conductivity with depth. Areas without much change in conductivity are depicted as yellow.*

4.7.3 Cross-sections

Six flight line sections across the western half of the area were generated using Profile Analyst™ (lines 6100701, 6101901, 6102201, 6102701, 6103302, 6103702). All but one of these lines (6103302) had geological control from the sonic drilling program. The lines were imported into Strater, along with the bore log (where present). Polygons showing stratigraphic units and the seawater intrusion zones were drawn in PowerPoint and likewise imported into Strater. Polygon interpretation was guided by conductivity patterns and the interpreted elevation slices.

5 Results

5.1 SONIC DRILLING RESULTS

A number of consistent patterns are evident in the combined borehole geophysical, spectroscopic and geochemical results, as shown in the Strater logs contained in Appendix 6.

Quaternary sediments were intersected in only one hole, RN37152, and only three samples were analysed. These show a positive association between As and Fe, indicating that the As is bounded to the Fe_2O_3, and a negative correlation between Al_2O_3 and $Fe2O_3$ consisted with the proportion of clay (kaolinite) decreasing as iron induration increases.

The general features in the Cretaceous sediments include:

- A gamma spike is present in all holes through the Cretaceous with the exception of RN37174 (where the Cretaceous is very thin and is probably a near-shore facies. Where analysed the gamma spike is associated with elevated P, U, Zn, As and sometimes S, consistent with pyritic sedimentary phosphate. A phosphate bed in the Bathurst Island Formation forms a marker bed in outcrops along the coast (Doyle 2001).
- A generally close association between the presence of saline groundwater and smectite clays. The exception to this occurs in the northernmost hole (RN37150) where the smectites are not associated with more saline water. In this hole the smectites appear associated with the clay-rich Wangarlu member of the Bathurst Island Formation.
- The basement rocks of the Mount Partridge Group, where present, are composed phyllites, formerly siltstones. No dolostone is present, despite several bores penetrating what is nominally KCD.
- High K with muscovite (grading to phengite) and elevated gamma as a consequence in all phyllitic units
- One hole (RN37152) has a zone of secondary induration, possibly associated with a fault, this shows elevated As, Zn and possibly Cu, suggesting weak mineralisation along a silicified fault zone. Iron is enriched in pore fluids from this interval.

5.1.1 Sonic bore RN37150

Bore RN37150 (Figure 61) is on gently undulating plains in the north of Koolpinyah station. Total drill depth was 54 m, and the hole ended in weathered Cretaceous sandy and silty claystone. The upper part of the drilled sequence has a slightly coarse texture, passing from muddy sand and siltstone into clay and weathered shale with minor bands of very fine sand. The drillhole was targeted to evaluate a highly conductive zone where prior knowledge from local bores indicated the presence of heavy clays overlying dark grey to black silty sediments (Fell-Smith and Sumner, 2011).

The muddy sand and siltstone are resistive (<20 mS/m), whereas the clays are moderately conductive, ranging from 300 to 500 mS/m. The gamma signature decreases from the surface to the base of the upper sequence (muddy sand and siltstone), and remain low in the clay. However, a band of high gamma spikes occur at 33-38 m depth, correlating with increased uranium associated with phosphate.

With respect to PIMA mineralogy (Figure 62), the upper part of the Cretaceous succession (0-15.5 m) consists mainly of inferred fine grained quartz with some kaolinite and iron-rich phases. Smectite-dominated clays correspond with the Wangarlu Member and are responsible for the conductivity bulge in the down hole log, despite the water not being saline (Appendix 6).

The gamma spike in the downhole log is associated with elevated phosphate, uranium,zinc, arsenic and sulphur. We correlate this with the widely distributed phosphate marker bed in the Bathurst Island Formation

(Doyle 2001), with uranium a common associate with sedimentary phosphate and the arsenic and zinc being associated with sulphides, also common in reduced sediments. Elemental geochemical cross plots (Figure 63) show that lanthanides do not correlate with Al_2O_3 but Zn, Cu and As appear to correlate with Fe_2O_3 with concentrations of up to 30ppm. For the middle of the Cretaceous succession (18.3-36.5 m) the mineralogy is a mixture of smectite, kaolinite and inferred quartz. There is good correlation between K_2O and SiO_2 which suggests that K-feldspar may occur, however there is no positive relationship between K_2O and Al_2O_3. There are also no obvious relationships between TiO_2, Zr, Th, Sn and Ta so these elements are not likely to be correlated with detrital grains. Lanthanides are not correlated with Al_2O_3 but show some relationship with Mo. The lower part of the Cretaceous section (38-52.4m) consists largely of smectite clays with some pyrite. Zr and Th correlate well indicating that they have been carried as a transported phase. As for the overlying unit, lanthanides are not locked up with Al_2O_3 but show some correlation with Mo.

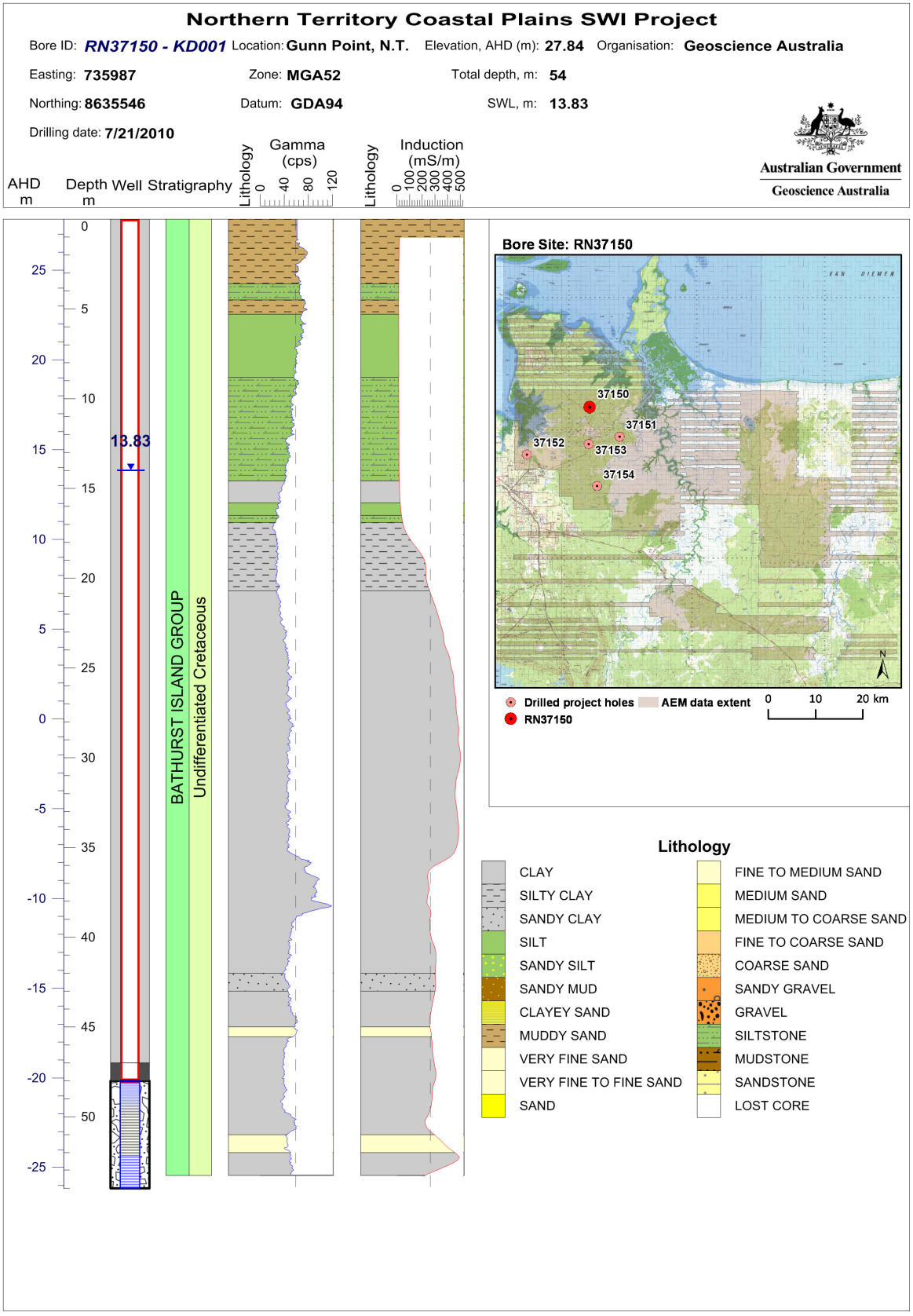

Figure 61: *Summary log of sonic bore RN37150 (KD001).*

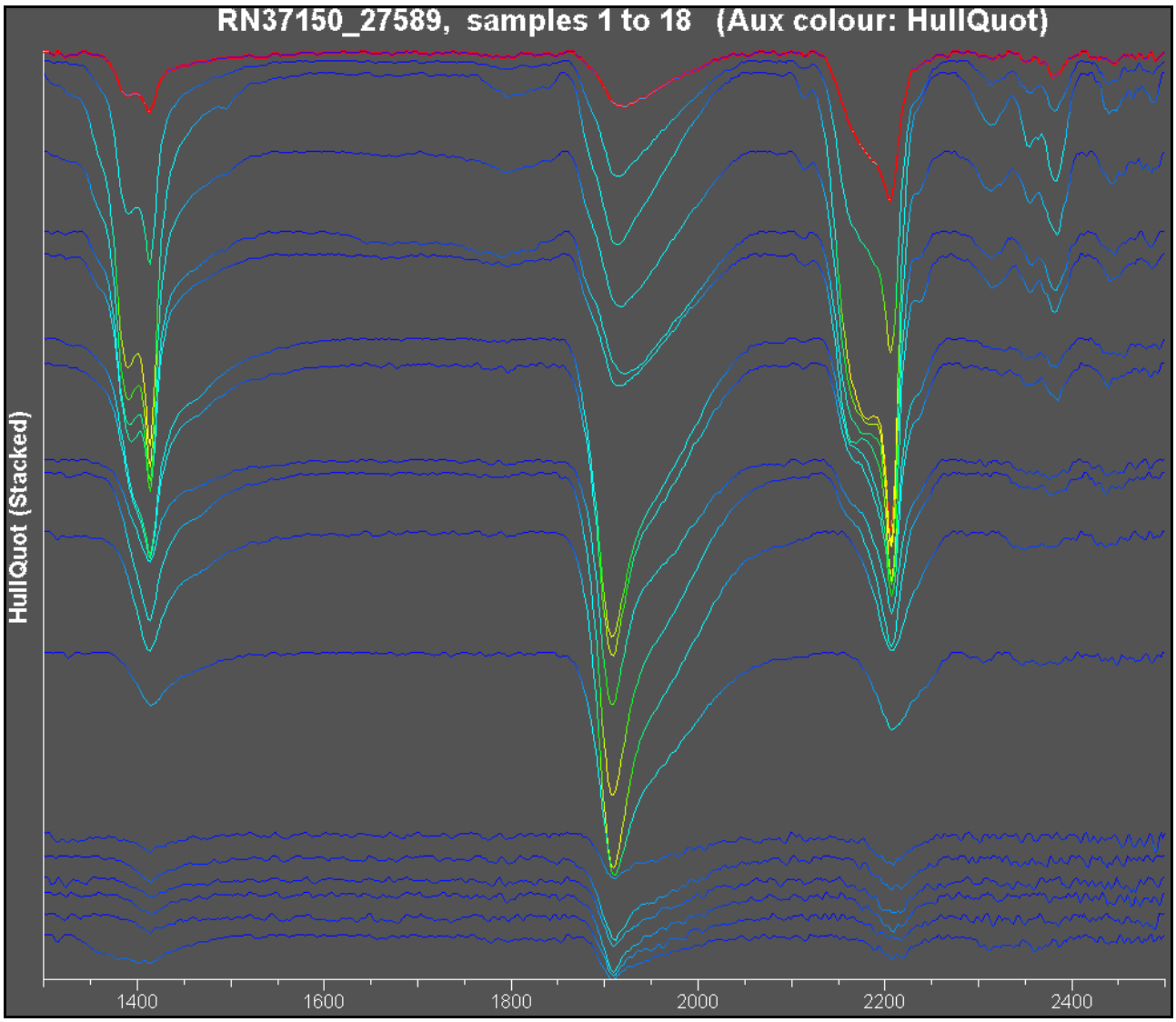

Figure 62: *Stacked PIMA results for RN37150. Strong absorption at 1910nm and 2210nm shows the presence of smectite and kaolinite respectively.*

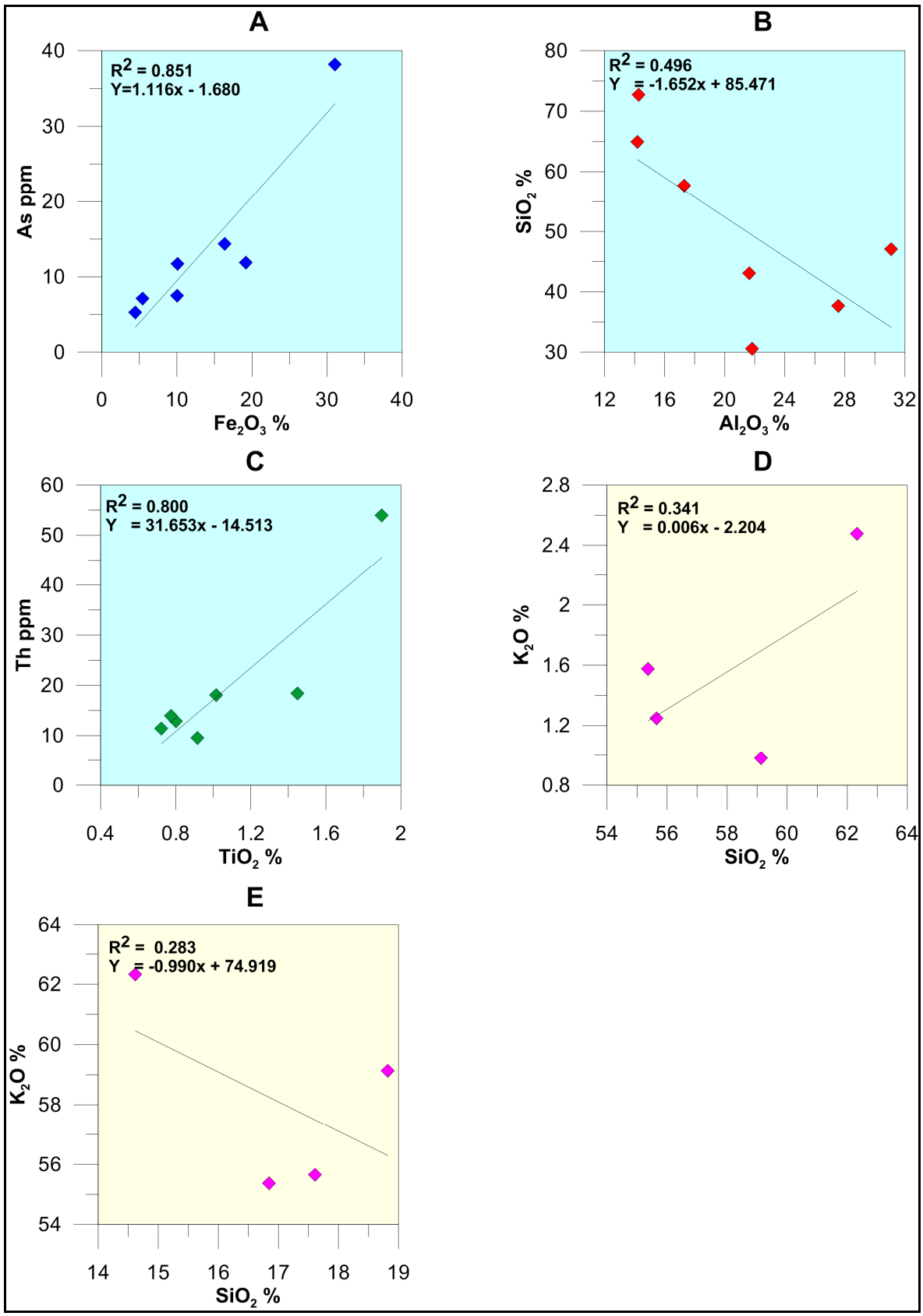

Figure 63: *Summary geochemical plots for drillhole RN37150. A-C upper (silt-rich) part Cretaceous section, D and E lower (clay-rich) part Cretaceous section. A - As/Fe_2O_3 association. B - SiO_2/Al_2O_3 association suggesting presence of clays. C – Th/TiO_2 association probably from detrital heavy minerals. D - Al_2O_3/K_2O association, probably from K-feldspar or muscovite. E - Al_2O_3/ SiO_2 association, probably from K-feldspar or muscovite.*

5.1.2 Sonic bore RN37151

Bore RN37151 (Figure 64) is on gently undulating plains near the airstrip in the centre of Koolpinyah station and is 50 m deep. The drillhole targeted an area of medium conductivity in the AEM data (Fell-Smith and Sumner 2011). The Cretaceous sedimentary rock section is 36 m thick, and consists mainly of siltstone and claystone, and two sand-bearing units approximately 3 m thick (from 9-12 m and 33-36 m depth). Underlying the Cretaceous sequence is at least 14 m of slightly metamorphosed (phyllitic) siltstone interpreted as the KCD of the Mount Partridge Group (dolostone, despite the hame of the Formation, is absent).

The induction log suggests an increasing conductivity trend, from resistive near the surface to moderately conductive (200-300 mS/m) at 22 to 33 m depths, which corresponds to the silty claystone and sandy mudstone containing more brackish water. The conductivity decreases in the KCD. The gamma signature varies throughout the Cretaceous strata, ranging from 20 to 60 API. A sharp increase in gamma responds to 80 API is present in the meta-siltstone of the KCD.

The soil contains slightly brackish (800 mg/l TDS) fluids, whereas the rest of the weathered Cretaceous rocks contain fresh fluids (<100 mg/l TDS). In contrast, the salinity in the meta-siltstone is more brackish (1,000 mg/l TDS). Chloride is the main anion in the Cretaceous strata, whereas sulfate appears to dominate in the soil horizons and the Proterozoic meta-siltstone.

With respect to PIMA mineralogy (Figure 65), the upper part of the Cretaceous section (0.2-20.5 m) consists of sandy-silty clay and is dominated by quartz and kaolinite. The lower part contains smectites, corresponding to the zone of brackish water. The presence of Fe_2O_3 in the profile suggests that Fe^{3+} minerals such as goethite and maghemite occur. The brownish yellow colours suggest more maghemite, although a mixture is more likely. PIMA also shows the presence of muscovite (or phengite) in the phyllitic Mout Partridge Group sediments.

The elemental geochemistry cross plots (Figure 66) show that Lanthanides do not correlate with Al_2O_3, but correlate with Fe_2O_3. The lower part of the Cretaceous section (25-34.8m) is clay to medium-grained sand. The minerals consist of quartz (inferred) and smectite (most likely montmorillonite). The Fe_2O_3/SiO_2 relationships indicate that maghemite and/or goethite is present. The primary colours for this section are yellowish brown and red which indicates a shift to a higher proportion of goethite. Th/Zr correlation shows that they are contained as detrital grains. Lanthanides in this less weathered part of the section are correlated with Al_2O_3, indicating that they are associated with micas. Although the gamma spike in the downhole log shows that the phosphate marker bed is present, it was not sampled, as it is difficult to recognise in core.

Accurate interpretation of the Proterozoic Mt Partridge Group is difficult due to the relatively small dataset from the phyllites at the bottom of the drillhole (36.5-47.2 m). However, the mineral composition is dominated by mica. The correlation of MgO with Al_2O_3 is consistent with phengite, whereas the correlation of K_2O with Al_2O_3 is consistent with muscovite. Fe_2O_3 does not show any reasonable correlation with the usual anions but does correlate well with K_2O which indicates jarosite, suggesting weathering of sulphides. Ta and Sn correlate well, which is consistent with them being associated with the original silty sediment protolith. Both Cu and Zn are correlated with Fe_2O_3 at concentrations of 80 and 120 ppm, respectively.

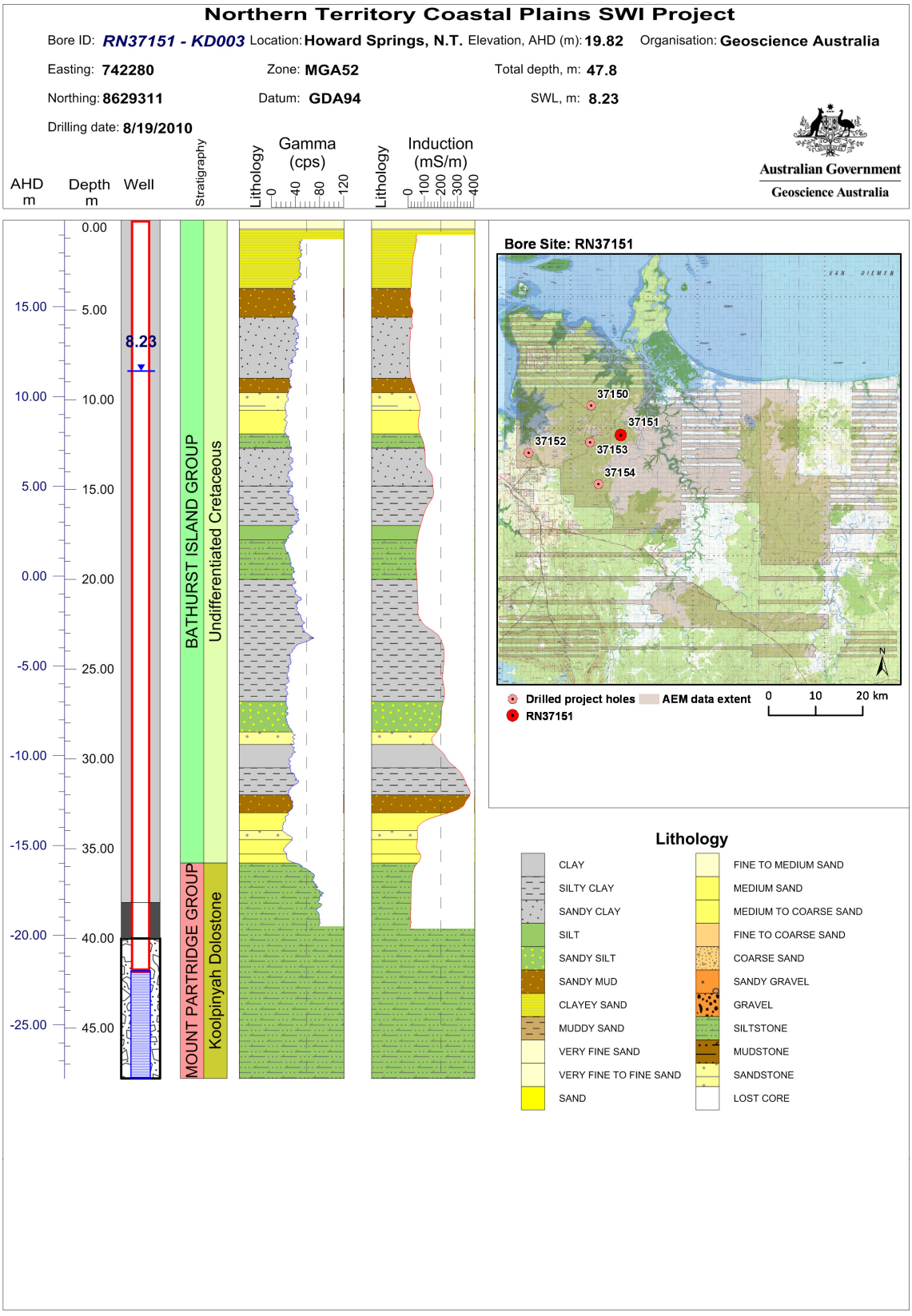

Figure 64: *Summary log of sonic bore RN37151 (KD003).*

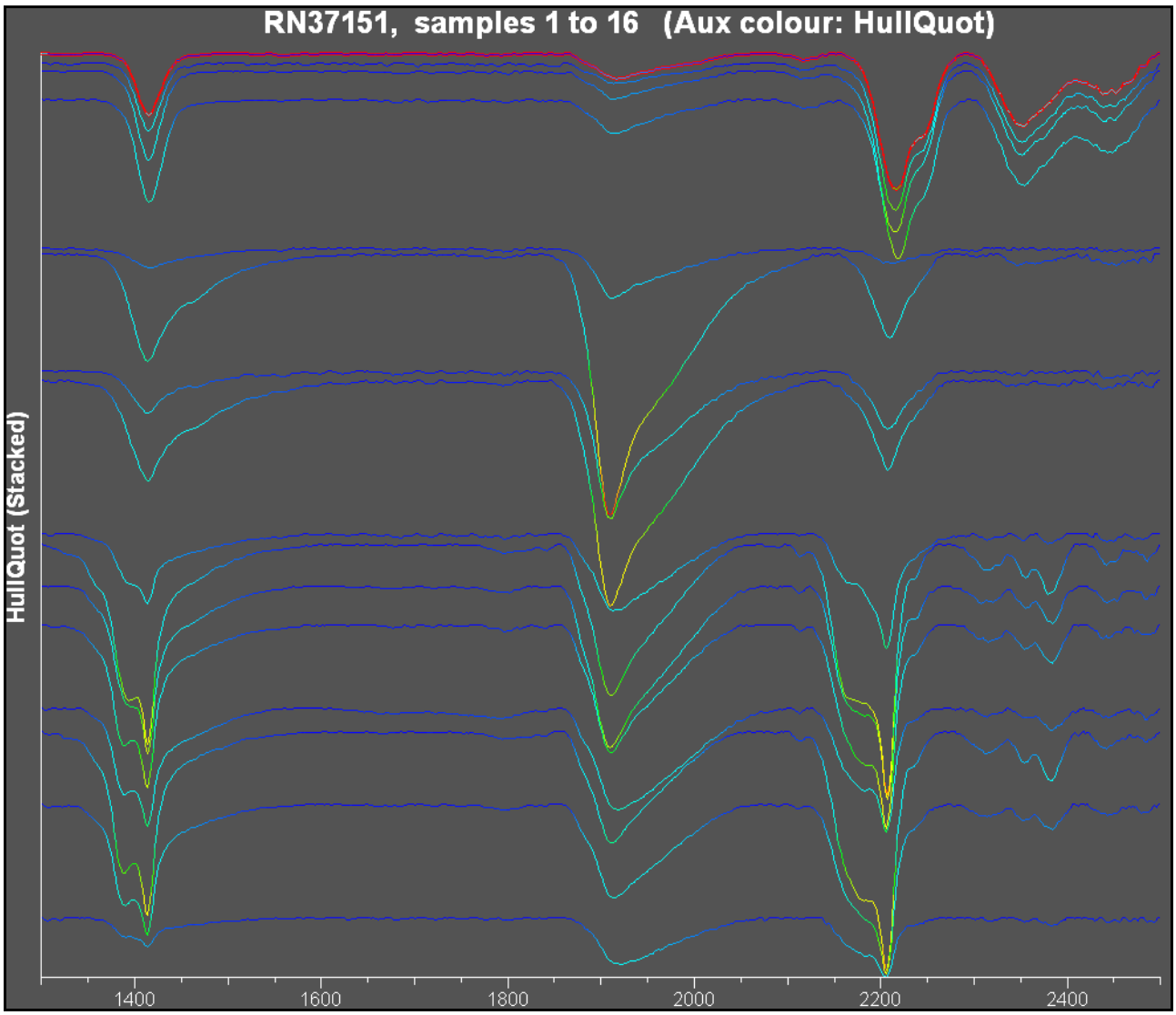

Figure 65: *Stacked PIMA results for drillhole RN RN37151. Sample with very low absorption indicates the absence of clay minerals. Strong absorption at 1910nm and 2210nm shows the presence of smectite and kaolinite respectively.*

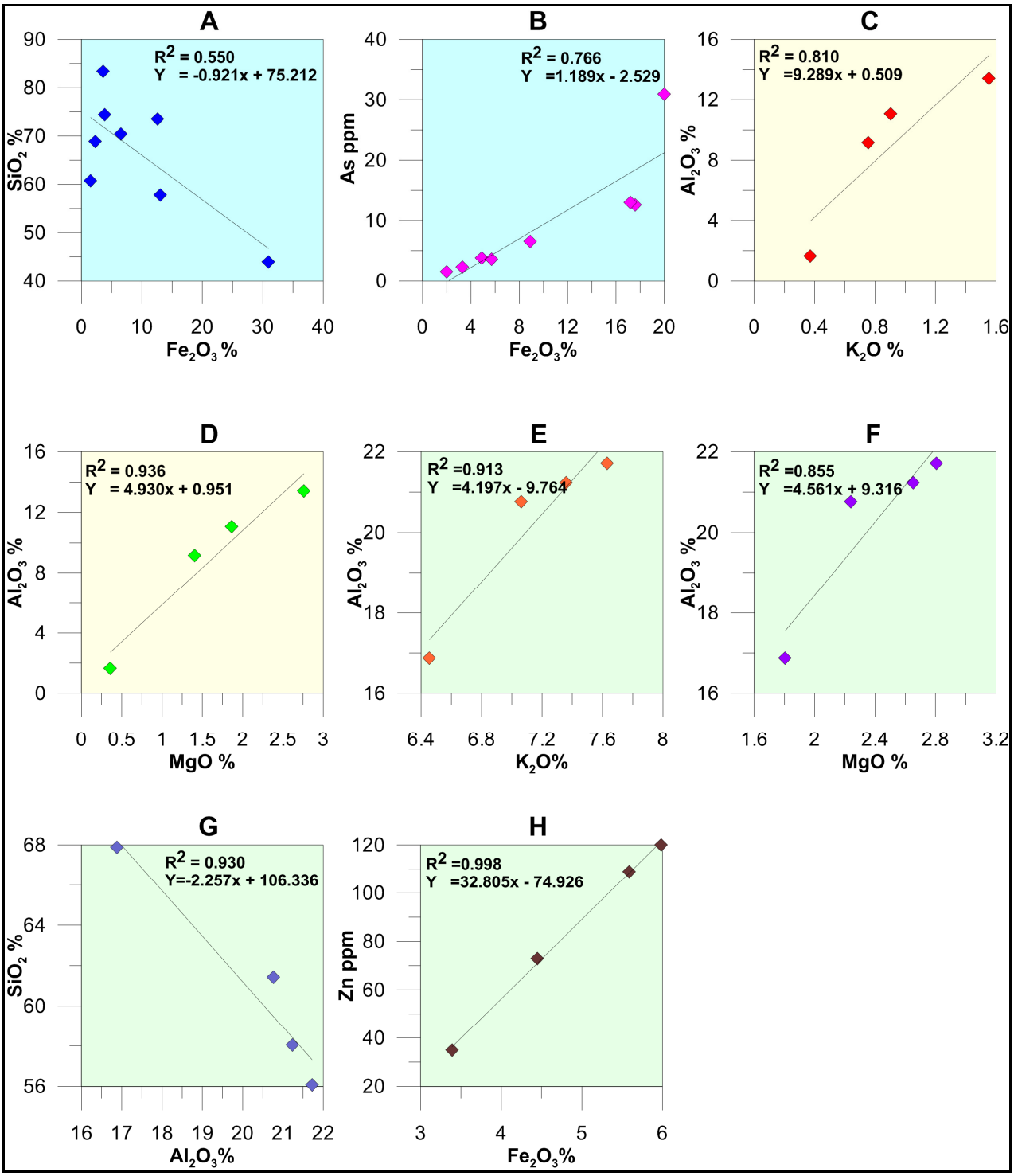

Figure 66: *(Geochemical plots shown on previous page) – Summary geochemical plots for borehole RN RN37151. A and B upper (silty) part Cretaceous section, C and D lower (clay-rich) part Cretaceous section, E-H Proterozoic section. A - SiO_2/Fe_2O_3 association. B - As/Fe_2O_3 association. C - Al_2O_3/K_2O association suggesting presence of glauconite. D - MgO/Al_2O_3 association suggesting presence of montmorillonite. E - Al_2O_3/K_2O association indicating the presence of muscovite. F - Al_2O_3/MgO association, possibly due to phengite. G - Al_2O_3/ SiO_2 co-variation suggesting presence of feldspar. H - Zn/Fe_2O_3 showing zinc being locked up with iron.*

5.1.3 Sonic bore RN37152

Borehole RN37152 (Figure 67) is on the floodplain of the Howard River, approximately 3.5 km north of Howard Springs, and reaches 52 m depth. The Quaternary sedimentary profile is 13 m thick, and composed moderately to poorly sorted fine to coarse sand and gravel. Underlying is at least 39 m of metamorphosed siltstone interpreted as the Proterozoic Wildman Siltstone of the Mount Partridge Group. A zone logged as "gravel" in the Wildman Siltstone at a depth of 30-32 m is a zone of secondary silification that has been fractured.

The induction log shows a very weak conductor (40-70 mS/m) in the upper part of the sediments, probably associated with brackish water from seawater wedge. The apparent conductivity for the rest of the hole is low (<20 mS/m) throughout the Cretaceous section and the Wildman Siltstone. The gamma response is low in the Cretaceous rocks (10-40 API) but increases (60-80 API) across the unconformity into the Wildman Siltstone. Mineral chemistry results indicate that the potassium (4 to 5 wt. % K_2O) is the cause of elevated gamma counts.

The salinity profile indicates fresh water (<200 mg/l TDS) in both the Cretaceous sedimentary rocks and the Proterozoic saprolith. Examination of the fluid chemistry suggests that Cl is the dominant anion.

With respect to PIMA mineralogy (Figure 68) and elemental geochemistry (Figure 69), the Quaternary cover of coarse sand (5-11.5 m depth) consists largely of quartz (inferred) and kaolinite. MgO and SiO_2 show good correlation which indicates small amounts of montmorillonite or phengite which are probably below PIMA detection limits. There is also a notable presence of Fe^{3+} minerals such as goethite. Th and Ta show good correlation, consistent with their occurrence as detrital grains in the sand. Lanthanides correlated well with Al_2O_3, suggesting a detrital association, and As appears associated with Fe_2O_3 (with concentrations of up to 12 ppm). MgO correlates with SiO2 which could point towards phengite. The Proterozoic rock section (14.5-50.7 m) consists of phyllite; the whole-rock geochemistry data suggests that quartz and muscovite are dominant. Iron species are not associated with SO_3 or SiO_2 and probably form goethite or haematite. The greenish colour may be due to phengite. Lanthanides appear locked up with Al_2O_3 and Zn is associated with Fe_2O_3 (with concentrations of up to 495 ppm). Elemental results over the zone of secondary induration as plotted Strater (Appendix 6) shows elevated zinc arsenic and nickel, and possibly copper, over this interval. Pore fluids are also enriched in iron.

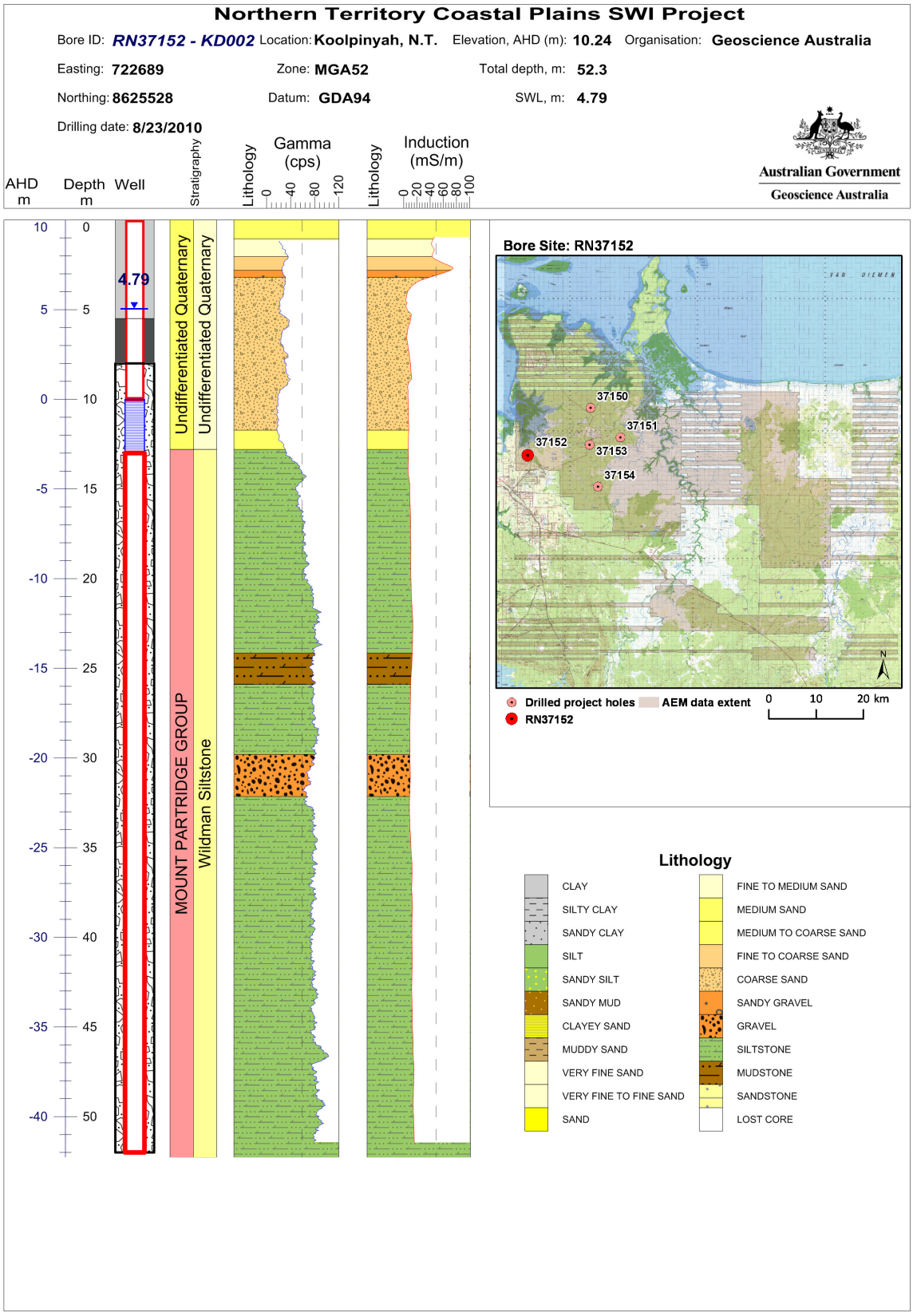

Figure 67: *Summary log of sonic bore RN37152 (KD002).*

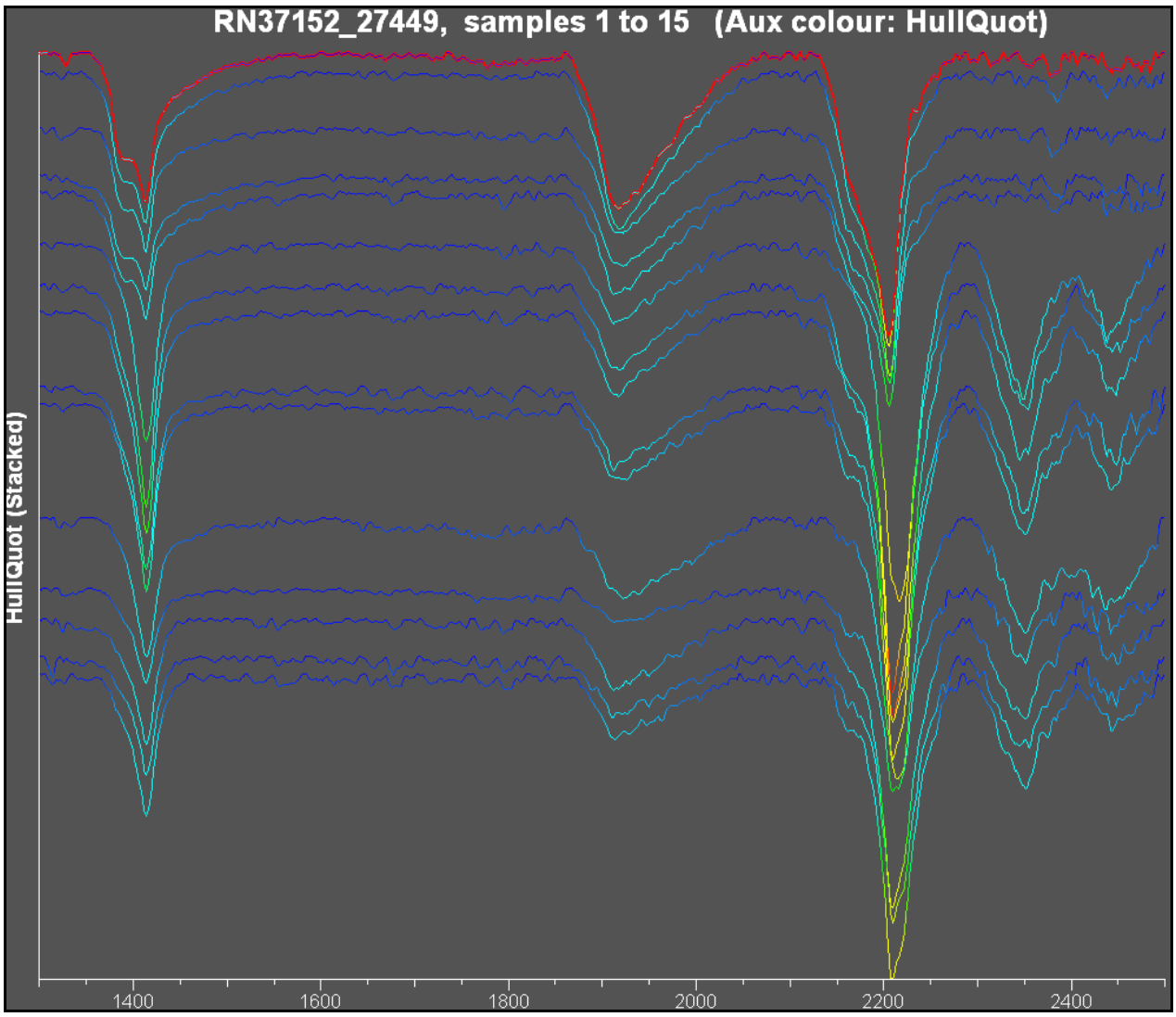

Figure 68: *Stacked PIMA results for borehole RN RN37152. Strong absorption at 2210nm coupled with moderate absorption at 1910nm shows the presence of kaolinite. Strong absorption at 2210nm coupled with weak absorption at 1910nm and moderate absorption at 2340nm shows the presence of muscovite (phengite).*

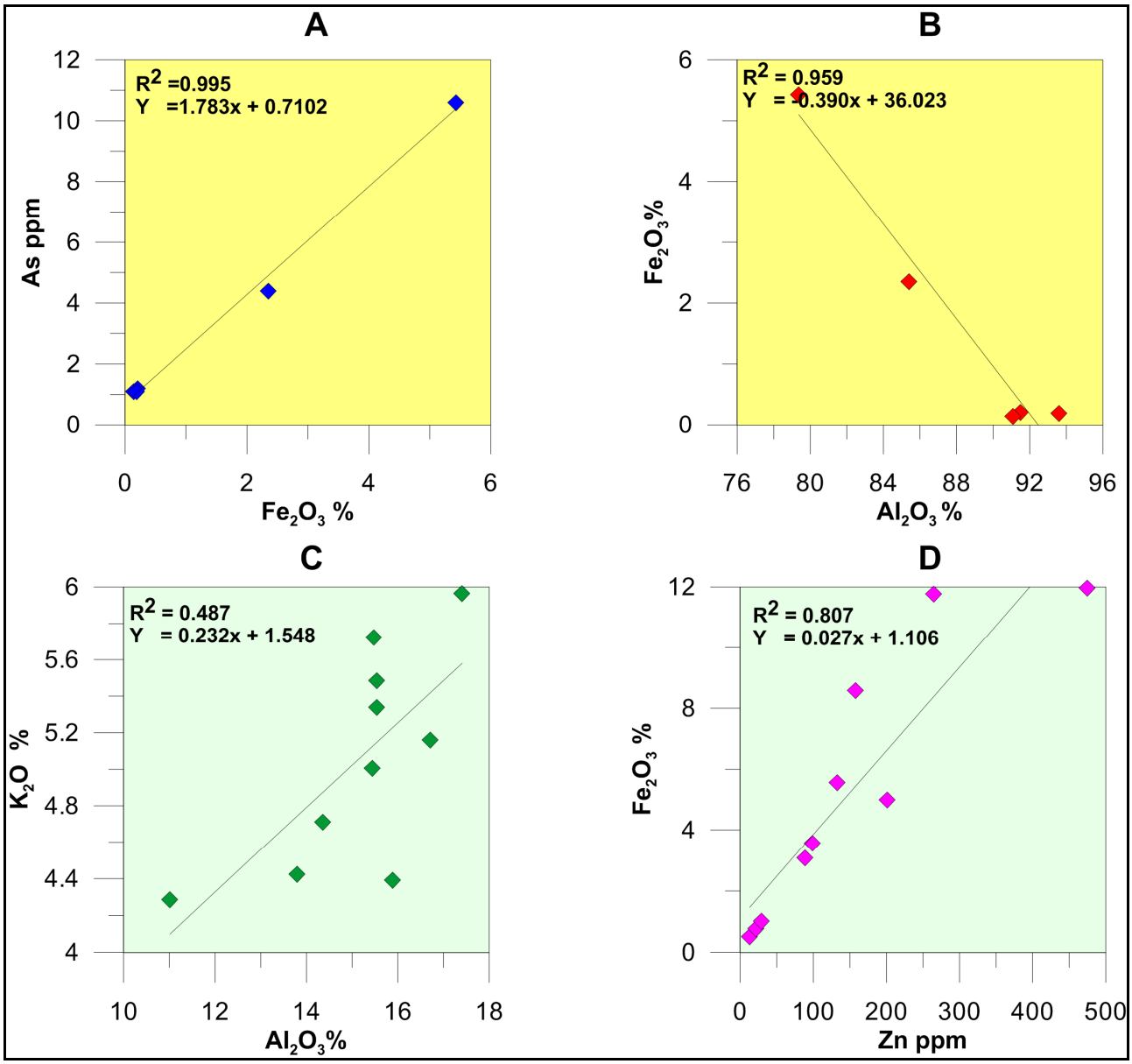

Figure 69: *Summary geochemical plots for drill hole RN RN37152. A and B: Quaternary; C and D: Proterozoic. A - Fe_2O_3/As association. B - Fe_2O_3/ SiO_2 association. C - K_2O/Al_2O_3 association suggesting muscovite. D - Zn/ Fe_2O_3 association.*

5.1.4 Sonic bore RN37153

Bore RN37153 (Figure 69) is on gently undulating plains 600 m east of Koolpinyah station main gates and reaches 72 m depth. This drillhole was targeted in an area of low conductivity in the AEM data (Fell-Smith and Sumner 2011). The only geological unit encountered in this drillhole was undifferentiated Cretaceous sedimentary rocks of the Bathurst Island Group. The upper part of the sequence is coarser textured, consisting mainly of clayey sand. The remaining sequence is dominantly clay, with a thin layer of sand from 69-72 m depth.

The induction log shows an overall resistive profile (<20 mS/m), with a slight elevated apparent conductivity near the surface probably associated with the ferruginous zone. The gamma log has a variable response across the Cretaceous sedimentary section, ranging from 40 to 60 API with several spikes to 80 API.

The fluid chemistry profile confirms that the pore waters are fresh, generally less than 100 mg/l TDS, and chloride is the dominant anion. This is consistent with AEM results.

The PIMA mineralogy (Figure 71) shows that the upper part of the Cretaceous sequence (0.3-27.2 m, composed of clayey sand) consists largely of quartz (inferred) with some clay minerals such as kaolinite. Maghemite is present at the surface and goethite and haematite occur at depth.

The elemental data cross plots (Figure 72) show some correlation between Fe_2O_3 and P_2O_5, possibly suggesting weathered phosphorite beds over this hole. This is born out by a gamma spike between 48 and 53 m depth, with enrichment in phosphorous and uranium. Associated with the gamma spike is elevated zinc and arsenic, sulphur is not enriched, suggesting that the phosphate bed was not in this location pyritic. A strong weathering overprint is indicated by the lack of correlation between Th, Zr, TiO_2 Ta and Sn. There is a strong association of As with Fe_2O_3 (As concentrations of up to 39 ppm). Lanthanides are not associated with Al_2O_3. The middle part of the Cretaceous sequence (30.2-61 m) is clay-rich and consists primarily of quartz (inferred) and kaolinite with small amounts of goethite and haematite. Good correlation between Th and Sn as well as Ta and Sn is consistent with them being hosted by detrital grains. As before, As is locked up with Fe_2O_3 (As concentrations up to 25 ppm) and lanthanides are not correlated with Al_2O_3. The lower part of the Cretaceous section (65.35-70 m) includes silt, clayey sand, and coarse sand. The mineralogy and geochemistry data indicates quartz and kaolinite, consistent with the mineral composition. The presence of Fe^{3+} minerals is also indicated. The interval possibly contains K-feldspar, indicated by the K_2O and Al_2O_3 relationship, and correlation of Ta and Sn indicates that these occur in detrital minerals. Both Zn and Cu are associated with Fe_2O_3 (Cu up to 38 ppm, Zn up to 160 ppm), and lanthanides are locked up with Al_2O_3.

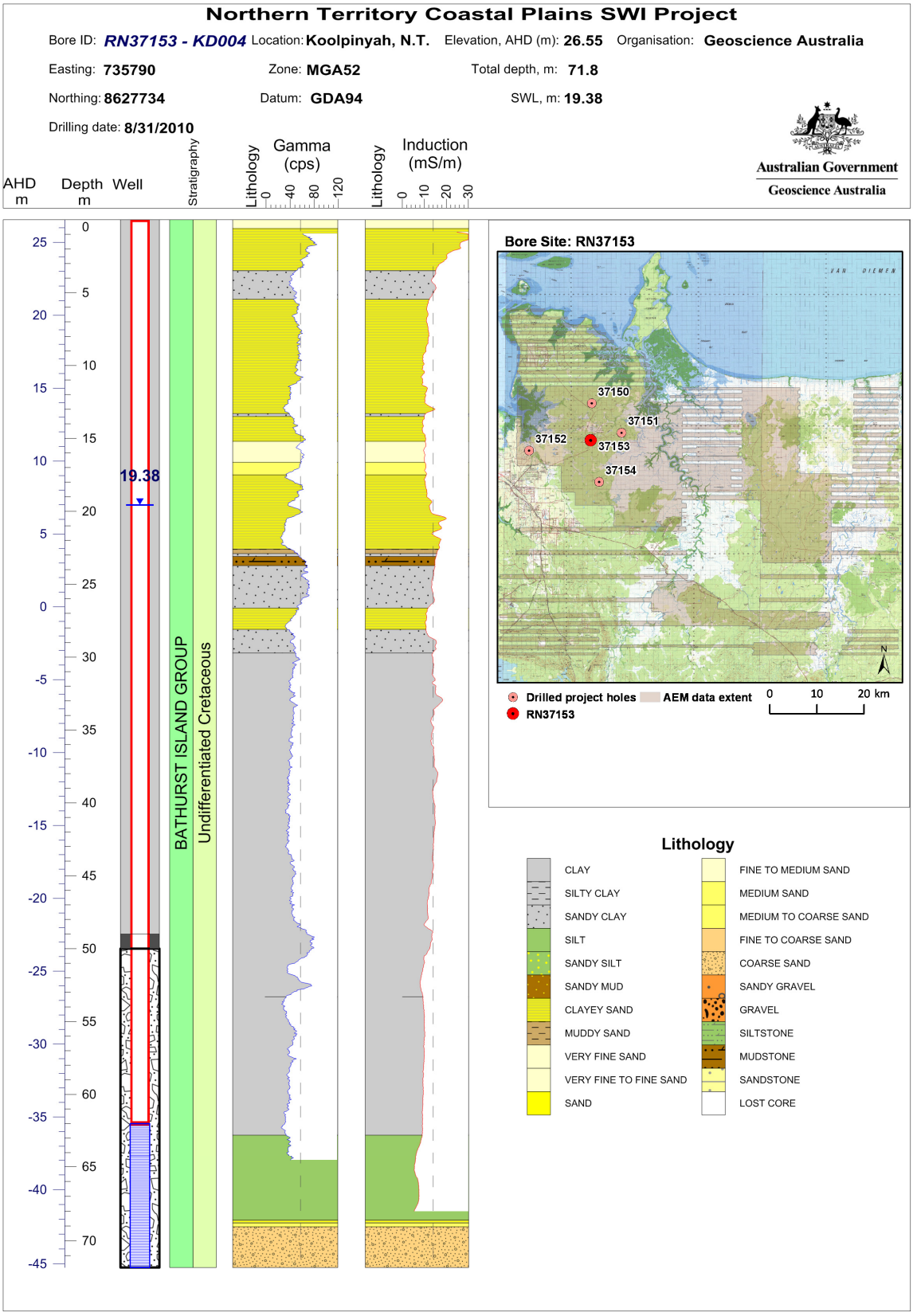

Figure 70: *Summary log of sonic bore RN37153 (KD004).*

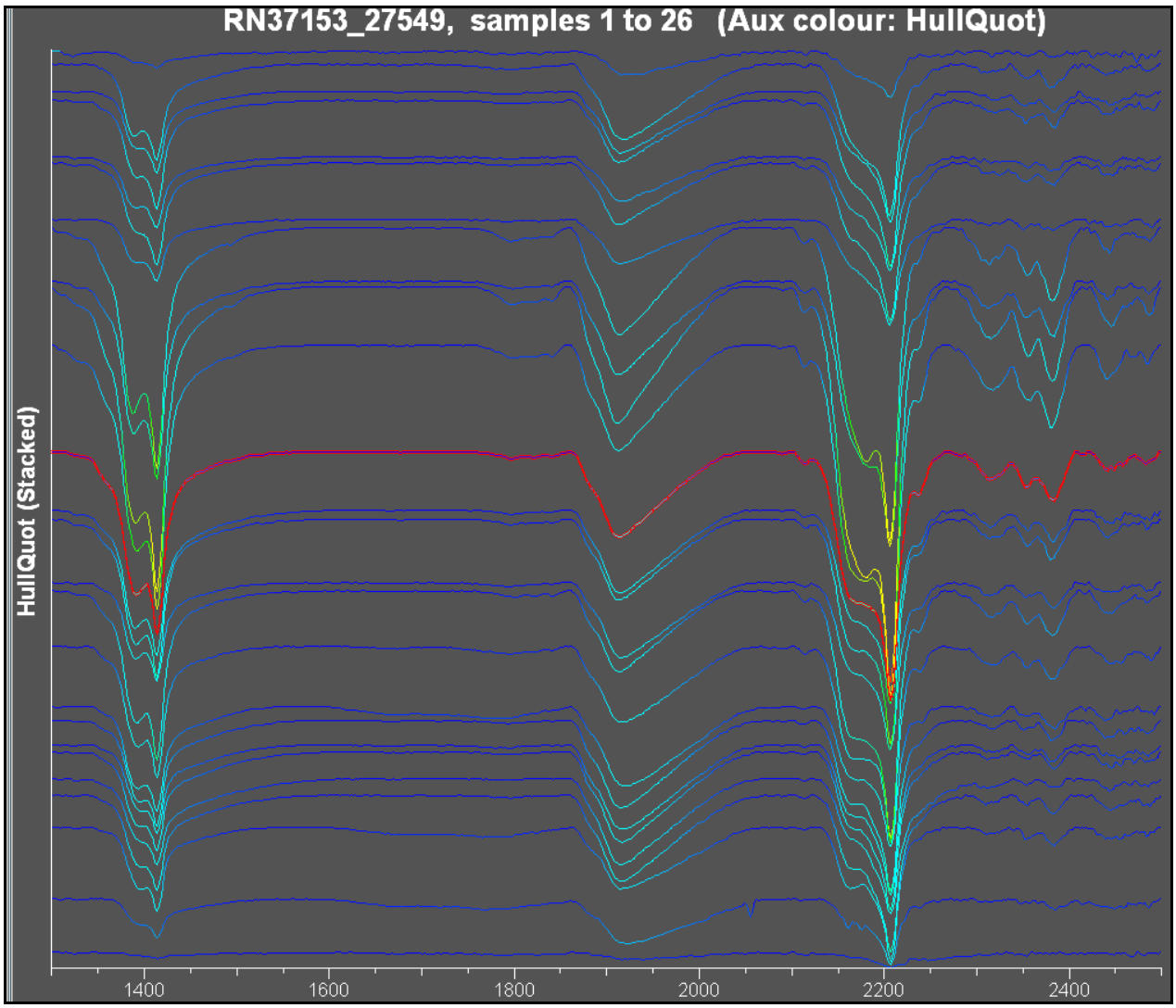

Figure 71: *Stacked PIMA results for drillhole RN RN37153. Strong absorption at 2210nm with coupled moderate absorption at 1910nm shows the presence of kaolinite.*

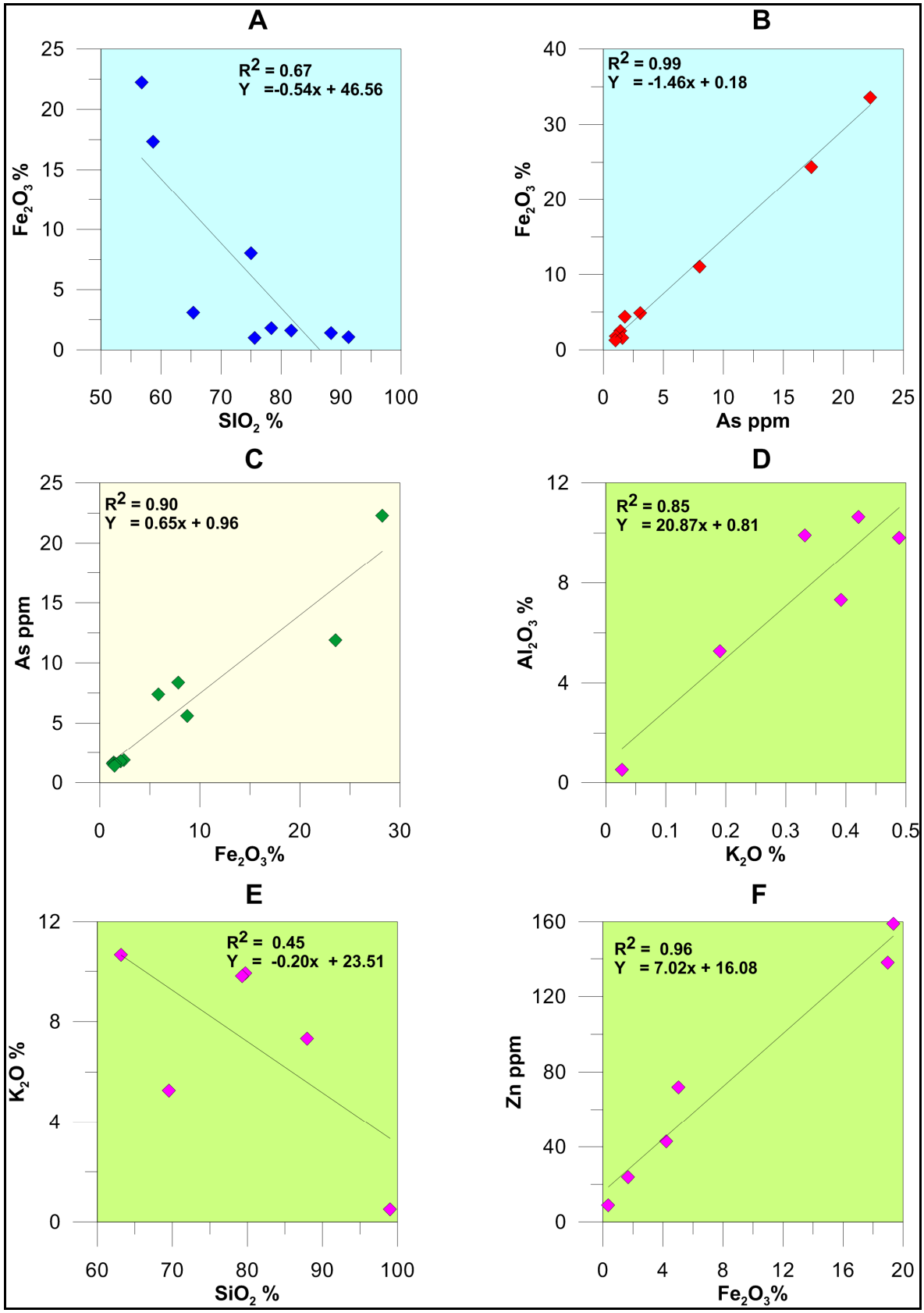

Figure 72: *Summary geochemical plots for drill hole RN37153. A-B Upper (silty) part of Cretaceous succession, C: middle (clay-rich) part of Cretaceous succession, D-F lower (sandy) part of Cretaceous succession. A - Fe_2O_3/ SiO_2 showing association of quartz and Fe^{3+} minerals. B: Fe_2O_3/As association in upper part of Cretaceous section. C: Fe_2O_3/As association in middle part of Cretaceous section. D - K_2O/Al_2O_3 suggesting presence of muscovite. E: SiO_2/Al_2O_3 suggesting presence of feldspar. F: Zn/ Fe_2O_3 association.*

5.1.5 Sonic bore RN37154

Bore RN37154 (Figure 73) is on gently undulating plains at the north boundary of the Black Jungle Conservation Reserve. The hole was targeted at an area of low conductivity (Fell-Smith and Sumner 2011). Total drill depth is 60 m, with the Cretaceous-Proterozoic unconformity at 15 m depth below surface. The weathered Cretaceous sedimentary profile includes thinly bedded sand, sandy mud, sandy silt and clayey sand. The Proterozoic rock consists of meta-siltstone interpreted as the KCD.

The induction log shows a weak conductor associated with the clayey sand at the base of the Cretaceous section. Apparent conductivity is low (~20 mS/m) and becomes lower (~10 mS/m) from 40 m depth, suggesting a boundary between saprolite and saprock. The gamma response is high (80 API) near the surface and decreases to 20 API at the base of the Cretaceous section. The gamma trace increases across the unconformity and remains consistently high (>80 API) in the Proterozoic phyllite.

The fluid in the Cretaceous rock is fresh (<100 mg/l TDS), and salinity levels increase slightly in the Proterozoic phyllite section (100-400 mg/l TDS). Fluid chemistry suggests that chloride, rather than sulfate, is the dominant anion.

PIMA mineralogy (Figure 74) shows that the Cretaceous section (1-13.3 m), logged as sandy silt and medium- to coarse-grained sand, largely consists of quartz (inferred) and kaolinite. The absence of smectite is consistent with the freshwater nature of the groundwater. Muscoite (or phengite) is present throughout the Proterozoic phyllites.

Geochemical cross plots shown that Fe2O3 and SO3 concentrations indicate the presence of pyrite, probably as a diagenetic phase (Figure 75). Feldspar may also occur as indicated by the SiO_2 and K_2O relationship. However, the stronger SiO_2 and Al_2O_3 relationship shows that quartz is predominant. Both Th and Sn show good correlation which is consistent with then occurring in detrital minerals. Lanthanides do not seem to be locked up with Al_2O_3 but this is difficult to determine due to the relatively low resolution of the data in this section. Both Cu and As correlate with Fe_2O_3 and have concentrations of up to 25 ppm and 60 ppm respectively. This suggests that they are associated with pyrite. Some correlation between MgO and SiO_2 are indicative of phengite, probably as a detrital phase. The uppermost 7 m show progressive enrichment in arsenic, bismuth and copper along with iron. This is probably a weathering-related feature, however the source of the heavy metals and the arsenic is unknown.

The Proterozoic section (17-59 m) of this drillhole consists of phyllite, largely composed of muscovite and inferred quartz. However, the strong yellow/red and grey colouring along with a seemingly independent Fe_2O_3 profile suggests the presence of goethite as well as haematite. Th and Sn relationships suggest that some of the material is in detrital minerals although the relationship is not uniform. Lanthanides are correlated with Fe_2O_3 in this section

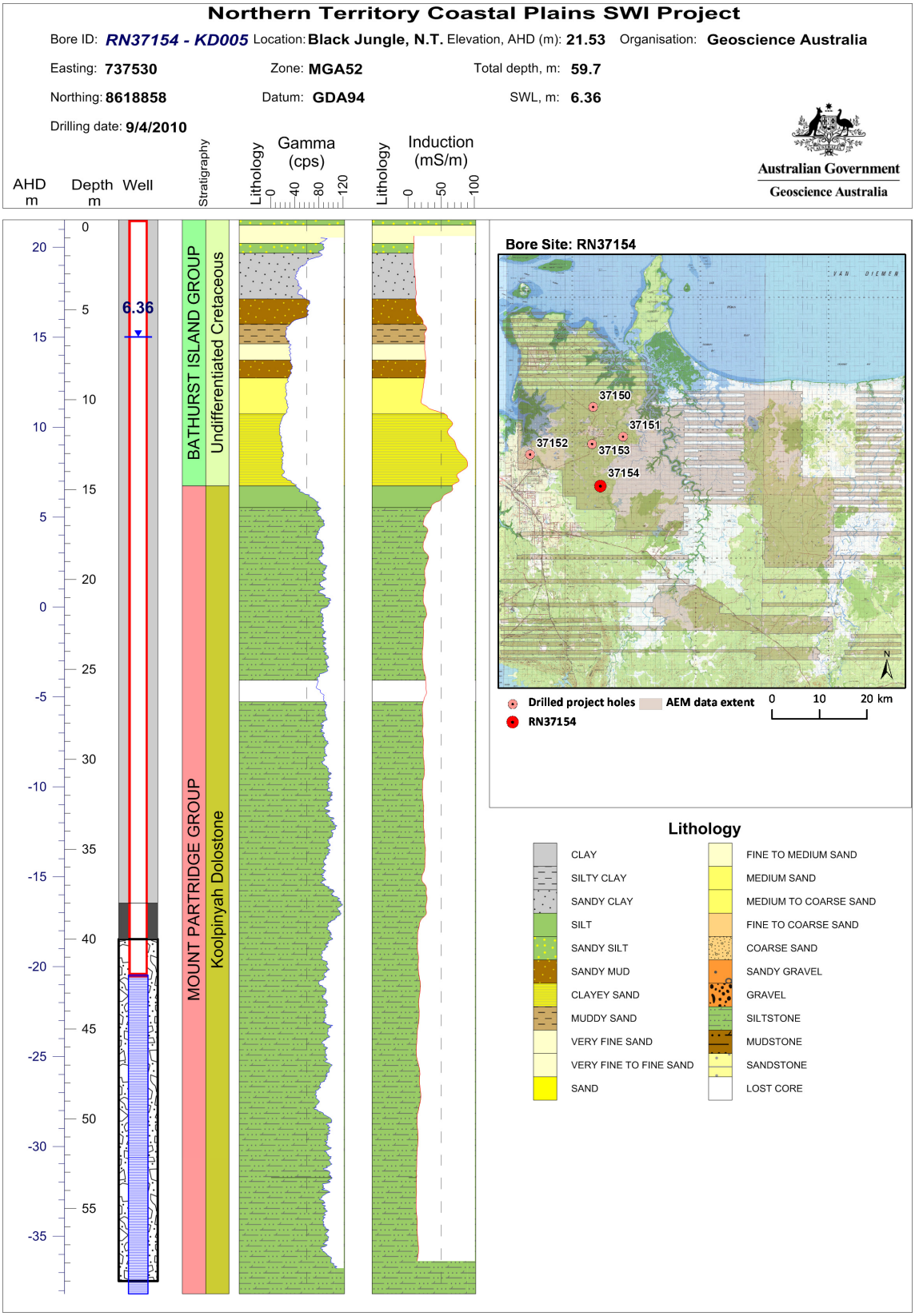

Figure 73: *Summary log of sonic bore RN37154 (KD005).*

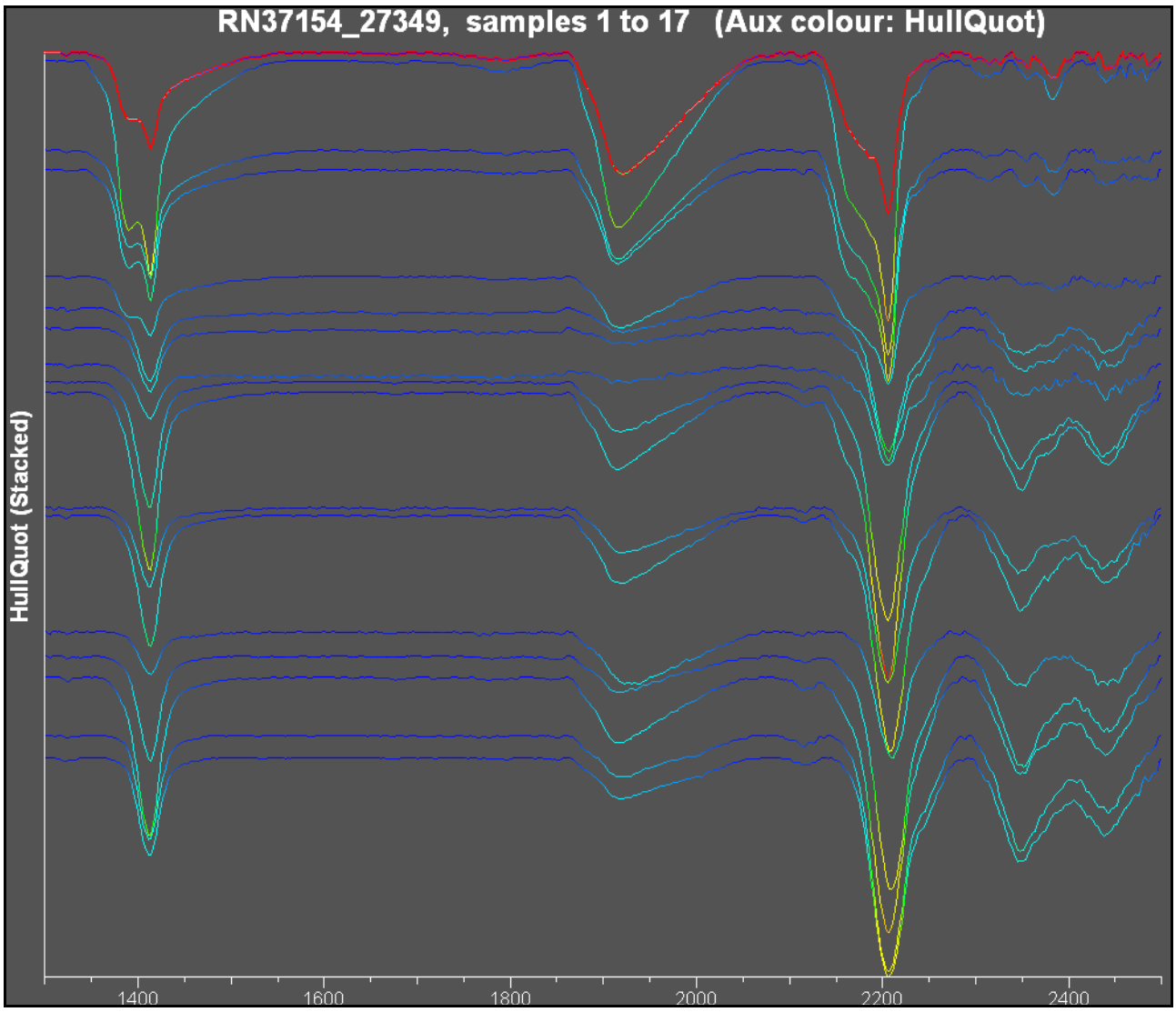

Figure 74: *Stacked PIMA results for drillhole RN RN37154. Strong absorption at 2210nm coupled with moderate absorption at 1910nm shows the presence of kaolinite. Strong absorption at 2210nm coupled with weak absorption at 1910nm and moderate absorption at 2340nm shows the presence of muscovite (phengite).*

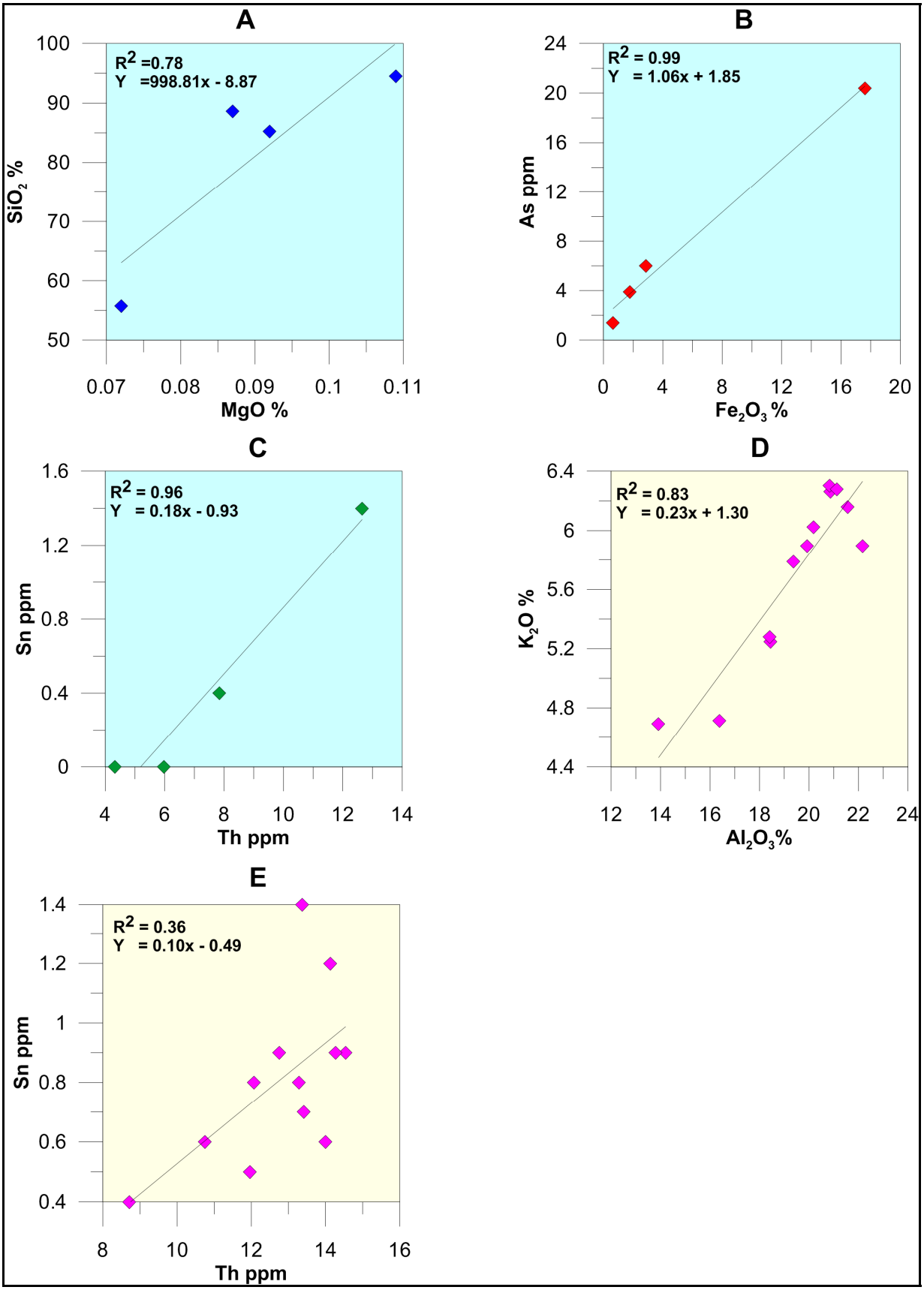

Figure 75: *Summary geochemical plots for drillhole RN37154. A–C Cretaceous, D–E Proterozoic. A: SiO_2/MgO suggests phengite; B: Fe_2O_3/As association; C: Sn/Tn relationship suggests detrital association; D: K_2O/Al_2O_3 relationship suggesting muscovite occurs.*

5.1.6 Conductive and Resistive Clays

The pore fluids extracted from the muddy sand and siltstone have low salinity (80-200 mg/l TDS). In contrast, the clays contain brackish to saline fluids, with TDS ranging 4,000-20,000 mg/l and corresponding EC values of 5,000-12,000 µS/cm. The fluid chemistry indicates that sulfate rather than chloride is the dominant anion in the clays, and calcium and magnesium both dominate over sodium.

Conductive Cretaceous clay facies (up to 500 S/m) is present in sonic bore RN37150. Four samples from the conductivity zone (20 to 36m depths) were extracted for fluids and the results indicate no sign of salinity. New set of samples were reanalysed and again the results show very low TDS (< 100 mg/l). This suggests the clay may be the cause for the elevated conductivity values.

90 samples were analysed using portable infrared mineral analyser (PIMA) to identify the dominant phyllosilicate (clay) minerals. The results show that kaolinite and montmorillonite (smectite) are the main clay types for the Cretaceous sedimentary rocks (66 samples), whereas muscovite is dominant in the Proterozoic phyllitic saprolith.

Using pore fluid or saturation extract TDS of 1000 mg/l to divide the samples into fresh and brackish, the data shows a single kaolinite population, i.e. they are all non-brackish. In contrast, there are two smectite populations, the first is non-brackish and the other is brackish. The PIMA method is not able to provide a quantitative result. However, the relative absorption of the wavelength spectrum allows the relative abundance to be determined. The background of the PIMA spectrum has a value of 1 and each mineral has a main diagnostic spectrum. For example, the main trough for kaolinite is at 2210nm and the main smectite trough is at 1910nm. Minerals with high abundance will have a deep absorption diagnostic trough approaching 0.5 whereas sample with low clay abundance will have absorption trough remaining close to the background of 1.

Plotting the PIMA absorption intensity against apparent conductivity from borehole induction logs reveals apparent trends (Figure 76). The relative abundance of kaolinite varies from low to moderate, these samples are non-brackish and has low apparent conductivity, dominantly less than 30mS/m with a few samples vary up to 140mS/m. The non-brackish smectite-rich sample has conductivity ranging from 150mS/m to 500mS/m. There is one non-brackish low smectite abundance sample with conductivity of 50mS/m. The population with low smectite abundance and brackish fluid has conductivity ranging from 230mS/m to 500mS/m. This result supports the presence of conductive Cretaceous sedimentary unit solely attributed to the presence of abundant smectite and not salinity.

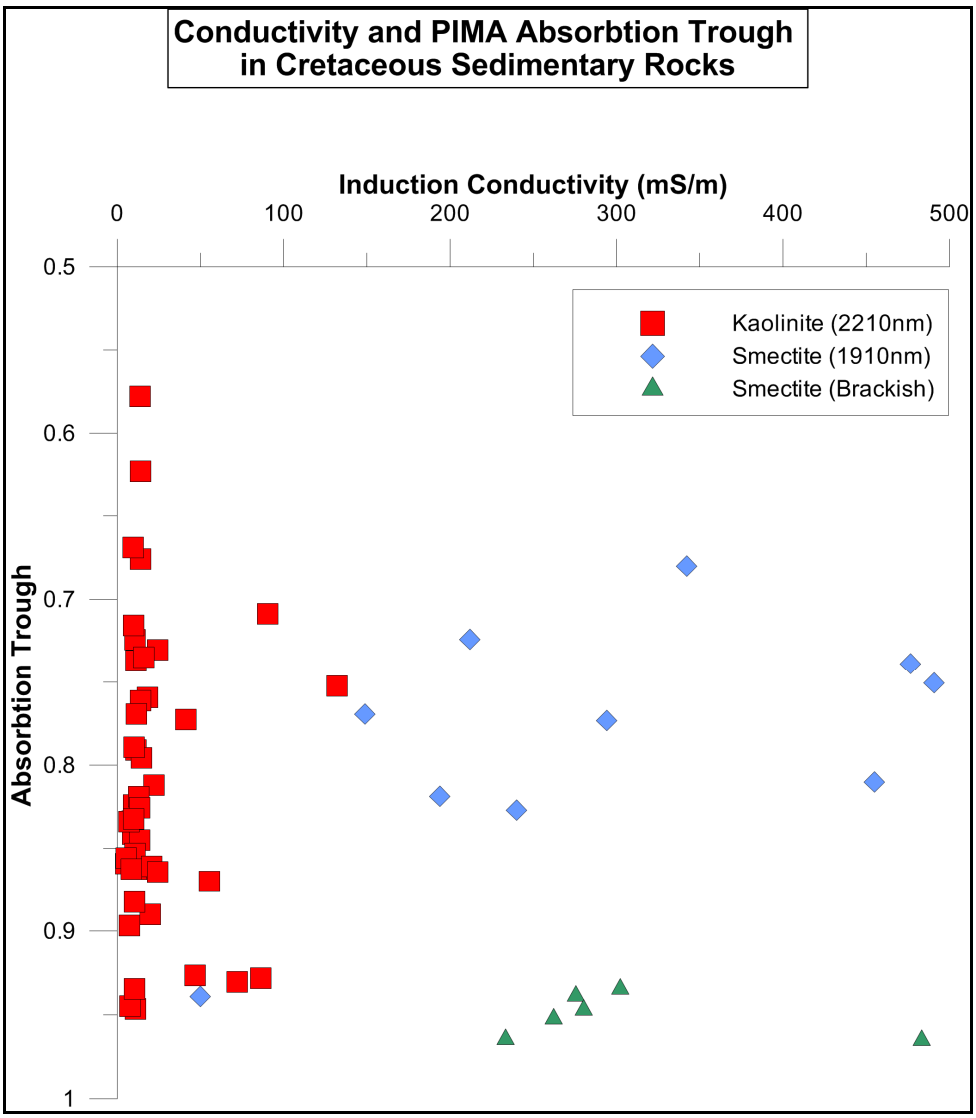

Figure 76: *Correlation between PIMA-derived clay mineralogy and conductivity (salinity). Kaolinite correlates strongly with fresh water and resistive zones, smectite with either fresh or brackish water and dominantly conductive zones.*

5.2 ROTARY DRILLING RESULTS

5.2.1 RN37216

This hole was drilled as a pair with RN37217, the pair being designed to test the magnetic feature that marks the dividing line between highly saline groundwater to the SE and fresh water to the NW. The hole was also designed to test the orientation of the intersected rock types. The holes were drilled 200 m apart with the aim of making stratigraphic correlations; however, the rock sequences dip steeply and correlations are not possible. The location is shown in Figure 54. A geological log from this hole is shown in Figure 77 (upper section) and Figure 78 (lower section). The top 21 m of RN37216 consists of Darwin Formation sedimentary rocks with mottled sandy clay and clay; these weathered rocks have no apparent aquifer characteristics.

The upper 65 m of the Proterozoic sequence is dominated by weathered schistose material and quartzite with two 10 m dolostone interbeds. From 88 m to EOH at 162 m dolostone is the dominant rock type with increasing phyllitic schist and quartzite down-hole.

Electrical conductivity (EC) data obtained from groundwater samples in this drillhole show that the groundwater within the KCD over this interval (50-160 m) is more conductive than seawater. The spatial distribution of this conductivity anomaly is consistent with a wedge of saline groundwater and is strongly indicative of seawater intrusion encroachment into the KCD. A conductivity section showing the seawater intrusion wedge through this feature is shown in Figure 79. Further analysis and interpretation is necessary; however the AEM survey data successfully mapped the seawater intrusion interface in the project area.

5.2.2 RN37218

This drill hole (Figure 80) was constructed on the floodplain to test the AEM data interpretation, which indicated possible low salinity water in an area previously considered to be saline (being well out on the floodplain). Sandy sediments of the Darwin Formation were encountered in the top 25 m with clay supported gravels to 32 m. Proterozoic dolostones then occurred to EOH at 72 m. On airlift the EC of groundwater at the Proterozoic unconformity was 696 µS/cm, whereas at the base of the drillhole groundwater was 2,400 µS/cm; these variations provided evidence to validate the AEM data.

5.2.3 RN37330

Drilled on an AEM conductivity anomaly centred at depth of around 110 m, this hole was designed to test whether the anomaly was due to lithology or the source of the modest rises in salinity that occurs in one of the bores 1,500 m away at Howard Springs. This hole encountered black siltstones of the Whites Formation that became pyritic (mainly veining) from about 87 m through to where the sequence is thrust faulted against the KCD at 128 m, indicating that the pyrite is probably the conductor (Figure 81 and Figure 82).

5.2.4 RN37331

This drillhole (Figure 83) was sited with the aid of AEM data, magnetic data and visual interpretation at a point where two crossing faults with apparent dolerite intrusive rocks coincide for a short distance in the AEM section (Figure 84). The intention was to target the dolerite dykes to ascertain whether they provide a barrier to groundwater flow. The drillhole intercepted fresh dolerite at 49 m and back logging indicated saprock and saprolite up to 9 m thick where there is a thin aquifer (pumping at 2 l/s) at the base of the Cretaceous units. Local bores indicate basement intersections around 35 m below surface, suggesting that the dolerite dykes were a significant ridge in the pre-Mesozoic topography.

The location of RN37331 was based on an AEM synthetic cross-section (Figure 84) showing that saprolitic material (doleritic) forms a conductive zone above intersecting dolerite intruded faults (centre of the image).

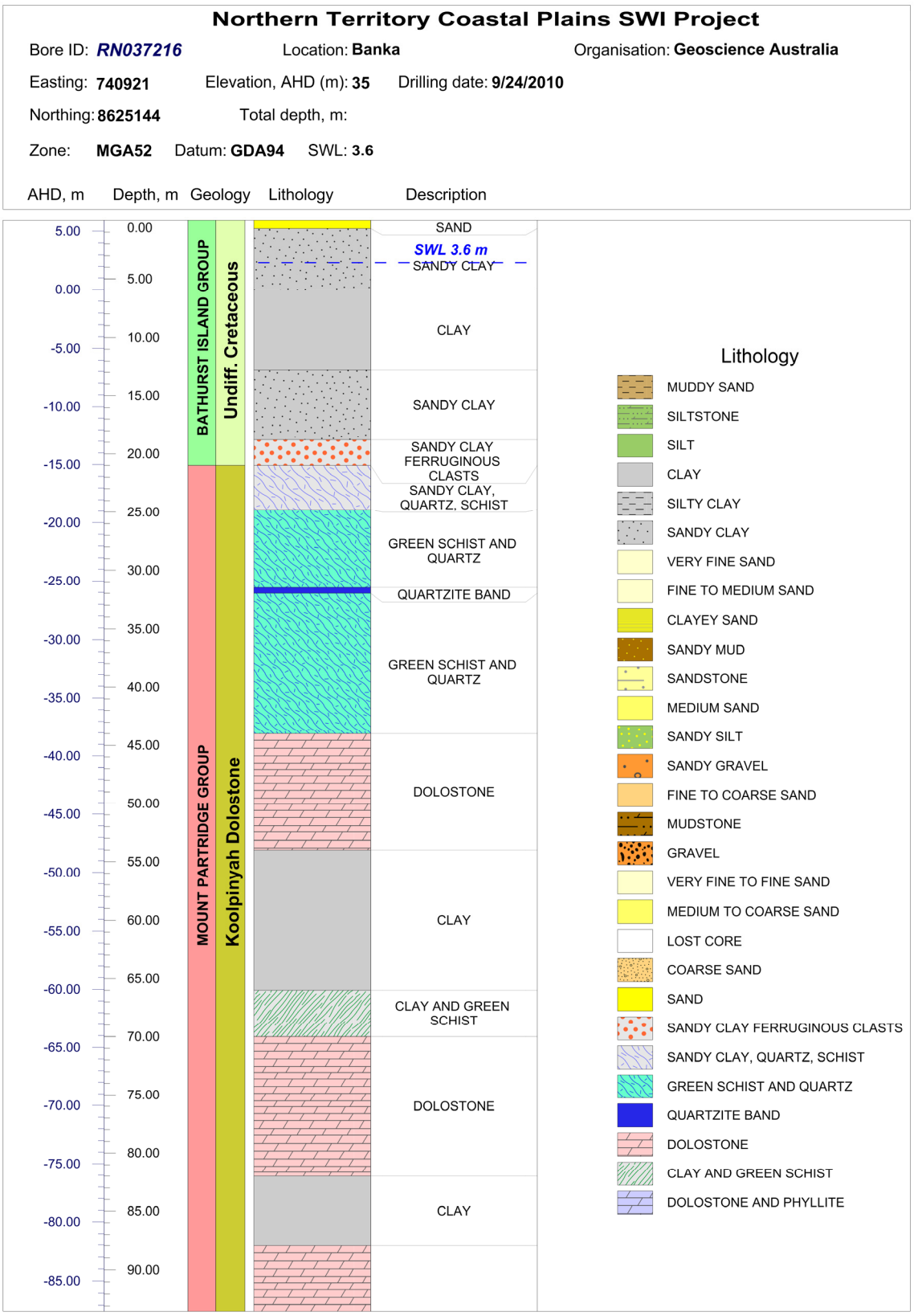

Figure 77: *Top of geological log of borehole RN37216. Groundwater sampling from this bore recovered saline groundwater (EC ~70,000 µS/cm) from depth within the Koolpinyah Dolomite.*

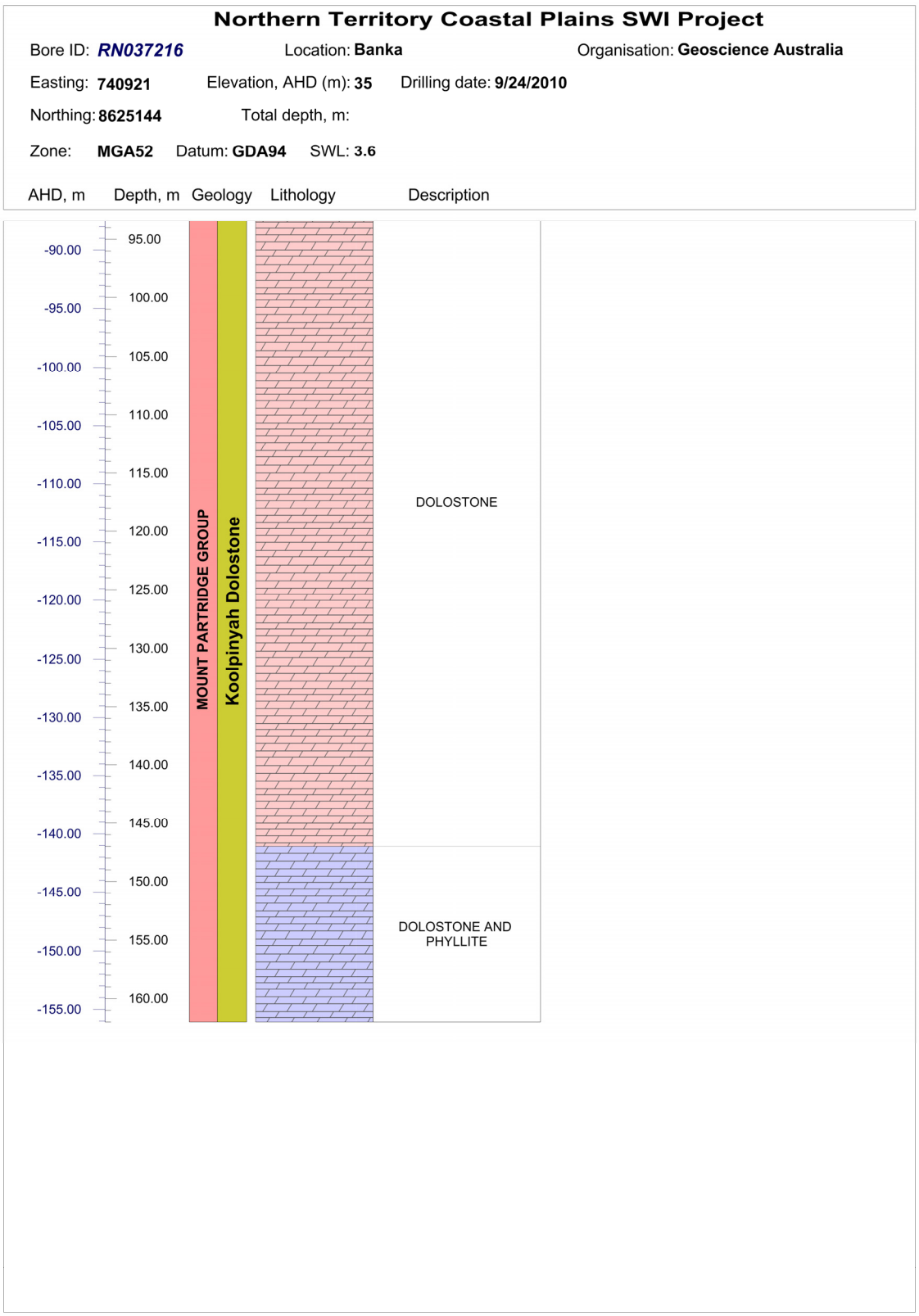

Figure 78: *Bottom of geological log of borehole RN37216. Legend in Figure 77.*

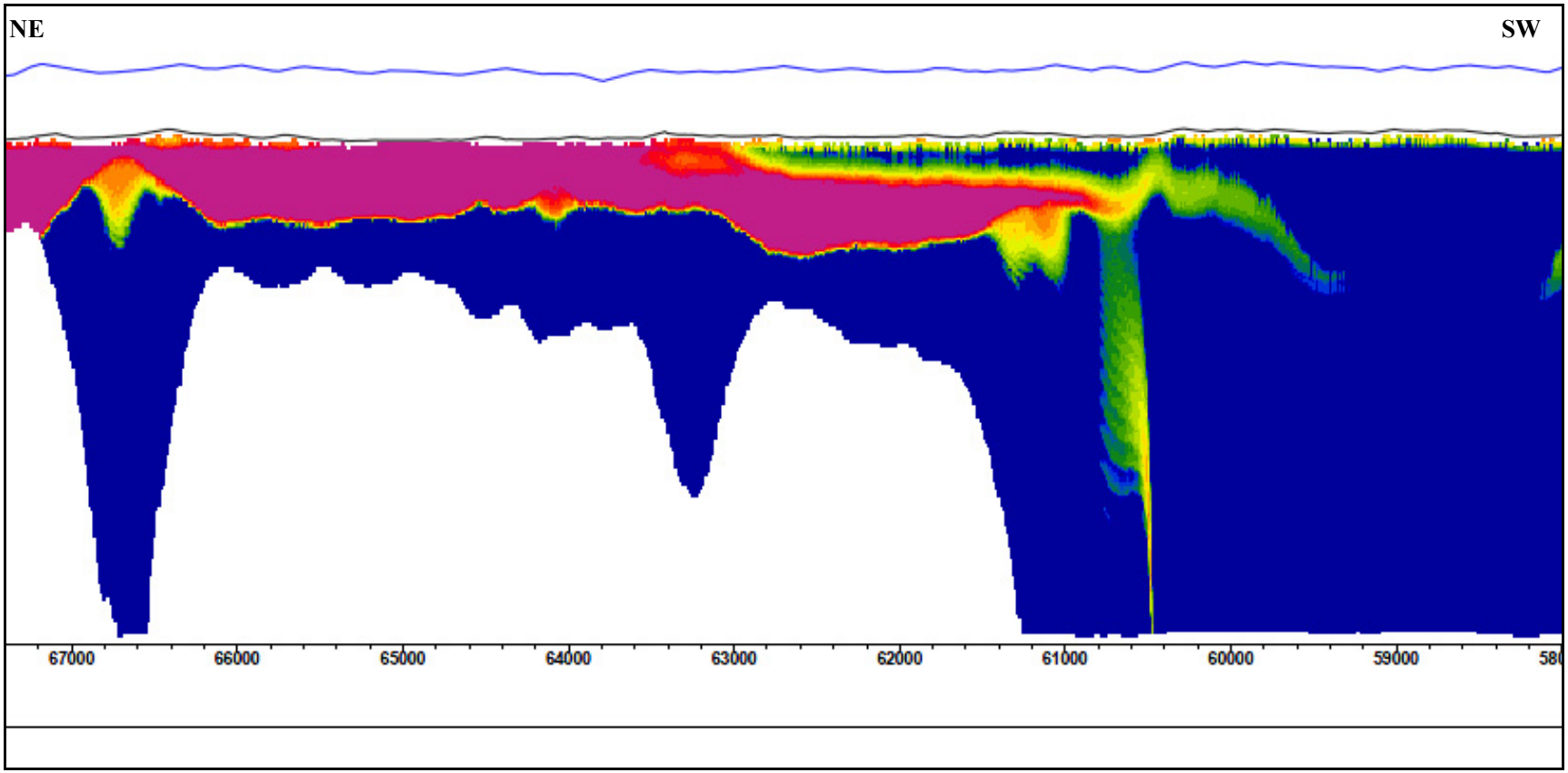

Figure 79: *Synthetic section AEM data acquired north-east from Darwin. The image depicts shallow (100 m deep) seawater to left in pink (highly conductive), which is wedged above resistive (blue) crystalline rock filled with fresh water, underlying the salt water intrusion (Tan et al., 2011).*

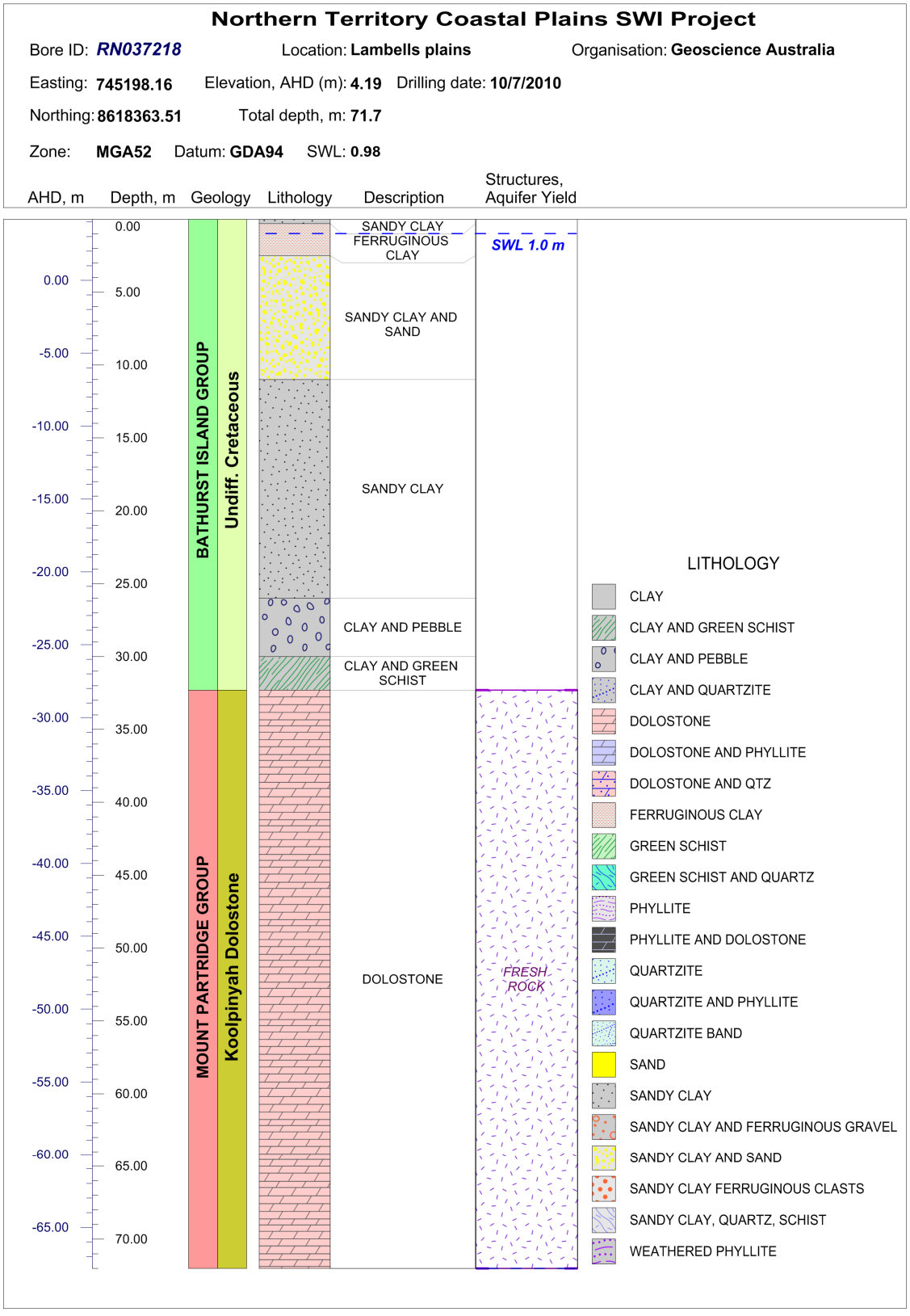

Figure 80: *Geological log of borehole RN37218.*

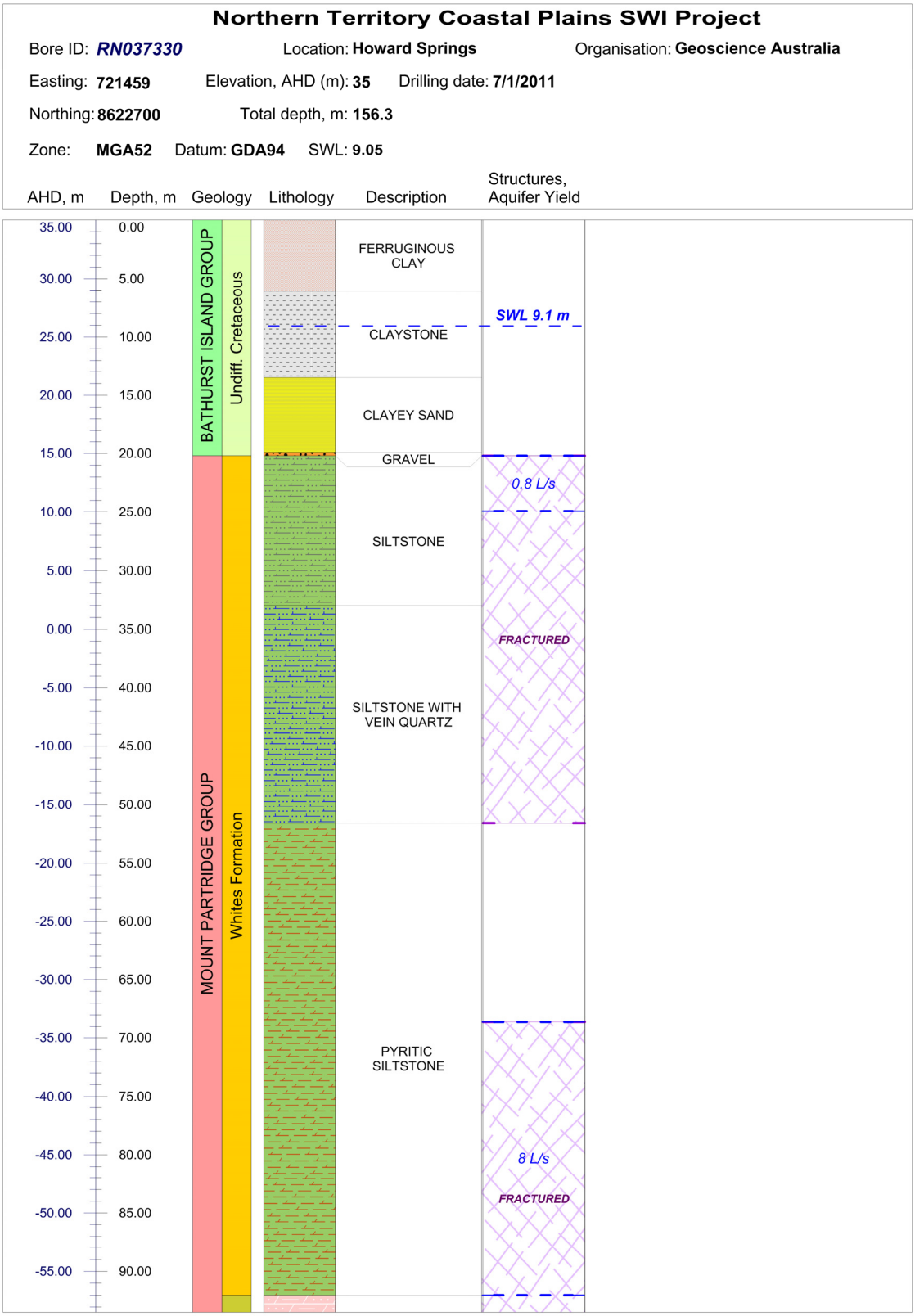

Figure 81: *Top of geological log of borehole RN37330. Legend contained in following Figure.*

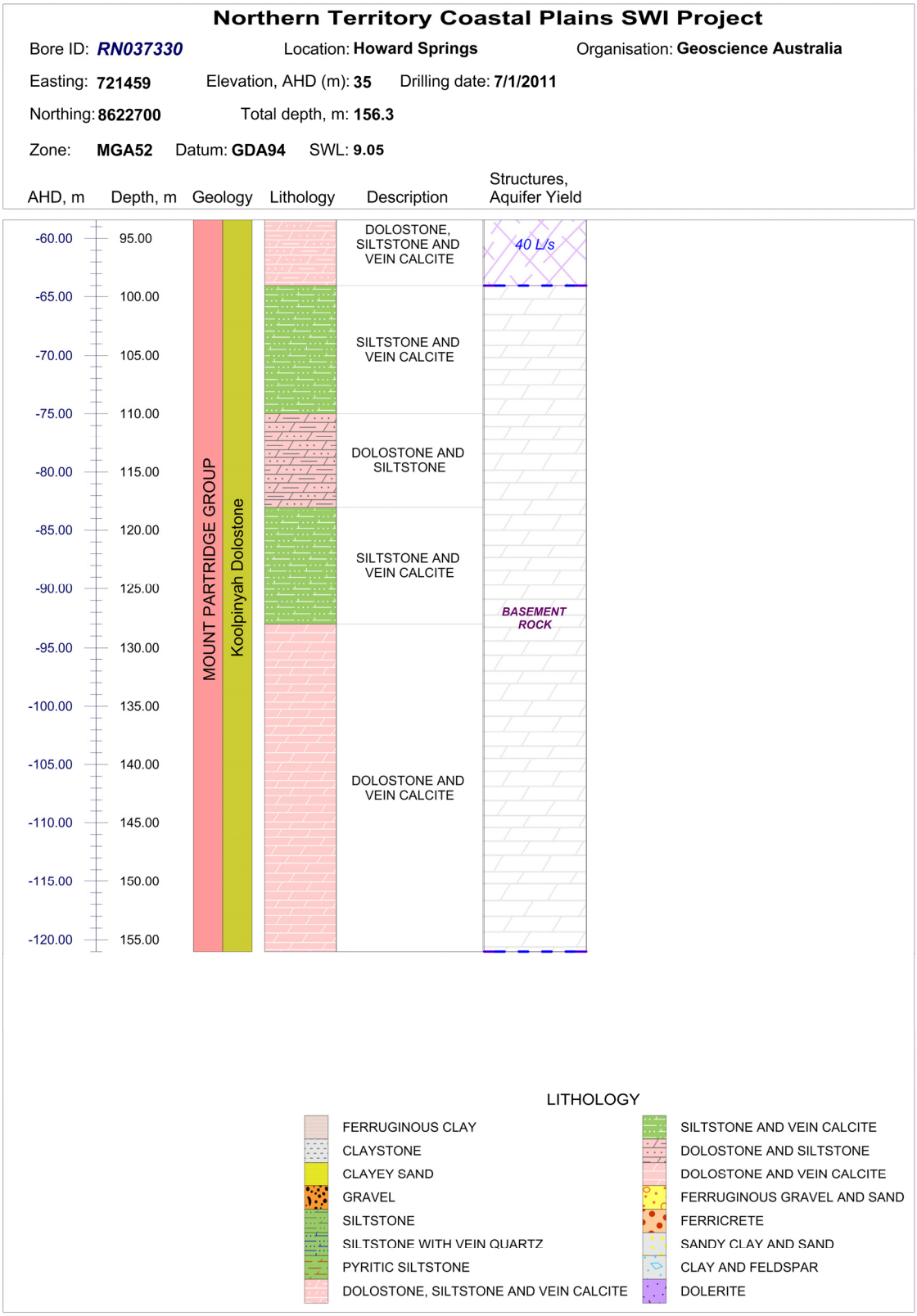

Figure 82: *Bottom of geological log of borehole RN37330.*

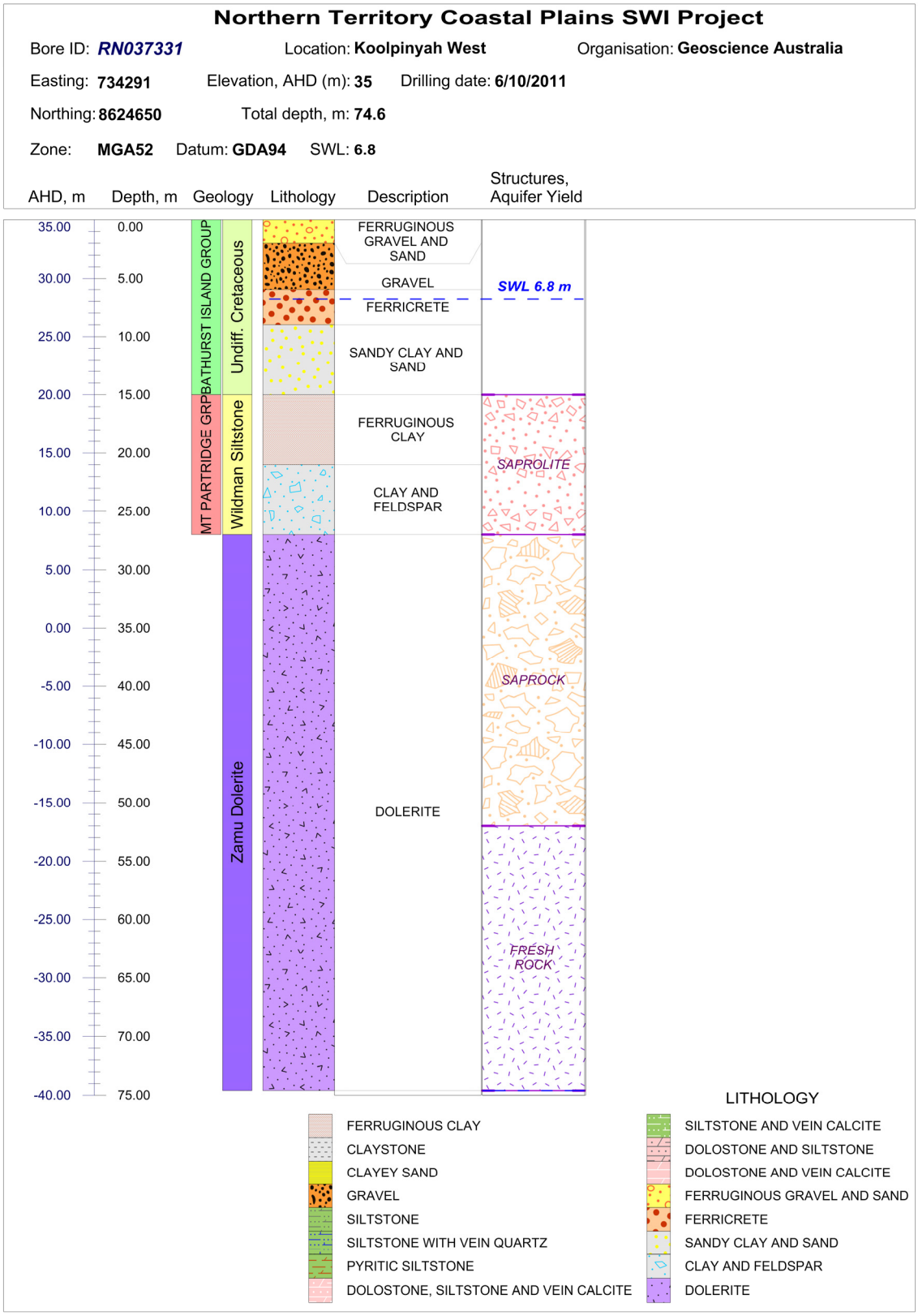

Figure 83: *Geological log of borehole RN37331.*

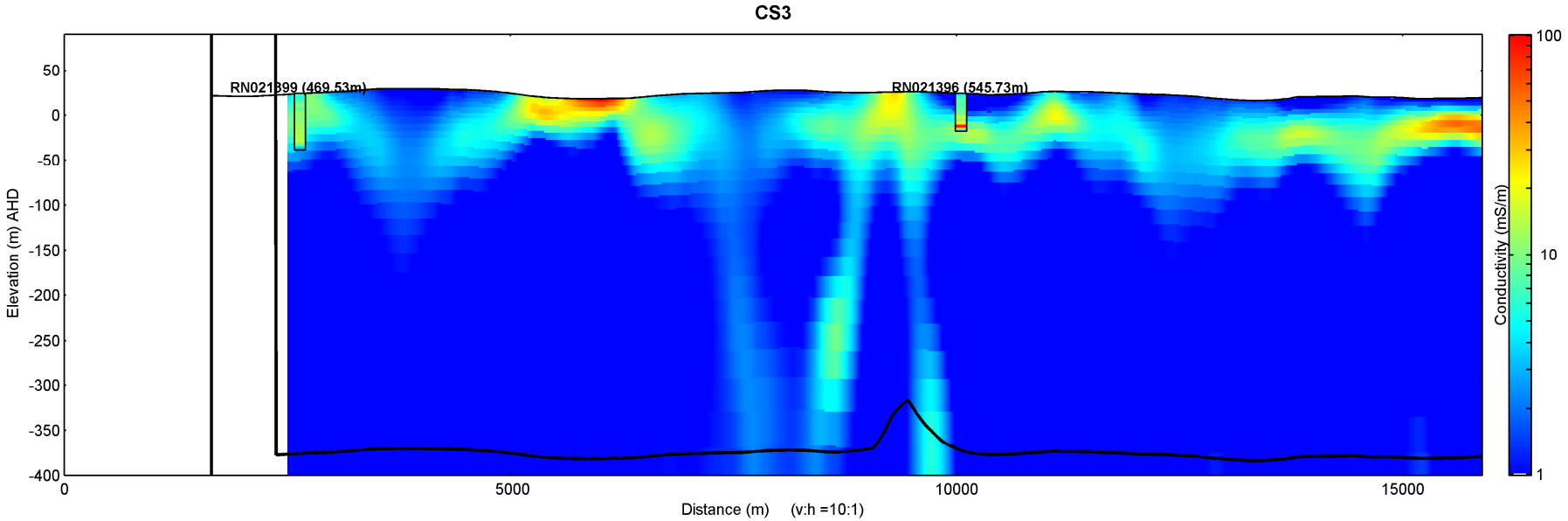

Figure 84: *Southwest to northeast synthetic AEM section through location of borehole RN37331 (Tan et al., 2011).*

5.3 GEOPHYSICAL LOGGING RESULTS

5.3.1 Results

NRETAS undertook all borehole logging for the project using Auslog brand equipment. Conductivity logs were taken at the time of flying of the AEM survey in 2008 but intermittent problems with the inductive conductivity tool rendered the data useless. A new tool was purchased and the logs were completed in PVC cased bores in 2010 and early 2011. Five sonic bores (RN037150, RN037151, RN037152, RN037153 and RN037154) were drilled and constructed by Boart-Longyear specifically for this project. All other bores were drilled and constructed by NRETAS since 1980. All bores were cased with PVC.

Down hole inductive conductivity and natural gamma logs were acquired for 36 bores in the Woolner AEM survey area, listed in Table 16. Figure 85 shows the locations of the logged bores. Twenty seven of the inductive conductivity logs were used to provide calibration for the AEM inversions. The remaining nine logs arrived after the comparison was performed. All borehole inductive conductivity and natural gamma logging data are shown in Appendix 2.

Table 16: *Bores logged with inductive conductivity and gamma in the Woolner AEM survey area (sonic bores in bold). All coordinates in Zone MGA52 using the GDA94 datum.*

Site	Easting	Northing	Area	Log Depth (m)	Point Comp.
RN020967	736687	8614360	Black Jungle	44.1	Y
RN021012	730707	8617353	Howard East	64.1	Y
RN021047	735101	8617719	Howard East	78.8	Y
RN021396	735110	8624739	Koolpinyah	41.6	Y
RN021399	730123	8619161	Howard East	62.4	Y
RN021762	729144	8622459	Howard East	71.5	Y
RN025420	728616	8627150	Hunting Reserve	34.2	Y
RN025421	733490	8629583	Koolpinyah	85.5	Y
RN025422	734519	8617719	Koolpinyah	68.5	Y
RN025423	735126	8627309	Koolpinyah	60.5	Y
RN025941	732519	8619169	Howard East	79.4	Y
RN031977	740422	8626287	Koolpinyah	23.9	Y
RN034679	733189	8631963	Koolpinyah	44.2	Y
RN035864	722518	8623580	Howard Springs	65.6	Y
RN035865	722977	8623637	Howard Springs	61.4	Y
RN035866	727438	8625262	Hunting Reserve	21.5	Y
RN035970	743188	8629815	Koolpinyah	59.8	Y
RN036536	742413	8637502	Gunn Point	67.3	Y
RN036537	737205	8635180	Gunn Point	102.2	Y
RN036810	783081	8613820	Marrakai	93.0	Y
RN036811	781146	8605016	Marrakai	63.7	Y
RN037150	735987	8635546	Gunn Point	53.3	Y
RN037151	742293	8629301	Koolpinyah	39.5	Y
RN037152	722689	8625528	Howard Springs	51.5	Y
RN037153	735787	8627728	Koolpinyah	68.0	Y
RN037154	737531	8618857	Black Jungle	57.9	Y
RN037218	745195	8618361	Koolpinyah	70.6	Y
RN021761	730002	8619158	Howard East	84.5	N
RN021765	731295	8619159	Howard East	49.7	N
RN021768	731114	8622945	Howard East	80.1	N
RN021769	729518	8622931	Howard East	54.5	N
RN022060	729490	8622930	Howard East	74.5	N
RN022063	729140	8622575	Howard East	23.9	N
RN022065	729170	8623733	Howard East	60.3	N
RN024390	731131	8618147	Howard East	75.4	N
RN024402	735124	8627159	Howard East	60.5	N

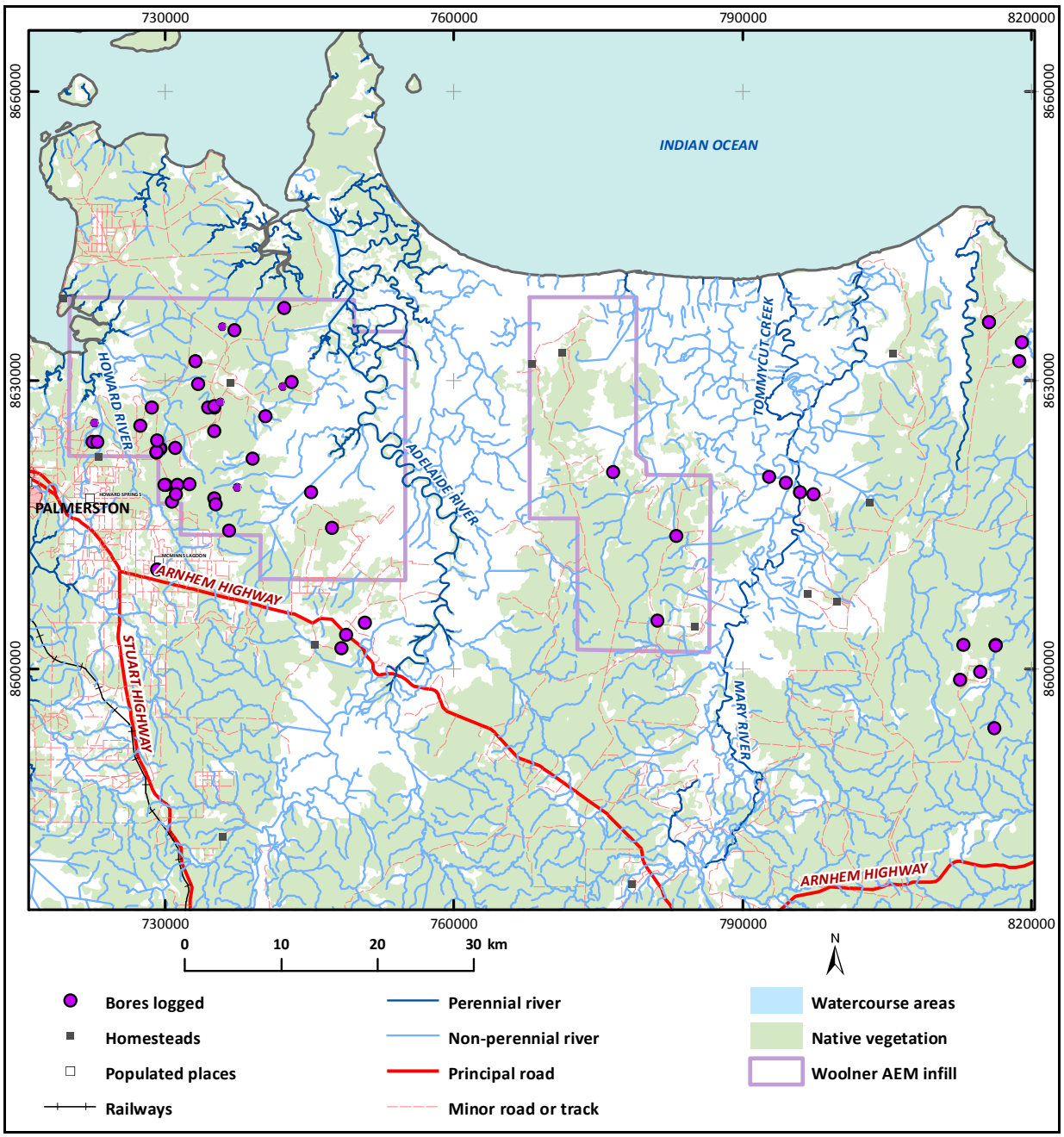

Figure 85: *Map of bores logged with inductive conductivity and gamma in the project study area.*

6 Interpretation of Geology and Landscape Evolution

6.1 INTERPRETED STRATIGRAPHY AND LITHOLOGY DISTRIBUTION

Five representative elevation slices are discussed in this section, these being the below sea-level intervals for 0-5 m, 10-15 m, 20-25 m, 30-35 m and 60-65 m. The depth slices show interpreted lithologic and stratigraphic features as derived from analysis of the AEM data, supported by borehole information where available. The five slices illustrate the results of using AEM data to map lithology, and a similar approach can be applied to other AEM depth slices to highlight the stratigraphic variations that occur with depth.

6.1.1 60-65 m interpretive elevation slice (below sea-level)

This is the deepest elevation slice (60-60 m below sea level) is shown in Figure 86 with accompanying interpretation (Figure 87), including all rock units mapped belong to the Proterozoic and older (Archaean) basement sequences. Consistent patterning in the AEM can be linked to specific lithostratigraphic units, as shown. Noteworthy is the complex structural architecture visible in the south-west of the mapped area, which corresponds to the Rum Jungle Complex (RJC). Faults in the western part of the mapped area mostly trend north- west to south-east and are part of the Pine Creek Shear Zone (PCSZ). In the central and eastern map area faults trend mostly north-easterly, parallel to the Giants Reef Fault (GRF). The major basement fault systems are commonly intruded by magnetic dolerite dykes. The subcrop of the folded dolostone units (Koolpinyah) trends in a similar direction, consistent with fold patterns evident in the aeromagnetic data.

6.1.2 30-35 m interpretive elevation slice (below sea-level)

Figure 88 and Figure 89 shows a slice through the basal Cretaceous unconformity. The unconformity slopes down to the north so that the far northern area is covered by Cretaceous rocks (the Bathurst Island Group) whereas the southern part is composed of Proterozoic lithostratigraphic units. The northward thickening of Cretaceous cover is consistent with the overall Cretaceous Basin architecture (Mory 1988). The Archaean inliers between the mouths of the Adelaide and Mary rivers (arrowed in white) formed by Woolner Granite and Dirty Water Metamorphics are surrounded by the Cretaceous sedimentary sequences, forming what would have been islands in the Cretaceous sea. Two other significant features of the basal Cretaceous unconformity are visible in this figure. These are the presence of interpreted palaeovalleys (blue arrows) and possible large to very large karst depressions infilled in the western region (orange arrows). The eastern palaeovalley approximately coincides with the courses of the Mary and Adelaide Rivers, indicating the considerable antiquity of the large-scale drainage systems in the region.

Two other significant features of the basal Cretaceous unconformity are visible in this figure. These are the presence of interpreted palaeovalleys (blue arrows) and possible large to very large karst depressions infilled in the western region (orange arrows). Both these features are of major hydrogeological significance to the region.

The eastern palaeovalleys are associated with the courses of the Mary and Adelaide Rivers, indicating the considerable antiquity of the large-scale drainage systems in the region. Palaeovalleys in other regions of Australia are extremely important features for groundwater resources (English *et al*. 2012) and both focus flow and provide pathways from recharge areas to basins along the continental margin (Alley *et al*. 1999, Clarke *et al*.2003). The examples in the western project areas are tributaries of Adelaide River, the trunk palaeovalley being largely beneath areas excluded from the survey. A strong structural control is evident in their orientation, which appears inherited from the underlying Proterozoic stratigraphy. The eastern example may be the edge of the trunk palaeovalley of the Mary, but may also be a tributary, the uncertainty arising because of the edge of the survey area cuts across the main part of the Mary River. We predict that they would focus groundwater flow and provide potential pathways for freshwater plumes to access the coastal environment, especially during and immediately following the wet season. This flow could be of great significance to the maintaining of groundwater dependent ecosystems, especially vine forests and habitats for freshwater breeding fish, and the recreational amenities reliant on these. Conversely, over-pumping from these palaeovalleys and adjacent areas could mean that they would provide a major ingress point for

seawater intrusions. This is possibly analogous to the situation that occurs in the Burdekin Delta (Queensland) within the Quaternary sediments of that system (Fitzpatrick *et al*. 2004; Lawrie *et al*. 2006).

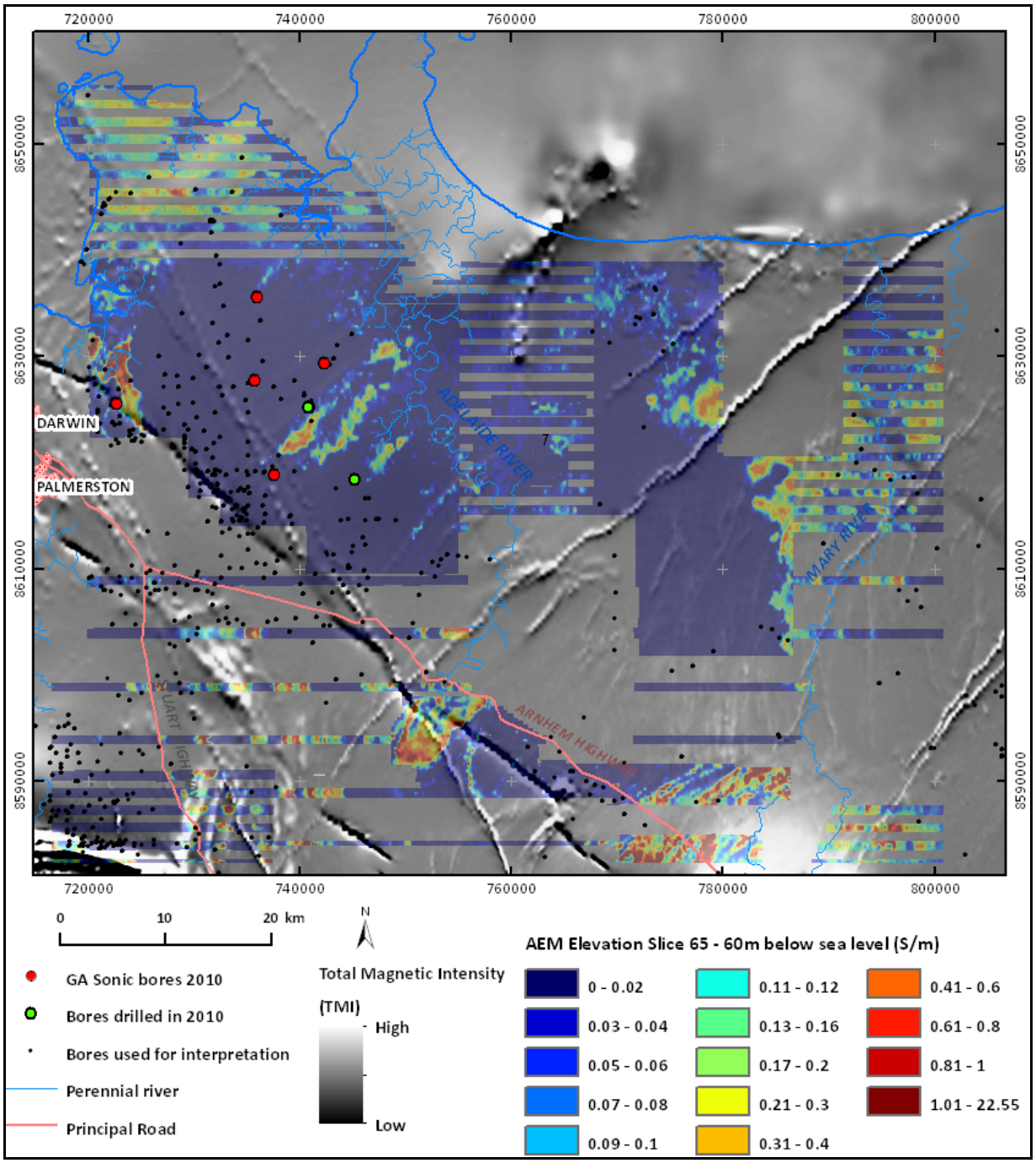

Figure 86. *AEM elevation slice at 60-65 m bsl overlain on 1st vertical derivative TMI image.*

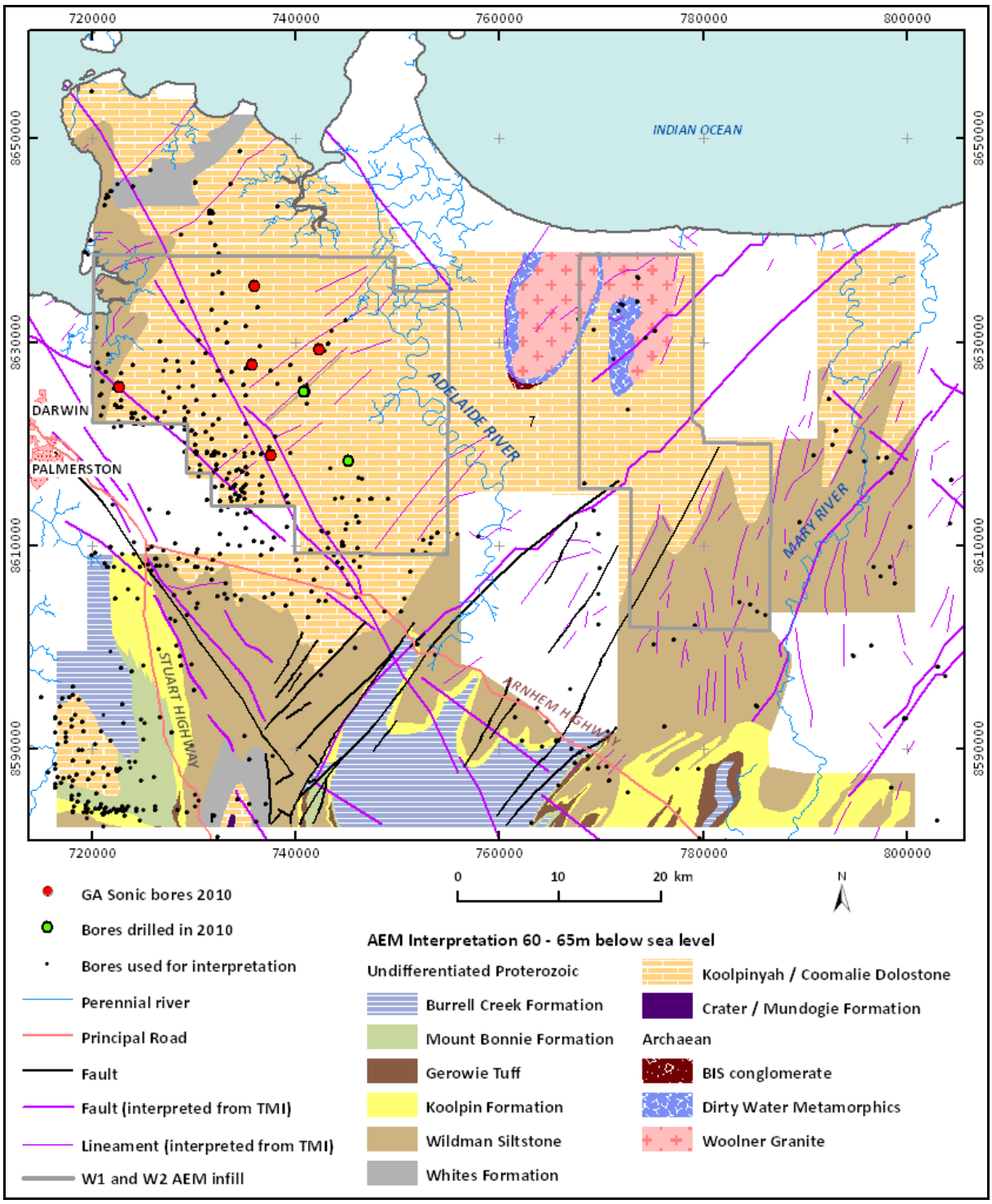

Figure 87: *Interpreted lithology and stratigraphy for the elevation slice 60-65 m bsl.*

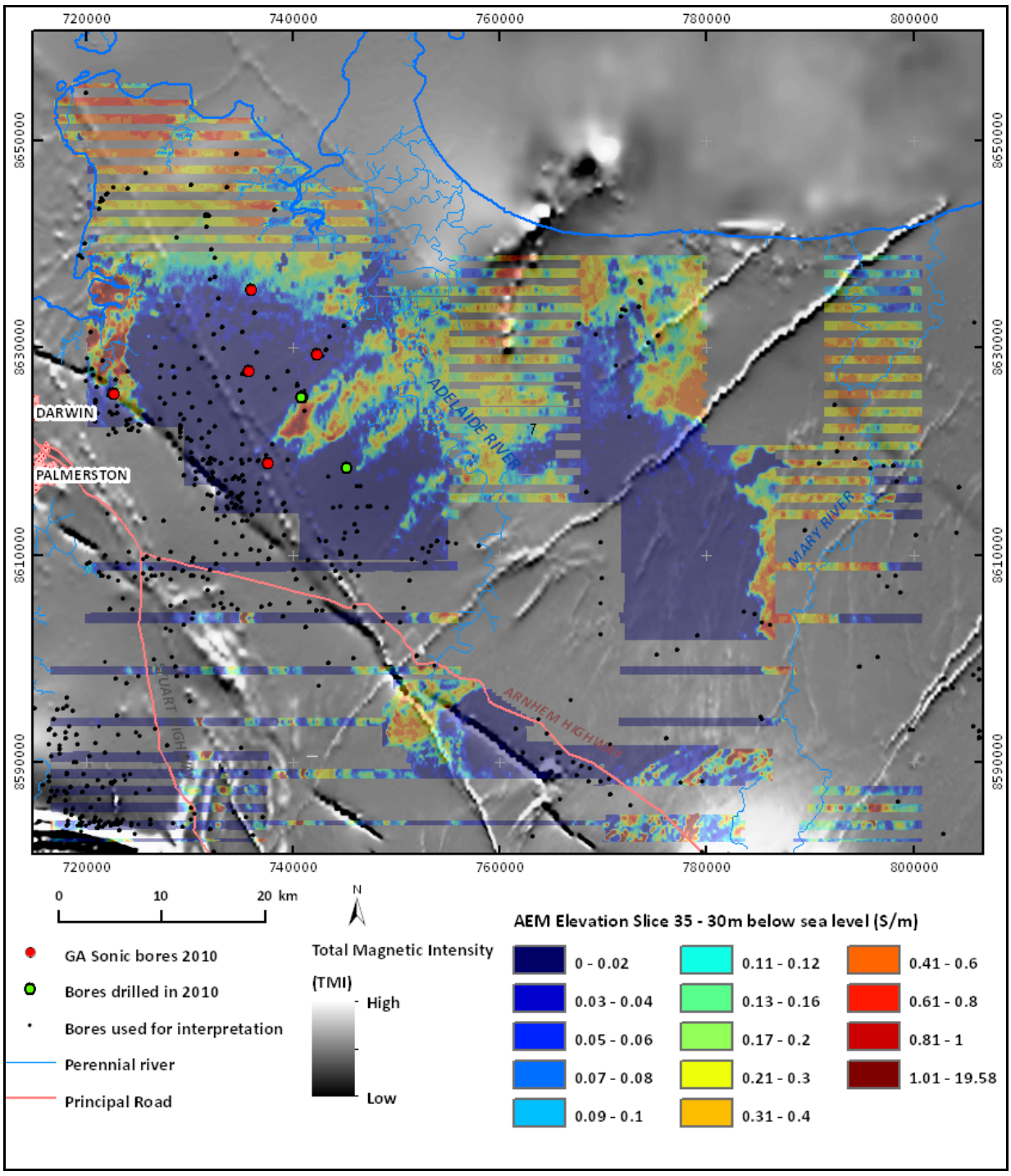

Figure 88. *AEM elevation slice at 30-35 m bsl overlain on 1st vertical derivative TMI image.*

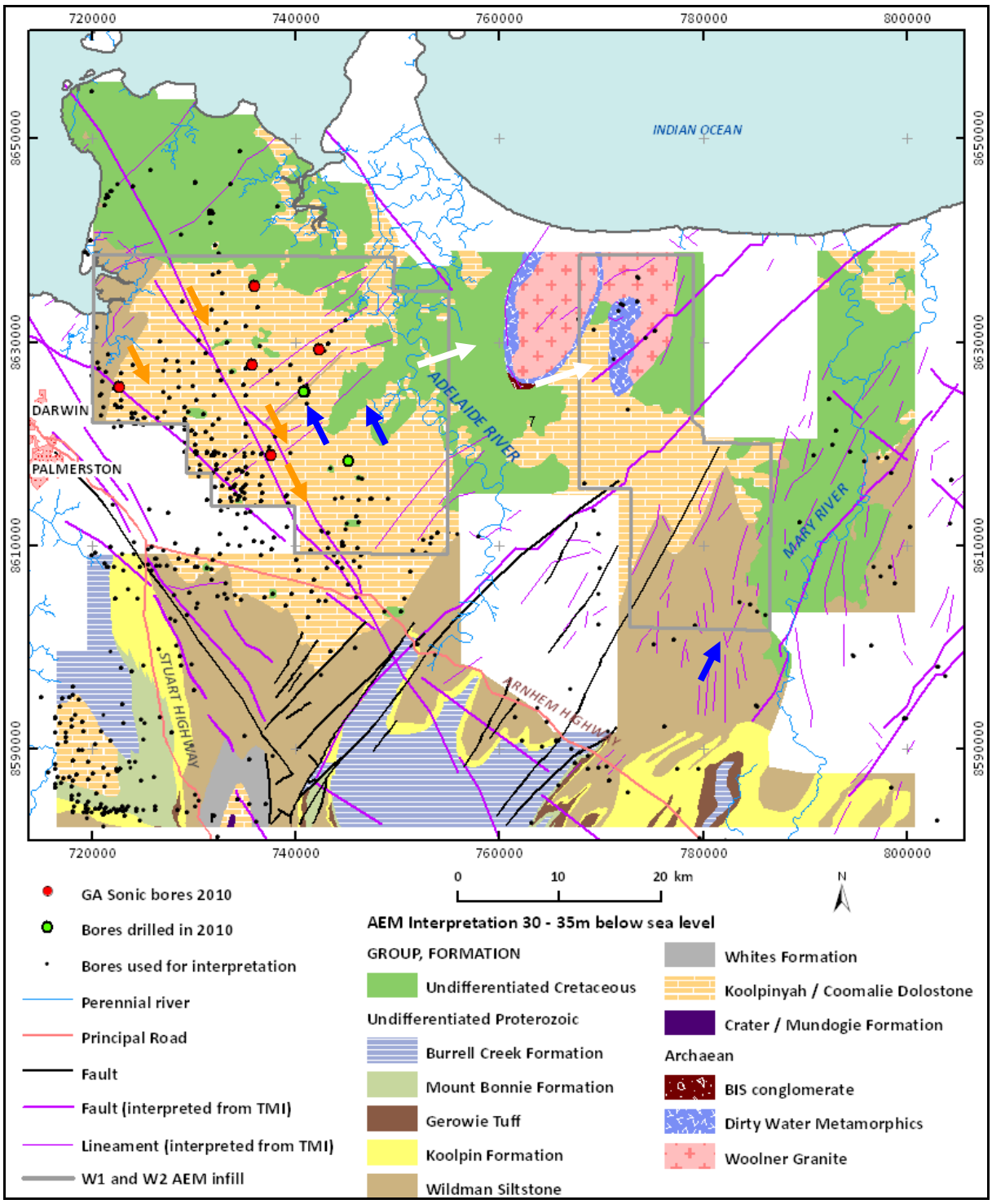

Figure 89: *Interpreted lithology and stratigraphy for the elevation slice 30-35 m bsl.*

The karstic depressions are much larger scale features than the surface dolines formed by subadjacent karst collapse. More than a km across, even in this depth slice, they most closely resemble the larges scale karst features known as poljes (Bloom 1978, Ford and Williams 2007). Strictly speaking these features are palaeo-poljes, as the formed prior to the Cretaceous and have no surface features associated with them. Under natural conditions the palaeo-poljes would act as large scale funnels at the base of the Cretaceous, focusing groundwater flows in the basal sands down into the most permeable and and strongly karstified parts of the KCD aquifer. Depending on the height of the water table, act as either major recharge points for the karstic aquifer in dolostones where and when the water table is low, or major discharge points where and when the water table is high. Should over-extraction lead to seawater intrusion, these features could act either as zones of seawater ingress into the aquifer, or as saline water discharge points.

Both the palaeovalleys and the karstic depressions warrant further and more detailed investigation of their structure, stratigraphy and hydrogeology.

6.1.3 20-25 m interpretive elevation slice (below sea-level)

Figure 90 and Figure 91 shows the area covered by Cretaceous rocks is broader and extends further south at this more elevated interval. The Archaean inlier between the mouths of the Adelaide and Mary Rivers (arrowed in white) are more spatially restricted. This is the result of the greater area inundated by the rising Cretaceous sea that deposited these sediments and infill of palaeotopography by the Cretacerou sediments, burying the palaeotopographic highs

The interpreted palaeovalleys of the Adelaide river tributaries (blue arrows) are still present, showing that these features extend over a vertical distance of at least 20 m. The eastern palaeovalley approximately coincides with the course of the present-day Mary River. Likewise the karstic depressions (palaeo-poljes) are now larger (orange arrows), and have widened out to being 5 to 10 km across at this level. As with the palaeovalley fills, these features which occur in both this an the previous section are therefireat least 20 m deep.

As noted, the palaeovalleys provide a focus for groundwater flow and potential pathways for freshwater plumes to access the coast. Conversely, over-pumping from these palaeovalleys and adjacent areas could make them major ingress points for seawater intrusion. Likewise, the karstic depressions, depending on the height of the water table, act as either major recharge points for the karstic aquifer in dolostones (where and when the water table is low), or as major discharge points (high water tables). Karstic features affected by seawater intrusion may act either as zones of seawater ingress into the aquifer or as saline water discharge points, depending on water table levels.

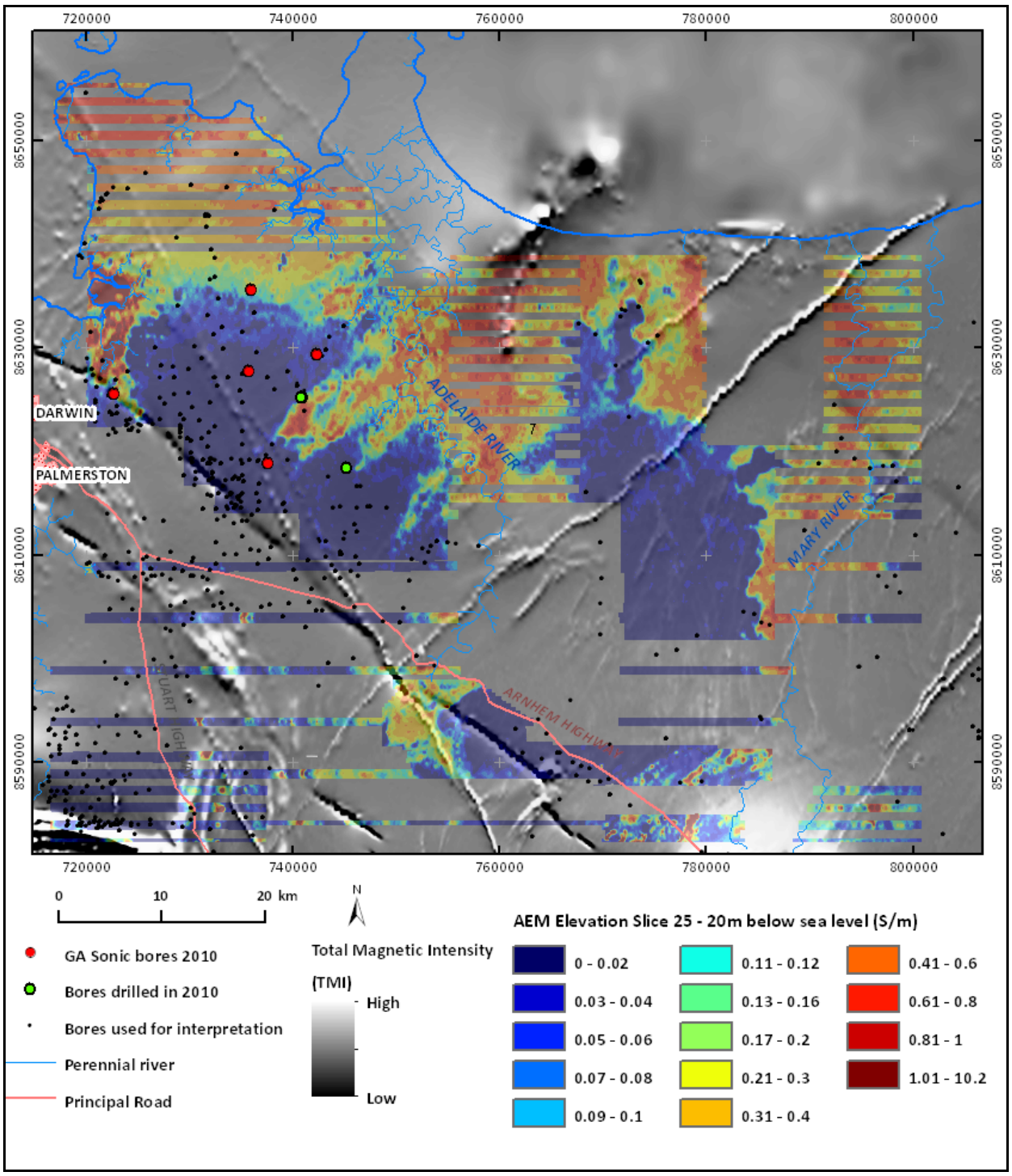

Figure 90. *AEM elevation slice at 20-25 m bsl overlain on 1st vertical derivative TMI image.*

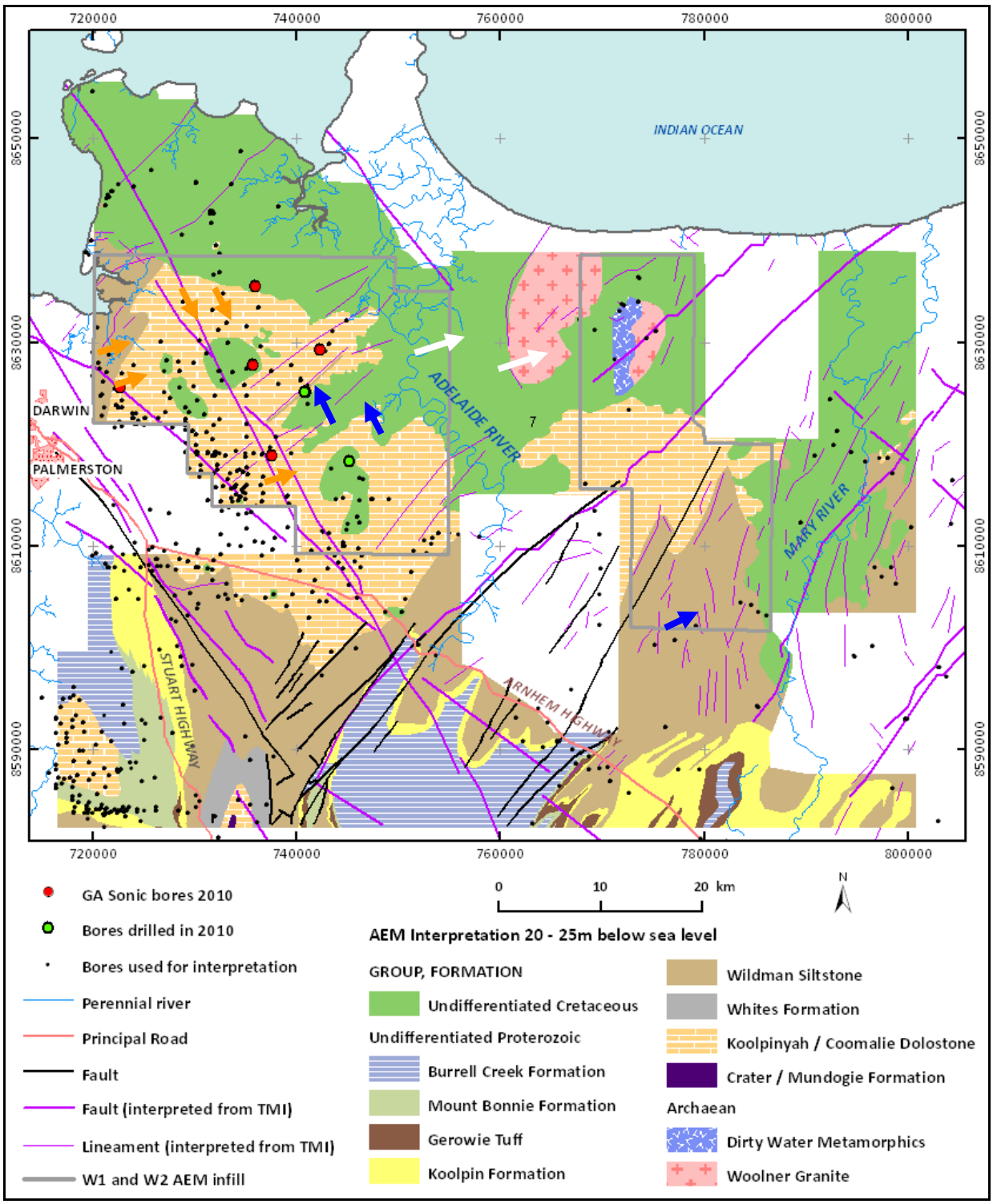

Figure 91. *Interpreted lithology and stratigraphy for the elevation slice 20-25 m bsl.*

6.1.4 10-15 m interpretive elevation slice (below sea-level)

Figure 92 and Figure 93 shows the broader extent of the Cretaceous cover in the area at higher elevation levels. Several relative high-points of Proterozoic bedrock are evident surrounded by the Cretaceous cover; these may have been islands during the time of deposition (pink arrows). Numerous additional smaller Proterozoic highs are also present, but are not visible at this scale. A palaeovalley, possibly associated with the course of the Adelaide River (blue arrow), has been filled by Cretaceous sedimentary rocks. This slice also shows the extent of Quaternary alluvial and estuarine sediments which have infilled palaeovalleys incised into the Cretaceous and basement units along the Mary and Adelaide Rivers.

As is the case for the deeper intervals, the palaeovalleys and karstic depressions provide a potential focus for groundwater flow and pathways for freshwater plumes to access the coast. Conversely, over-pumping from these areas could mean that they provide a major ingress point for seawater intrusions. The full extent of these features warrant further and more detailed investigation. The Quaternary sediments are the primary flow path for seawater intrusion with direct connection to the sea. They also have high permeability in sandy units, with the possibility of tidal pumping effects and storm surges providing a forcing mechanism to pump groundwater through the system. The detailed hydrogeology of these Quaternary units and their connectivity with underlying and laterally equivalent Proterozoic and Cretaceous units are another potential area for further investigation.

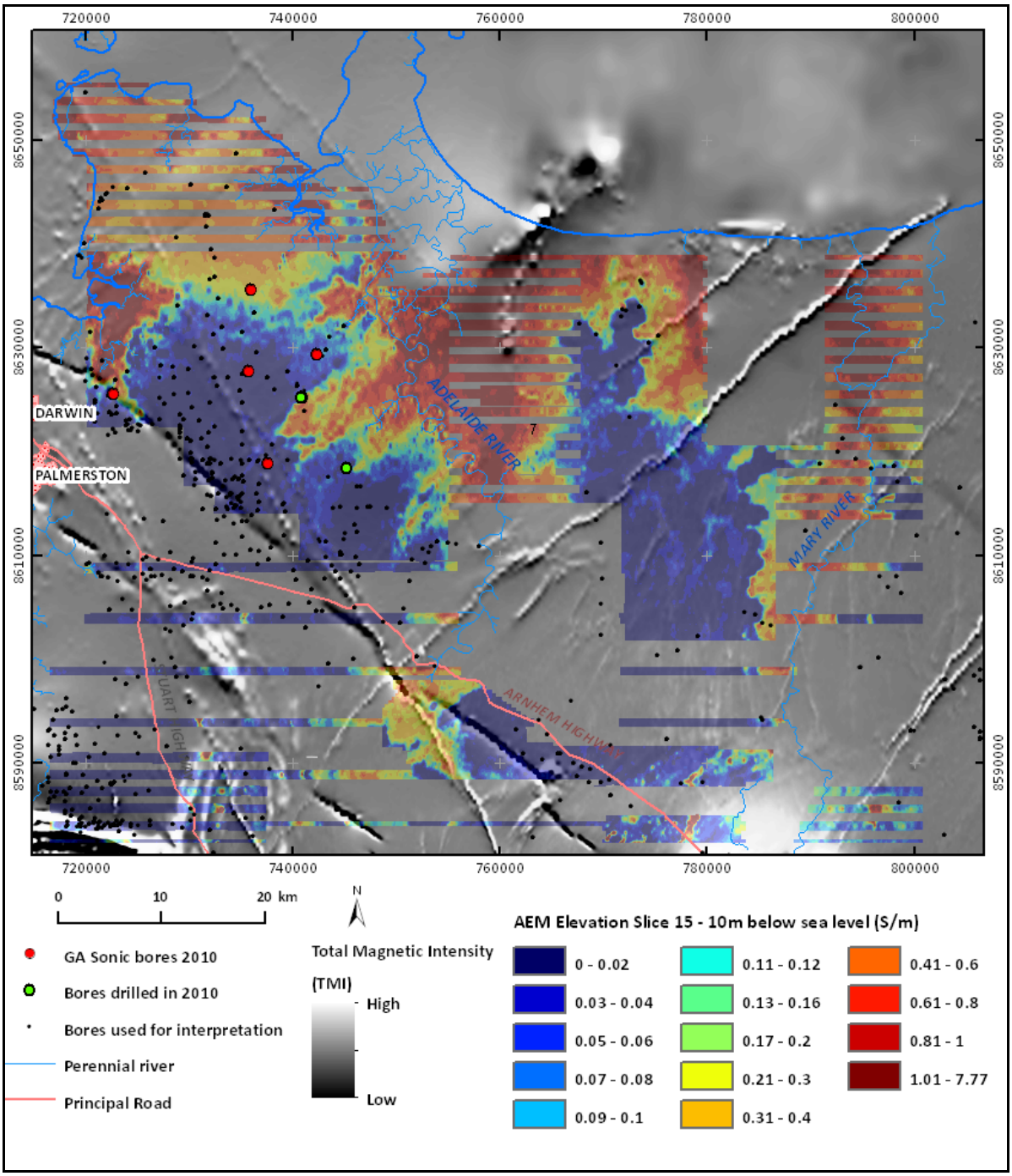

Figure 92. *AEM elevation slice at 10-15 m bsl overlain on 1st vertical derivative TMI image.*

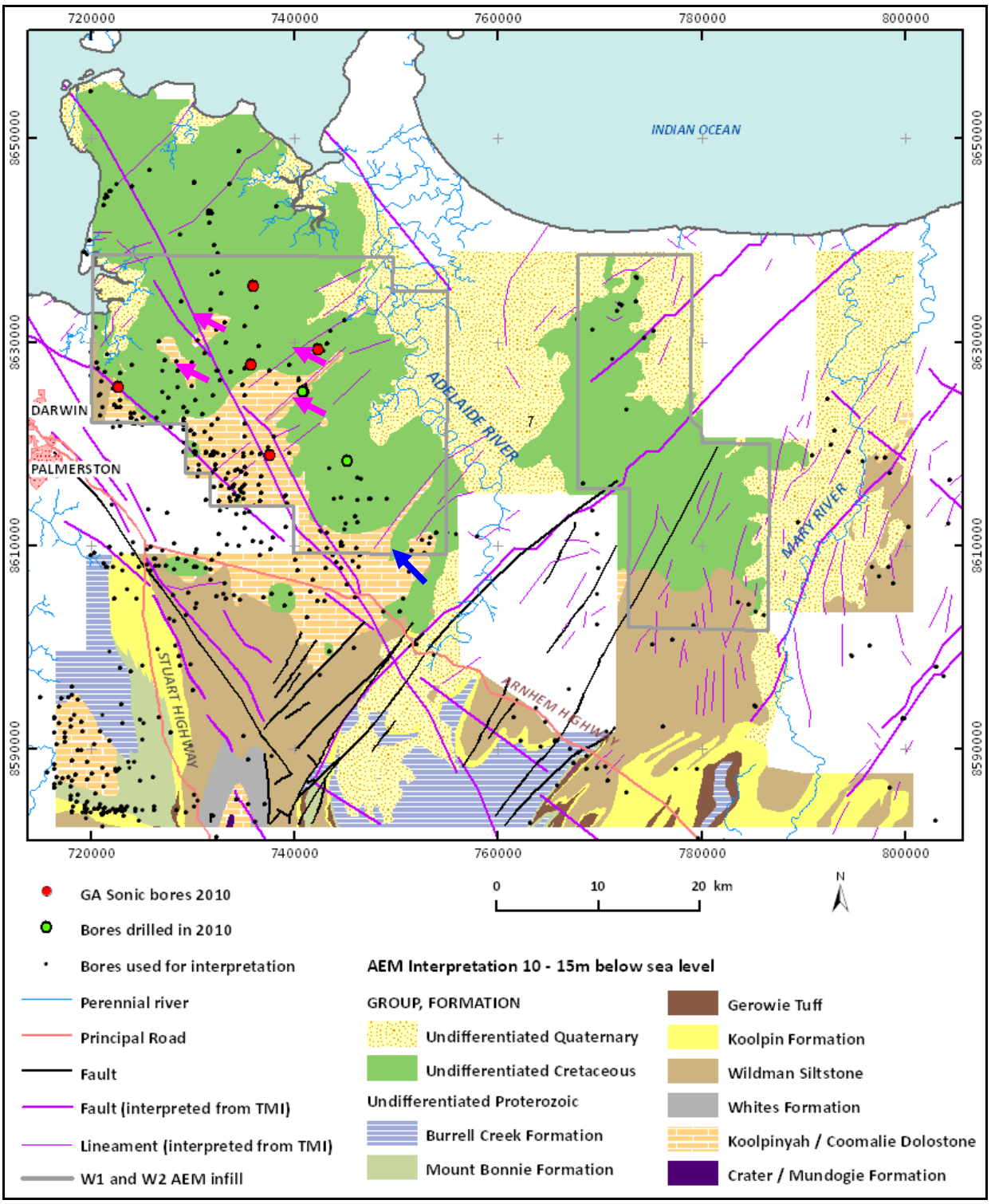

Figure 93. *Interpreted lithology and stratigraphy for the elevation slice 10-15 m bsl.*

6.1.5 0-5 m interpretive elevation slice (below sea-level)

Figure 95 shows the wider southward distribution of Cretaceous sedimentary cover. There are fewer Proterozoic bedrock highs at this depth level, as most are obscured by deposition of the Cretaceous sedimentary cover. This interpretive slice also shows the extent of Quaternary alluvial and estuarine sediments which have infilled palaeovalleys incised in the Cretaceous and basement units along the Mary and Adelaide Rivers. The distribution of Quaternary sediments is more extensive for the elevation slices closer to the surface.

Although not visible in this slice, the collapse zones associated with the KCD would persist and provide a potential focus for groundwater flow and pathways for freshwater plumes to access the coast. Conversely,

over-pumping from these areas could mean that they would provide a major ingress point for seawater intrusions. The full extent of these features warrant further and more detailed investigation.

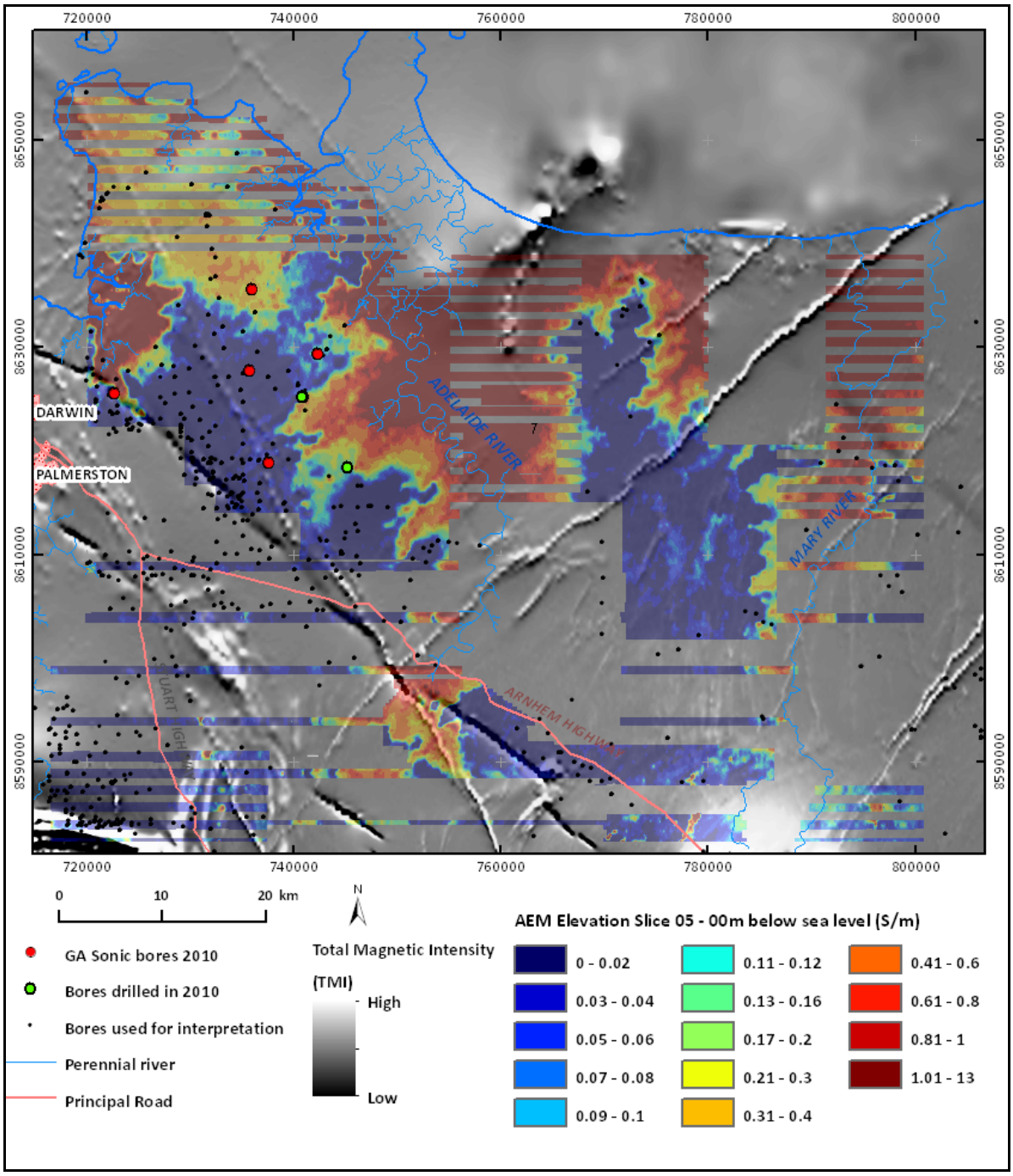

Figure 94. *AEM elevation slice at 0-5 m bsl overlain on 1st vertical derivative TMI image.*

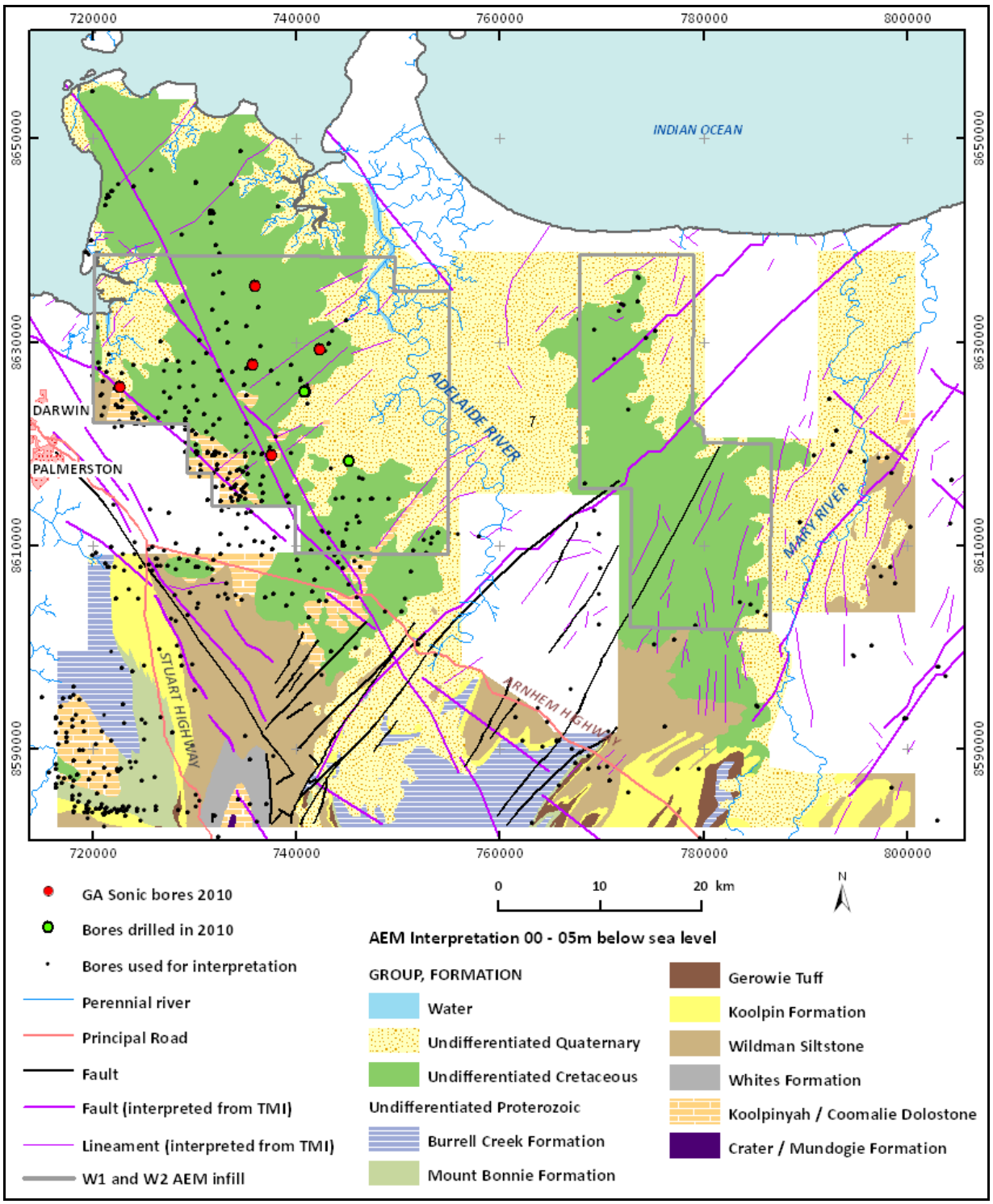

Figure 95: *Interpreted lithology and stratigraphy for the elevation slice 0-5 m bsl.*

6.2 INTERPRETED GEOLOGICAL PRODUCTS

6.2.1 Quaternary thickness

The thickness of the Quaternary sediments in shown in Figure 96. All Quaternary sediments are included as a single unit, be they fluvial, estuarine, or beach in deposition.

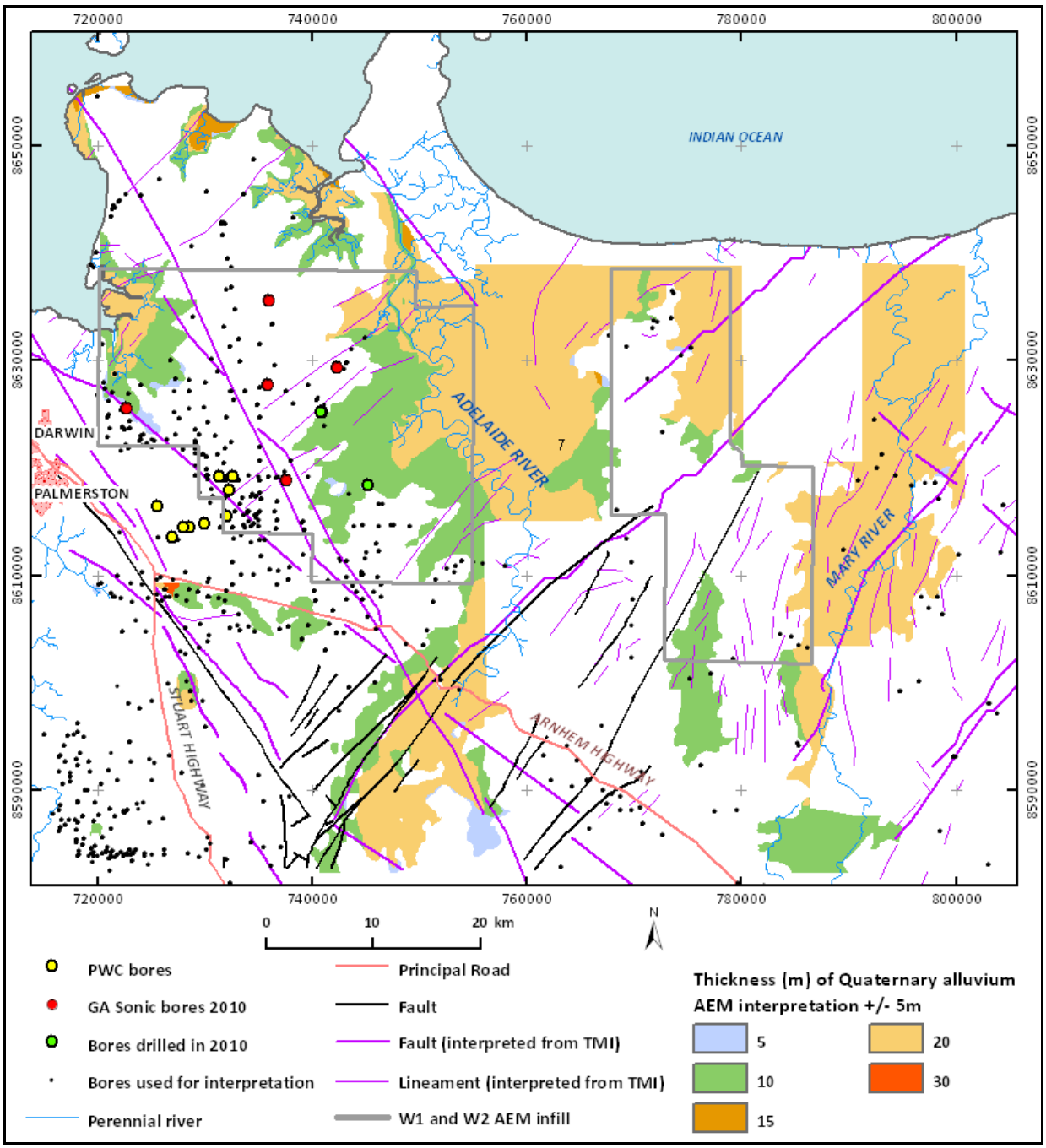

Figure 96. *Interpreted thickness of Quaternary sediments.*

Although representation of the extent and thickness of the Quaternary succession is constrained by the survey limits, very limited number of bores, and the masking of key interfaces by the sea water wedge, the above figure clearly shows the thickest (up to 20 m) sediments are in the valleys of the Adelaide and Mary Rivers and beneath the coastal plain. Less extensive areas of similar thickness occur beneath beaches southwest of Gunn Point and the Howard River estuary.

Figure 96 shows that the areas overlain by Quaternary sediment are, for the most part flat-floored or of low gradient. Limited drilling data, mostly from the estuary of the Mary River, is consistent with this. However the critical interface between the Quaternary sediments and older units is almost everywhere obscured by the

sea water wedge, and the flatness is also due largely to interpolation. In reality, considerable small scale variation, due to buried fluvial valley incision, is to be expected.

Small and localised areas of thin (<10 m) of Quaternary sediment are also present. These do not appear to be related to modern drainage or other topographic features. They may low amplitude indurations from tectonic or pseudokarstic processes affecting the Cretaceous.

6.2.2 Elevation top of Cretaceous

The map of the elevation of the top of the Cretaceous units is shown in Figure 97. The map closely matches the Quaternary thickness map in Figure 96. Noteworthy are a number of buried palaeovalleys in the top of the Cretaceous that are associated with the Adelaide River. These are arrowed and are potential pathways for the ingress inland of the coastal saline wedge. When compared with the underlying elevation of the top of Proterozic map it is evidence that these partly overly palaeovalleys in that surface also, suggesting that there has been compactional sag of the Cretaceous over these features allowing preferential fluvial flow.

6.2.3 Cretaceous thickness

The Cretaceous isopach map (Figure 98) shows that the thickness of the Cretaceous marine sediments is remarkably uniforming, thinning only gradually from 80 m to zero over a distance of 60 km, north to south.

The thickest part of the Cretaceous section is in the north western part of the project area, close to Gunn Point, where it reaches a thickness of 80 m. This thickening is due to the greater part of the Cretaceous basin being located offshore and is accompanied by an increase in the amount of fine-grained (clay rich) sediment in the section and a decrease in the sandy units. The Cretaceous has been extensively thinned by Cenozoic erosion beneath the Howard, Adelaide and Mary Rivers. Localised (on the 5 km scale) thickening by 20 m south of the Arnhem Land highway may be related to large scale karst features (poljes).

6.2.4 Depth to Top of Proterozoic

Elevation of the top of the Proterozoic is shown in Figure 99. Noteworthy features include the presence of palaeovalleys (blue arrows) and poljes (orange arrows). The tributary palaeovalleys show a strong structural control in a northeast-southwest direction. The poljes do not show obvious structural control, although there must be a lithological control as they can only form on a carbonate substrate.

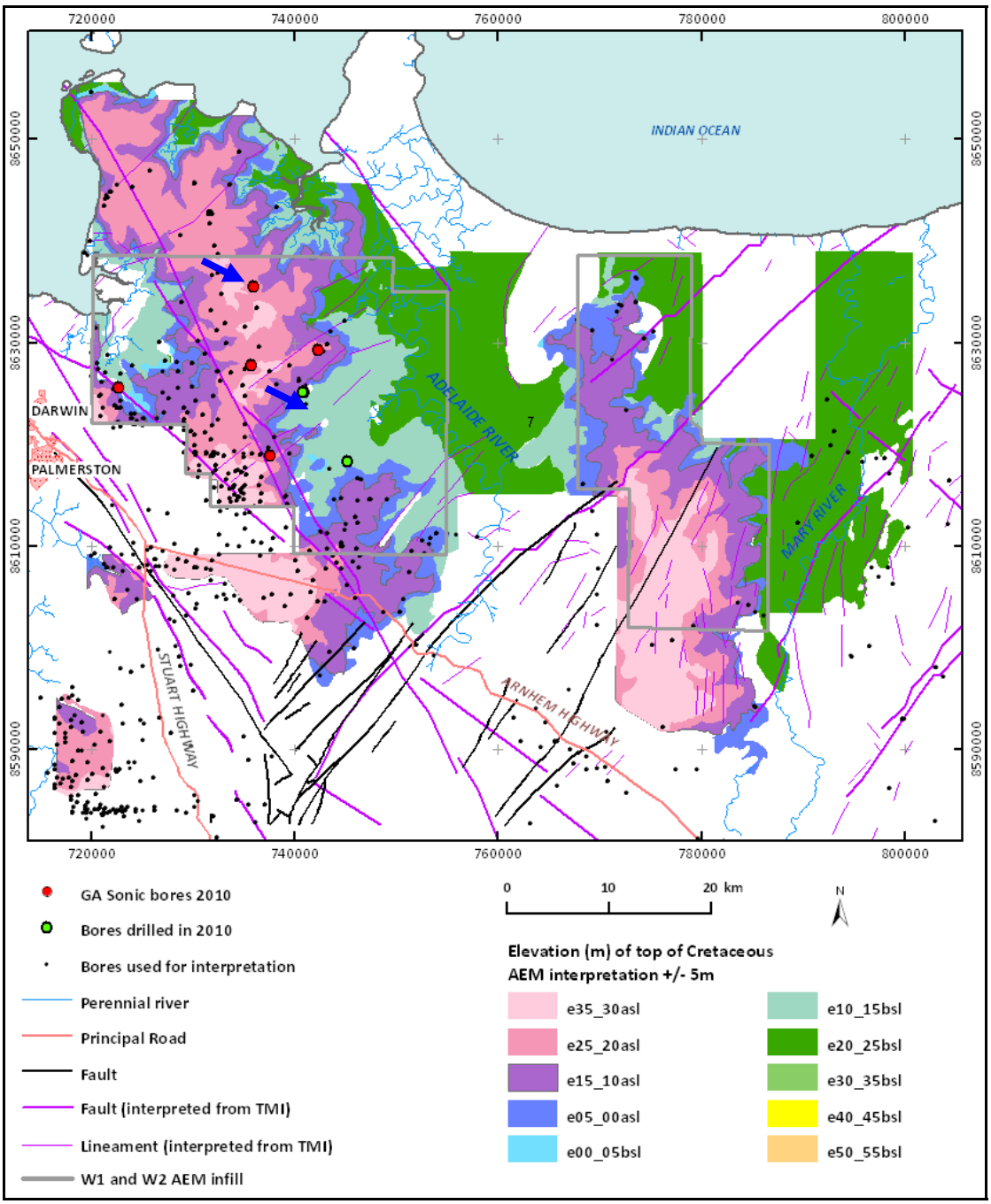

Figure 97*. Interpreted elevation of top of Cretaceous. Tributary palaeovalleys of the Adelaide River are arrowed.*

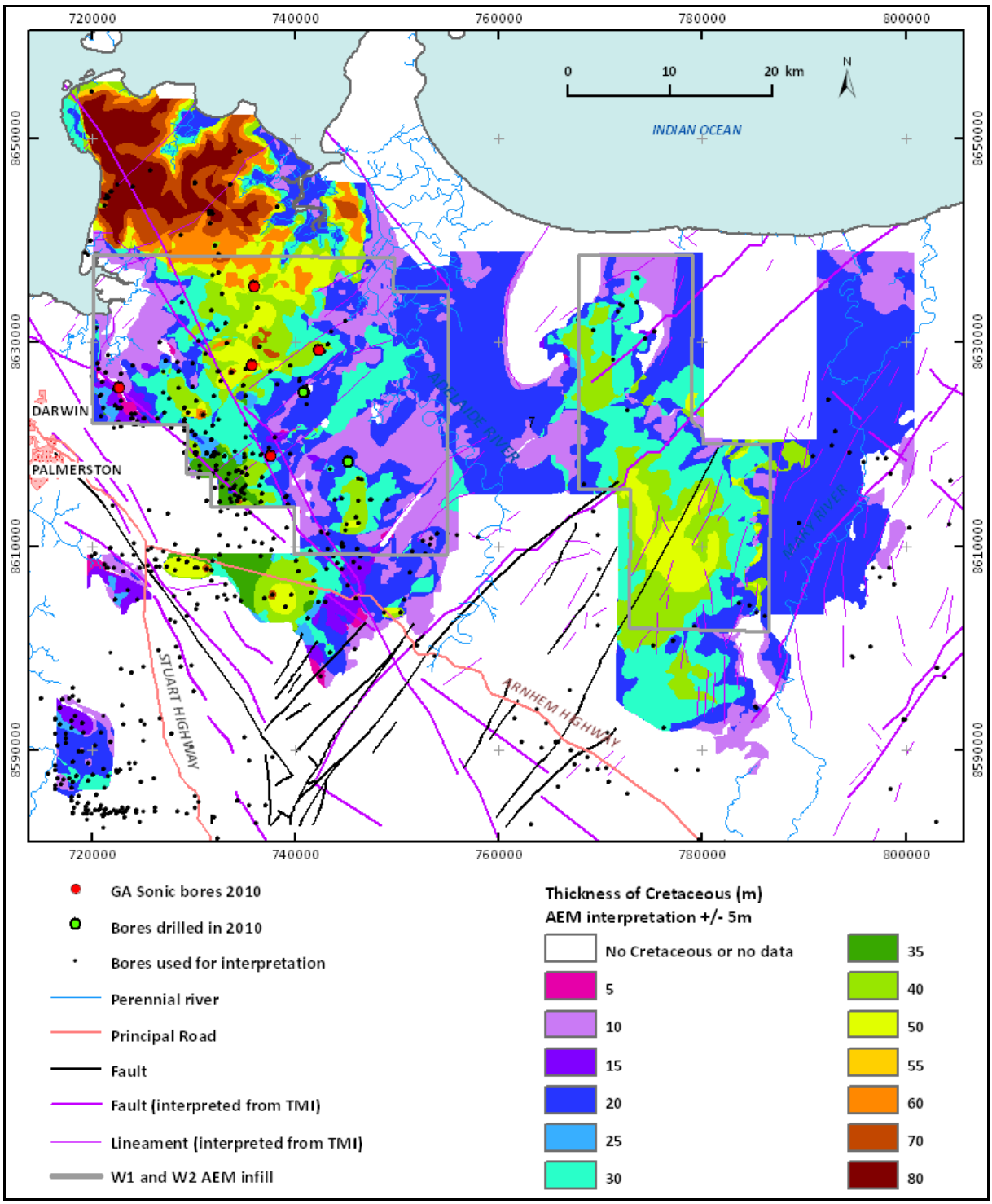

Figure 98. *Interpreted thickness of the Cretaceous succession in the project area.*

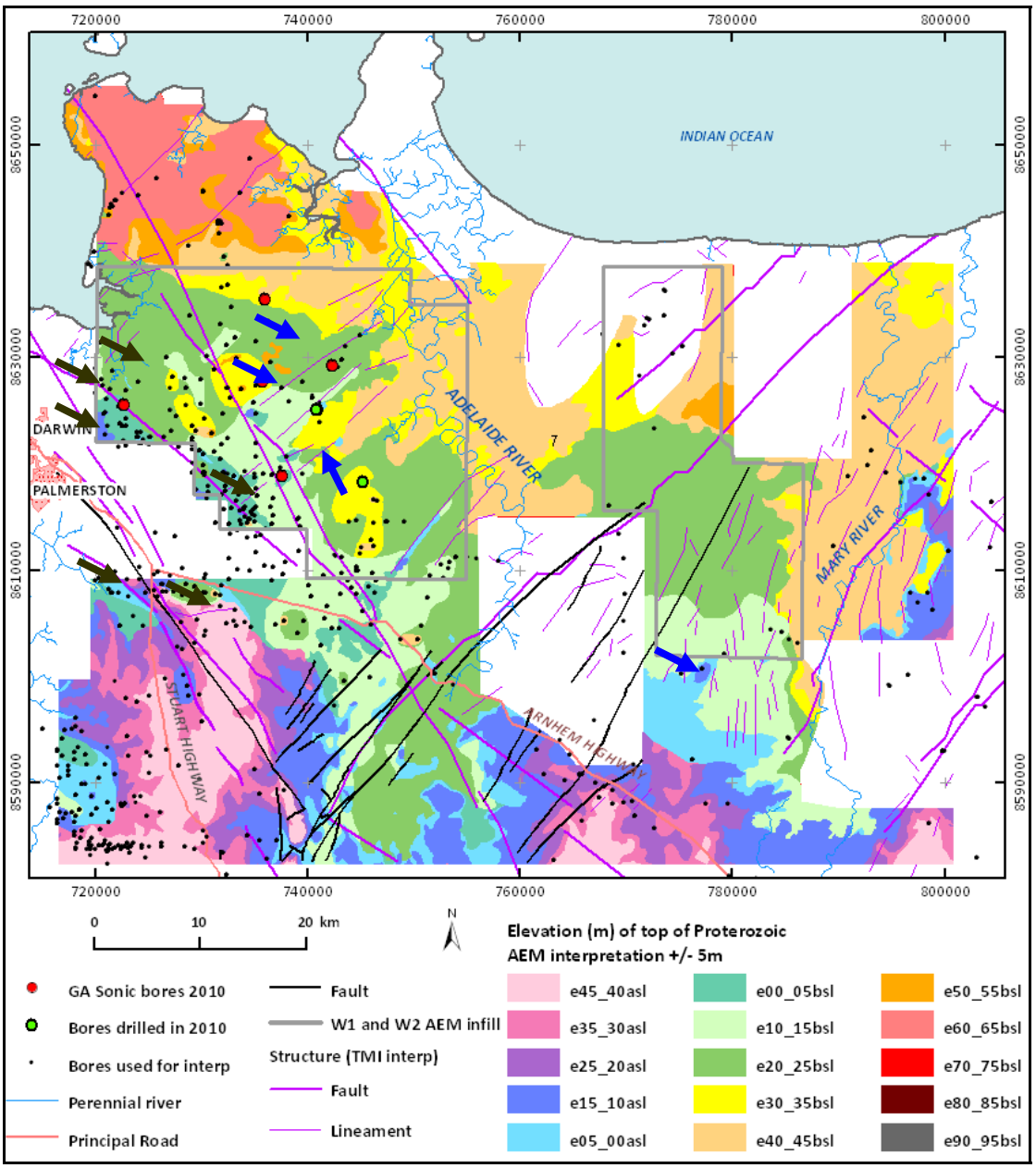

Figure 99. *Elevation of the top of the Proterozoic. Palaeovalleys arrowed in blue. Poljes in olive.*

6.2.5 Recharge controlling features

AEM mapping has revealed a number of potentially significant features of the palaeotopography underlying the Cretaceous that may influence recharge. These are shown in Figure 100. The features are of two types, palaeodrainage features and large scale karst features. Narrow bedrock structural features may also locally divert groundwater flow. These also are shown in Figure 5.

The palaeodrainage features are associated the Adelaide and Mary Rivers, thus showing the antiquity of the large scale fluvial drainage features of the project area. Not all fluvial drainage is of such antiquity, however. The Howard River, for example, lacks evidence for pre-Cretaceous antecedents. Their extent has not been fully mapped because of exclusions from the survey area associated with national parks. However, the map shows that the Cretaceous-filled trunk palaeovalleys are of the order of 10-15 km wide and 20 m deep. Several tributary palaeovalleys are also filled by Cretaceous sediment, these are also about 20 m deep but are only 1-5 km in width. The tributaries on the western side of the Adelaide river show strong structural control inherited from the underlying Proterozoic bedrock. The largest of these are indicated by blue arrows in Figure 100.

The palaeovalleys have the potential to both funnel discharge from the Cretaceous out towards the fluvial and estuarine plains under conditions where the hydraulic head is from the Cretaceous towards the coast and, where the head has been reversed by severe drought and over pumping, to allow sweater ready pathways in ingress further inland.

Large scale (5-10 km) closed karst depressions known as poljes have be recognised by outliers of Cretaceous sediment along the top of Proterozoic/base of Cretaceous unconformity in the 10-15 and 20-25 m interpreted elevation slices. These are between ten and 20 m deep and eight have been mapped. They are indicated by olive arrows in Figure 100. These have not been tested by sonic drilling so their fill is poorly understood, however, as low points in the palaeo-landscape, their fill is likely to be sandier than the surrounding sediments on higher parts of the palaeotopography. Thus the palaeo-poljes are likely to focus groundwater flow into them from the surrounding Cretaceous and along the basal Cretaceous-top of Proterozoic unconformity. While exposed, their floors would be likely sites for the development of dolines. Karst processes are likely to continue subadjacently after burial, possibly leading to localised fracturing and collapse of the overlying Cretaceous strata. Both palaeodolines and more recent subadjacent features would provide ready pathways for ground water to enter into cavernous porosity in the KCD.

Under current hydrologic regimes the poljes and associate features offer major potential for recharge. Should groundwater gradients be reversed, however, they may act as discharge zones for saline waters, were they to be reached in ingress of the salt water wedge.

The structural features in Figure 5 fall into one of three orientations, a north-northwest set, associated with the PCSZ, and north east-south west set, associated with the GRF, and a north west-south east set conjugate to those. These structural trends are often represented by bedrock ridges, some reaching the surface, composed of quartz veins, quartzite beds, dolerite dykes, and silicified faults. The largest of these are indicated by red arrows in Figure 100. While they appear very continuous in Figure 5, there extent is much more localised, being locally disrupted by features such as cross faults and variable silicification. These structures divert flow along them and impede cross flow. They may be particularly significant in association with the structurally controlled tributaries of the Adelaide River palaeovalley, and may serve to funnel groundwater flow into and out of them.

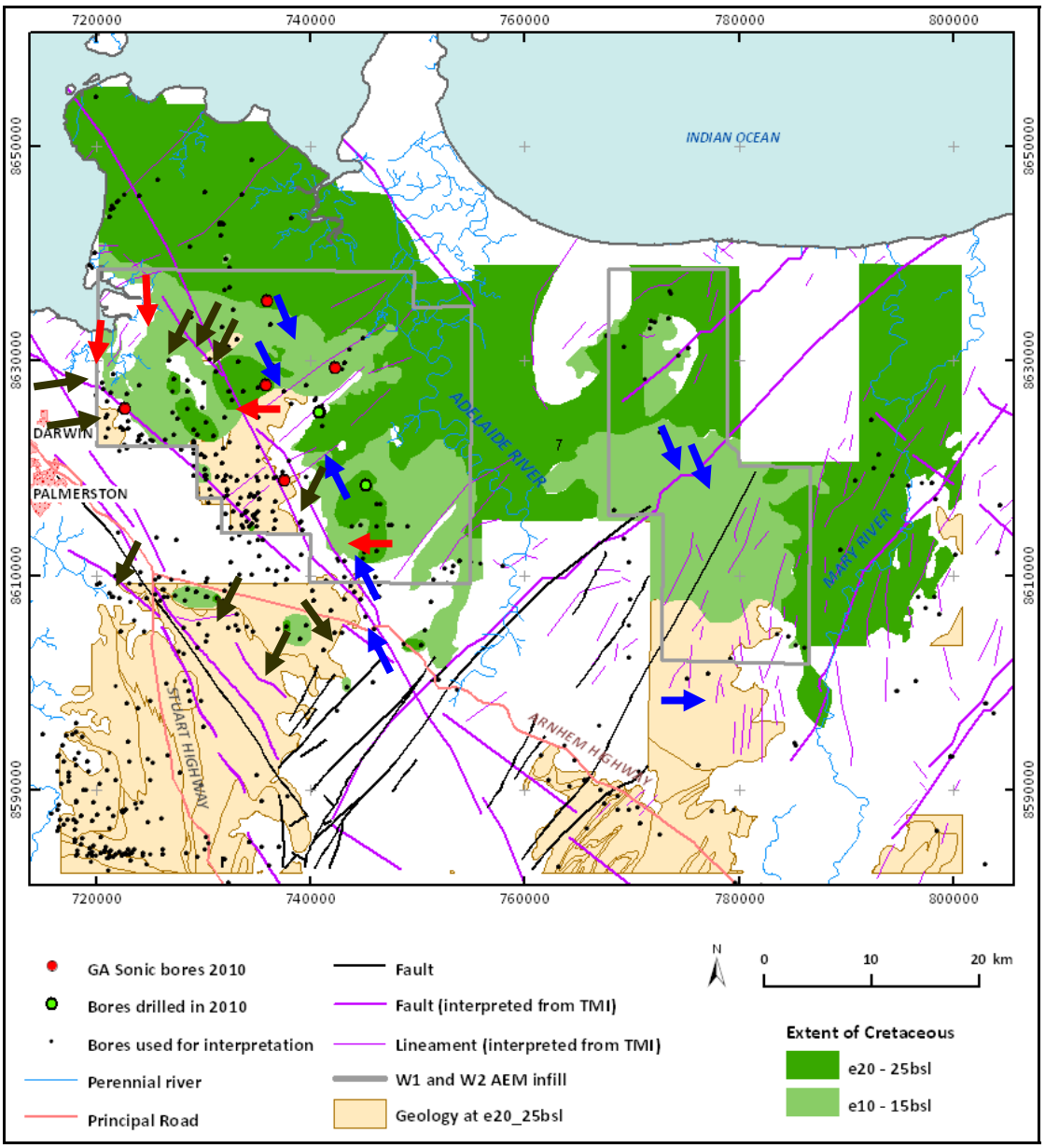

***Figure 100**. Hydrogeological features that may control recharge and groundwater flow. Palaeovallyes (blue arrows), poljes (olive arrows), and structural ridges (red arrows) indicated).*

6.3 SYNTHESIS OF GEOLOGY AND LANDSCAPE EVOLUTION

The geomorphic and stratigraphic history for the Northern Territory Coastal Plain project area can be summarised as occurring in the following phases:

Formation of the basement rocks, the mechanical properties and structural fabric of which are important in the development of fracture and karst porosity, and architecture of the overlying Cretaceous aquifers. Major events include:

- Formation of the Archaean succession (Woolner Granite and Dirty Water Metamorphics) over 2520-2675 Ma.
- Erosion of the Archaean basement and deposition of overlying sediments of the Mount Partridge Group (Crater Formation, Koolpinyah/Coomalie Dolomite, Whites Formation, Wildman Siltstone, and Koolpin Formation) at ~2019 Ma. All these except the KCD were clastic sediments, however the KCD is also predominantly clastic dominated in the project area. This was followed by deformation and metamorphism.

- Erosion of the folded and metamorphosed Mount Partridge Group and deposition of the overlying clastic and volcanic sediments of the South Alligator Group(Gerowie Tuff, Mount Bonnie Formation and Burrell Creek Formations) at ~1885 Ma. This was followed by further deformation and metamorphism
- On-going deformation associated with the Pine Creek Shear Zone and Giants Reef fault, with late dyke intrusion at ~1870 Ma (Zamu Dolerite) along the structures.
- Widespread erosion and weathering between from 1870 through to the Cretaceous. This resulted in a series of hydrostratigraphic features important in the control of large scale groundwater flow, in particular:
- Formation of the Wave Hill Surface, with relief on the order of tens of m that became the regional unconformity between the Proterozoic bedrock and younger sediments.
- Development of karstic landforms at various scales from poljes at the km to 10 km scale and dolines at the 100 m scale. Some caverns have also formed at this time, although they have not been dated directly.
- More resistant lithologies, especially quartzites, become ridges though differential erosion.
- Local accumulation of coarse detritus in low points of the landscape.
- Incision of a structurally palaeodrainage system ancestral to the modern Adelaide and Mary Rivers, with numerous tributaries.
- The Cretaceous transgression resulted in the rapid inundation of the Wave Hill Surface, forming the regional unconformity. Deposition in the Cretaceous Sea led to:
- Wave action locally adding to and modifying the coarse detritus in low points of the landscape.
- Widespread upward-fining sands were deposited, across the flooded area, forming the basal Cretaceous aquifer. These were thicker to the south where shallower water conditions prevailed, in karstic depressions at all scales, and close to quartzite ridges.
- Carbonaceous shales, thickest furthest of shore to the north were deposited in the peak of the transgression. Associated with the carbonaceous shales are a radiolarite bed and a phosphatic bed.
- Regression of the Cretaceous sea led to deposition of upward coarsening silts at the top of the successions
- Intense Cenozoic weathering affected much of the Cretaceous succession and the underlying Proterozoic. The weathering was very important in generating smaller scale flow pathways and aquifers. The weathering is expressed as:
- Continued dissolution of the KCD beneath Cretaceous cover, resulting in subadjacent karst and collapse of Cretaceous into sinkholes, forming water-filled springs.
- Extensive remobilisation of iron and silica in the Cretaceous sediments resulting in
- Dissolution of iron and silica minerals, especially along burrows and root channels, the formation of pseudokarstic depressions and bleached horizons, and intergranular secondary porosity.
- Precipitation of iron and silica minerals, the former as ferruginous bands and mottles, the latter forming porcellanite beds out of the radiolarite.
- Formation of an iron pisolite soils across the land surface.
- Incision of the courses of the Howard, Adelaide, and Mary Rivers into the Cretaceous, the course of the last two approximately continuous with their predecessors prior to the deposition of the Cretaceous sediments.

The Quaternary consisted of infill of the incised courses of the Howard, Adelaide, and Mary Rivers with fluvial and estuarine sediments. These infilled valley systems became the prime pathways for the ingress of saline water during Quaternary sea level highs, bringing saline marine water in contact with structural and karstic features along which the migrated to further depths and greater distances from the sea. There was also local reworking of the pisolitic Cretaceous-derived soils as slope deposits and ongoing weathering of local importance to recharge and discharge.

7 Hydrogeology Interpretation

7.1 INTERPRETED SALINITY DISTRIBUTION

The distribution of groundwater salinity across the project area was interpreted for the same five elevation slices discussed in the previous section, these being the below sea-level intervals for 0-5 m, 10-15 m, 20-25 m, 30-35 m and 60-65 m. The depth slices show the distribution of salinity as derived from the AEM conductivity data, as determined using the method outlined in Section 4.2. These five slices illustrate the potential for mapping SWI from regional AEM survey data.

7.1.1 60-65 m interpretive elevation slice

This is the deepest of the five interpreted salinity depth slices below sea level (Figure 101). The slice is entirely through Proterozoic and Archaean rocks, except for the northern part of the Gunn Peninsula where Cretaceous sedimentary rocks occur. The source of the saline water in the northern area is interpreted to be caused by present (and possibly past) lenses of seawater which have infiltrated the fresher groundwater reservoirs. These zones of seawater intrusion have probably percolated downwards from overlying seawater-saturated sediments particularly beneath the Howard, Adelaide, and Mary rivers, and also including the Cretaceous cover sequences to the north.

The strong structural control on the distribution of saline zones in the central part of the area is evident by the dominant north-east to south-west trend, where advection westward has occurred from a source zone beneath the Adelaide River. Highly conductive areas in the southern part, mostly south of the Arnhem Highway, are attributed to pyritic sedimentary rocks and other conductive units in the Proterozoic bedrock sequences.

7.1.2 30-35 m interpretive elevation slice

The depth slice cuts through the unconformity between the basement rocks in the south and the Cretaceous sedimentary sequences in the north (Figure 102). There is also an inlier of Archaean basement rocks between the Adelaide and Mary Rivers in the northern part of the project area. Highly conductive zones in the southern part of the area, mostly south of the Arnhem Highway, are attributed to pyritic sediments and other conductive basement rock units.

The source of the saline water is interpreted to be contemporary (and possibly past) seawater lenses infiltrating the fresher groundwater system. The strong north-east to south-west trend in the saline zones suggests that basement structures have played an important role in the infiltration of saline groundwater to the Proterozoic section, at least in the central part of the project area. Convective draw-down of saline groundwater from the Cretaceous rocks may have occurred along these structural corridors. The pattern of the overlying alluvial and estuarine plains of the Howard, Adelaide, and Mary Rivers that host seawater intrusion is strongly superimposed on underlying units. The saline areas are significantly more widespread at this depth than the 60-65 m interval.

7.1.3 20-25 m interpretive elevation slice

This depth slice also cuts through the unconformity between the basement rock units in the south and the Cretaceous sedimentary sequences in the north (Figure 103). However, at this depth the Cretaceous cover extends further southwards. The spatial extent of the Archaean basement rock inlier between the Adelaide and Mary Rivers in the north is also reduced at this level. Highly conductive zones in the southern part, mostly south of the Arnhem Highway, are attributed to pyritic rock units and other conductive sedimentary sequences.

Similar to the deeper elevation slices, the source of saline water evident at this depth is interpreted to be present and perhaps past seawater lenses. These occur within the Cretaceous rocks and have also infiltrated downwards from the Quaternary sediments along permeable basement structures; the dominant north-east to south-west structural trend is evident in the central part of the project area. The strong structural control on

the distribution of saline groundwater zones appears to have propagated upwards through the lower part of the Cretaceous units, probably through sequential inheritance from the basement structures.

The salinity pattern in the overlying alluvial and estuarine plains of the Howard, Adelaide, and Mary Rivers affected by seawater intrusion is strongly superimposed on underlying units. The saline areas at this elevation level are more extensive than those formed at greater depths.

7.1.4 10-15 m interpretive elevation slice

In this slice the distribution of Cretaceous sedimentary rocks is close to their maximum extent, with Proterozoic metasedimentary units only in the southern part of the study area (Figure 104). The Archaean inliers are completely obscured by the Cretaceous rocks at this depth. Quaternary alluvial and estuarine sediments of the Howard, Adelaide and Mary Rivers are evident in this slice. The seawater intrusion zone associated with these sediments is significantly more widespread than for the deeper slices, and large areas contain groundwater which has salinity levels close to that of seawater concentration.

The presence of possible fossil (and perhaps concentrated) seawater in the subsurface is consistent with the extensive estuarine–mangrove swamp facies which developed in the early Holocene (the so-called “Big Swamp” phase, see Woodroffe *et al.,* 1993).

Highly conductive areas in the southern region, mostly south of the Arnhem Highway, are attributed to pyritic sedimentary units and other conductive rock types.

7.1.5 0-5 m interpretive elevation slice

The extent of Cretaceous sedimentary units in this slice remains largely unchanged from the previous level (Figure 105). Quaternary alluvial and estuarine sediments associated with the Howard, Adelaide and Mary Rivers and their tributaries are more widely distributed. The areas of seawater intrusion associated with these sediments have increased further, especially the distribution of groundwater with salinity levels approaching or exceeding that of seawater.

Highly conductive areas in the southern part of the survey region, mostly south of the Arnhem Highway, are attributed to pyritic rocks and other highly conductive units.

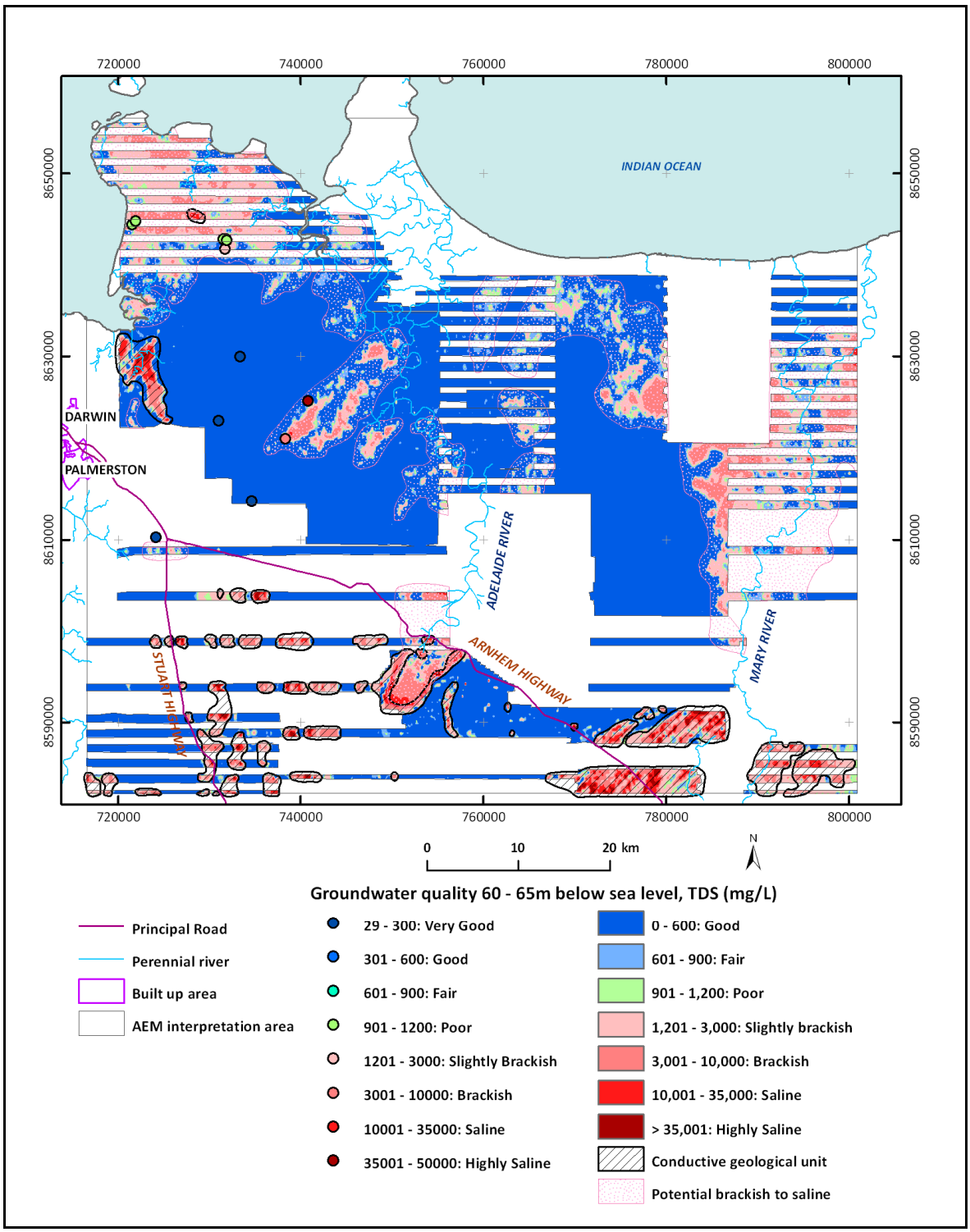

Figure 101: *Interpreted distribution of groundwater salinity for elevation slice 60–65 m below sea-level (bsl). The saline zones occur in Proterozoic and Archaean bedrocks. High salinity zones are evident beneath the Howard and Mary Rivers associated with seawater intrusion infiltrating downwards from overlying sediments. Similarly, a saline zone is visible at Gunn Point, associated with downward migration of seawater from the overlying Cretaceous rocks. Seawater movement into basement structures occurs west of the Adelaide River.*

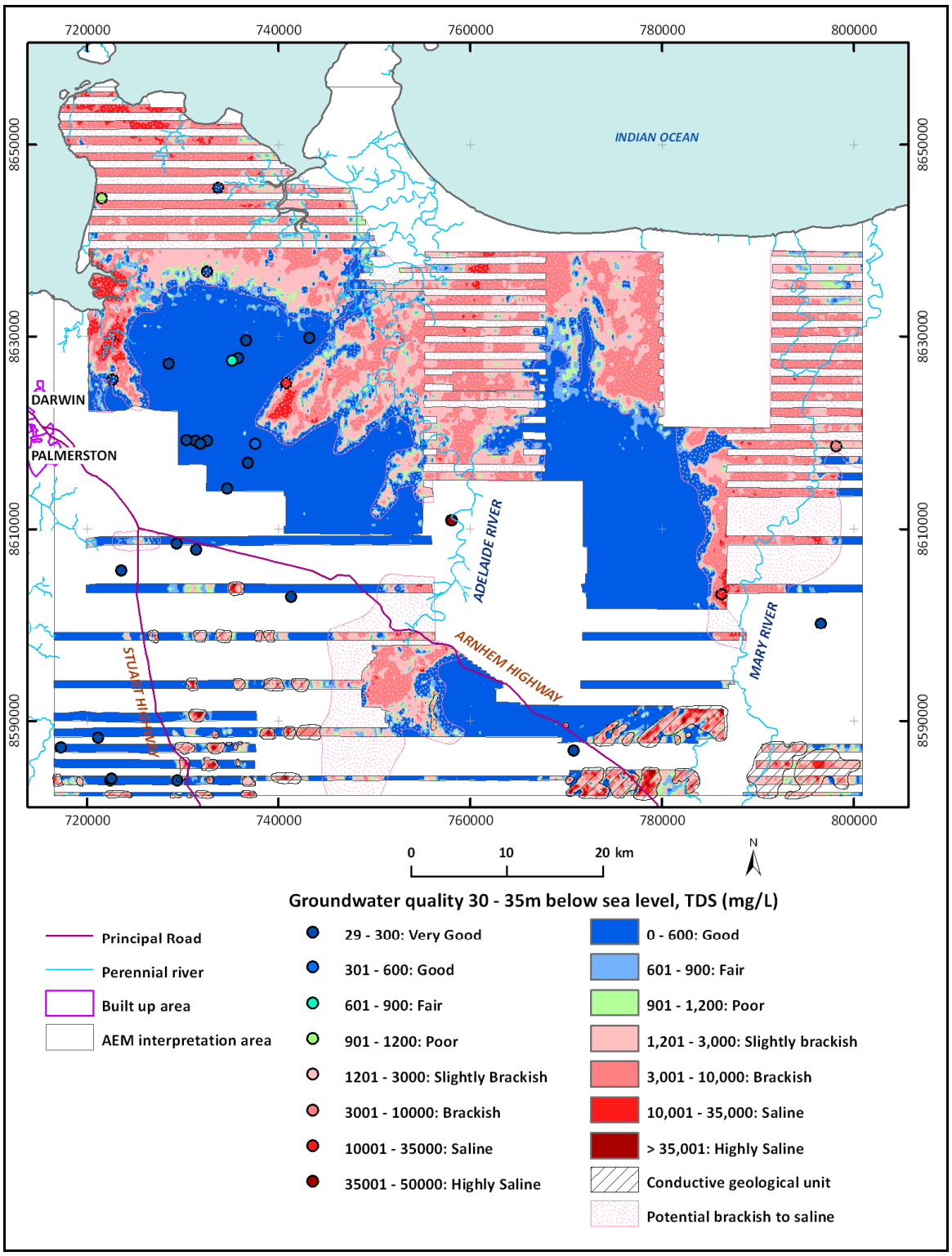

Figure 102: *Interpreted groundwater quality distribution for 30 to 35 m slice bsl. Zones of seawater intrusion are more widespread. In the northern region saline groundwater occurs in Cretaceous sedimentary rocks. Seawater intrusion has preferentially occurred downward along zones of structural weakness into Proterozoic basement rocks from the overlying sediments of the Howard, Adelaide, and Mary River floodplains.*

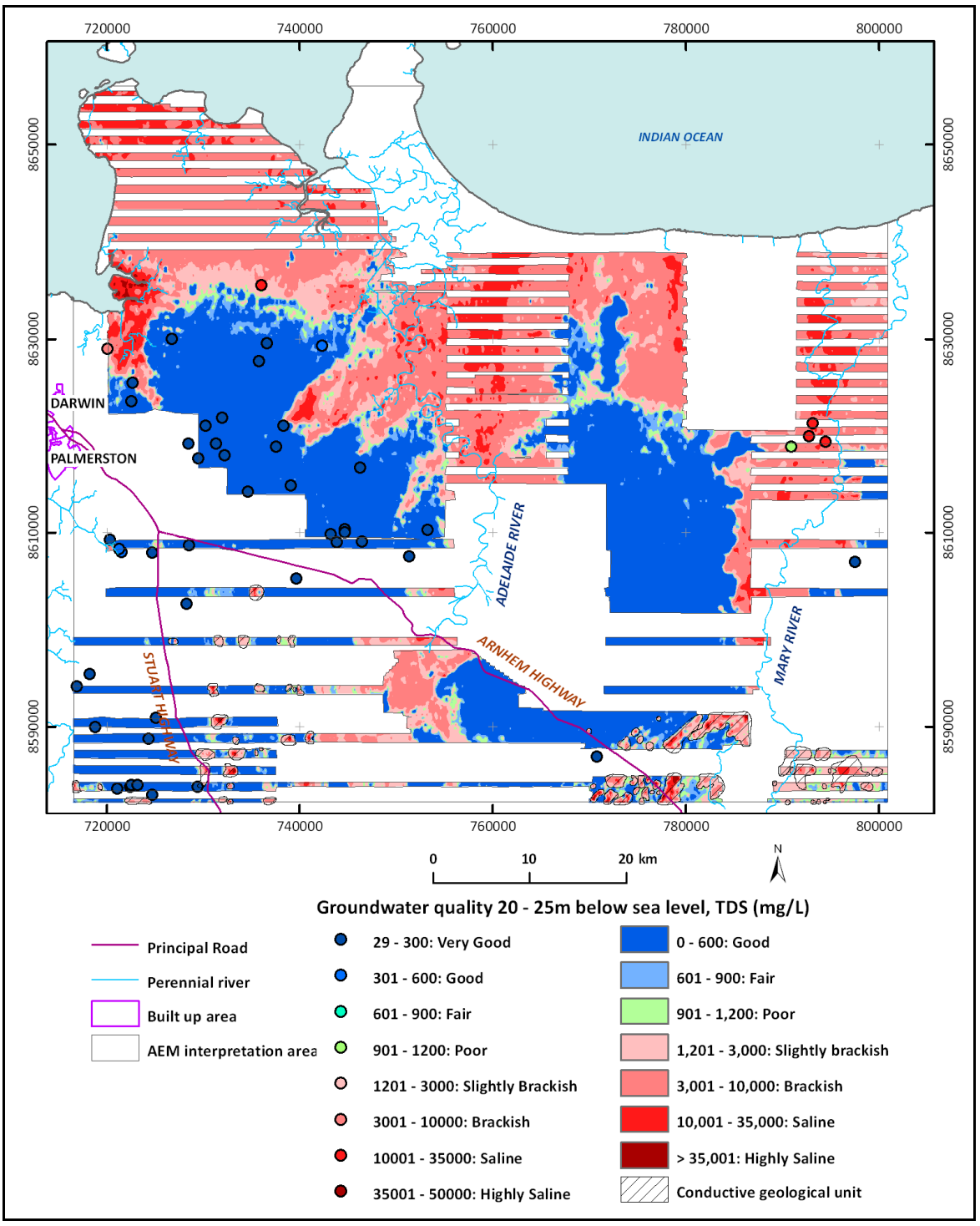

Figure 103: *Interpreted groundwater quality distribution for elevation slice 20 to 25 m bsl. The extent and magnitude of seawater intrusion is more widespread than at deeper intervals, and is mostly contained in Cretaceous sedimentary rocks, though inherited structural control is evident.*

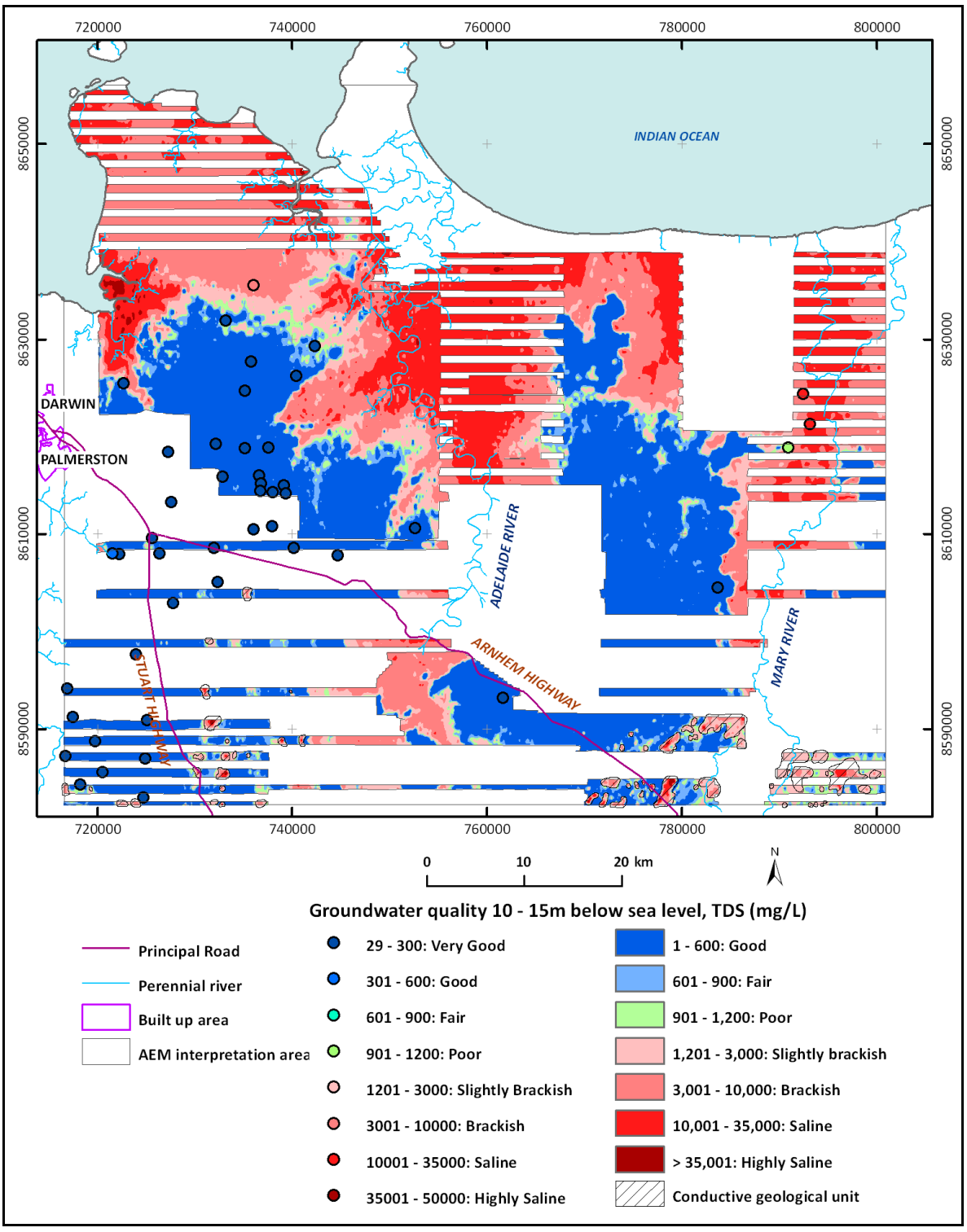

Figure 104: *Interpreted groundwater quality distribution for elevation slice 10 to 15 m bsl. This map highlights the maximum extent of Cretaceous rocks and is the deepest slice with Quaternary fluvial and estuarine sediments affected by seawater intrusion. Seawater intrusion is more widespread at this level than in the deeper slices.*

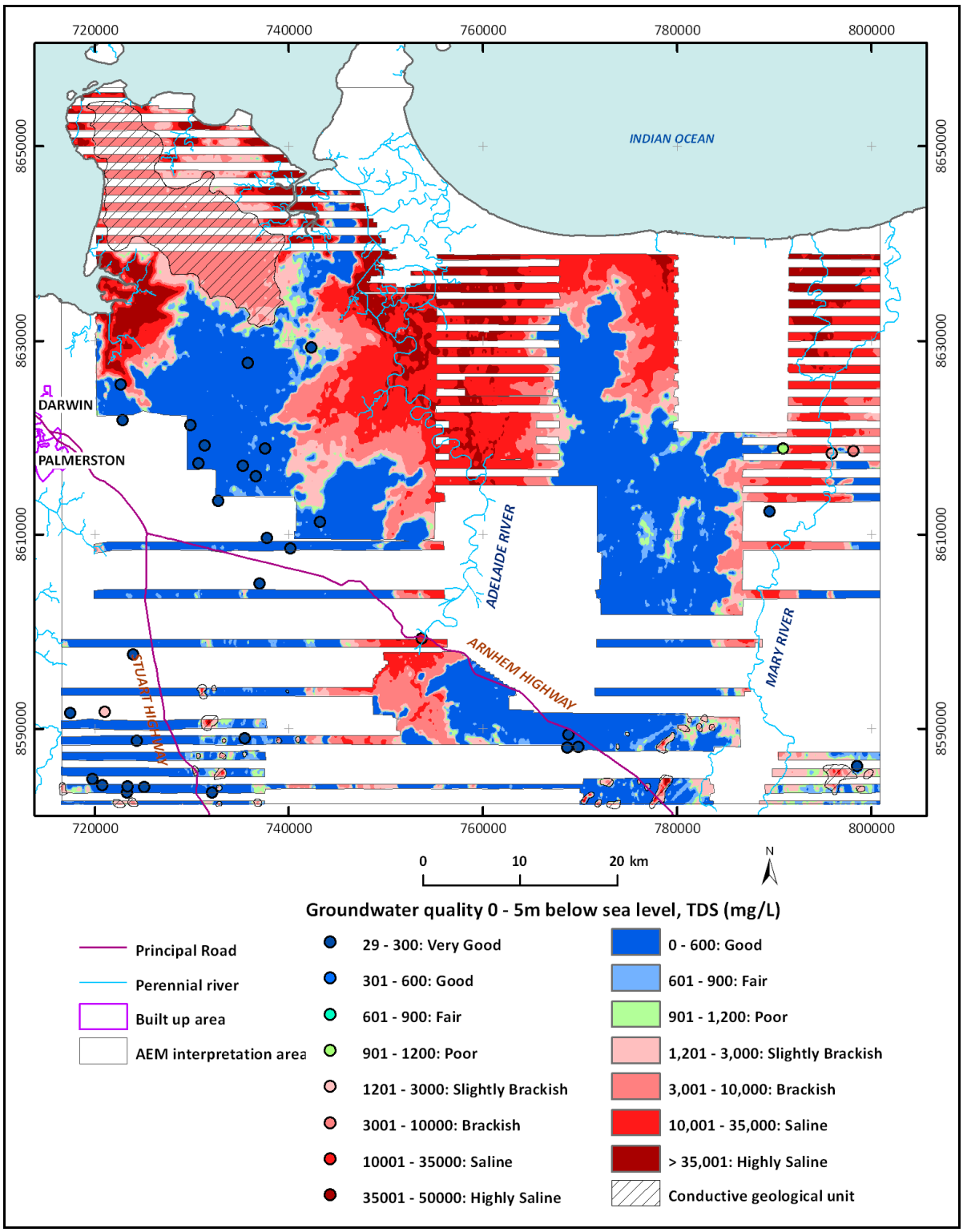

Figure 105: *Interpreted groundwater quality distribution for the 0 to 5 m bsl depth slice. This map shows the maximum extent of Quaternary sediments and the greatest extent and magnitude of seawater intrusion into the NTCP project area.*

7.2 STACKED INTERPRETED SALINITY LAYERS

The individual layers showing calculated groundwater salinity are presented as stacked layers in Figure 106. Layer depths remain unchanged. A noteworthy feature emphasised in the stacked sections are the relatively shallow elevated groundwater salinity levels in the estuarine floodplains of the Howard, Adelaide and Mary Rivers. These highly saline zones are interpreted to be caused by the combined effects of the current salt water intrusion wedge, and remnant Early Holocene saline waters from the "Big Swamp" phase of

widespread mangrove development. The presence of the saline water wedge beneath the weathered Cretaceous sedimentary rocks south of Gunn Point is particularly evident.

7.2.1 Flight line sections

Six AEM flight lines (or segments of longer flight lines) were selected for detailed interpretation as part of this study. This selection provides for a relatively wide spatial analysis of the AEM dataset across the main part of the coastal plain study region (Figure 107). The AEM flight lines were: 6100701, 6101901, 6102201, 6102701, 6103302, 6103702, and these interpreted sections, as well as the actual AEM data and satellite imagery, are shown in Figures 82-Figure 87, respectively. In the 1-D inversions portrayed below the interpreted section geometry has not been corrected and must be taken as indicative only.

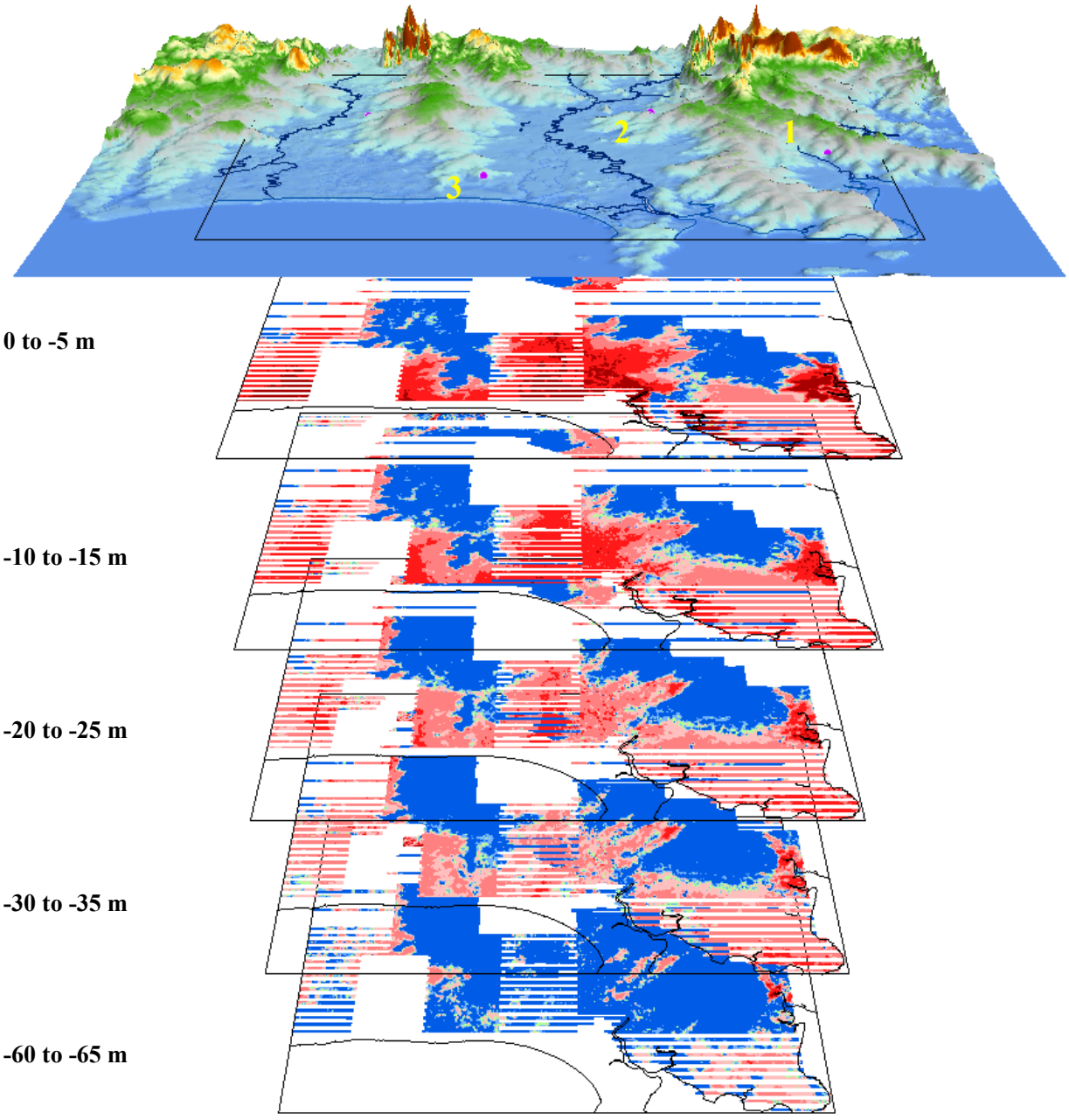

Figure 106: *Stacked calculated groundwater salinity layers for the five interpreted depth slices, highlighting variations in salinity with different depths in the project area. The uppermost level is combined SRTM and LIDAR DEM (with vertical exaggeration). Labelled on the uppermost level are: 1=Howard Springs, 2=Koolpinyah, 3=Woolner. View from above the Clarence Strait looking due south.*

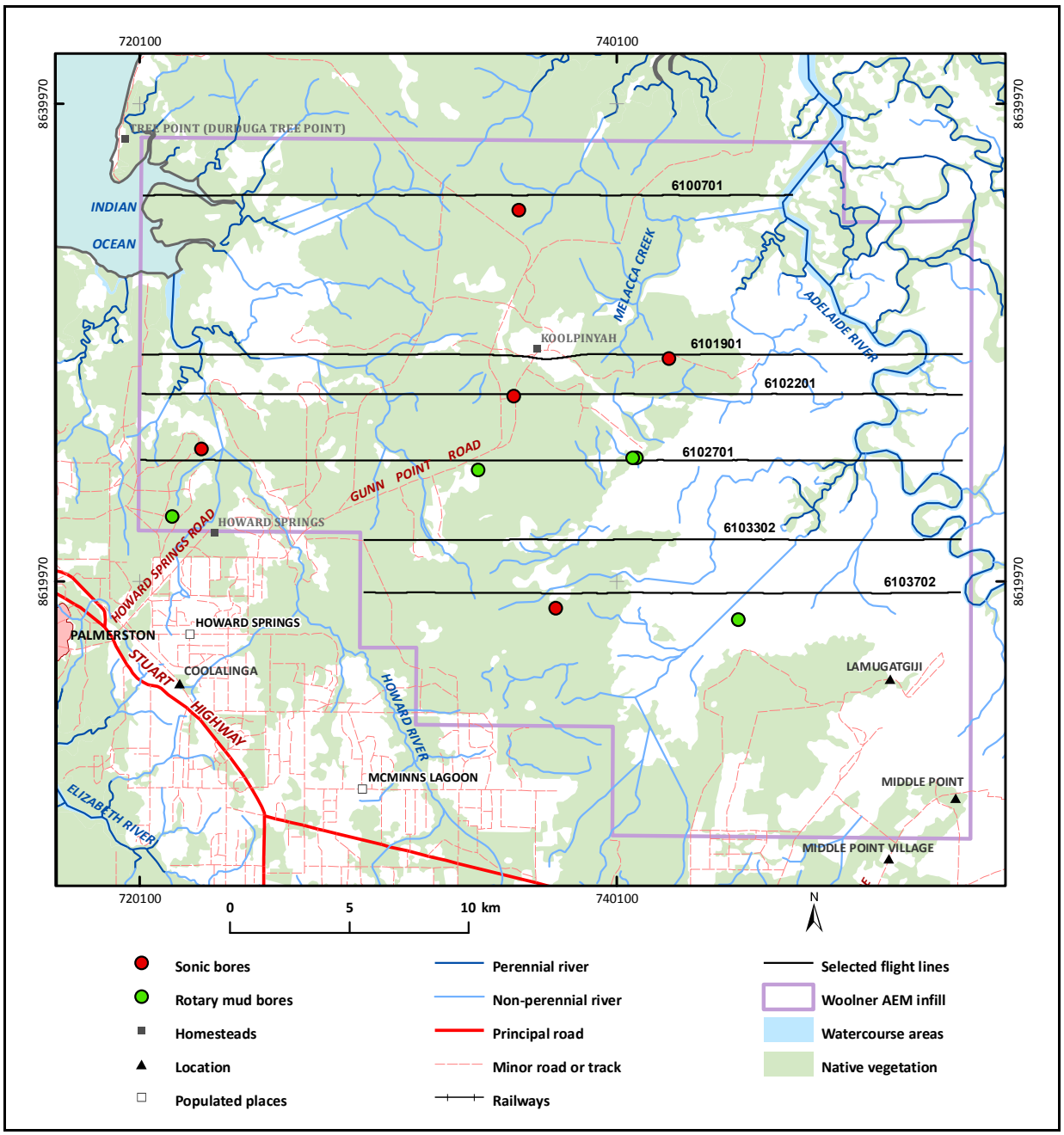

Figure 107: *Location of AEM flight line sections interpreted for this study.*

7.2.1.1 Interpreted flight line section 6100701

This section (Figure 108) shows the highly conductive zone of seawater intrusion in the west associated with the Howard River and, in the east, the edge of the seawater intrusion zone associated with the Adelaide River. Between them is a moderately conductive zone with brackish water contained within the undifferentiated Cretaceous sedimentary rocks. The highest conductivity groundwater (coloured pink on the section) is contained within the shallow Quaternary sediments and extends downwards along fractures and faults associated with Proterozoic dykes following the fault systems of the PCSZ. Beneath the Howard River floodplain the Proterozoic units are the Wildman Siltstone. In the remainder of the section the Proterozoic rocks are the KCD, although drilling shows that the formation contains significant proportion of siltstone.

7.2.1.2 Interpreted flight line section 6101901

This section (Figure 109) again shows the highly conductive zone of seawater intrusion in the west associated with the Howard River and, in the east, the seawater intrusion zone associated with the Adelaide River. Between them is a weakly conductive zone with brackish water contained within the Cretaceous sedimentary rocks. Unlike the section to the north (6100702) the conductive zone in the Cretaceous

sedimentary section is restricted to the eastern half and the intensity is considerably weaker. The highest conductivity groundwater occurs within the Quaternary sediments and extends downwards along fractures and faults. In places, these zones may be associated with Proterozoic dykes but the conductivity overprint of the seawater intrusion is so strong in this section that the dykes, if present, are obscured and cannot be conclusively identified. The most noteworthy features on the sections are two zones interpreted as collapse features formed by sub-adjacent karsts; the eastern zone corresponds to Quambi Lagoon and the western zone with Lumul Limul Lagoon. The Proterozoic rocks below these lagoons are interpreted as the Koolpinyah-Coomalie Dolomite (KCD). Beneath the Howard River the Proterozoic section is composed of the Wildman Siltstone

7.2.1.3 Interpreted flight line section 6102201

This section (Figure 110) also shows the zone of seawater intrusion in the west associated with the Howard River and, in the east, the sea water intrusion associated with the Adelaide River. Between them is a weakly conductive zone with brackish water contained within the Cretaceous sedimentary rocks. Compared to the section to the north (6100702) the conductive zone in the Cretaceous rocks covers a smaller area situated further to the east, and the overall conductivity signature is less pronounced. The highest conductivity water is contained within the Quaternary sediments and extends downwards along fractures and faults, some of which are associated with Proterozoic dykes (evident in TMI data). In other areas dykes may also act as sub-vertical pathways for ingress of saline groundwater, but the conductivity overprint related to seawater intrusion is so strong for these that the dykes, if present, are obscured. West of the Howard River the Proterozoic is composed of the Wildman Siltstone, in the rest of the section it is composed of the KCD, although a significant amount of siltstone exists in the dolostone sequence (shown by drilling).

7.2.1.4 Interpreted flight line section 6102701

This section (Figure 111) shows the zone of seawater intrusion in the west associated with the Howard River and, in the east, the seawater intrusion associated with the Adelaide River. The Howard River salt water wedge is less pronounced than in the sections further north and the sub-vertical distribution is strongly controlled by basement structures. The highly conductive Adelaide River salt water wedge is strong in the near-surface Quaternary sediments and likewise penetrates downwards along basement structures. The Cretaceous rocks along this section are confined to relatively thin and discontinuous strata on the higher hills.

7.2.1.5 Interpreted flight line section 6103302

This is the only cross section in the report that does not have a sonic bore to provide geological control (Figure 112). It is relatively short and consists of the Adelaide River floodplain to the west and a low plateau of Cretaceous rocks overlying Proterozoic bedrock in the east. The Adelaide River salt water wedge is strongly developed in the upper sequence of Quaternary sediments. The highly conductive seawater intrusion wedge associated with the Adelaide River penetrates both downwards along basement structures and laterally into the Cretaceous sediments. The eastern-most structural zones likely form part of the GRF.

7.2.1.6 Interpreted flight line section 6103702

This is the southernmost line and, as with line 6103302, is relatively short (Figure 113). Quaternary sediments of the Adelaide River floodplain underlie the western half of the line. Most of the eastern half consists of Proterozoic basement rocks, apart from a thin relic cover of Cretaceous strata in topographically elevated areas. Seawater intrusion occurs in the floodplain sediments of the Adelaide River, and infiltrates downwards and along basement structures. The structures in the eastern half of the line may offset the base of the Cretaceous sequence and possibly influence the distribution of the Quaternary sediments. They are at least in part associated with the GRF.

This page was left blank intentionally

Section 6100701

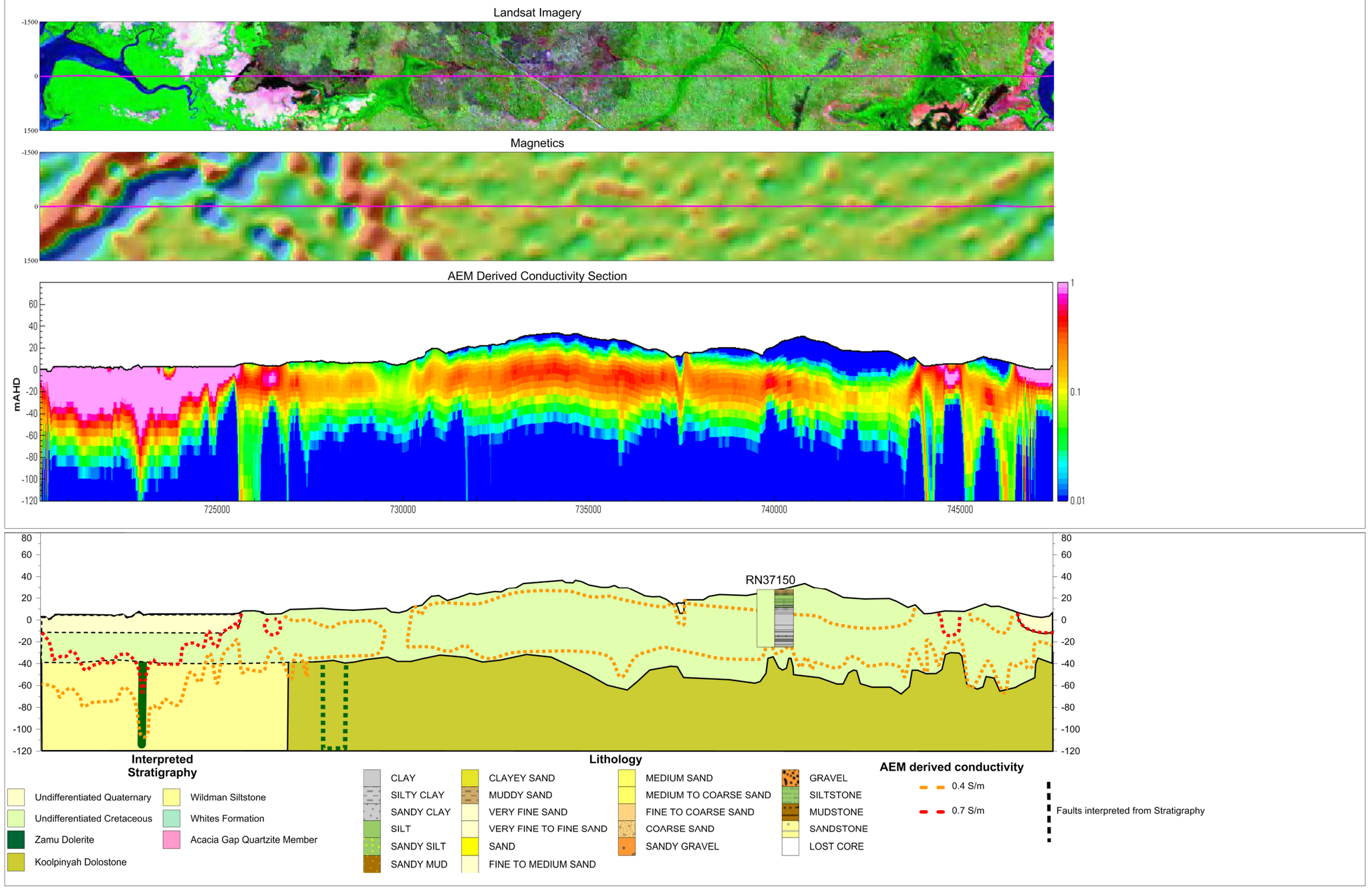

Figure 108: *Flight line section 6100701. Upper two images: Landsat image showing flight line trace, underlain by total magnetic intensity strip. Middle image: Conductivity section along flight line. Lower image: Interpreted geology and seawater intrusion zones with superimposed sonic bore hole (RN37150). Dashed lines show lower confidence in interpretation, based on either extrapolation (where stratigraphic contacts are masked by conductivity or for basement structures where these are supported by only one line of data). The highest conductivity zones shown in pink (arbitrarily defined here as having AEM conductivity >0.7 S/m) are caused by saline groundwater.*

Section 6101901

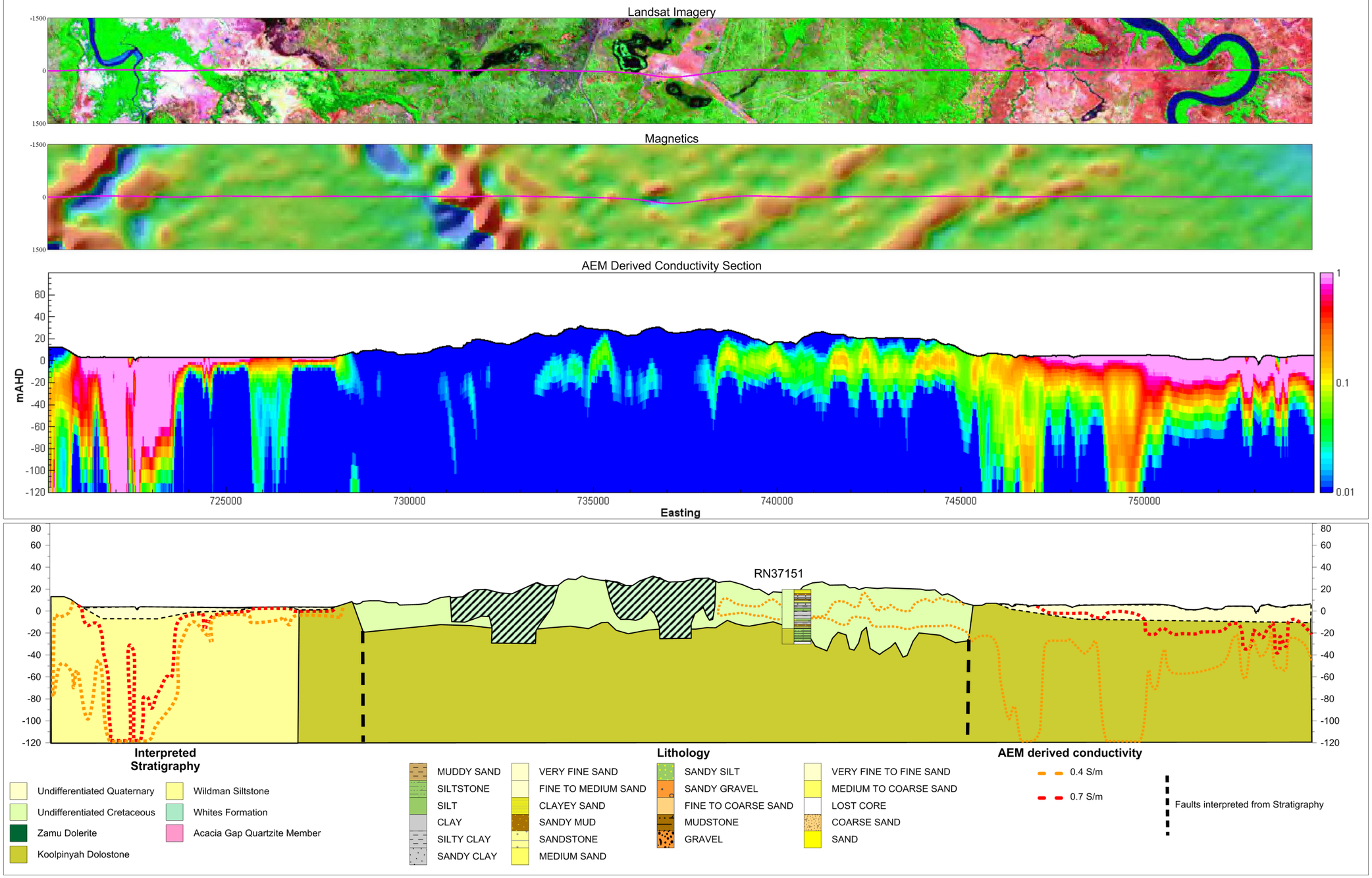

Figure 109: *Flight line section 6101901. Upper two images: Landsat image showing flight line trace, underlain by total magnetic intensity strip. Middle image: AEM conductivity section along flight line. Lower image: Interpreted geology and seawater intrusion zones with superimposed sonic bore hole (RN37151). Dashed lines show lower confidence in interpretation, based on either extrapolation (where stratigraphic contacts are masked by conductivity or for basement structures where these are supported by only one line of data). The two hashed areas in the Cretaceous section are interpreted as collapse features formed by sub-adjacent karsts; the eastern collapse zone coincides with Quambi Lagoon, and the western collapse zone coincides with Lumul Limul Lagoon. The highest conductivity zones shown in pink (arbitrarily defined here as having AEM conductivity >0.7 S/m) are caused by saline groundwater.*

Section 6102201

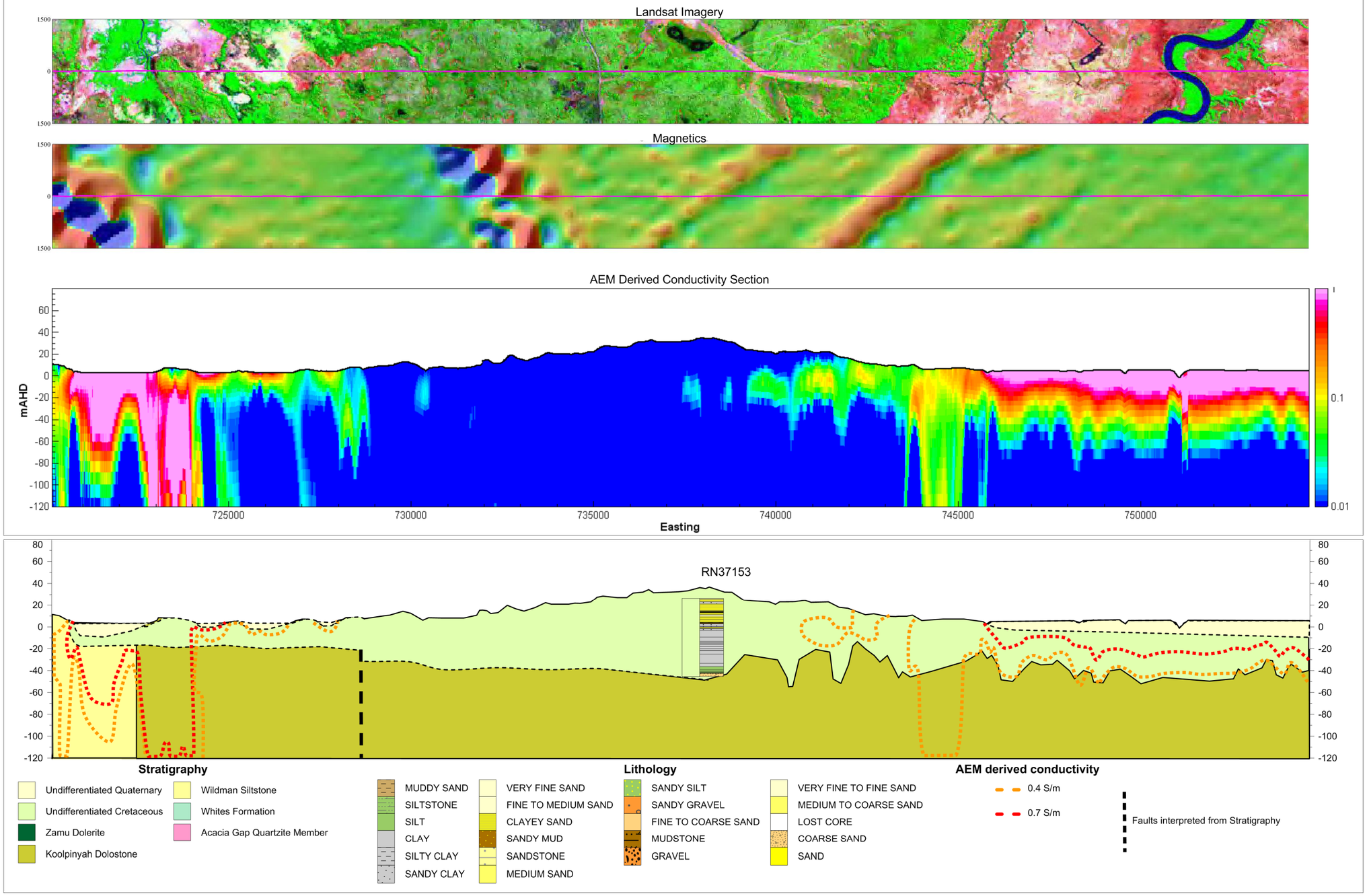

Figure 110: *Flight line section 6102201. Upper two images: Landsat image showing flight line trace, underlain by total magnetic intensity strip. Middle image: AEM conductivity section along flight line. Lower image: Interpreted geology and seawater intrusion zones with superimposed sonic bore hole (RN37153). Dashed lines show lower confidence in interpretation, based on either extrapolation (where stratigraphic contacts are masked by conductivity or for basement structures where these are supported by only one line of data). The highest conductivity zones shown in pink (arbitrarily defined here as having AEM conductivity >0.7 S/m) are caused by saline groundwater.*

Section 6102701

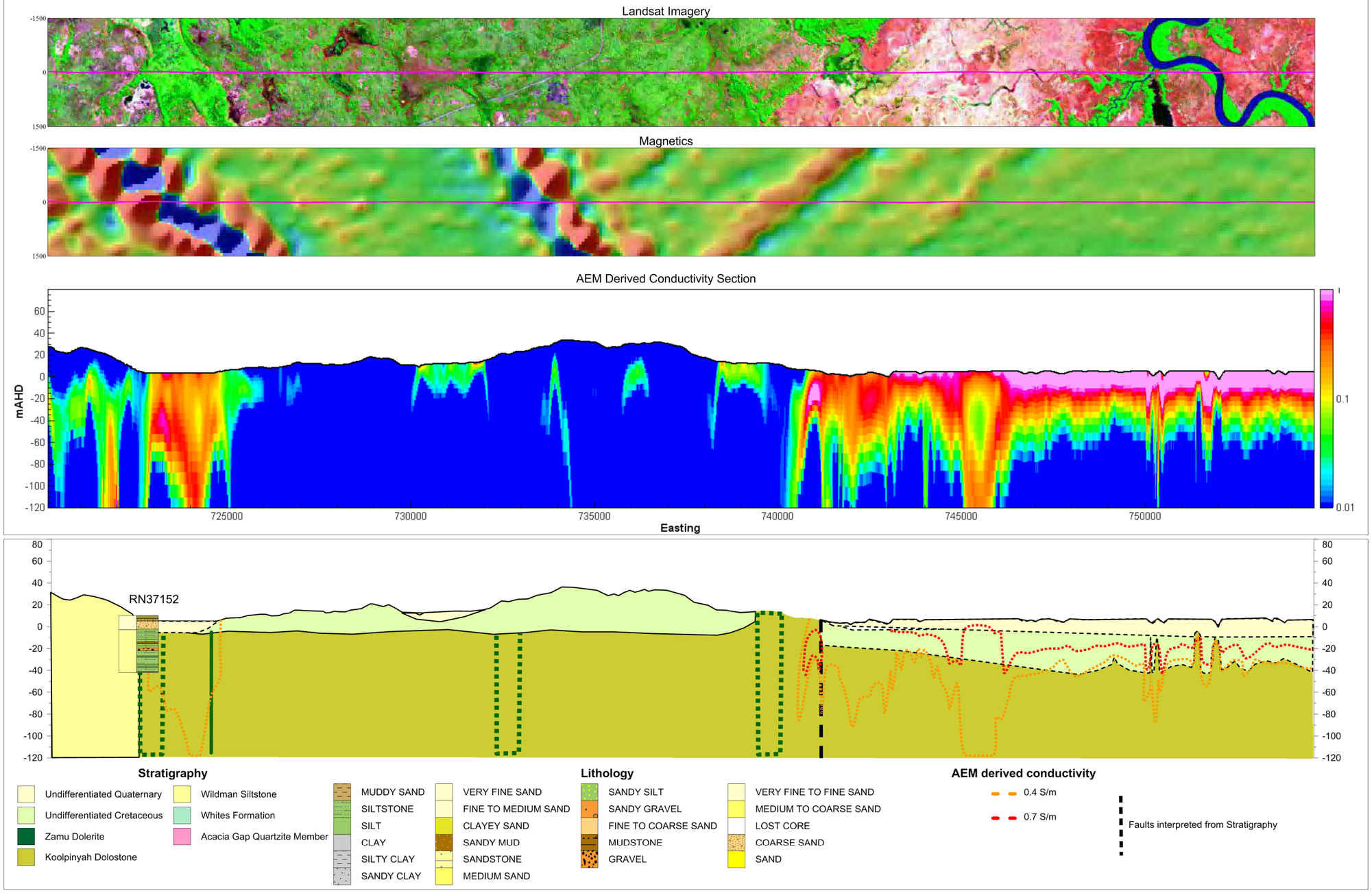

Figure 111: *Flight line section 6102701. Upper two images: Landsat image showing flight line trace, underlain by total magnetic intensity strip. Middle image: AEM conductivity section along flight line. Lower image: Interpreted geology and seawater intrusion zones with superimposed sonic bore hole (RN37152). Dashed lines show lower confidence in interpretation, based on either extrapolation (where stratigraphic contacts are masked by conductivity or for basement structures where these are supported by only one line of data). The highest conductivity zones shown in pink (arbitrarily defined here as having AEM conductivity >0.7 S/m) are caused by saline groundwater.*

Section 6103302

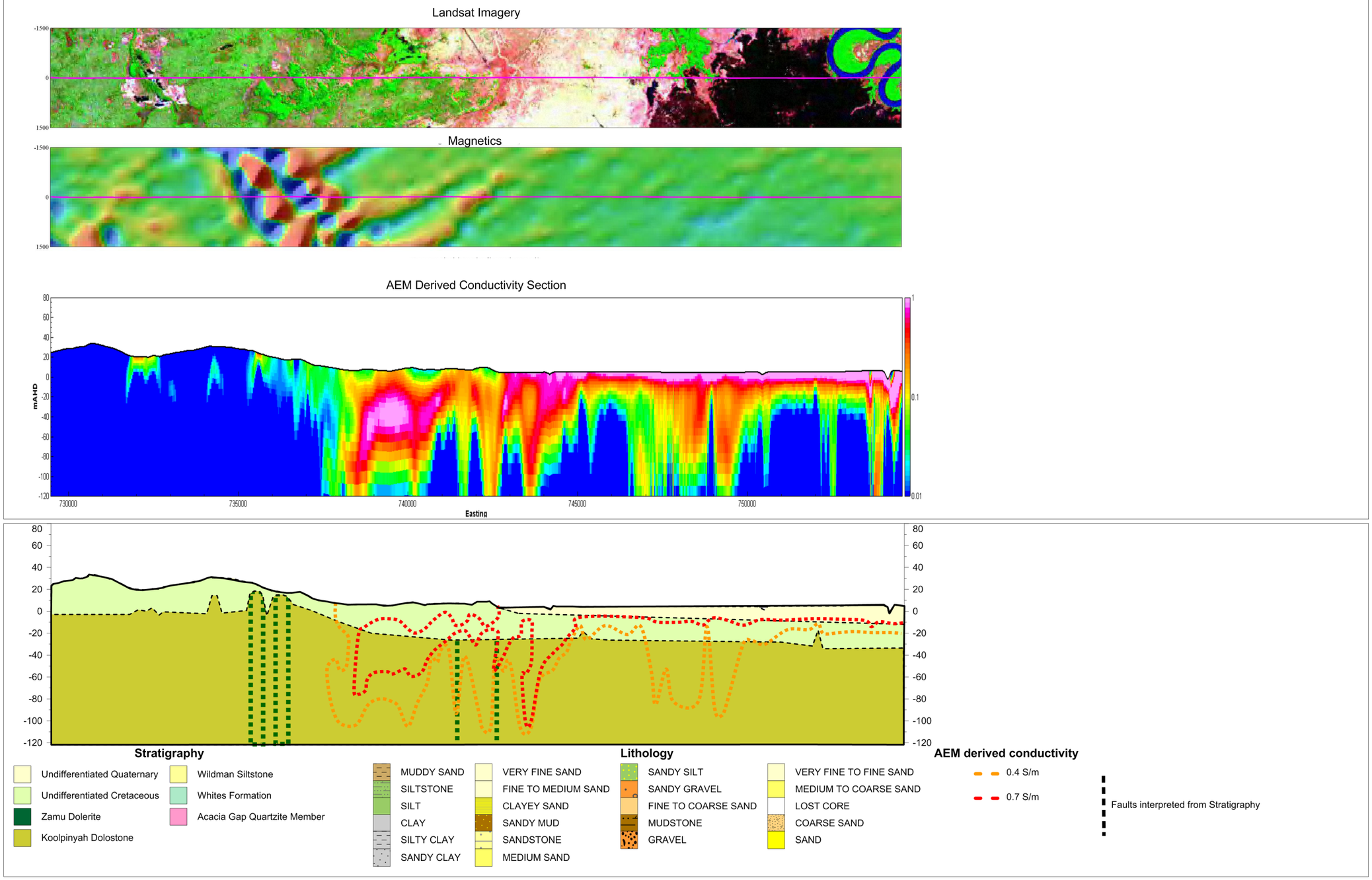

Figure 112: *Flight line section 6103302. Upper two images: Landsat image showing flight line trace, underlain by total magnetic intensity strip. Middle image: AEM conductivity section along flight line. Lower image: Interpreted geology and seawater intrusion zone. No sonic bore occurs in this section. Dashed lines show lower confidence in interpretation, based on either extrapolation (where stratigraphic contacts are masked by conductivity or for basement structures where these are supported by only one line of data). The highest conductivity zones shown in pink (arbitrarily defined here as having AEM conductivity >0.7 S/m) are caused by saline groundwater.*

Section 6103702

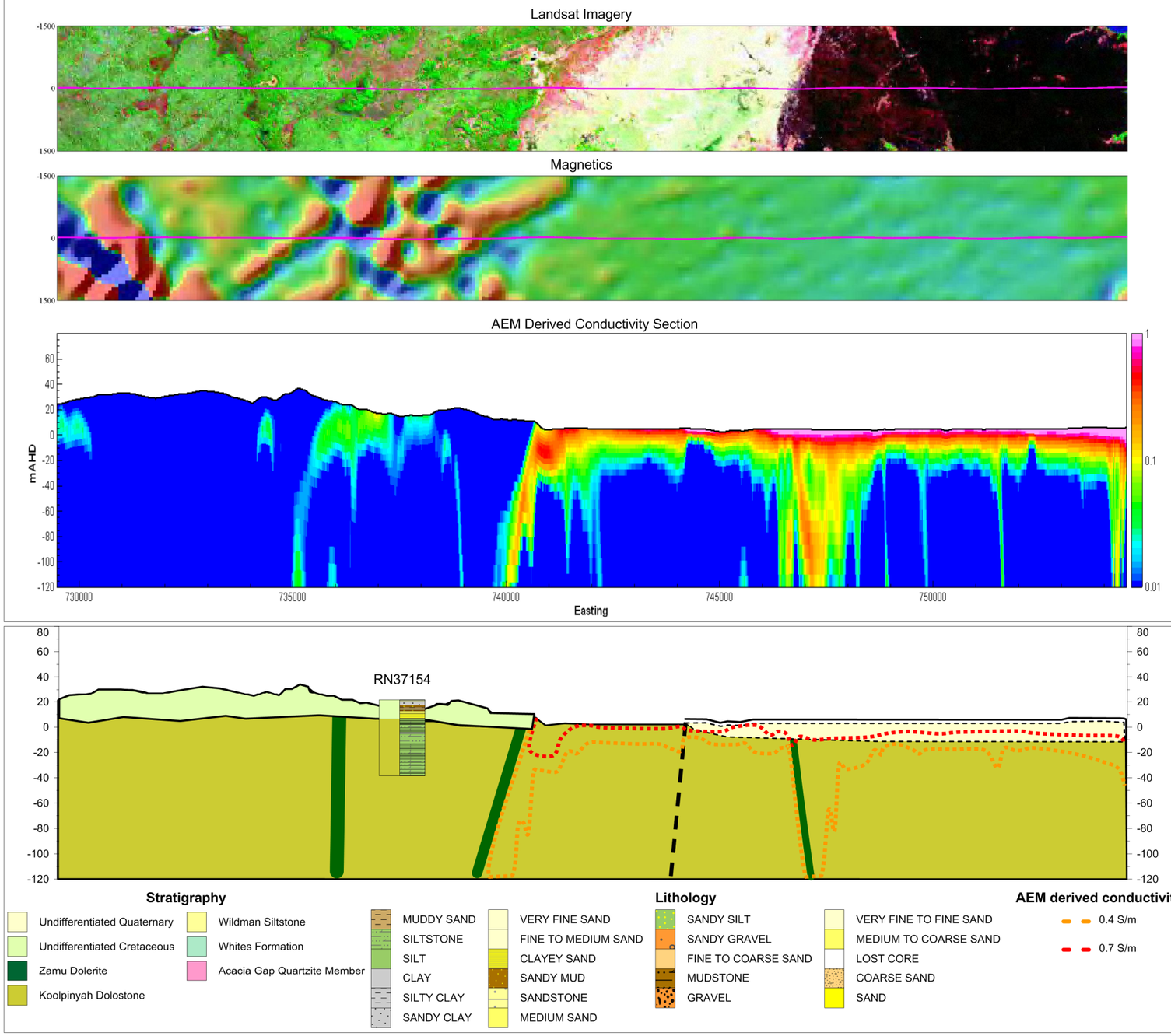

Figure 113: *Flight line section 6103702. Upper two images: Landsat image showing flight line trace, underlain by total magnetic intensity strip. Middle image: AEM conductivity section along flight line. Lower image: Interpreted geology and seawater intrusion zones with superimposed sonic bore hole (RN37154). Dashed lines show lower confidence in interpretation, based on either extrapolation (where stratigraphic contacts are masked by conductivity or for basement structures where these are supported by only one line of data). The highest conductivity zones shown in pink (arbitrarily defined here as having AEM conductivity >0.7 S/m) are caused by saline groundwater.*

8 Conclusions: Is it Possible to Map Seawater Intrusion in the Northern Territory Coastal Plain using AEM Data?

AEM data is particularly useful in helping to map the distribution and extent of seawater intrusion (SWI) in near-coastal aquifers due to the elevated sub-surface conductivity contrasts that exists between saline and fresh groundwater. Previous SWI investigations using AEM data have occurred in the USA (Fitterman and Deszcz-Pan, 1998), Indonesia (Siemon and Steuer, 2011), Mexico (Supper *et al*., 2009) and the Galapagos Islands (D'Ozouville *et al*., 2008). Prior to this study AEM has been used to map SWI in Coffin Bay (Munday *et al*., 2007; Auken *et al*., 2009a; Ward *et al*., 2009), and more recently in the Gascoyne coastal region (Munday, pers. comm. 2011).

The 'Northern Territory Coastal Plain: Mapping Seawater Intrusion (SWI) in Coastal Plain Aquifers Using Airborne Electromagnetic (AEM) Data' project has used a multidisciplinary geoscientific approach to assess the potential for SWI to impact on aquifers within the Darwin Rural Water Control District (DRWCD). The project entailed acquisition of regional AEM data over the priority areas within the DRWCD as well as small-scale sonic and rotary drilling programs, borehole geophysical logging, groundwater sampling, laboratory analysis of pore fluids and groundwater samples, and integration, analysis and interpretation of these data.

SWI has previously been reported from an area within the project study site although the threat posed by SWI is considered to be much greater. The project focussed on assessing the threat to the main producing aquifer (the Howard East Aquifer), which represents a significant water source to an estimated 30,000 residents (predicted to double by 2021), a strong horticultural industry, market gardens, and a public utility providing 20% of Darwin's municipal supply.

A total of 3,875 line km of AEM data were acquired in 2008-2009 within the 3,775 km^2 of the project area, using an AEM survey configured to map regional-scale variations in ground conductivity that might be associated with the character of the SWI wedge, regional aquifer characteristics, groundwater conductivity and salinity.

Data obtained from an advanced drilling technology in conjunction with existing hydrogeological information and hydrogeochemical analysis undertaken in this study provided the basis for the validation and interpretation of the AEM dataset, and the production of a suite of derived products including maps of key elements of the aquifer system, groundwater quality (salinity) and SWI hazard.

Overall, the study has demonstrated the potential for large survey areas to be assessed rapidly for SWI using an integrated approach based on AEM that has been validated by drilling and chemical analysis, with a high degree of confidence in the survey results.

The project has mapped a SWI interface throughout the project area that has been confirmed by limited drilling and hydrochemical analysis. This interface extends a considerable distance (up to 50km) inland associated with the upper reaches of the Adelaide and Mary Rivers, and 10km inland at Howard Springs (Figure 114). Potential SWI hazards to the Howard East Aquifer were identified in four areas: Lambells Lagoon, Howard Springs, Gunn Point and Middle Point. In each case, highly saline groundwater, interpreted as SWI ingress, appears to be facilitated by the presence of higher transmissivity structural corridors (e.g. faults at Howard Springs and faults and fractured quartz ridges at Lambells Lagoon), and/or where there are potential preferential recharge pathways in the overlying aquifer system (e.g. through overlying palaeochannels at Gunn Point). The greatest concern is at Lambells Lagoon, where highly saline groundwater is present at depth within 2 km of producing bores. Further data and groundwater modelling is required to understand the groundwater and salinity processes and dynamics in each of these hazard areas.

The holistic systems analysis approach taken in this study has effectively enabled the subdivision of the HEA into functional hydrogeological zones based on water quality and other aquifer characteristics. These zones consist of: confined aquifer, low salinity aquifer, the main aquifer and saline groundwater and/or floodplain (Figure 115). The approach has also effectively mapped variations in ground conductivity at scales relevant to the regional characterisation of the SWI interface, and key elements of the hydrostratigraphy in three dimensions over most of the project area. However the scale of the regional mapping, and lack of suitable borehole data in appropriate locations, generally precluded the mapping of karstic porosity in the aquifer system.

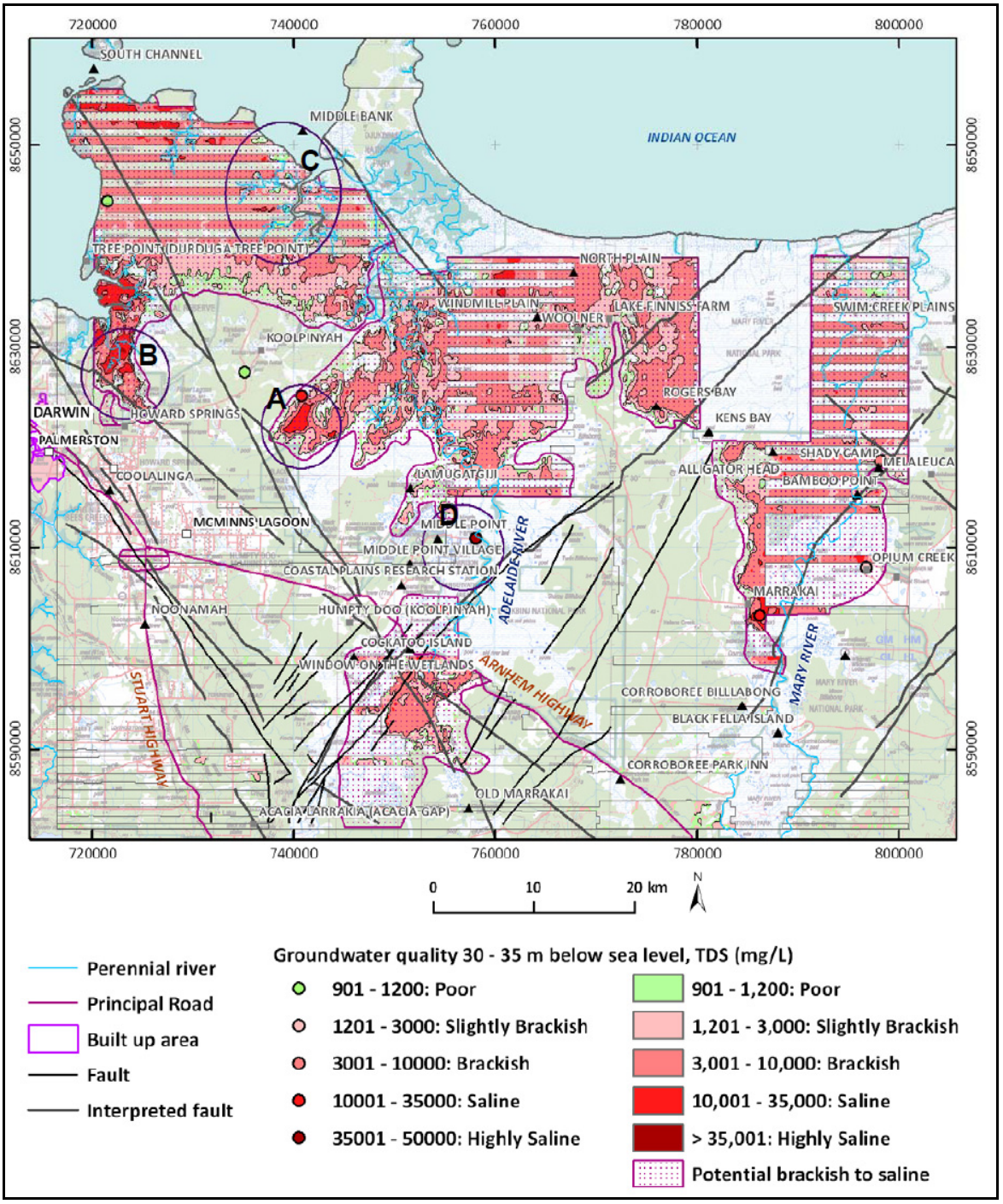

Figure 114. *Map of SWI in the project area based on the AEM depth slice 30-35m below sea level. Salinity hazard areas at (A) Lambells Lagoon, (B) Howard Springs, (C) Gunn Point and (D) Middle Point, are shown.*

The study has made the following specific findings in relation to mapping of the geology and hydrogeology:

1. The AEM data mapped Tertiary weathering surfaces in the area where these are electrically resistive. However, in places, it is not possible to discriminate this unit, particularly where more saline water overprints the weathering front. The base of weathering interface is geometrically irregular.

2. The floodplain sediments were successfully mapped using a combination of borehole information and AEM data. It was possible to map both the thickness and extent of these sediments, including the base of the floodplain sediment sequence. Most floodplain sediments are highly conductive and water quality variations within them need to be displayed based on fine threshold intervals. Correlation between laboratory results and conductivity data allows groundwater quality within the sediments to be derived from the AEM data.

3. Cretaceous sedimentary rocks could be mapped as undifferentiated Bathurst Island Group in the study area, but it was not possible to map individual sand bodies with the regional AEM data. Furthermore, groundwater storage in these sand units is likely to be low.

4. Drilling data and existing water bore data suggest there may be perched water tables above impermeable stratigraphic or secondary weathering-related horizons.

5. Borehole and coastal outcrop information show that the basal surface of the Cretaceous rocks is highly irregular. Most Cretaceous sedimentary rocks are electrically resistive and have no significant contrast with underlying dolostone sequences; this makes it impossible to map the interface between Cretaceous rocks and dolostone using AEM data alone. Consequently, validation using borehole and laboratory data is essential for this task. Integration of AEM and borehole data has enabled the thickness and extent of the Cretaceous sequence, and water quality variations within the sediments, to be mapped.

6. A basal Cretaceous lag of variable thickness and very coarse grainsize composed of quartz and dolostone boulders has been described in pre-existing water bores. These lag deposits do not appear to have significant lateral extent and their distribution is probably controlled by karstic palaeo-topography beneath Cretaceous rock cover. They cannot be mapped with AEM data.

7. Proterozoic and Archaean ‘Basement’.

   - The depth to the top of the Proterozoic and Archaean successions was mapped successfully. The extent of these rocks was mapped through a layer by layer interpretation of the AEM depth slices and validated by boreholes. In general, these rocks are structurally complex, with large-scale fold patterns and faults evident in the AEM data. Interpretation of faults and dykes was assisted by integration of AEM and drilling data with airborne magnetic data.
   - There is less reliability in mapping the Proterozoic and Archaean basement in the eastern part of the project area due to a paucity of drillholes of sufficient depth to reach the basement.
   - Most of the basement rocks are of the Mount Partridge and South Alligator Group. The Finniss River Group occurs only in the south and south-west of the mapped area and the only unit known in this region is the Burrell Creek Formation. The Finniss River Group has been mapped using a combination of AEM, outcrop and borehole data.
   - Most dolostones in the Koolpinyah-Coomalie Dolomite (KCD) are crystalline and impermeable. Where cavernous because of dissolution or fracturing they have relatively high groundwater yields. These zones could be mapped only by using drillcore data collected at high density, together with airborne magnetics data. AEM is not able to map connectivity between sinkholes owing to the highly resistive nature of the dolostones and the presence of fresh water in the aquifers.

8. A number of dolerite dykes were mapped in the project area using airborne magnetics and AEM data. An example is the north-west trending dolerite intrusive associated with the north-eastern Pine Creek Shear Zone. Dolerite dykes that cross-cut the Proterozoic successions are potential barriers to groundwater flow.

9. Quartz or quartzite ridges. Quartz-rich zones coincident with magnetic lineaments have also been mapped. These may be quartz veins, or the quartzite member (Acacia Gap Member) of the Mount Partridge Group. The quartz or quartzite is highly fractured and borehole information suggests high

groundwater yields occur from this unit when it outcrops. Production bore and pump test data indicate that these may be zones of preferential recharge and groundwater flow (Fell-Smith & Sumner, 2011).

In this project, survey line-spacing was based largely on matching the project area with available funds, rather than modelling of optimal survey design. Fortuitously, the infill line-spacing (550 metres) was adequate to show regional 3D patterns in electrical conductivity, and has successfully mapped the SWI interface at a broad-scale in the project area. A broader line-spacing of 1,666 metre and 5,000 metre has also been useful in defining the SWI wedge, which in this instance appears to have a relatively simple structure. In both instances, the approach has been successful due to the broad-scale variations in electrical conductivity patterns observed with SWI. Analysis of the broader 5,000 m line-spacing data shows that encroachment of the SWI interface towards the fresher groundwater resources tapped by borefields would only have been evident along individual flight lines that traversed the interface.

The AEM survey was not designed to map ‘within-borefield’ variations in texture and groundwater quality. Hints of significant variations in lithology and karstic porosity are evident in the data within individual flight lines, but the line-spacing (550 m or greater) restricts finer-scale interpretation.

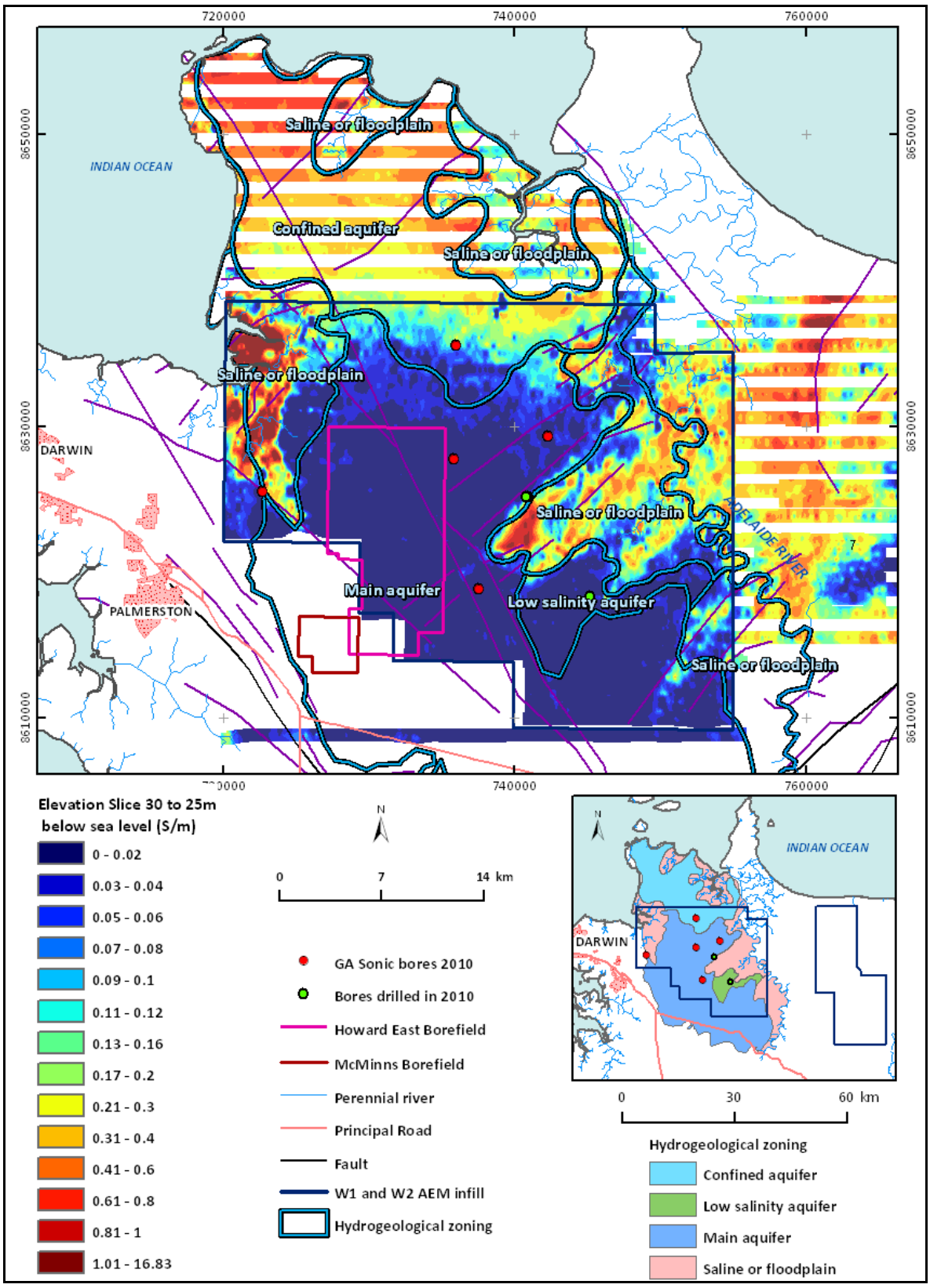

Figure 115: *Hydrogeological zoning in the HEA, based on the AEM, airborne magnetics data validated by drilling. The boundaries use AEM data from several different conductivity depth slices. Comparison of the boundaries with the AEM conductivity depth slice 30-35m b.s.l. shows the correspondence with the more saline aquifer at these depths.*

9 Recommendations and Further Work

NTCP PROJECT AREA-SPECIFIC RECOMMENDATIONS

There remain specific knowledge and data gaps in our understanding of the distribution of SWI, the hydrogeochemistry and hydrodynamics, and recharge and discharge processes. To assist with refining conceptual models and to improve groundwater model parameterisation and outcomes, we recommend the following:

1. A phase of additional drilling should be undertaken, targeted using the AEM-based interpretation products, to provide validation of areas of high electrical conductivity considered to result from SWI. Specifically, this will improve the validation of potential SWI encroachment at the margins of the borefield. It is recognised that this provides significant logistic difficulties, however additional data is required in key areas if the groundwater model is to be adequately parameterised. Specific sites that should be prioritised due to the higher salinity hazard, include: Lambells Lagoon, Howard Springs, Gunn Point, and Middle Point.
2. Additional drilling data and hydrogeological investigations are required to validate the revised conceptual model for recharge to the groundwater system, and to confirm potential discharge pathways, in particular the large scale karstic features (poljes) and palaeovalley tributaries identified in the AEM. Additional drilling data in specific areas may also enable further refinement of existing AEM inversions.
3. Compilation and analysis of existing hydrogeochemical data should be undertaken to understand more fully the potential risks to water quality in the borefield, and to help with developing a conceptual groundwater model.
4. New maps of surface recharge are required. Following the approach taken in previous investigations (e.g., Lawrie *et al*., 2010), these should incorporate existing soil and regolith maps, the new high resolution Digital Elevation Model (1-arc second SRTM), satellite remote sensing data (including vegetation change detection), radiometric data, the 0-4 m AEM depth slice, and should take into account the new conceptual model for recharge developed in this project. If possible, a high resolution LiDAR dataset should also be acquired over the project area to improve the spatial resolution of topographic features.
5. There is sufficient confidence in the inverted electrical conductivity data and AEM-derived interpretation products to recommend that groundwater modelling, utilising these products, be undertaken to assess the SWI risk to the DRWCD and the Howard East Aquifer in particular. However, model predictions would be improved with further refinements in model conceptualisation and parameterisation. Modelling should incorporate the latest sea-level rise modelling scenarios, as well as projected population growth, expected changes to land use and variations in other environmental or socio-economic factors that may be impacted by SWI (BMT WBM, 2010).

BROADER RECOMMENDATIONS

1. Future AEM surveys should consider the scale of the key elements of the hydrogeological system to be mapped, with the survey designed to match this requirement. This will optimise available resources and maximise the potential for a successful project outcome. This project has highlighted that more traditional, close line spacing (100-200 m) is not always necessary (Lawrie *et al.,* 2004), depending on project objectives.
2. As with several earlier AEM-based studies (Lawrie, 2008, Lawrie *et al*., 2010, 2011), a phased or staged approach should be employed for future AEM-based SWI or karstic mapping projects and include:

    – Collation and review of existing information for the purpose of identifying critical knowledge gaps;

- Scoping and technical risk evaluation to assess the methods and technologies best suited to address identified knowledge gaps, and to assist with survey design;
- Integrated geoscientific studies to enable key elements of the hydrogeological system to be mapped, and groundwater flow and hydrogeochemical processes to be understood;
- Data synthesis and interpretation using contemporary 'systems' approaches (Lawrie et al., 2000; Lane et al., 2004a, b; Spies andWoodgate, 2005; Lawrie et al., 2008, 2010, 2011), with an emphasis on delivering products that address specific issues and assist with the improved parameterisation of hydrogeological models; and
- Groundwater, surface-groundwater modelling and land use modelling to ascertain the sustainability of proposed developments. Modelling should use the best available climate data and modelling scenarios.

3. The acquisition of ground and airborne geophysical data for SWI or karstic mapping should only be considered within the broader context of integrated hydrogeological assessment of an area (Lawrie et al., 2010). Technical risk evaluation is required to gauge the merits of employing different geophysical approaches and technologies.

   - Acquisition of AEM data should only proceed after completion of scoping studies to assess the likelihood of success arising from their acquisition.
   - Scoping studies are required to identify target aquifers and groundwater systems, and the scale, depth and orientation of target objectives (where possible). This should be followed by review and assessment of suitable technologies in each area. Technology selection should include forward modelling of system responses, and should follow the best practice procedures developed by the Commonwealth, taking particular note of the ability of AEM system to map key elements of relevant elements of the hydrogeological system.
   - AEM data analysis and interpretation should follow a 'hydrogeological systems' approach based on the methodology recommended by the Joint Academies of Science Review of Salinity Mapping Methods in the Australian Landscape Context (Spies & Woodgate, 2005). Based on these recommendations, AEM-based projects need to incorporate a drilling program, complementary ground investigations and hydrogeochemical studies to ensure appropriate survey calibration, validation and interpretation.
   - Future AEM surveys for mapping SWI and karstic systems should carefully consider the merits of using calibrated AEM systems and inversion software that can significantly shorten data acquisition and delivery schedules, and the overall project time and budget.
   - The use of sonic drilling technology was a success in this project with nearly 100% core recovery in wide range of unconsolidated and consolidated geological materials, and delivery of uncontaminated core for hydrogeochemical investigation. The use of this technology in similar studies is strongly recommended.

4. This project differed from previous federally-funded groundwater and salinity mapping projects carried out over the past decade in Australia. Specifically, the project was developed opportunistically, piggy-backing on the acquisition of a survey designed to map bedrock features as part of GA's Onshore Energy Security Program. In future, we recommend that:

   - Where possible, forward modelling should be carried out using available ground and borehole geophysical data and relevant hydrogeological models to ascertain whether the selected technology can map the key elements of the hydrogeological system, and to aid survey design. This is also essential to assist in project planning and resourcing.
   - Stakeholder consultation should be undertaken at an early stage to ascertain the areas and scales of interest, and the types of products required.

10 References

ABS, 2001. Australian Bureau of Statistics. Website address when accessed 22/6/11 http://www.abs.gov.au/ausstats/abs@.nsf/mediareleasesbytitle/B70B578965453B57CA256A9400814AFD?OpenDocument

Ahmad, A., Lally, J.H., and McCready, A.J., 2006. Economic geology of the Rum Jungle mineral field. Northern Territory Geological Survey Report 19. Website address when accessed 26/5/11 http://www.nt.gov.au/d/Minerals_Energy/Geoscience/Content/File/Pubs/Report/NTGSRep19.zip

Allen, D., 2005. A Review of Geophysical Equipment applied to Groundwater and Soil Investigation. ANCID/Sustainable Irrigation Travel Fellowship Report. 77p.

Alley N. F., Clarke J. D. A., Macphail M. and Truswell E. M., 1999. Sedimentary infillings and development of major tertiary palaeodrainage customs of south-central Australia. Special Publication of International Assessment of Sedimentologists 27, 337–366.

ANZECC, 1992. Australian water quality guidelines for fresh and marine waters, National water quality management strategy, Australian and New Zealand Environment and Conservation Council, Canberra.

ANZECC, 2000, Water quality and monitoring guidelines, National water quality management strategy, Australian and New Zealand Environmental and Conservation Council, Canberra.

Auken, E., Christiansen, A. V., Westergaard, J. H., Kirkegaard, C., Fopged, N., Viezzoli, A., 2009. An integrated processing scheme for high-resolution airborne electromagnetic surveys, the SkyTEM system. Exploration Geophysics, 40, p. 184-192Barlow, P.M., 2003. Ground water in freshwater-saltwater environments of the Atlantic Coast. USGS Circular 1262, U.S. Geological Survey, Reston, Virginia.

Beringer, J., Hutley, L.B., Tapper, N.J., Coutts, A. Kerley, A. and O'Grady, A.P., 2003, Fire impacts on surface heat, moisture and carbon fluxes from a tropical savannah in north Australia, International Journal of Wildland Fire, Special Issue: 'Fire and savannah landscapes in northern Australia: regional lessons and global challenges', 12: 333-340.

Bloom, A. L., 1978. Geomorphology, Prentice-Hall, Englewood Cliffs, New Jersey, 510p.

BOM, 2011. Monthly rainfall data for Darwin Airport. Website address when accessed on 9/6/11 http://www.bom.gov.au/jsp/ncc/cdio/weatherData/av?p_nccObsCode=139andp_display_type=dataFileandp_startYear=andp_c=andp_stn_num=014015

Brodie, R and Fisher, A., 2008. Inversion of TEMPEST AEM survey data, Honeysuckle Creek, Victoria. Unpublished report produced by Geoscience Australia for the Bureau of Rural Sciences.

BMT WBM, 2010. Kakadu – Vulnerability to climate change impacts. A report to the Australian Government Department of Climate Change and Energy Efficiency.

Carey, H., Lenkopane, M.K., Werner, A.D., Li, L. and Lockington, D.A., 2009. Tidal controls on coastal groundwater conditions: field investigation of a macrotidal system. Australian Journal of Earth Sciences, 56(8): 1165-1179.

Chamberlain, T., and Wilkinson, K., 2004 (eds.). Salinity investigations using airborne geophysics in the Lower Balonne area, Southern Queensland. Queensland Department of Natural Resources and Mines, 257p.

Chin, D., 1991. Millikapiti water supply and alternative resource investigation 1991, NT Power and Water Authority Technical report (unpublished).

Chin, D., Martin, K., Schwartz, T. and Jolly, P., 1993. Power and Water Authority Darwin report 20/93D.

Clarke, J. D. A., Gammon, P. R., Hou, B., and Gallagher, S. J., 2003 Middle to Upper Eocene stratigraphic nomenclature and deposition in the Eucla Basin Australian Journal of Earth Sciences 50, 231–248

Cresswell R. G., Mullen, I. C., Kingham, R. Kellett, J., Dent, D. L., and Jones, G. L., 2007. Airborne electromagnetics supporting salinity and natural resource management decisions at the field scale in Australia. International Journal of Applied Earth Observation and Geoinformation 9(2), p. 91-102.

Cobb, S.M., Saynor, M.J., Eliot, M., Eliot, I. and Hall, R., 2007. Saltwater intrusion and mangrove encroachment of coastal wetlands in the Alligator Rivers Region, Northern Territory, Australia. Supervising Scientist Report 191, Office of the Supervising Scientist, Darwin NT.

Constable, S., Parker, R., and Constable, C., 1987. Occam's inversion; a practical algorithm for generating smooth models from electromagnetic sounding data. Geophysics, 52, 289-300.

Cook, P.G., Hatton, T.J., Eamus, D., Hutley, L., and Pidsley, D., 1998a. Hydrological investigation and Howard East, N.T. CSIRO Land and Water Technical Report 41/98 Web address when accessed on 9/6/11 http://www.clw.csiro.au/publications/technical98/tr41-98.pdf.

Cook, P.G., Herczeg, D., Pidsley, D., and Farrow, R., 1998b. Hydrological investigation at Howard East, NT, 2. Eucalypt savannah site: soil physics and groundwater geochemistry, CSIRO Australia Land and Water Technical Report 13/98.

Costelloe, M.T., and Hutchinson, D.K., 2010. Woolner Granite and Rum Jungle TEMPESTTM AEM Survey: Inversion Report. Geoscience Australia internal report.

Costelloe, M., Sorensen, C. and English, P., 2009. Pine Creek airborne electromagnetic survey Onshore Energy and Minerals Division, Geoscience Australia. ASEG Extended Abstracts 2009.

CSIRO, 2009a. Water in the Gulf of Carpentaria Drainage Division. A report to the Australian Government from the CSIRO Northern Australia Sustainable Yields Project, CSIRO Water for a Healthy Country Flagship, Australia, 479p.

CSIRO, 2009b. Water in the Timor Sea Drainage Division. A report to the Australian Government from the CSIRO Northern Australia Sustainable Yields Project., CSIRO Water for a Healthy Country Flagship, Australia.

Custodio, G.E., and Bruggeman, G.A., 1987. Groundwater problems in coastal areas, studies and reports in hydrology, 45, UNESCO, Paris.

DCC, 2009. Climate change risks to Australia's Coast, Department of Climate Change, Commonwealth of Australia, Canberra.

Dixon-Jain, P., Ivkovic, K.M., Clarke, J.D.A, Wallace, L., Werner, A.D., and Sundaram, B., 2010. National-scale vulnerability assessment of seawater intrusion project, Milestone 2 progress report to National Water Commission.

Dixon-Jain, P., Ivkovic, K.M., Morgan, L.K., Werner, A.D., Clarke, J.D.A., Garlapati, N., Wallace, L., and Sundaram, B., 2011. National-Scale vulnerability assessment of seawater intrusion project, Milestone 3 progress report to National Water Commission.

Doble, R., Walker, G., and Simmons, C., 2005. Understanding spatial patterns of discharge in semi-arid regions using a recharge-discharge balance to determine vegetation health. CSIRO Land and Water Technical Report No 13/05. Adelaide: CSIRO. http://www.clw.csiro.au/publications/technical2005/tr13-05.pdf

Doble, R. C., Connor, J., Stenson, M., Elmahdi, A., Jolly, I. D., Miles, M., and Walker, G. R., 2008. Future landscape scenarios in the lower River Murray, south-eastern Australia and their implications for river salinity and floodplain health. Final papers of the 2nd International Salinity Forum, Adelaide, March 30-April 3rd, 2008. http://www.internationalsalinityforum.org/Final%20Papers/doble_E3.pdf

Doyle, N., 2001. Extractive minerals within the outer Darwin area. Northern Territory Geological Survey Report 15. Website address when accessed 26/5/11 http://www.nt.gov.au/d/Minerals_Energy/Geoscience/Content/File/Pubs/Report/NTGSRep14.pdf

d'Ozouville, N., Auken, E., Sorensen, K., Violette, S. Marsily, G. de, Deffontaines, B., and Merlen, G., 2008. "Extensive perched aquifer and structural implications revealed by 3D resistivity mapping in a Galapagos volcano." Earth and Planetary Science Letters 269(3): 518-522.

EHA, 2007. Integrated hydrologic modelling of the Darwin Rural Area and development of an integrated water resource monitoring strategy, report for hydrogeological conceptualisation and groundwater modelling, Report to Department of Natural Resources, Environment and the Arts and Natural Systems, June 2007.

EHA, 2009. Groundwater modelling of the Darwin Rural Area – McMinns – Howard East Section for a range of current and future development and climate scenarios, Report for CSIRO Northern Australia Sustainable Yields project, June 2009.

English, P. *et al*. 2012. Groundwater resources in palaeovalleys summary report. Geoscience Australia Record (in prep.)

FAO, 1997. Seawater intrusion in coastal aquifers, Guidelines for study, monitoring and control, Food and Agricultural Organisation of the United Nations, Rome.

Fell-Smith, S.A., and Sumner, J., 2011. Technical report – Koolpinyah Dolomite Aquifer Characteristics Project. Department of Natural Resources, Environment, the Arts and Sport, Report 26/2011D.

Fitterman, D.V., and Deszcz-Pan, M., 1998. Helicopter EM mapping of saltwater intrusion in Everglades National Park, Florida: Exploration Geophysics, v. 29, p. 240-243.

Fitzpatrick, A., Apps, H., Clarke, J. and Lawrie, K., 2004. Mapping salt water intrusion and understanding water-rock interactions in saline aquifers in the lower Burdekin Delta: Phase 1 report. CRC LEME Restricted Report 210R, Cooperative Research Centre for Landscape Environments and Mineral Exploration, Perth, 141p.

Fogarty, P., 1980. The land resources of the Marrakai Area. Land Conservation Unit, Conservation Commission of the Northern Territory Technical Report LRD 80001. Website address when accessed on 9/6/11 http://www.ntlis.nt.gov.au/hpa-services/techreport?report_id=LRD80001

Ford D. C. and Williams, P. W., 2007. Karst hydrogeology and geomorphology. John Wiley and Sons, 562p.

George, R., Lawrie, K.C. & Woodgate, P., 2003. "Convince me all your bloody data and maps are going to help me manage salinity any better ?" A review of remote sensing methodologies for salinity mapping. In Proceedings 9th PURSL (Productive Use of Saline Land) Conference, Yepoon, Qld. 14p.

Ghyben, B.W., 1888. Nota in verband met de voorgenomen putboring nabij Amsterdam (Notes on the probable results of the proposed well drilling near Amsterdam), Tijdschrift van het Koninklijk Institunt van Ingeniers, The Hague.

Haig, T., and Townsend, S., 2003. An understanding of the groundwater and surface water hydrology of the Darwin Harbour Plan of Management area. Proceedings of the Darwin Harbour Public Presentations - February 2003. Website address when accessed 10/3/11 http://www.nt.gov.au/nreta/water/aquatic/publications/pdf/2003/understanding.pdf

Hallenburg, J.K., 1984. Geophysical logging for mineral and engineering applications, Penn Well Books, Tulsa, Oklahoma.

Herzberg, A., 1901. Die Wasserversorgung einiger Nordseebader (The water supply on parts of the North Sea coast in Germany). Journal Gabeleucht ung und Wasserversorg ung 44: 815-819, 824-844.

IPCC (Editor), 2007. Climate Change 2007: The Physical Science Basis. Contribution of Working Group I to the Fourth Assessment Report of the Intergovernmental Panel on Climate Change. Solomon, S., Qin, D., Manning, M., Chen, Z., Marquis, M., Averyt, K.B., Tignor, M., and Miller, H.L. (eds.).

Jolly, P., 1983. McMinns-Benham Lagoon borefield investigation 1981-1982, Water Division, Department of Transport and Works, Darwin, report 17/83D.

Jonauskas, P., and Sterling, L., 1992. A report on accessing shallow groundwater hydrology of the lower Mary River Plains. Conservation Commission of the Northern Territory Technical Report EXTD0650. Website address when accessed on 9/6/11 http://www.ntlis.nt.gov.au/hpa-services/techreport?report_id=EXTD0650

Keys, W.S., 1990, Borehole geophysics applied to ground water investigations: U.S. Geological Survey Techniques of Water-Resources Investigations, book 2, chap. E2.

Kingston, D., Port, G., Marquardt, A., and Deacon, G., 1982. Upper Adelaide River agriculture hydrological aspects of rice growing. Northern Territory Department of Transport and Works, Water Division Technical Report WRD 82025. Website address when accessed on 9/6/11 http://www.ntlis.nt.gov.au/hpa-services/techreport?report_id=WRD82025

Lane, R., 2000. Conductive unit parameters: summarising complex conductivity distributions, 70th Meeting, SEG, Calgary, Expanded Abstracts, Volume 1, Section EM 4.2, 328-331.

Lane, R., 2002. Ground and airborne electromagnetic methods. Geophysical and Remote Sensing Methods for Regolith Exploration Volume, CRC LEME Open File Report 144, 53-79.

Lane, R., Brodie, R.C., and Fitzpatrick, A., 2004a. Constrained inversion of AEM data from the Lower Balonne area, Southern Queensland, Australia. CRC LEME Open File Report 163.

Lane, R., Brodie, R.C, and Fitzpatrick A., 2004b. A revised inversion model parameter formulation for fixed wing transmitter loop – towed bird receiver coil time-domain airborne electromagnetic data. ASEG 17th Geophysical Conference and Exhibition, Sydney 2004.

Lane, R., Green, A., Golding, C., Owers, M., Pik, P., Plunkett, C., Sattel, D., and Thorn, B., 2000. An example of 3D conductivity mapping using the TEMPEST airborne electromagnetic system. Exploration Geophysics, 31, 162-172.

Lawrence, M., and Stenning, L., 2009a. Woolner airborne electromagnetic (AEM) mapping survey acquisition and processing report for Geoscience Australia.

Lawrence, M., and Stenning, L., 2009b. Rum Jungle airborne electromagnetic (AEM) mapping survey acquisition and processing report for Geoscience Australia.

Lawrie, K. C., Munday, T. J., Dent, D. L., Gibson, D. L., Brodie, R. C., Wilford, J., Reilly, N. S., Chan, R. A. & Baker, P., 2000. A 'Geological Systems' approach to understanding the processes involved in land and water salinisation in areas of complex regolith- the Gilmore Project, central-west NSW. AGSO Research Newsletter, v. 32, p. 13-32, May 2000.

Lawrie, K.C., Gray, M. Fitzpatrick, A., Wilkes, P., Lane, R., Pain C. & Lambert, I., 2003a. Assessing cost-effective salinity mapping strategies using a landscape- based approach for methodology and technology selection. In Submission to National Review of Salinity Mapping Methods and Technologies in the Australian Context. CRC LEME Open File Report.

Lawrie, K.C., Gray, M., Fitzpatrick, A., Wilkes P., and Lane, R., 2003b. Reducing the Acquisition Costs of Airborne Electromagnetics Surveys for Salinity and Groundwater Mapping. Preview, October 2003.

Lawrie, K.C., 2006. Land use questions and models of AEM targets report by technical working group chair on proposed River Murray Corridor (South Australian border to Gunbower) Victorian AEM mapping project. CRC LEME Restricted Report 265r. 27p.

Lawrie, K. C., Clarke, J., Hatch, M., Price, A., and Wilkes, P., 2006b. Improving hydrogeological models of aquifer systems in the Ord Irrigation area: assessing the potential of geophysics and other Geoscience methods. In Proceedings of the ANCID Conference, October 2006, Darwin.

Lawrie, K., 2008. To what extent can recent advances in salinity mapping and assessment create new salinity management and policy opportunities? 2nd International Salinity Forum (Plenary Address) Ext. Abs. http://www.internationalsalinityforum.org/Final%20Papers/lawrie_plenary.pdf

Lawrie, K.C., Tan, K.P., Halas, L., Cullen, K., Pain, C.F., Brodie, R.C., Apps, H., Wong, V., Reid, M., Clarke, J.C. & Gibson, D., 2009a. River Murray Corridor (RMC) Salinity Mapping and Interpretation Project: Report on the Barr Creek to Gunbower Island Region. Geoscience Australia Professional Opinion 2009/13, 186 p.

Lawrie, K.C., Brodie, R.S., Gibson, D.L., Ley-Cooper, Y., Davis, A., Magee, J., Cullen, K., Halas, L. & Apps, H., 2009b. Broken Hill Managed Aquifer Recharge Project, Phase 2. Conceptual Managed Aquifer Recharge and Groundwater Resource Targets Identified from Preliminary Analysis of Airborne Electromagnetic Data. Geoscience Australia Professional Opinion 2009. 103p.

Lawrie, K.C., Brodie R.S., Dillon, P., Tan, K.P., Halas, L., Christensen, N.B., Ley-Cooper, A.Y., Davis, A., Somerville, P., Smith, M.S., Apps, H.E., Magee, J., Gibson, D., Clarke, J.D.A., Page, D., Vanderzalm, J., Miotlinski, K., Barry, K., Levett, K., and Gow, L., 2011. Securing Broken Hill's water supply: Assessment of groundwater extraction and conjunctive water supply options at Menindee Lakes. Geoscience Australia Professional Opinion 2011/02.

Lawrie, K.C. Brodie, R.S., Dillon, P., Tan, K.P., Gibson, D., Magee, J., Clarke, J.D.A., Somerville, P., Gow, L., Halas, L., Apps, H.E., Page, D., Vanderzalm, J., Abraham, J., Hostetler, S., Christensen, N.B., Miotlinksi, K., Brodie, R.C., Smith, M. and Schoning, G., 2012. BHMAR Project: Assessment of conjunctive water supply options to enhance the drought security of Broken Hill, regional communities and industries – Summary report. Geoscience Australia Record, 2012/15, 213p.

Lawrie, K., Fitzpatrick, A., Clarke, J., Hatch, M., Kepic, A., and Apps, H., 2006. Mapping salt water intrusion and understanding water-rock interactions in saline aquifers in the lower Burdekin delta: Phase 2 Report, CRC LEME Restricted Report.

Lawrie, K. C., Munday, T. J., Dent, D. L., Gibson, D. L., Brodie, R. C., Wilford, J., Reilly, N. S., Chan, R. A., and Baker, P., 2000. A 'Geological Systems' approach to understanding the processes involved in land and water salinisation in areas of complex regolith- the Gilmore Project, central-west NSW. AGSO Research Newsletter, 32, 13-32, May 2000.

Lawrie, K.C., Tan, K.P., Clarke, J.D.A., Munday, T.J., Fitzpatrick, A., Brodie, R.S., Apps, H., Halas, L., Cullen, K., Pain, C.F., Kuske, T.J. ,Cahill, K. and Davis, A., 2010. Using the SkyTEM time domain airborne electromagnetics (AEM) system to map aquifer systems and salinity hazard in the Ord Valley, Western Australia. Geoscience Australia Professional Opinion 2010/01, 500p.

Ley-Cooper Y. and Davis A. 2010. Can a borehole conductivity log discredit a whole AEM survey? ASEG Extended Abstracts 2010(1) 1 - 5.

Macnae, J., King, A., Stolz, N., Osmakoff, A., Blaha, A., 1998. Fast AEM processing and inversion: Exploration Geophysics 29, 163-169.

Mayo, M., Kaestli, M., Harrington, G., Cheng, A.C., Ward, L., Karp, D., Jolly, P., Godoy, D., Spratt, B.G., and Currie, B.J., 2011. Burkholderia pseudomallei in un-chlorinated domestic bore water in tropical northern Australia. Emerging Infectious Diseases (in press).

McFarlane, M.J., Rigrose, S., Giusti, I. and Shaw, P.A., 1995. The origin and age of karstic depressions in the Darwin-Koolpinyah area in the Northern Territory of Australia. In: Brown, A.G. (ed.) Geomorphology and groundwater. John Wiley and Sons, London, pp.93-120.

McNally, G.H., Clarke, G., and Weber, B.W., 2000. Porcelainite and the urban geology of Darwin, Northern Territory, Australian Journal of Earth Sciences, 47:1, 35-44.

McNeill, J. D., Bosnar, M., and Snelgrove, F. B., 1990. Resolution of an electromagnetic borehole conductivity logger for geotechnical and ground water applications. Geonics Limited, Mississauga, Ontario. Technical Note TN-25, 29p.

Meisler, H., Leahy, P.P. and Knobel, L.L., 1985. Effect of eustatic sea-level changes on saltwater-freshwater relations in the northern Atlantic Coastal Plain, U.S. Geological Survey water supply paper, 2255.

Menke W. 1989. Geophysical data analysis: Discrete inverse theory. Academic Press Inc.
Mory, A. J. 1988. The North West Shelf Australia. In: Purcell, P.G. and Purcell, R.R. (eds.). Proceedings, North West Shelf Symposium, Perth, WA 1988, Petroleum Society of Australia Ltd, 287-309.
Moser, A. and Chin, D., 1994. Warankuwu groundwater resource evaluation, NT Power and Water Authority Technical report WRD94028.
Mullen, I.C., Wilkinson, K.E., Cresswell, R.G., and Kellett, J., 2007. Three-dimensional mapping of salt store in the Murray-Darling Basin, Australia 2. Calculating landscape salt loads from airborne electromagnetic and laboratory data. International Journal of Applied Earth Observation and Geoinformation, 9, 103-115.
Munday, T., Walker, G., Cresswell, R., Wilford, J., Barnett, S. & Cook, P., 2003a. South Australian Salt Mapping and Management Support Project –An example of the considered application of airborne geophysics in natural resource management. 16th ASEG Conference, Adelaide.
Munday, T., Green, A., Brodie, R., Lane, R., Sattel, D., Barnett, S., Cook, P. & Walker, G., 2003b. Developing recharge reduction strategies in the Riverland of South Australia using airborne electromagnetic data – a case study in tailoring airborne geophysics given a particular target and a desired set of outcomes. 16th ASEG Conference, Adelaide.
Munday, T.J. Overton, I. Fitzpatrick, A. Cahill, K. Berens, V. Hatch, M. & Brodie, R. C., 2007. Spatio-temporal monitoring of floodplain environments using electromagnetic methods: a scaled approach to understanding surface water- groundwater interactions on the Chowilla floodplain, S. Australia. In 20th SAGEEP, Denver.
Munday, T., Fitzpatrick, A. and White, J., 2008. Spatial Patterns of Groundwater Induced Salt Accumulation in a Salinising Floodplain and links with the Murray River, South Australia. AGU.
Mulrennan, M. E. and Woodroffe, C. D., 1998. Holocene development of the lower Mary River plains, Northern Territory, Australia. The Holocene 1998(8), 565-579.
Narayan, K.A., Schleeberger, C., Charlesworth, P.B., and Bristow, K.L., 2003. Effects of groundwater pumping on saltwater intrusion in the Lower Burdekin Delta, north Queensland. In: D.A. Post (ed.), MODSIM 2003. Modelling and Simulation Society of Australia and New Zealand, 224-229.
Needham, R.S., and Stuart-Smith, P.G., 1984. Geology of the Pine Creek Geosyncline, Northern Territory, 1:500,000 scale map. Bureau of Mineral Resources, Australia and Geological Survey of NT.
NRETAS, 2011. Website address when accessed 14/6/11 http://150.191.80.22/nreta/water/ground/springs/howard.html.
Nott, J.F., 2003. The urban geology of Darwin, Australia. Quaternary International, 103, 83-90.
Paine J. G., 2003. Determining salinization extent, identifying salinity sources, and estimating chloride mass using surface, borehole, and airborne electromagnetic induction methods, Water Resour. Res., 39 (3), p. 3-1–3-10
Pavelic, P., Dillon, P., Barber, C., Toze, S., Yin Foo, D., Jolly, P., and Knapton, A., 2002. Water banking trial and Warruwi, South Goulburn Island, NT: stage 3 report to Department of Infrastructure Planning and Environment, Northern Territory, Conservation and Natural; Resources Report 35/2002.
Pietsch, B.A., 1985. Explanatory notes for Koolpinyah 1:100,000 geological series, Sheet 5173. Northern Territory Geological Survey, Darwin.
Pietsch, B.A., and Stuart-Smith, P.G., 1987. Darwin 1: 250,000 scale geology map sheet SD54-2 explanatory notes and accompanying map, published by BMR and NTGS, Darwin.
Pittock, B., (ed.), 2003. Climate Change: An Australian guide to the science and potential impacts. Australian Greenhouse Office.
Radke, B., Watkins, K.L., and Bauld, J., 1998. A groundwater quality assessment of shallow aquifers in the Darwin rural area, Northern Territory. AGSO Record 1998/020, Vol. 1-2.
Richardson, S. Evans, R., Haworth, D., and Prider, J., 2007. Tri-State Hydrogeological Benchmark Assessment. Resource & Environmental Management Pty Ltd. (Unpublished report).
Richter, B.C., and Kreitler, C.W., 1993. Geochemical techniques for identifying sources of ground-water salinisation, CRC Press, Boca Raton, FL.
Reid, J.E., and Vrbancich, J., 2004. A comparison of the inductive-limit footprints of airborne electromagnetic configurations. Geophysics, 69, 1229-1239.
Rodriguez, E., Morris, C. S. & Belz, J. E. 2006. A global assessment of the SRTM performance. Photogrammetric Engineering and Remote Sensing, 72, 249-260.
Siemon, B., Steuer A., Ullmann, A., and Vasterling, M., 2011. "Application of frequency-domain helicopter-borne electromagnetics for groundwater exploration in urban areas." Physics and chemistry of the earth. Parts A/B/C 36(16): 1373-1385.

Simpson, C.J., Huntington, J.F., Leishman, J., and Green, A.A., 1980. A study of the Pine Creek Geosyncline using integrated Landsat and aeromagnetic data. In: Ferguson, J. and Goleby, A.B. (eds.) Uranium in the Pine Creek Geosyncline. Proceedings of the International Uranium Symposium on the Pine Creek Geosyncline. Sydney, Australia, 4-8 June 1979.

Spies, B., and Woodgate, P., 2005. Salinity mapping methods in the Australian context. Land and Water Australia, Department of the Environment and Heritage; and Agriculture Fisheries and Forestry, June 2005. 236p. Website addressed when accessed 14/6/11 at http://www.nrm.gov.au/publications/books/pubs/salinity-mapping.pdf

Spies B and Woodgate P., (2005). Salinity Mapping Methods in the Australian Context. Land and Water Australia, Department of the Environment and Heritage; and Agriculture Fisheries and Forestry, June 2005. 236p. http://www.nrm.gov.au/publications/salinity-mapping

Sumner, J., 2008. Ngukurr groundwater investigation 2006-07, NT Water Resources Branch report 16/2008D.

Supper, R., Ahl, A., Motschka, K., Ottowitz, D., Bauer, P., Alonso, G. M., Jochum, B. and Gondwe, B., 2009. "Spatial Mapping of Submerged Cave Systems by Means of Airborne Electromagnetics: Results from the 2008 Mapping Campaign in the Area Around Tulum, Yucatan." Symposium on the Application of Geophysics to Engineering and Environmental Problems 22(1): 499-510.

Tan, K.P., Apps, H., Halas, L., Gibson, D., and Lawrie, K., 2005. Utilizing airborne electromagnetic data to model the subsurface salt load. In: Zerger, A. and Argent, R.M. (eds.). A catchment, Bland Basin, NSW. MODSIM 2005, International Congress on Modelling and Simulation. Modelling and Simulation Society of Australia and New Zealand, 1478-1484. Website address when accessed 14/6/11 http://www.mssanz.org.au/modsim05/papers/ascough_1.pdf

Tan, K. P., Halas, L., Lawrie, K., Clarke, J. D. A., Apps, H. E., Costelloe, M1, Sumner, J., Fell-Smith, S., Ley, Y., Schoning, G. L., and Halas, V., 2011. Northern Territory Coastal Plain: Mapping seawater intrusion in coastal plain aquifers using airborne electromagnetic data. Geoscience Australia Professional Opinion 2011/05, 146p

Tan, K.P., Lawrie, K.C., Halas, L., Pain, C.F., Clarke, J.D.A., Gibson, D., Apps, H., Cullen, K., Brodie, R.C., and Wong, V., 2009. Methodology for the customised products developed as part of the River Murray Corridor Victorian AEM mapping project. Geoscience Australia, Professional Opinion 2009/12, 75p.

Tan, K.P., Munday, T.J., Fitzpatrick, A., Lawrie, K., and Gibson, D.L., 2007. Integrating electromagnetic data, petrophysics, sedimentological/regolith and hydrological information for salinity management. Symposium on the application of geophysics to engineering and environmental problems (SAGEEP). Seattle, Washington. 11p.

Tickell, S.J., 2009. Investigation drilling in the Koolpinyah Dolomite. Northern Territory Government Department of Natural Resources the Environment the Arts and Sport, Technical Report No. WRD09028.

Tien, A.T., 2006. Influence of deep aquifer springs on dry season stream water quality in Darwin rural area. Northern Territory Government Department of Natural Resources, Environment, and The Arts, Water Monitoring Branch Natural Resource Management Division Report 6/2006D.

Tyson, P. and Yin Foo, D., 1991. Umbakumba groundwater resource evaluation. Northern Territory Power and Water Authority Report, 32/91.

Urangesellschaft Australia Pty. Ltd., 1981, Annual Report 1980 EL1709 Northern Territory Koolpinyah project A8/819, NT Geological Survey report CR80/246.

Verma, M.N., 2002. Hydrogeological map of Darwin. Explanatory Notes 1:250,000 scale map. Northern Territory Department of Infrastructure, Planning and Environment Report 34/2002, Darwin, Australia.

Walker, G., Cresswell, R., Munday, T. and Liddicoat, C., 2004. South Australian Salinity Mapping and Management Support Project: Final Report (Overall Project Summary Report), South Australia. Department of Water, Land and Biodiversity Conservation. Report, DLWBC 2004/39.

Walker, G., Doble, R., Mech, T., Lavis, T., Bluml, M., MacEwan, R., Stenson, M., Wang, E., Jolly, I., Miles, M., McEwan, K., Bryan, B.A., Ward, J., Rassam, D., Connor, J., Smith, C., Munday, T., Nancarrow, B., and Williams, S., 2005. Lower Murray Landscape Futures Phase One Report. Final Year 1 Technical Report prepared for the Centre for NRM, the Victorian NAP Office and CSIRO Water for a Healthy Country. Water for a Healthy Country report. Adelaide: CSIRO. Address when accessed http://www.clw.csiro.au/publications/consultancy/2005/LMLF_Project_Phase_One_Report.pdf

Wang, E., Miles, M., Schultz, T., Cook, P., Maschmedt, D., Munday, T., Leaney, T., Walker, G., and Barnett, S., 2005. Targeting Dryland Areas in the Mallee for Controlling Groundwater Recharge and

Salt Load to the Murray River. Report to Client No. #/2005. CSIRO Canberra, ACT, Australia. Address when accessed http://www.clw.csiro.au/publications/consultancy/2005/WfHC_targeting_dryland_areas.pdf

Ward, J. D., Werner, A. D. and Howe, B., 2009. Saltwater intrusion in Southern Eyre Peninsula: Report developed through the Eyre Peninsula Groundwater Allocation and Planning Project.

Water Monitoring Branch, 2005. The Health of the Aquatic Environment in the Darwin Harbour Region. Natural Resource Management Division, Department of Natural Resources, Environment and the Arts, Darwin. Report 5/2005D.

Werner, A.D., and Lockington, D.A., 2006. Tidal impacts on riparian salinities near estuaries. Journal of Hydrology, 328: 511-522.

Werner, A.D., and Simmons, C.T., 2009. Impact of sea-level rise on sea water intrusion in coastal aquifers. Ground Water, 47(2), 197-204.

Wood, B., 2002, Draft Darwin regional water resources management strategy, Resource Assessment Division, Department of Infrastructure, Planning and Environment, Darwin, report XX/02D.

Woodroffe, C.D., Mulrennan, M.E. and Chappell, J., 1993. Estuarine infill and coastal progradation, southern van Diemen Gulf, northern Australia. Sedimentary Geology, 83, 257-275.

Worden, K., Carson, C., Scrimgeour, I., Lally, J., and Doyle, N., 2008. A revised Palaeoproterozoic chronostratigraphy for the Pine Creek Orogen, northern Australia: Evidence from SHRIMP U-Pb zircon geochronology. Precambrian Research, 166, 122-144.

Yan, W. and Howe, B., 2008. Chowilla Floodplain Groundwater Model. Water Down Under Conference, Adelaide. p 1260-1271.

Yin Foo, D., 1980. Milingimbi water supply - investigation of the island aquifer system, NT Power and Water Authority Technical report WRD87057.

Yin Foo, D., 1982. Milingimbi water supply - investigation of water resources 1982, NT Power and Water Authority Technical report WRD83007.

Yin Foo, D., 1984. Galiwinku groundwater resource investigation, Water Division, Department of Transport and Works report 6/1984.

York D., Evensen N., Martinez M. and Delgado J. 2004.Unified equations for the slope, intercept, and standard errors of the best straight line. Am. J. Phys. 72 (3) March 2004.

11 Acknowledgements

This project would not have been possible without the invaluable support from staff at the Northern Territory Department of Natural Resources, Environment, the Arts and Sport (NRETAS). In particular, Des Yin Foo is thanked for his unwavering support for the project, and for finding additional resources when field validation and interpretation of the AEM dataset was required. Jon Sumner is thanked for his stalwart efforts with the field geophysical program, Simon Fell-Smith showed great patience in managing a difficult drilling program, while, Des, Jon, Simon and Steven Tickell greatly assisted the interpretation with their knowledge of local hydrogeology. The sonic drilling crews from Boart-Longyear did a great job (in often difficult circumstances) in drilling the five sonic boreholes which helped to validate the AEM data.

Ross C. Brodie is thanked for giving up his weekends to carry out the final inversions of the AEM dataset, and producing a set of reliable conductivity products. Murray Richardson and Ned Stolz are thanked for providing the geophysical resources required to complete the project appropriately. Niels Christensen is also thanked for performing the FiD point comparisons. Also a special thanks to the Graphics and Visualisation team, Michael de Hoog, James Navin, Neil Caldwell, Julie Silec and Michael O'Rourke.

This project also benefited greatly from discussions held with many staff from within the Groundwater Group at Geoscience Australia. In particular, we thank the team members of the National Seawater Intrusion project (another NWC-funded project), including Baskaran Sundaram, Prachi Dixon-Jain, Hashim Carey, Luke Wallace, Sarah Marshall, Rebecca Norman and Karen Ivkovic. Tim Ransley provided considerable assistance with some of the early fieldwork conducted for the project, and Yusen Ley-Cooper (now with the CSIRO) worked with the initial AEM data.

Pauline English from Geoscience Australia is recognised for the original conceptualisation and development of the NTCP project, and gaining organisational support within GA for the initial project. We would also like to acknowledge the funding and support provided by the National Water Commission, particularly their support for additional funding and an extension to the project timeframes when it became apparent that additional resources were required to calibrate and validate the AEM dataset, and produce interpretation products. In particular, we would like to acknowledge the input and assistance provided by NWC staff particularly Matt Kendall, Adam Sincock, Alastair Usher and Shane Hogan. The members of the project Steering Committee are also thanked for their guidance.

Peter Jolly and Colin Pain are thanked for their in-depth technical reviews of the initial draft report which have significantly improved the manuscript. Jane Coram, and her predecessor, Matt Hayne, are thanked for supporting the project. Barry Drummond and Stuart Minchin are thanked for providing high-level support for the project within GA.

12 Abbreviations and Acronyms

AEM – Airborne Electromagnetics
AHD – Australian Height Datum
ANZECC – Australian and New Zealand Environment and Conservation Council
API – American Petroleum Institute (API units commonly used for down-hole gamma logging)
DEM – Digital Elevation Model
DRWCD – Darwin Rural Water Control District
FAS – Fugro Airborne Systems
GA – Geoscience Australia
Ga – Billions of years ago
GDE – Groundwater-Dependent Ecosystem
GIS – Geographic Information System
GPS – Global Positioning System
HEA – Howard East Aquifer
KCD – Koolpinyah-Coomalie Dolomite
KDAC – Koolpinyah Dolomite Aquifer Characteristics project
Ma – Millions of years ago
NTCP – Northern Territory Coastal Plain
NRETAS – Northern Territory Department of Natural Resources, Environment, the Arts and Sport
NT – Northern Territory
NWC – National Water Commission
NWQMS – National Water Quality Management Strategy
OESP – Onshore Energy Security Program
PIMA – Portable Infrared Mineral Analyser
PVC – Poly Vinyl Chloride
RX – Receiver (coils in AEM systems)
SRTM – Shuttle Radar Topographic Mission
SWI – Seawater Intrusion
SWL – Standing Water Level
TDS – Total Dissolved Solids
TWOH – Tidal Water Over-height
TX – Transmitter (loop in AEM systems)
WAP – Water Allocation Plan
WCD – Water Control District

13 Units

cm – centimetres
km – kilometres
L/s – litres per second
m – metres
mg/l – milligrams per litre
mS/m – milli-Siemens per metre
S/m – Siemens per metre
µS/cm – micro-Siemens per centimetre

14 Glossary

Airborne Electromagnetic (AEM) survey: A geophysical survey method that maps the subsurface conductivity structure of the survey area using a loop mounted on a fixed-wing aircraft or carried beneath a helicopter. Many such systems exist with different performances, allowing the survey to be tailored to the needs of the end users.

Alluvial/alluvium: Sediments deposited by the action of rivers.

Aquifer: A geological horizon that holds and conducts water, the water is contained within the porosity of the aquifer. Aquifers may be unconfined, meaning they are open to the atmosphere, or confined, meaning they are capped by a relatively impermeable unit, or aquitard.

Aquitard: A relatively impermeable geological layer that caps a confined aquifer.

Archaean: Spelled Archaean in older literature; rocks older than 1.5 billion years.

Artificial recharge: The deliberate recharge of aquifers through pumping water into them via bores or increasing surface water infiltration through pits. Also known as managed aquifer recharge. Artificial recharge in coastal aquifers may be used to slow, contain, or reverse seawater intrusion.

Architecture: The relationship of different geological units to each other in space. For example, regolith architecture, sedimentary architecture etc.

Bedrock: Loose term given to any geological material that underlies the stratum of interest. Bedrock commonly consists of crystalline rocks such as granite or metasedimentary rocks.

BSL: below sea level

Confined: See *aquifer.*

Conglomerate: A sedimentary deposit formed by cementing gravels and cobbles together with minerals precipitated from groundwater.

Consolidated: See *cemented.*

Diagenesis: The changes that occur to sediments after they are deposited, including cementation and weathering.

DEMs: See *Digital Elevation Models.*

Digital Elevation Models (DEMs): Digital representations of the topography of the earth that are important components of geographic information systems (GIS). DEMs are obtained by many systems, including ground surveying, airborne radar and laser surveys, or from satellite radar.

Discharge: The flow of groundwater to surface water, bores, from one aquifer to the other or the sea. Also includes evapotranspiration from shallow aquifers.

Dissected: A term applied to landscapes which have been extensively eroded by valleys and gullies.

Dolerite: A dark, medium-grained rock, similar in mineral and chemical composition to basalt but coarser grained. Commonly intruded as molten rock into older rock bodies.

Dolines: A depression formed by the dissolution and collapse of the underlying rocks through the percolation of groundwater. It is a karst landform. Dolines can form directly in the soluble rocks or in insoluble rocks when the underlying soluble rocks are dissolved, forming cavities into which the insoluble rocks collapse. This is known as sub-adjacent karst.

Dolostone: A sedimentary rock consisting largely of the calcium-magnesium carbonate mineral dolomite, older literature refers to these rocks as dolomite.

Down-hole logging: A method of measuring the geophysical properties of the rocks, soils, or sediments penetrated by a drill hole. A tool that measures properties such as conductivity and natural gamma radioactivity is lowered down the borehole; data is recorded during both descent and ascent of the tool. Down-hole logging is a vital technique to calibrate conductivity and surveys and interpret geological logs.

Duricrust: A hardened layer formed in the regolith by cementation of soil or sediment, generally by minerals rich in iron, sulfate, silica, or carbonate.

Estuary: A funnel shaped inlet formed where a river meets the sea along a wave or tide-dominated coastline.

Evapotranspiration: The total water loss from the soil through the combined effects of evaporation and transpiration.

Feldspar: A common rock-forming mineral consisting of aluminium, silicon, oxygen and varying amounts of calcium, sodium, and potassium.

Ferricrete: An iron-rich duricrust.

Fracture: Cracks in indurated rocks formed by stress and strain. Fractures along which significant movement has occurred are called faults.

Freshwater lens: A lens-shaped body of less dense fresh water floating on top of denser saline water in an unconfined coastal aquifer. See *Ghyben-Herzberg lens*.

Gamma ray logging: Down-hole geophysical logging technique that maps the gamma radiation released by naturally occurring uranium, thorium and radioactive potassium within rocks and regolith.

Geomorphology: The study of landforms.

Geophysics: The study of the physical properties of the earth, in particular magnetic, conductivity, and radiometric properties, or variations in the earth's gravity. Geophysical techniques are widely used in mineral exploration and can help to understand the subsurface structure of the earth, locate groundwater, and map salinity (as well as many other applications).

Geographical Information Systems (GIS): GIS are computer-based systems for creating, storing, analysing and managing multiple layers of spatial data. These datasets include maps of geology, topography, infrastructure, soils, vegetation, and land use. GIS allow users to create interactive queries to analyse trends and patterns in spatial information.

Goethite: A yellowish-brown iron hydroxide mineral that is common in soils and regolith.

Granite: A coarse-grained igneous rock consisting mainly of quartz and feldspar.

Granules: Gravel-sized sediment between 2-4 mm in diameter.

Gravel: All loose, coarse-grained sediments with grains greater than 2 mm diameter.

Haematite: A reddish-brown iron oxide mineral that is common in soils and regolith.

Hydrogeology: The study of geological properties of rocks, soils, and sediments as they relate to groundwater movement and storage.

Hylogger: A system developed and marketed by CSIRO systems to provide a means to routinely and objectively capture detailed mineralogical information from drill core, chips and powder using reflectance spectroscopy. Hylogger collects data using spectrometers which measure the reflectance spectra over a range of wavelengths Visible-Near Infrared (VNIR) through Short Wave Infrared (SWIR) to Thermal Infrared (TIR).

Indurated: The process of hardening, such as occurs when sediments are turned into rock by various cementing agents, or surface hardening of some exposed rock surfaces that can occur during weathering.

IPCC: Inter-governmental Panel on Climate Change.

LIDAR: Light Detection And Ranging. A means of highly accurate topographic surveying using an aircraft-mounted laser scanner to measure the variation in altitude. Also written as LIDAR, Lidar or lidar.

Lithic: A term applied to sand or gravel where the particles are made up of rock fragments.

Incised channel: A river channel, such as that of the Ord River in the Ord Irrigation Area, that has cut down below its original flood plain. This commonly occurs in response to changes in river flow conditions or geological uplift.

Karst: A landscape formed by the dissolution of soluble rocks, such as dolostones. Karst features include caves and *dolines.* Karst-like features formed in normally non-soluble rocks, such as sandstones and siltstones, through the action of exceptionally aggressive groundwaters, is termed pseudokarst.

LANDSAT: A polar-orbit satellite launched by NASA to collect *multispectral* images of the Earth surface. Seven satellites have been launched in the series. Commonly written as "Landsat".

Magnetic survey: A geophysical survey method that maps the distribution of magnetic materials in the earth. Magnetic surveys can be carried out on the ground or from aircraft.

Metadata: Information about the source and accuracy of information used in a *GIS.*

Metamorphics: General term for rocks that have been recrystallised as a result of heat and pressure.

Multispectral imagery: Images acquired by satellites or aircraft that capture more than the three colour bands visible to the human eye. Multispectral images can be manipulated and combined in a *GIS* to emphasise subtle features such as variations in soil composition or vegetation.

Palaeochannels: Former river channels that are recognised in the surface (from aerial or satellite images) or subsurface (typically in *AEM* surveys or drilling).

Palaeovalley: Ancient valley filling sediments including (but not restricted to) those of *palaeochannels*. Typically palaeovalley sediments are not associated with currently active river processes.

Pediment: A gently-sloping apron of exposed or shallowly buried bedrock surrounding hills and rises.

Pedogenic: Processes or features pertaining to soil formation.

Phyllite: A fine-grained rock formed by the recrystallisation (metamorphism) of siltstone or shale under elevated temperatures and pressures, characterised by well developed parting (cleavage) and a sheen formed by the crystallisation of mica minerals.

PIMA: Portable **I**nfrared **M**ineral **A**nalyser. A short-wavelength infrared spectrometer that allows semi-quantitative assessment of the abundance of minerals containing CO_3, OH, H_2O, etc. and thus useful to detect clays, carbonates and other minerals formed during aqueous alternation.

Polje: The largest scale closed karst depressions, of the order of km to tens to km in width. From the Serbo-Croatian word for "field"

Porcelainite: A fine-grained *sedimentary* rock modified by *silicification* through *diagenesis* so that its fractured surfaces resemble broken porcelain. In the Darwin area porcelainites are associated with *radiolarites*.

Porosity: Open spaces in rocks and sediments that can hold water. *Primary porosity* formed when the sediments were laid down; these spaces may be variably infilled by *cement*, leaving remnant primary porosity. *Secondary porosity* forms through modification of rocks, such as by dissolution of soluble grains, formation of *fractures*, or solution-forming *karst.*

Progradation: The seaward movement of the coastal zone caused by infilling of coastal environments by sediments derived from the land after a *transgression.*

Proterozoic: A geological era that encompasses the time between 2,500 and 545 million years ago. The Proterozoic is formally divided into the Paleoproterozoic (2,500 and 1,600 million years), Mesoproterozoic (1,600-1,000 million years), and Neoproterozoic (1,000-545 million years).

Quartz: A very common mineral consisting of silicon dioxide that commonly occurs in river sands and as the main mineral in sandstones.

Quartzite: *Sandstone* consisting largely of quartz that has been recrystallised (metamorphosed) by exposure to geological heat and pressure.

Radiolarite: A *sedimentary* rock formed largely from the remains of Radiolaria, microscopic marine plankton whose skeletons are composed of opal. *Silica* mobilised from the Radiolaria and precipitated in siltstones leads to formation of *porcelainite.*

Recharge: The process by which water is added to an aquifer.

Regolith: The earth materials that occur between fresh rock and fresh air, including *weathered* rocks, soils, shallow groundwater and sediments.

Relict: A term applied to landscape features that are no longer being actively formed. For example, the floodplain of the Ord River is regarded as relict because, prior to dam construction, it was not being inundated during seasonal floods.

Rotary mud drilling: A relatively cheap drilling method that uses a rotating cutting bit to drill a hole. Samples are brought to the surface as cuttings supported by a circulated drilling fluid containing mud, and this also keeps the hole open. Samples are contaminated by the drilling fluid, and these are averaged over the sample interval (typically 1-5 m). Material from shallower depths can also contaminate samples drilled further down-hole. Also known as mud drilling or rotary drilling.

Salinity: Areas where salt is being deposited in the near-surface environment. Salinity is a natural phenomenon but can be increased through land use practices involving inappropriate types of soil management, vegetation clearing, cropping, and irrigation.

Sandstone: A *sedimentary* rock composed of sand-sized particles.

Saltwater wedge: Saltwater has a greater density than freshwater, and as a result it moves in the form of a seawater wedge beneath freshwater on the landward side of the coastline.

Saprock: Compact, slightly weathered rock with low porosity; defined as having less than 20% of weatherable minerals altered but generally requiring a hammer blow to break. It may still contain rock structure.

Saprolite: Saprolite is weathered rock in which more than 20% of the weatherable minerals in the original rock have been altered *in situ*, with interstitial grain relationships being undisturbed. Saprolite is altered from the original rock by mainly chemical alteration and loss without any change in volume. This is sometimes referred to as constant volume alteration. Saprolite can be highly porous and permeable and may be an important aquifer.

Saprolith: Saprolith is all those parts of a weathering profile that have been formed strictly *in situ*, with interstitial grain relationships being undisturbed. This contrasts with residual material or pedolith, which has been disturbed. Saprolith is altered from the original rock by mainly chemical alteration and loss without any change in volume. It is subdivided into *saprock* and *saprolite*.

Seawater interface: The front that exists between seawater and freshwater in a coastal aquifer, whereby less dense freshwater sits above, and adjacent to, a denser seawater wedge.

Seawater intrusion: The landward movement of seawater into coastal aquifers, due to natural or human-related changes in groundwater dynamics.

Sedimentary: Pertaining to deposition of sediments and sedimentary process, for example, a sedimentary rock is a rock once composed of sediments such as sand, gravel, silt, etc.

Shale: A *sedimentary* rock composed of clay particles.

Silica: Term applied to fine-grained *quartz* cement in sediments and soils.

Silicification: Process by which silica is deposited.

Siltstone: A *sedimentary* rock composed of silt-sized particles.

Sonic drilling: A relatively high-cost drilling method that relies of acoustic-frequency vibrations and slow rotation to recover core of relatively undisturbed material uncontaminated by drilling fluids and shallower intervals.

Succession: Term applied to a series of sedimentary or volcanic deposits.

Stratigraphy: The study of how different layers of sediments can be related to each other.

SRTM: *Digital Elevation Model* data collected during the 2000 STS-99 **S**huttle **R**adar **T**opography **M**ission by the Space Shuttle Endeavour. SRTM data is widely available at 3-arc second (~90 m) horizontal resolution and on a restricted basis at 1-arc second (~30 m) horizontal resolution.

SWI: See *Seawater Intrusion*.

Transgression: A long-term rise in relative sea-level causing flooding of the coastal zone, for example, after the end of the last ice age.

Transgressive: Pertaining to processes or sediments resulting from a *Transgression.*

Transmissivity: A measure of the ability of groundwater to pass through soil, sediment or rock.

Transpiration: Water given off by plants via pores in the surface tissues.

Unconfined: See *aquifer.*

Unconformity: A *bounding surface* where the rocks below rest at a different angle to those above, for example, where alluvial gravels rest on bedrock.

Unconsolidated: See *uncemented.*

Vulnerability: The characteristics and circumstances of a community, system or asset that make it susceptible to the damaging effects of a hazard.

Watertable: The surface below which an *unconfined aquifer* is saturated with water. See also *potentiometric surface.*

Weathered/weathering: The physical and chemical changes that a rock undergoes when it is exposed to the atmosphere and shallow groundwater.

Wetlands: Low-lying areas subject to partial or continuous inundation. Also called swamps.

XRD: X-ray diffraction. An analytical method used to determine the mineral composition of soil, sediment, and rock samples.

15 Appendices

There are eight appendices in this report. These are included in digital format on the DVD that accompanies the hard copy version of the report, and (from July 2012) the appendices are also available for download with the pdf version of the report from the Geoscience Australia website at:
http://www.ga.gov.au/cedda/publications/96

The appendices include the following information:

Appendix 1 – AEM sections
This appendix contains all AEM flight line sections (approximately 190 jpeg files) for the project survey area. Each section shows five images: 1). Topographic variation along the flight line as shown from the 1-arc second SRTM digital elevation model (shaded with NW gradient), 2). Landsat image, 3). Regional aeromagnetic data showing the 1st vertical derivative data reduced to the pole, 4). Linear colour stretch of the GA-LEI AEM conductivity data (in S/m), and 5). A logarithmic colour stretch of the GA-LEI AEM conductivity data (S/m).

Appendix 2 – Geophysical logging data
This appendix contains the recorded downhole logging data for gamma and induction logs collected for the five sonic core holes drilled for this project. The data are contained in separate Excel spreadsheet files.

Appendix 3 – Borehole stratigraphic and lithologic data
This appendix contains the stratigraphic and lithologic logging data for the five sonic boreholes drilled for the project. Detailed lithologic logging of the sonic core was carried-out in the Geoscience Australia core laboratory in Canberra. The data are contained in separate Excel spreadsheet files.

Appendix 4 – Borehole sonic core photographs
This appendix contains photographs of each box of sonic drill core collected for this project. The photographs are provided as jpeg and pdf files.

Appendix 5 – Grainsize data for sonic core
This appendix contains grainsize information for selected sonic core intervals. The data are contained in Excel spreadsheet and pdf files.

Appendix 6 – Borehole geochemistry data
This appendix contains geochemistry data obtained from analysis of the sonic drill cores obtained for this project. Solid phase data were obtained by X-ray fluorescence (XRF) analysis for major elements, and by inductively coupled plasma–mass spectrometry (ICP-MS) for trace elements. The pore fluid geochemistry data were analysed in the Geoscience Australia Hydrogeochemistry Laboratory using standard analytical techniques. The data are provided in Excel spreadsheet and pdf files.

Appendix 7 – Compiled sonic borehole logs
This appendix contains compiled borehole logs for each sonic drillhole completed for this project. These logs have been created using the Strater software application. These logs show the down—hole variation in pore fluid and solid phase geochemistry data (for both major elements and trace elements), as well as the PIMA data. The data are presented as pdf files.

Appendix 8 – Groundwater salinity data
This appendix contains compiled down-hole data from NRETAS for existing bores in the project study area. These include groundwater salinity and lithologic data. The information is presented in an Excel spreadsheet.